# Fundamentals for modeling of micro climate, plant growth and plant quality development in field vegetable production below plastic covers

## D i s s e r t a t i o n

**zur Erlangung des akademischen Grades**
**doctor rerum horticulturarum**
**(Dr. rer. hort.)**

**eingereicht an der**
**Lebenswissenschaftlichen Fakultät**
**der Humboldt-Universität zu Berlin**

von

M.Sc. Martin Sandmann

Präsident der Humboldt-Universität zu Berlin:
Prof. Dr. Jan-Hendrik Olbertz

Dekan der Lebenswissenschaftlichen Fakultät:
Prof. Dr. Richard Lucius

Gutachter: 1. Prof. Dr. Christel Richter
2. Prof. Dr. Eckhard George
3. Prof. Dr. Thomas Rath

Tag der mündlichen Prüfung: 20. April 2015

# I. Content

# II. Figures

# III. Tables

# IV. Symbols

**Latin symbols**

## A

| | |
|---|---|
| $a$ | temperature response function of leaf area index [LAI/h], parameter of the Skartveit model |
| $A$ | test area size [cm²] |
| $a_1$ | empirical coefficient |

## B

| | |
|---|---|
| $b$ | constant in SVM |
| $b_0$ | estimate of the regression constant |
| $b_1$ to $b_4$ | estimate of the regression coefficient |

## C

| | |
|---|---|
| $c$ | fitting parameter for $CO_2$ compensation point estimation |
| $C$ | constant in SVM |
| $c_0$ | speed of light in vacuum [m/s] |
| $C_1$ | first radiation constant [$W\mu m^4/m^2$] |
| $C_2$ | second radiation constant [$\mu mK$] |
| $c_s$ | $CO_2$ concentration at the leaf surface [mol $CO_2$/(mol air)] |

## D

| | |
|---|---|
| $d$ | number of independent variables of each observation in SVM |
| $D$ | dry matter [g] |
| $D_0$ | empirical coefficient |
| $d_{min}$ | minimum diffuse fraction |
| $D_s$ | humidity deficit [kPa] |

## E

| | |
|---|---|
| $E$ | blackbody spectral emissive power [$W/(m^2\mu m)$] |
| $E_\lambda$ | sensor specific calibration factor of TP01 [V/K] |

## F

| | |
|---|---|
| $f^d$ | relative diffuse fraction of global radiation |

## G

| | |
|---|---|
| $G$ | mean projection of unit foliage area |
| $g_0$ | stomata conductance when there is no irradiation and A is zero [$mol/(m^2s^1)$] |
| $g_1$ to $g_3$ | fitting parameters |
| $g_{sc}$ | stomatal conductance [$mol/(m^2s)$] |

## H

| | |
|---|---|
| $h$ | universal Planck constant [Js], water tension [hPa] |

## I

| | |
|---|---|
| $I_0$ | incident direct radiation [W/m²] |
| $I_a$ | total radiation which is absorbed by the canopy [$W/m^2$] |
| $I_{a,cy}$ | direct radiation which is absorbed by the canopy [$W/m^2$] |
| $I^d_0$ | incident diffuse radiation [W/m²] |
| $I^d_{a,cy}$ | diffuse radiation which is absorbed by the canopy [$W/m^2$] |
| $I_g$ | global radiation, measured above canopy and cover [W/m²] |

## J

| | |
|---|---|
| $J$ | number of independent variables in the logistic regression model |

## K

| | |
|---|---|
| $k$ | Boltzmann constant [JK], clearness index |
| $K$ | unsaturated water conductivity [$cm\ d^{-1}$], kernel function in SVM |
| $k_0$ | parameter of the Skartveit model |
| $k_1$ | clearness index at $d_{min}$ |

| | |
|---|---|
| $K_c$ | Michaelis-Menten constant for $CO_2$ [µbar] |
| $K_o$ | Michaelis-Menten constant for $O_2$ [mbar] |
| $K_s$ | saturated conductivity [cm $d^{-1}$ |

## L

| | |
|---|---|
| $L$ | likelihood function |
| $L_0$ | likelihood of the intercept-only model |
| $LAI_0$ | initial leaf area index [$m^2/m^2$] |
| $LAI_{eff}$ | effective leaf area index from indirect measurements [$m^2/m^2$] |
| $LAI_{max}$ | maximum leaf area index [$m^2/m^2$] |
| $LL$ | log likelihood function |
| $L_\beta$ | likelihood of the fitted model |

## N

| | |
|---|---|
| $n$ | sample size |
| $n_d$ | number of days before harvest |
| $n_f$ | ratio of false predictions on non-marketable plants |
| $n_i$ | pore size distribution |
| $n_t$ | ratio of correctly predicted non-marketability of plants |

## O

| | |
|---|---|
| $O$ | partial pressure of oxygen in the leaf air [mbar] |
| $OP$ | output |

## P

| | |
|---|---|
| $p$ | adjustable parameter of kernel functions in SVM, probability |
| $P$ | period [µs] |
| $p_1$ to $p_4$ | fitting parameter |
| $P_c$ | soil temperature corrected period [µs] |
| $p_f$ | ratio of false predicted marketable plants |
| $p_t$ | ratio of correctly predicted marketability of plants |

## Q

| | |
|---|---|
| $q$ | water flow [cm/h] |
| Q | heating power per meter of TP01 sensor [W/m] |

## R

| | |
|---|---|
| $R$ | molar gas constant [kJ $K^{-1}$ $mol^{-1}$], incident global radiation [$Wh/m^2$] |
| $R^2$ | coefficient of determination |
| $R^2_{adj}$ | $R^2$ adjusted for the degree of freedom |
| $R^2_{LR}$ | generalized coefficient of determination in the logistic regression analysis |
| $R_d$ | mitochondrial |

## S

| | |
|---|---|
| $s_1$ to $s_6$ | fitting parameters from the soil reflectance model |

## T

| | |
|---|---|
| $t$ | time step |
| $T$ | air temperature [K], absolute temperature of a black body [K] |
| $T_a$ | air temperature below a cover [°C] |
| $T_{inside}$ | daily mean air temperature below the cover [°C] |
| $T_k$ | leaf temperature [K] |
| $T_{max}$ | maximum temperature above which lettuce cannot form any side shoots [°C] |
| $T_{min}$ | minimum temperature below which no side shoots can be formed in lettuce [°C] |
| $T_{outside}$ | daily mean air temperature in 2 m height [°C] |
| $T_{ref}$ | reference temperature [K] |
| $T_s$ | soil temperature [°C] |

## U

| | |
|---|---|
| $u$ | residual |
| $U_0$ | voltage output of TP01 sensor before heating procedure [V] |
| $U_{180}$ | voltage output of TP01 sensor after heating procedure [V] |

## V

| | |
|---|---|
| $V$ | visibility function, volume [$cm^3$] |
| $V_{cmax}$ | maximum carboxylation velocity [µmol $m^{-2}$ $s^{-1}$] |

## W

| | |
|---|---|
| $w$ | parameterizing vector of the hyperplane in SVM |
| $WC$ | soil water content |
| $w_i$ | weights of the partial van Genuchten functions |

## X

| | |
|---|---|
| $x$ | ratio of vertical to horizontal projections of canopy elements, vector of observations of the independent variable in SVM |

## Y

| | |
|---|---|
| $y$ | vector of observations of the dependent variable in SVM, dependent variable in logistic regression analysis |

## Z

| | |
|---|---|
| $z$ | height of soil sample [cm], vectors within the optimal hyperplane in SVM |
| $z_i$ | realization of the latent variable of the $i^{th}$ observation in the logistic regression analysis |

**Greek symbols**

— A —

| | |
|---|---|
| $\alpha$ | absorbtance coefficient, type 1 error, leaf inclination angle [°] |
| $\alpha_b$ | current total cover roughness |
| $\alpha_{cy}(\theta)$ | direct radiation absorptance coefficient of the canopy |
| $\alpha^d_{cy}$ | diffuse radiation absorptance coefficient of the canopy |
| $\alpha_i$ | inverse value of the bubble point potential [$cm^{-1}$] |

— B —

| | |
|---|---|
| $\beta_0$ | regression constant |
| $\beta_j$ | regression coefficient of the $j^{th}$ independent variable |

— Γ —

| | |
|---|---|
| $\Gamma$ | $CO_2$ compensation point [µbar] |
| $\Gamma^*$ | $CO_2$ compensation point without dark respiration [µbar] |

— Δ —

| | |
|---|---|
| $\delta$ | incidence angle [°] |
| $\Delta A$ | absolute relative difference of LI-3100 measurements and test size area [$cm^2$] |
| $\Delta A_{\%}$ | relative difference of LI-3100 measurements and test size area [%] |
| $\Delta H_\alpha$ | fitting parameter for $CO_2$ compensation point estimation |

— Θ —

| | |
|---|---|
| $\theta_l$ | mean leaf inclination angle [°] |
| $\theta_{max}$ | water content at field capacity [$cm^3/cm^3$] |
| $\theta_{min}$ | water content at wilting point [$cm^3/cm^3$] |
| $\theta_{res}$ | residual water content [$cm^3/cm^3$] |
| $\theta_s$ | volumetric soil water content [$cm^3/cm^3$] |
| $\theta_{sat}$ | water content at saturation [$cm^3/cm^3$] |

— Λ —

| | |
|---|---|
| $\lambda$ | wavelength [nm], soil thermal conductivity [W/(m·K)] |
| $\lambda_r$ | thermal conductivity in dry soil [W/(m·K)] |
| $\lambda_s$ | thermal conductivity of water saturated soil [W/(m·K)] |

— Ξ —

| | |
|---|---|
| $\xi$ | slack variable in SVM |

— P —

| | |
|---|---|
| $\rho$ | reflectance coefficient, distance between upper and lower hyperplane in SVM |
| $\rho_b$ | bulk density [$g/cm^3$] |

— Σ —

| | |
|---|---|
| $\sigma$ | adjustable parameter of kernel functions in SVM |
| $\Sigma T_{max}$ | maximum value of temperature sum which is necessary for lettuce to achieve the adult growing stage [°C] |

— T —

| | |
|---|---|
| $\tau$ | threshold ratio for marketability of lettuce plants according side shoots, transmittance coefficient, tortuosity |
| $\tau(\delta)$ | directional-hemispherical transmittance of cover materials |
| $\tau_{DIR}(\delta)$ | directional-directional light transmittance of cover materials |

— Φ —

| | |
|---|---|
| $\Phi$ | separation function in SVM, cumulative distribution function of the standard normal distribution |

— Ω —

| | |
|---|---|
| $\Omega$ | clumping index |

# V. Units

| | |
|---|---|
| *µbar* | microbar |
| *µm* | micrometer |
| *µmol* | micromole |
| *µs* | microsecond |
| *C* | celsius |
| *cm* | centimeter |
| *d* | day |
| *g* | gramm |
| *ha* | hectare |
| *hPa* | hectopascal |
| *Hz* | hertz |
| *J* | joule |
| *Js* | joule-second |
| *K* | kelvin |
| *kJ* | kilojoule |
| *kPa* | kilopascal |
| *m* | meter |
| *mbar* | millibar |
| *min* | minute |
| *mm* | millimeter |
| *mol* | mole |
| *N* | newton |
| *s* | second |
| *t* | tonne |
| *W* | watt |

# VI. Abbreviations

| | |
|---|---|
| ASTM | American Society for Testing and Materials |
| BEREST | Beregnungssteuerung |
| $CO_2$ | carbon dioxide |
| DAP | days after planting |
| DLR | Dienstleistungszentrum ländlicher Raum Rheinpfalz |
| ER | Erbs et al. (1982) |
| FF | double layer cover consisting of non-woven fabric and perforated film |
| GO | Golzow |
| GR | Großbeeren |
| GRG | generalized reduced gradient |
| Hyprop | Hydraulic properties measurement system |
| LAI | leaf area index |
| LOOCV | leave-one-out cross-validation |
| LR | logistic regression |
| LUE | light use efficiency |
| NWF | non-woven fabric |
| $O_2$ | oxygen |
| PAR | photosynthetic active radiation [W/m²] |
| PF | perforated film |
| PVC | polyvinyl chloride |
| RF | random forest |
| SC | Schifferstadt |
| SK | Skartveit and Olseth (1987) |
| SP | Spitters et al. (1986) |
| SVM | support vector machines |
| UV | ultraviolet radiation |
| VIS | visible radiation |

# VII. Preliminary considerations

There are two published works attached to this thesis, which contain a significant portion of the results of my work. In this thesis I cite these works several times and give some extensions which are not part of the original works. The attached published works should be regarded as a part of this thesis:

1. Sandmann, M., Graefe, J. & Feller, C. (2013): Optical methods for the non-destructive estimation of leaf area index in kohlrabi and lettuce. *Scientia Horticulturae*, 156, 113-120.

2. Graefe, J. & Sandmann, M. (2015): Shortwave radiation transfer through a plant canopy covered by single and double layers of plastic. *Agricultural and Forest Meteorology*, 201, 196-208.

Results and methods from soil hydraulic measurements (see section 3.2.1.1) were used in the following published works:

3. Schreiter, S., Ding, G.C., Heuer, H., Neumann, G., Sandmann, M., Grosch, R., Kropf, S. & Smalla, K. (2014) Effect of the soil type on the microbiome in the rhizosphere of field-grown lettuce. *Frontiers in microbiology*, 5, Article Number 144.

4. Bitterlich, M., Vetter, A., Sandmann, M., Graefe, J. & Franken, P. (2014) Impact of arbuscular mycorrhizal substrate and root colonization on host photosynthesis. *Soil Biology & Biochemistry* (submitted 3/2014)

5. Schreiter, S., Sandmann, M., Smalla, K. & Rita Grosch, R. (2014) Soil type dependent rhizosphere competence and biocontrol of two bacterial inoculant strains and their effects on the rhizosphere microbial community of field-grown lettuce. *PLoS ONE* 9(8): e103726 doi: 10.1371/journal.pone.0103726

# 1. Introduction

## 1.1. Field vegetable production in early spring

Customers in Germany want to buy vegetables the whole year. They prefer vegetables, which were grown in Germany. This statement is supported for Germany by results of empirical studies from von Alvensleben (2000) and Henseleit et al. (2007). A similar consumer behavior can be observed e.g. in the USA (Loureiro & Umberger 2005). However, the climatic conditions in Germany are not suitable to completely satisfy this need of the consumers. Especially in the winter period, temperatures are often too low for most vegetables for growing or even for surviving. But there are some strategies to beneficially regulate climatic conditions around the vegetable plants in the field in a certain temperature range. To extend the growing and harvest-period of spring vegetables it is possible to protect the plants from late frosts by using a cover. Another effect of covering the plants is a mean rise of temperature below the cover of about $5.5\,K$ (own data; measured $10\,cm$ above soil surface) compared to no cover, which results in an accelerated plant development. This figure fits well to data obtained by Maync (1989), who found a cover induced air temperature rise of $4.5\,K$ at $5\,cm$ above the soil surface.

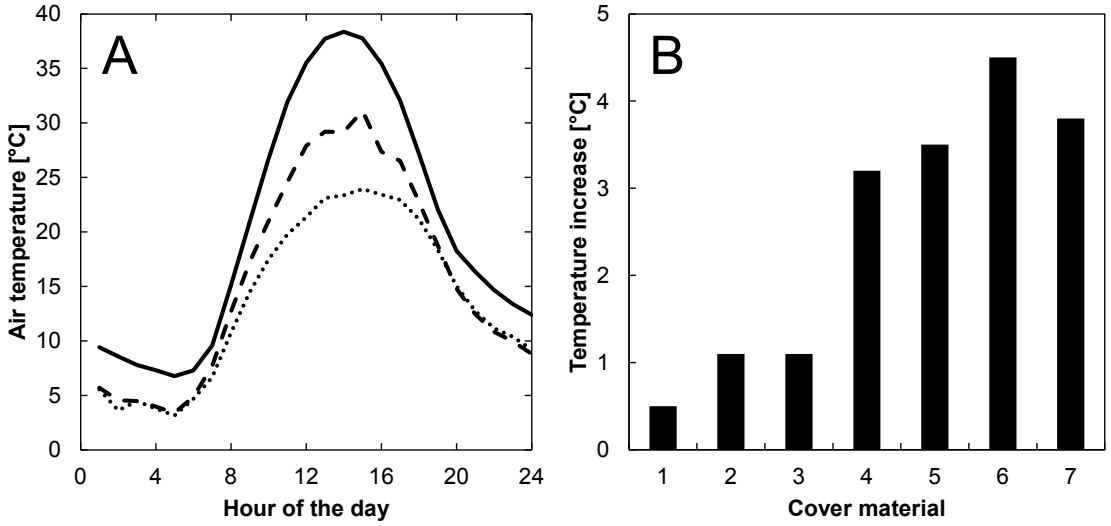


**Figure 1.1** (A) Hourly mean air temperature at $10\,cm$ above soil surface in kohlrabi (Großbeeren, 13.04.2010, sunny weather, 12 days after planting). Solid line = double layer consisting of non-woven fabric (NWF) and perforated film (PF), dashed line = NWF, dotted line = without cover. (B) Mean daily temperature increase at $5\,cm$ above soil surface in kohlrabi for different cover materials in comparison to no cover treatment. Data are from Maync et al. (1985) (Schifferstadt, 06.03.1985-21.04.1985). Cover materials: 1 = new NWF, 2 = new PF, 3 = used PF, 4 = new NWF and new PF, 5 = 2× new PF, 6 = 2× used PF, 7 = 2× new PF anti-drop.

Figure 1.1A shows a bit more in detail the diurnal change of the air temperature below different covers. It can be said that the cover material leads to a rising temperature compared to no cover treatment. The temperature rise usually has its maximum in the afternoon. Results from Maync et al. (1985) are summarized in Figure 1.1B. They compared seven cover materials and showed that covers, consisting of two layers, increased air temperature by at least 3 $K$ whereas the increase goes up to only 1 $K$ for single layer covers.

Except for strawberries and asparagus, the most important crops for this production system in Germany are head lettuce (*Lactuca sativa var. capitata* L.) and kohlrabi (*Brassica oleracea var. gongylod*es). Non-woven fabric (NWF) in combination with perforated film (PF) is in common use as cover material. According to data from the German Federal Statistical Office (2014), head lettuce was grown on an area of 1789 $ha$, where 62595 $t$ were harvested in Germany in 2013. These absolute numbers are equivalent to 4 % and 10 % of the total growing area and total harvest of leafy and stem vegetables, respectively, where 17 different species in this group of vegetables were considered. The same measures for kohlrabi were 1873 $ha$ and 64840 $t$, related to the total values of all nine brassica vegetables, included in this inquiry, this is equal to 10 % and 8 %, correspondingly. Unfortunately, data ascertainment was not done separately for field vegetable production in early spring. All data refer to the whole year 2013. Nevertheless, both vegetable species have a medium importance in Germany for the whole year, whereas their importance can be assumed to be significant higher if only early spring production was considered.

### 1.1.1. The production system

For the protected production of field vegetables in early spring, many different cover materials are available. Usually, NWF or PF are utilized by the growers. Often, two layers of cover material are put on the crops simultaneously: first, a layer of NWF with direct contact to the plants and, second, a layer of PF. Commonly, there is no mechanical structure which supports the cover material (Figure 1.2). So the weight of the covers has to be carried solely by the plants. Especially plants on the corners of the edge of the cover may suffer from deformations, because the cover material not only exerts pressure from the top but also from the side. But in practice only a negligible number of plants are affected. So

the weight of the cover material seems to be not a significant economic problem. The cover needs to be relatively taut to prevent damages of the plant during spells of strong wind. If the cover was installed too loose, then the wind would cause a rhythmic motion of the cover in vertical direction which moves like waves in horizontal direction across the field. Every time the cover moves downward, the plants are hit and the young leaves are rubbed or they even kink.

There are two main strategies to face this problem. (1) During the growing process, the cover is loosened to fulfill the increased space needs of the plants. This strategy requires that there is additional cover material at the edge of the field. (2) Another strategy may be to form little banks at the edges of the field and in regular distances across the field. The cover material is put taut on top of the banks. In the space between them, the plants are able to grow until they reach marketability (Seitz 1985).

To prohibit the possibility that wind could remove the cover from the plants completely, the edges of the cover material are either plowed into the soil or they are loaded e.g. with sandbags.

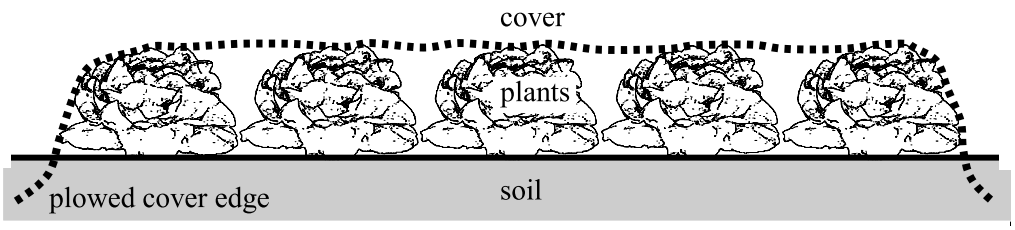


**Figure 1.2** Schematic of the production system

This production system has some important advantages and disadvantages. Positive aspects are the accelerated plant grows and the increased production security. Short periods of very cold weather affect the covered plants to a much lesser extent. The risk of yield and quality losses becomes lower for the grower and the accelerated plant growth makes it possible to bring the vegetables earlier to the market and to gain more money per plant. The last fact is the main reason for growers in Germany to apply this production system, as long as the higher prizes, which can be realized in early spring, outweigh the main disadvantage of the production system: the additional costs for the cover material and its deploying and removal.

From the environmental point of view, the cover material should be used as efficient as possible to save fossil raw materials which are used to produce the NWF and PF. But it is hard or even impossible

to use the cover material several times due to its ageing process during the growing period (it is getting frail, dirty and bumpy). Mostly the cover material is given to the recovered substance cycle after the first use.

The most recent statistic which was available according to the development of area of cultivated land in Germany, where this production system is applied, was provided by Schlaghecken et al. (2002). Their data are plotted in Figure 1.3. The increasing importance of the described production system in Germany can be deduced from the increasing area where it was applied from 1975 to 2002. The strongest increase of cultivated area shows NWF (up to almost $9000\,ha$), whereas usage of double layer covers (NWF and PF) also increased up to almost $2000\,ha$ during this period. Single layer PF covers application became more common in the 1970s and 1980s and remained constant on an absolute scale since 1990. It can be assumed that the importance of the plastic cover usage at least did not decrease since 2002 in Germany.

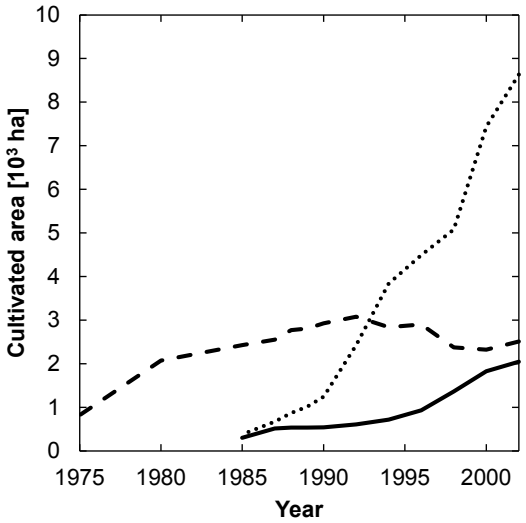


**Figure 1.3** Development of cultivated area which is covered by plastics during field vegetable production in early spring in Germany from 1975 to 2002. Solid line = double layer cover consisting of non-woven fabric and perforated film, dashed line = perforated film, dotted line = non-woven fabric. Data are from Schlaghecken et al. (2002).

### 1.1.2. Conventional plastic film management

The described production system requires one important decision to be made by the growers: When to remove the cover from the plants? On the one hand, it is problematic to leave the cover too long on the plants. In that situation there is a serious risk for crop quality losses if air temperature below the cover

rises too high. Commonly observed plant symptoms are then low head consistency, burns of the outside leaves and the appearance of side shoots in lettuce and an altered turnip form in kohlrabi. On the other hand a too early removal of the cover results in a suboptimal use of the temperature advantage and the harvest may be not at the earliest time, possible.

To minimize those risks it is necessary to make a scientific sound decision when to remove the cover. Currently, a temperature sum approach is used which takes into account the daily maximum temperature above the cover since planting. This approach was developed by Maync in the 1980s (Laun 14.05.2014, personal communication). Air temperature data at $2\ m$ height from nearby weather stations are used for this purpose. If a certain temperature sum is reached (e.g. $300\ °C$), the PF is removed, while NWF usually stays on the crop until harvest. Clearly, this approach does not consider the complexity of the micro climate below the cover. The plant development below the cover is depending on far more factors than the temperature in $2\ m$ height.

An empirical approach for the prediction of temperature below covers was proposed by Fink (2009). From measured daily data he found the relationship

$$T_{inside} = T_{outside} + p_1 R \tag{1.1}$$

where $T_{inside}$ is the daily mean air temperature below the cover, $T_{outside}$ is the daily mean air temperature at $2\ m$ height, $R$ is incident global radiation in $\frac{Wh}{m^2}$ and $p_1$ is a dynamic fitting parameter which is recalculated daily. Measured data for $T_{inside}$, $T_{outside}$ and $R$ from the previous nine days are used for fitting $p_1$ via linear regression. Predictions of future $T_{inside}$ realizations are provided using weather forecast data of $T_{outside}$ and $R$. Fink (2009) mentioned one important weakness of this approach: the situation of strong changes of $T_{outside}$ and $R$ during the prediction period. Two cases can be separated: (1) unstable strong changes of $T_{outside}$ and $R$ with duration of only a few days before the values return to "normal" magnitude and (2) stable strong changes of $T_{outside}$ and $R$ from one magnitude to another. In both cases precision of the prediction will be decreased as long as the period of strong change is among the "learning data set" of the previous nine days. In other words: transients of $p_1$ and the predictions occur during this period of time. Another weakness of the approach is the necessity of $T_{inside}$ measurements for the estimation of $p_1$. To get this information, test plots with different covers and data acquisition hardware need to be established. This is costly and

labor expensive. From predictions of $T_{inside}$, a removal of PF can be derived, if a rise of $T_{inside}$ above a critical temperature ($\approx 35°C$) can be expected. Common practice in the Pfalz region is to supply the vegetable growers with the output of the Maync and the Fink model via the online portal of the Dienstleistungszentrum ländlicher Raum Rheinpfalz (DLR).

However, neither the Maync nor the Fink model is precise enough for contemporary requirements in production safety because for growers it might be economic disastrous to produce low quality lettuce due to a wrong time of cover removal.

## 1.2. Objectives of the thesis

In this dissertation, the foundations for a more sophisticated model than the Maync and the Fink models are proposed, which will be based on an energy balance approach, to improve the recommendation for the removal of the cover. This goal should be reached by using only standard weather station data as regular model-input, which are now commonly available in vegetable growing regions. Besides weather data several model parameters describing covers, soils and plants are required. In the context of the described production system (section 1.1.1) three compartments need to be considered: the plant, the soil, the cover. Furthermore, the two physical states of the climatic conditions above and below the cover need to be taken into account. The microclimate beneath the cover is the key-component of the system (especially the air temperature and the radiation budget), because it is crucial for plant growth and quality differentiation.

For modeling the microclimate beneath a cover, it is necessary to parameterize submodels which describe physical and biological processes and their states. Required auxiliary functions and parameters of these processes are another output of the submodels. Two important auxiliary functions of the soil compartment are the water retention function content and the thermal conductivity-water content relation. Leaf growth and the stomata conductance, which is related to the mean stomata aperture, are examples for an important biological process and a state in this case. For these and more processes, where ever possible, well-proven published submodels were parameterized for the actual production system. In cases of non-availability of suited submodels, new ones were created.

Using extensively measured micro climate states below the cover, a second necessary step will be the development of a new quality model which is able to predict and quantify the risk for quality losses of lettuce and kohlrabi as a function of micro climate below the cover. Using measured data of micro climate below the cover in this thesis is a simplification and should be replaced by modeled data in future works.

Quality is a highly complex and fundamental plant characteristic. In practice it is an aggregated characteristic, which is formed from different product features. The purchaser mentally aggregates the quality aspects via weights to account for the relative importance of each feature – a highly subjective process.

The same subjectivity in the evaluation of plant quality occurs in experimentation. Therefore, preceding the quality model formulation the methodological problem of subjectivity has to be considered. Commonly, scorings are used. But those values strongly depend on the person performing the scoring. So first different quality measures of lettuce and kohlrabi are evaluated, then the most essential ones concerning their importance for marketability are chosen and their scorings are attempted to be objectified, respectively.

In summary, Table 1.1 gives an overview of the various submodels which are involved in the modeling of micro climate, plant growth and plant quality development in field vegetable production below plastic covers. Submodels in Table 1.1 are grouped in already established and new parameterized ones, in this thesis new developed ones and in those which are not yet developed.

**Table 1.1** Summary of submodels which are required for modeling micro climate, plant growth and plant quality development in field vegetable production below plastic covers.

| Component | New parameterized established submodels | In this thesis new developed submodels | Not yet developed/used submodels |
|---|---|---|---|
| Air above the cover | • Fractions of diffuse and direct incident radiation → *section 2.5.4.1* / 3.2.4.1 | | • Relative humidity |
| Cover material | | • Shortwave radiation transfer (transmittance, reflectance, absorptance) → *section 3.3.2 / Graefe & Sandmann (2014)*<br>• Wetness status → *section 3.3.2 / Graefe & Sandmann (2014)*<br>• Surface morphology → *section 3.3.2 / Graefe & Sandmann (2014)* | • Longwave radiation transfer (transmittance, reflectance)<br>• Heat transfer via conduction and convection<br>• Energy balance (cover temperature) |
| Air below the cover | | | • Scalar transport (temperature, relative humidity, $CO_2$ concentration)<br>• Airflow |
| Plants | • Stomata conductance → *section 2.5.3* / 3.2.3<br>• Shortwave radiation transfer (extinction coefficient) → *section 3.3.2 / Graefe & Sandmann (2014)*<br>• Canopy structure (leaf angle, clumping factor) → *section 2.5.4.3* / *3.2.4.3* | • Dry matter accumulation → *section 3.3.3*<br>• Leaf area growth → *section 3.3.1.1* / *3.3.1.2*<br>• Plant quality (marketability) → *section 3.4* | • Leaf gas exchange<br>• Longwave radiation transfer (emissivity)<br>• Energy balance |
| Soil surface | | • Shortwave radiation transfer (reflectance, absorptance) → *section 3.2.4.2.3* | • Longwave radiation transfer (emissivity) |
| Soil | • Unsaturated water conductivity → *section 2.5.1 / 3.2.1.2*<br>• Water content → *section 2.5.1 / 3.2.1.1*<br>• Thermal conductivity → *section 2.5.2 / 3.2.2* | | • Heat transfer<br>• Water transport and root water uptake |

# 2. Material and Methods

To generate the necessary data for model formulation and validation of micro climate and plant development below plastic covers, field experiments at different sites and for several years were carried out. In the following sections the field experiments (sites and layout) and the data collection (micro climate, plant growth and plant quality) are described.

## 2.1. Field experiments

Several field experiments were carried out at the experimental sites of the Leibniz-Institute of Vegetable and Ornamental Crops in Großbeeren (GR; 52°21' N, 13°19' E) and Golzow (GO; 52°34' N, 14°30' E) and at the experimental site of the Dienstleistungszentrum Ländlicher Raum Rheinpfalz in Schifferstadt (SC; 49°24' N, 8°21' E) in the years 2010-2013. Due to bad weather conditions in 2013, only one trial in Schifferstadt could be performed. The plants were supplied with nutrients in step with actual practice. At GR site and GO site irrigation was carried out following the BEREST (**Bere**gnungs**st**euerung) software recommendations (Gutezeit et al. 1993). At SC site the Geisenheim method was applied, accordingly to Beck & Kleber (2014).

### 2.1.1. Treatments and experimental layout

The tested treatments changed over the years. In general, the number of different treatments and the removal strategy for the perforated film varied in later field trials due to gained experiences from previous seasons. In this study, there was a special interest in the two vegetable species head lettuce (*Lactuca sativa var. capitata* 'Torpedo') and kohlrabi (*Brassica oleracea var. gongylodes* 'Lech'). Those species were grown under differently applied covers:

- without cover
- NWF
- PF
- NWF+PF (Abbreviation: FF)

Covers were placed directly on the plants without any supporting structures. The NWF (material: polypropylene) had a weight of 19 $g/m^2$ and the film (material: polyethylene) was perforated by 500 holes/$m^2$, where each hole has a diameter of 1 $cm$ which corresponds to an area gap fraction of 3.93 %. The cover removal strategy in 2010 and 2011 in GR and GO was to remove the perforated film from the FF at prior fixed dates (weekly from week 2 to week 5 after planting) whereas in SC a temperature sum strategy was applied. Due to too bad plant quality at harvest in 2010 and 2011 in GR and GO (especially concerning sun burns of the outer leaves and decay of the plants in lettuce), the temperature sum strategy was applied at these sites in 2012, too. Based on experience of Fink (personal communication) and Maync in SC and compared to fixed dates, this strategy makes it possible to react on actual weather conditions and resulted in a wider range of plant quality. A regular planting grid of 0.3 × 0.3 m (distance between rows × within the row) was adopted, resulting in a planting density of about 111,000 plants/ha. Plots consisted of five rows in GR and SC and six rows in GO. In 2010 and 2011 in GR and GO there were two planting dates (first and second batch) realized, resulting in an additional inspection factor. The strategies for the removal of the perforated film from FF treatments are summarized in Table 2.1, whereas the layouts of the ten field trials and the plot designs are listed in the appendix (see sections 6.1 and 6.2). Altogether, 18 cover treatments were realized: 15 removal strategies (Table 2.1) and the treatments "without cover", NWF and PF.

**Table 2.1** Strategies for the removal of the perforated film (PF) from treatments with covers consisting of non-woven fabric (NWF) and perforated film. $\Sigma T_{max}$= sum of the daily maximum temperature ($°Cd$) at 2 m height since planting.

| No. | Strategy | No. | Strategy |
|---|---|---|---|
| 1 | without removal | 9 | remove if $\Sigma T_{max} \geq 300$ |
| 2 | first fixed time of removal | 10 | remove if $\Sigma T_{max} \geq 350$ |
| 3 | second fixed time of removal | 11 | remove if $\Sigma T_{max} \geq 400$ |
| 4 | third fixed time of removal | 12 | remove if $\Sigma T_{max} \geq 500$ |
| 5 | fourth fixed time of removal | 13 | $\Sigma T_{max} \geq 200$ and more than three hours > 30°C |
| 6 | remove if $\Sigma T_{max} \geq 150$ | 14 | $\Sigma T_{max} \geq 200$ and more than three hours > 35°C |
| 7 | remove if $\Sigma T_{max} \geq 200$ | 15 | removal after occurrence of quality losses |
| 8 | remove if $\Sigma T_{max} \geq 250$ | | |

An overview of planting dates and days of PF removal is given in Table 2.2. Not all cover treatments were realized at every site and in every year. There were two replications per treatment. Additional plots were established which were excluded from intermediate harvests for intensive measurements via sensors. Altogether the experimental layout was a randomized block design. An overview of the established cover treatments per site and per year is given in Table 2.3

**Table 2.2** Planting dates and number of days since planting when the perforated film was removed from plots with covers, which initially consisted of non-woven fabric and perforated film (GB = Großbeeren, GO = Golzow, SC = Schifferstadt, removal 1 to removal 6 = different removal treatments for each year and location). The number of the applied removal strategy is given in brackets (for the meaning of the strategy number see Table 2.1).

| Location | Batch | Planting date | Removal 1 | Removal 2 | Removal 3 | Removal 4 | Removal 5 | Removal 6 |
|---|---|---|---|---|---|---|---|---|
| GB | 1 | 13.04.2010 | 15 (2) | 22 (3) | 28 (4) | 42 (5) | | |
| GB | 2 | 22.04.2010 | 13 (2) | 19 (3) | 33 (4) | 40 (5) | | |
| GO | 1 | 14.04.2010 | 15 (2) | 22 (3) | 30 (4) | 43 (5) | | |
| GO | 2 | 23.04.2010 | 13 (2) | 21 (3) | 34 (4) | 41 (5) | | |
| SC | 1 | 02.03.2010 | 22 (7) | 27 (9) | 35 (11) | 36 (13) | 41 (12) | 45 (14) |
| GB | 1 | 17.03.2011 | 14 (2) | 28 (3) | 34 (4) | | | |
| GB | 2 | 31.03.2011 | 20 (2) | | | | | |
| GO | 1 | 25.03.2011 | 12 (2) | 26 (3) | | | | |
| GO | 2 | 06.04.2011 | 14 (2) | | | | | |
| SC | 1 | 24.02.2011 | 24 (13) | 26 (9) | 32 (14) | 38 (12) | | |
| GB | 1 | 14.03.2012 | 14 (7) | 19 (9) | 30 (11) | 37 (12) | 47 (15) | |
| GO | 1 | 19.03.2012 | 16 (7) | 25 (9) | 32 (11) | 39 (12) | 44 (15) | |
| SC | 1 | 22.02.2012 | 23 (13) | 27 (9) | 33 (14) | 38 (12) | | |
| SC | 1 | 04.03.2013 | 28 (6) | 32 (8) | 38 (13) | 41 (9) | 43 (10) | 45 (11) |

**Table 2.3** Established cover treatments in the field experiments at Großbeeren site (GB), Golzow site (GO) and Schifferstadt site (SC) in 2010 to 2013. NWF = non-woven fabric, PF = perforated film, FF = double layer cover consisting of NWF and PF, FF 1 to FF 15 is the number of the cover removal strategy (see Table 2.1).

| Site | Year | Without Cover | NWF | PF | FF 1 | FF 2 | FF 3 | FF 4 | FF 5 | FF 6 | FF 7 | FF 8 | FF 9 | FF 10 | FF 11 | FF 12 | FF 13 | FF 14 | FF 15 |
|---|---|---|---|---|---|---|---|---|---|---|---|---|---|---|---|---|---|---|---|
| GB | 2010 | X | X | | X | X | X | X | X | | | | | | | | | | |
| GB | 2011 | X | X | | X | X | X | X | X | | | | | | | | | | |
| GB | 2012 | X | X | | X | | | | | | X | | X | | X | X | | | X |
| GO | 2010 | X | X | | X | X | X | X | X | | | | | | | | | | |
| GO | 2011 | X | X | | X | X | X | X | X | | | | | | | | | | |
| GO | 2012 | X | X | | X | | | | | | X | | X | | X | X | | | X |
| SC | 2010 | | X | | | | | | | | X | | X | | X | X | X | X | |
| SC | 2011 | X | X | X | | | | | | | | | X | | | X | X | X | |
| SC | 2012 | X | X | X | | | | | | | | | X | | | X | X | X | |
| SC | 2013 | X | X | | | | | | | X | | X | X | X | X | | X | | |

### 2.1.2. Site descriptions

Mean monthly air temperatures and mean monthly sums of precipitation of the three sites GR, GO and SC are presented in Figure 2.1. SC site is warmer than the GR and GO sites, which are very similar regarding mean temperature. Mean annual temperatures are $11.4\,°C$, $9.6\,°C$ and $9.4\,°C$ for SC, GR and GO, respectively. There is a remarkable precipitation peak in GO around august. Mean annual precipitation sums are for SC $555\,mm$, GR $467\,mm$ and GO $525\,mm$. The fractions of sand/silt/clay are for the haplic luvisol in SC $34/47/19\,\%$ (Nett et al. 2011), the arenic luvisol in GR $91/4/5\,\%$ (Graefe et al. 2005) and the gleyic fluvisol in GO $47/25/28\,\%$ (Ruehlmann & Ruppel 2005). Therefore a certain range of mean annual temperatures and soil textures were covered by the three sites.

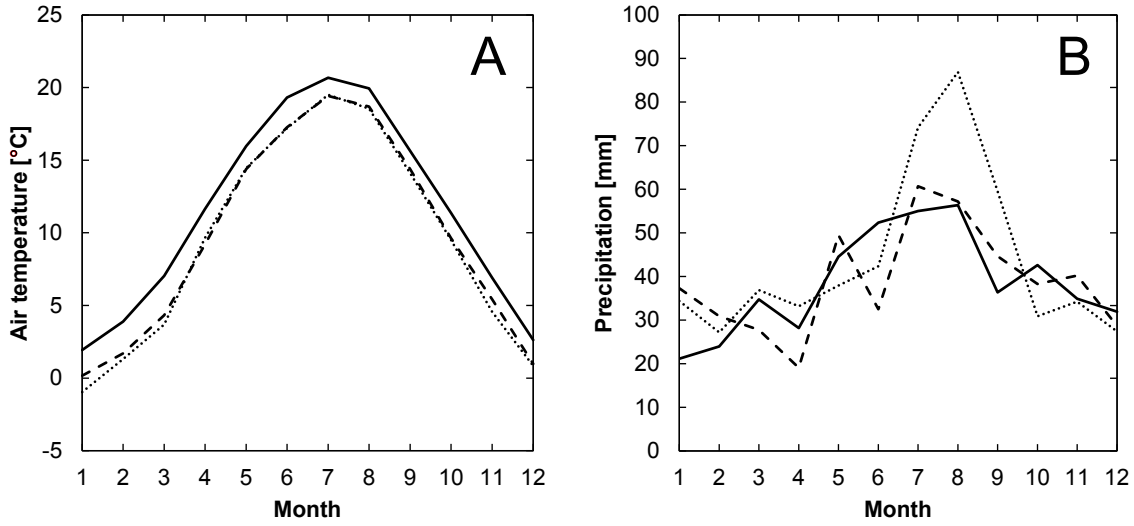


**Figure 2.1** Climatic characteristics of field trial sites. A = monthly mean air temperature [$°C$] in 2 $m$ height. B = monthly mean sum of precipitation [$mm$]. Solid line = Schifferstadt, dashed line = Großbeeren, dotted line = Golzow (all means based on data from 2000 to 2010).

### 2.1.3. Data collection

An extensive data collection was gathered during field trials, where three main strategies of measuring were applied. Microclimatic conditions were measured automatically using electronic sensors and data loggers, plant growth parameters were estimated both destructively and non-destructively and plant quality measures were determined via scoring several plant traits. Especially intensive data collection

by electronic sensors was established at GB site, where the amount of data collection was increasing from 2010 to 2012. The details will be described in the following three sections.

#### 2.1.3.1. Microclimate

A variety of microclimatic parameters were measured every ten minutes. Those parameters were air temperature, soil temperature, relative air humidity, wind speed, soil volumetric moisture content, air $CO_2$ concentration, photosynthetic active radiation (PAR) and crop surface temperature. The number and spatial locations of the sensors are listed together with the adopted experimental layouts in the appendix (section 6.1). Air temperature was measured $10\ cm$ above the ground among the plants. For this purpose PT100 sensors (Service für Messtechnik Geraberg GmbH, Germany) were placed into a radiation shield (PVC pipe, $3\ cm$ in diameter, $27\ cm$ long, covered with aluminum foil) which was equipped with a fan for continuous air flow around the sensor. Relative air humidity, wind speed and air $CO_2$ concentration were also measured at $10\ cm$ above the soil surface within the crops. For relative air humidity measurements, synthetic fiber sensors (TFG80J, Galltec Mess- und Regeltechnik GmbH, Germany) were placed into a radiation shield (PVC pipe, $5\ cm$ in diameter, $32\ cm$ long, covered with aluminum foil) which was equipped with a fan for continuous air flow around the sensor, very similar to the PT100 sensor radiation shields. Horizontal wind speed below covers was measured with thermal anemometers (velocity transducers model 8455, TSI Inc., USA). Air was sampled at five locations and continuously pumped towards a central located IRGA $CO_2$/$H_2O$ Analyzer (LI-840, LICOR Bioscience Inc., USA). The air flow arriving from one sample location was analyzed for $CO_2$ concentration over two minutes, so that one multiplexing cycle with 5 sample channels was completed within $10\ min$. Soil temperature was measured in two soil depths: $5\ cm$ and $15\ cm$ (PT100, mostly WTE 10 type, Service für Messtechnik Geraberg GmbH, Germany) and volumetric soil water content was measured in 0 to $30\ cm$ soil depth via time-domain reflectometry (TDR) sensors (CS625, Campbell Scientific Inc., Utah, USA) placed vertical into the soil. The CS625 output ($OP$) is a frequency in $Hz$. It has to be transformed into a period ($P$) in $\mu s$ via $P = OP^{-1} \cdot 1000000$. Due to the temperature dependence of CS625 sensors, a temperature correction is necessary: $P_c = P + (20 - T_s)(0.526 - 0.052P + 0.00136P^2)$, where $T_s$ is soil temperature. Soil water content ($WC$) is

then $WC = -0.0663 - 0.0063P_c + 0.0007P_c^2$ (Campbell Scientific Inc.USA 2011). Total PAR was measured with line quantum sensors (LI-191, LICOR Biosciences Inc., Nebraska, USA) placed below the canopy. Plant surface temperature was measured in lettuce using infrared sensors (IR120, Campbell Scientific Ltd., UK) while each sensor was targeting essentially a single lettuce head in its field of view. As a reference, all parameters were also measured next to the plots, but $40\ cm$ above the ground, where a cup anemometer (4.3519.00.173, Adolf Thies GmbH & Co. KG, Germany) was used for reference wind speed measurements.

For the test of the diffuse fraction of incident shortwave radiation (see section 3.2.4.1), a reference dataset was created using a sunshine sensor (BF5, Delta-T Devices Ltd, UK) which was placed in about $1\ m$ height next to the plots. The following microclimatic parameters are used for modeling in this thesis: air temperature, soil temperature, soil volumetric moisture content, air $CO_2$ concentration, PAR, diffuse fraction of incident shortwave radiation.

#### 2.1.3.2. Plant growth

The plant growth was monitored by regular destructive harvests of twelve non-edge plants per plot. Plot design generally allowed seven intermediate harvests (see section 6.2), where it was not always necessary to fully utilize this amount of intermediate harvests. Intermediate harvests were not performed on plots intensive microclimatic measurements via electronic sensors (see section 6.1). Usually, the sampling interval was once a week. But during the first weeks, when the plant growth is very slow, the sampling interval was extended to two weeks. Intermediate sampling was not realized at the SC site, because the required man power was not available.

The measured attributes differed per species, due to their diverging morphology. Measured characteristics for lettuce are:

- plant fresh mass [$g$]; head fresh mass [$g$]
- {number of leaves (only during first weeks until the plants had around 20 leaves)}
- plant diameter [$cm$]; head diameter [$cm$]
- length of stalk [$cm$]
- plant dry mass content [$g/g$]
- leaf area index (LAI) [$m^2/m^2$] (where the leaf area was defined as the sum of the one-sided projected area of hull leaves and half the surface area of the head (Sandmann et al. 2013))

Plant characteristics in curly brackets were measured but not used for further considerations. For plant dry mass content measurements in lettuce, a mixed sub sample of all harvested plants was oven dried (200 $g$ to 250 $g$ fresh mass, 65 °$C$, until weight constancy [about 3 to 5 $d$]).

Measured characteristics for kohlrabi are:

- leaves fresh mass [$g$]; tuber fresh mass [$g$]
- {number of leaves}
- {length of the longest leaf [$cm$] (including the petiole)}
- tuber diameter [$mm$]
- tuber height [$mm$]
- leaves dry mass content [$g/g$]; tuber dry mass content [$g/g$]
- LAI [$m^2/m^2$]

Plant characteristics in curly brackets were measured but not used for further considerations. For plant dry mass content measurements in kohlrabi, a mixed sub sample of all harvested plants (separately for leaves and tubers) was oven dried (each about 200 $g$ fresh mass, 65 °$C$, until weight constancy [about 3 to 5 $d$]).

Leaf area was measured in 2010 and 2011 directly with an LI-3100 Area Meter (LICOR Bioscience USA 1996). The LAI was computed from plant spacing (0.3 $m$ × 0.3 $m$). In 2012 the LAI was measured indirectly via a method outlined in Sandmann et al. (2013). Leaf area was not assessed in SC.

#### 2.1.3.3. Quality measures

A species specific range of potential useful quality measures was assessed on the same twelve plants obtained during destructive harvest. A screening of all initially assessed quality measures revealed, that only a small number of variables are suitable quality measures. Two were chosen for lettuce and one for kohlrabi: head consistency and formation of side shoots in lettuce and turnip form in kohlrabi. The main advantages of these properties are: they are especially critical for plant quality and their scoring schemes have the potential to be objectified.

Usually, quality measures are assessed using scorings, where this is a procedure influenced by subjectivity. Objectification of data assessments is necessary to gain more reliable data, which are independent of the scoring person. A long-term objective of the objectification is to replace scorings by other methods. The first step to objectify the scorings is to diminish the traditional number of scores from nine to three. At the SC site head consistency has been scored from 1 (very soft) to 9 (very hard) since decades. It is very hard to distinguish reliable between two neighboring scores – even if there is a lot of expert knowledge. One can think of an alternative scoring system where the even scores 2, 4, 6 and 8 are left out to gain more reliable data. In practice there is an interest whether the plants are marketable or not. So it is appropriate to merge the scorings into the three scores marketable, not marketable and intermediate. Transforming the detailed scorings into the combined ones, leads to more reliable information about the plant characteristic considering marketability. In the case of properties, which have their optimum at one end of the scoring scale, there is no real loss of information because the higher information content of the detailed scores is just an illusion due to their high uncertainty (e.g. formation of side shoots in lettuce in Table 2.4). If the optimum of the property is at an intermediate position in the scoring scale, no information according to marketability is lost due to diminishing the scoring schemes. But the information whether the property is too strong or too weak in the case of non-marketability is no more in the data (head consistency in lettuce and turnip form in kohlrabi in Table 2.4). However, this is not a problem as long as only the decision of marketability is of interest. The quality measure “formation of side shoots” was scored in a semi-quantitative way where number and estimated size of side shoots are combined to yield a scoring

estimate. Turnip form of kohlrabi was objectified via measurements of turnip height and diameter. The ratio of height and diameter was than related to the given scoring (Table 2.4).

**Table 2.4** Traditional and reduced scoring schemes for head consistency and formation of side shoots in head lettuce and turnip form in kohlrabi. For turnip form of kohlrabi also the related ratio of turnip height to diameter is given.

| Head consistency | | Formation of side shoots | | Turnip form | | |
|---|---|---|---|---|---|---|
| Old scoring | New scoring[a] | Old scoring | New scoring[a] | Old scoring | New scoring[a] | Ratio |
| 1 (very soft) | 3 | 1 (none) | 1 | 1 (flat) | 3 | ≤ 0.58 |
| 2 | 2 | 2 | 1 | 2 | 2 | 0.67 |
| 3 (soft) | 2 | 3 (some) | 1 | 3 | 1 | 0.75 |
| 4 | 1 | 4 | 2 | 4 (flat-round) | 1 | 0.83 |
| 5 (intermediate) | 1 | 5 (intermediate) | 2 | 5 | 1 | 0.92 |
| 6 | 1 | 6 | 2 | 6 (round) | 1 | 1.00 |
| 7 (hard) | 2 | 7 (much) | 2 | 7 (high-round) | 2 | 1.09 |
| 8 | 2 | 8 | 3 | 8 | 3 | 1.20 |
| 9 (very hard) | 3 | 9 (very much) | 3 | 9 (high) | 3 | ≥ 1.33 |

[a] 1= marketable; 2 = intermediate; 3 = not marketable

## 2.2. Additional experiments

To objectify the scorings of head consistency, an additional test was made in 2012, where 63 plants from the SC site, representing the whole “old scoring” scheme range of head consistency, were scored by three persons independently. Person 1 has decades of experience in scoring the head consistency and persons 2 and 3 do not. So the scorings of person 1 were taken as a reference. Persons 2 and 3 repeated the scoring three times. The scoring was performed by squeezing the head with one hand. All persons scored independently from each other and the repetitions of persons 2 and 3 were also performed independently to minimize the subjective component of the scoring-procedure. Scorings were done using the old scoring scheme. To objectify the property of head consistency, a force-path analysis during machine performed squeezing of heads (Instron, Series IX automated Material Testing system 8.30.00.) was carried out. This material testing device squeezed the head from the side with a circular stamp (stamp diameter = 5.8 cm) and measured squeeze-path and squeeze-force for all scored plants. The hypothesis was that plants with lower scorings would show a smaller resistance for

squeezing, so that the squeezing-force is smaller than for plants with higher scorings. The data for squeezing-forces from 10 to 20 N were used for further analysis because within this interval there is a linear relationship between path and force. The regression coefficient of this linear relationship was compared with the scoring of each plant by a linear regression analysis.

Among the persons, linear regressions of the scorings were also performed. Uncertainties in the scorings among the repetitions per person were quantified by calculating the mean-range of scorings which were given to the same plant by the same person (for results see section 3.4.1).

More additional experiments are described in detail in the following sections:

- Leaf area index in section 2.4 and Sandmann et al. (2013); conducted in GB (2011)
- Soil water flow in section 2.5.1.2; conducted using samples from GB and GO (both 2012)
- Soil heat flow in section 2.5.2.2; conducted using samples from GB and GO (both 2012)
- Optical properties of flux participating surfaces in section 2.5.4.2, where further details for each surface can be found here:
    - Covers (transmittance, reflectance and absorbtance) in section 3.2.4.2.1; conducted using samples from GB and GO (both 2011 and 2012)
    - Leaves (transmittance, reflectance and absorbtance) in section 3.2.4.2.2; conducted using samples from GB (2012)
    - Soils (reflectance) in section 3.2.4.2.3; conducted using samples from GB and GO (both 2013)

## 2.3. Statistical and computational methods

Statistical and computational methods used in this thesis were realized with several software packages and specialized analysis programs. For most statistical and data management problems SAS 9.2 (SAS Institute Inc. 2008) was used. Realization of the proposed models was done in MATLAB R2006b (The MathWorks Inc. 2006). Data presentation and simple analyses were conducted via Microsoft Excel 2010. Specialized analysis programs, used in this thesis, are mentioned in the particular text passages.

### 2.3.1. Parameter estimation methods

Several parameter estimation methods were used for this thesis. With SAS 9.2 the procedures REG, LOGISTIC and MODEL were applied, where the REG procedure performs simple and multiple linear regressions, the LOGISTIC procedure performs logistic regressions (section 2.3.2.1) and the MODEL procedure provides several parameter estimation methods and is able to fit any kind of model equation or system of equations. In MATLAB the estimation of parameters was performed with the "lsqnonlin" function, which solves nonlinear least squares problems via a subspace trust region method. Parameter estimation in Microsoft Excel 2010 was performed via the add-in "Solver", which uses the generalized reduced gradient (GRG) method for solving nonlinear optimization problems. For all software packages and parameter estimation methods, except for the REG procedure of SAS 9.2, initial values had to be provided to start the estimation procedure. Proper initial values were set either directly or by trial and error until the used optimization procedure converged. Boundaries which define intervals with plausible upper and lower limits for each parameter, were also used in the parameterization process.

### 2.3.2. Data mining methods for classification and regression

To test the predictability of the quality measures described in section 2.1.3.3, several data mining methods are suitable. Three of them were used and will be presented in detail in the following three sections. The main intention will be to find a statistical classification system which discriminates between good and bad plant qualities based on environmental features. In this case air temperature data was considered. Thus, a binary classification problem needs to be solved by the data mining methods.

#### 2.3.2.1. Logistic regression

This section is mainly based on chapter 5 of Backhaus et al. (2011). Logistic regression (LR) aims to find the probability $p$ for the realization of a certain event $y$, e.g. the marketability, $p(y = 1)$, of a lettuce head or its non-marketability, $p(y = 0)$. This approach can be extended to more than two discrete realizations of an event (Krishnapuram et al. 2005). Obviously, this method can be used for

classification purposes. The main difference towards the classical linear regression analysis is that the dependent variable is not necessarily of metric scale (e.g. ordinal or alternative scales are possible), i.e. the estimated probability in the LR (dependent variable) is in the interval [0,1] whereas the dependent variable in the linear regression analysis is in the interval $[-\infty, +\infty]$. Compared to the discriminant function analysis the main difference is that LR is more robust because fewer assumptions are made. The probability for $p_i$ of the $i^{\text{th}}$ observation to have the value 1 as the realization of the event $y$ is defined as

$$p_i(y = 1) = \frac{1}{1 + \exp(-z_i)} \tag{2.1}$$

with

$$z_i = \beta_0 + \sum_{j=1}^{J} \beta_j x_{ij} + u_i \tag{2.2}$$

where Eq. (2.2) is a linear equation containing the influence on $p_i$ of all $J$ independent variables. $\beta_0$ is the regression constant, $\beta_j$ is the regression coefficient of the $j^{\text{th}}$ independent variable and $u_i$ is the residual of the $i^{\text{th}}$ observation. Eq. (2.1) is the link between the desired probability $p$ and the independent variables $x_j$ and is also called "link function". Besides Eq. (2.1), which is also called "logit function" due to its structure, there are also other link functions possible, e.g. the probit function $p_i(y = 1) = \Phi(z_i)$ ($\Phi$ is the cumulative distribution function of the standard normal distribution) or the complementary log-log function $p_i(y = 1) = 1 - \exp(-\exp(z_i))$ (SAS Institute Inc. 2008). The most simple version of Eq. (2.2) is $z_i = \beta_0 + \beta_1 x_i + u_i$, where only one independent variable $x_i$ describes $z_i$.

Obviously, $p_i(y = 0) = 1 - p_i(y = 1)$. Due to the fact that every observation $y_i$ is either 1 or 0 and under the assumption of independence of the observations $y_i$, one can generalize Eq. (2.1) to

$$p_i(y) = \left(\frac{1}{1 + \exp(-z_i)}\right)^{y_i} \cdot \left(1 - \frac{1}{1 + \exp(-z_i)}\right)^{1-y_i}. \tag{2.3}$$

If $y_i = 1$ than the second factor of Eq. (2.3) will be 1 and if $y_i = 0$ than the first factor of Eq. (2.3) will be 1. To get the maximum likelihood estimation of the parameters $\hat{\beta}_0 = b_0$ and $\hat{\beta}_1 = b_1$ the

product of the probabilities $p_i$ for all $n$ observations has to be determined (which is the likelihood function $L$):

$$L = \prod_{i=1}^{n} \left[ \left( \frac{1}{1 + \exp(-z_i)} \right)^{y_i} \cdot \left( 1 - \frac{1}{1 + \exp(-z_i)} \right)^{1-y_i} \right]. \quad (2.4)$$

The favored parameter estimates are found when $L$ is maximized (maximum likelihood). For easier calculations the product in Eq. (2.4) can be transformed to a sum via logarithmic calculus, resulting in the log likelihood function $LL$, which also has to be maximized:

$$LL = \sum_{i=1}^{n} \left( y_i \cdot \ln\left( \frac{1}{1 + \exp(-z_i)} \right) \right) + \left( (1 - y_i) \cdot \ln\left( 1 - \frac{1}{1 + \exp(-z_i)} \right) \right). \quad (2.5)$$

To check the goodness-of-fit of the LR-model a generalized coefficient of determination was introduced by Nagelkerke (1991):

$$R_{LR}^2 = \left( 1 - \left( \frac{L_0}{L_\beta} \right)^{\frac{2}{n}} \right) \cdot \left( 1 - (L_0)^{\frac{2}{n}} \right)^{-1} \quad (2.6)$$

where $L_0$ is the likelihood of the intercept-only model and $L_\beta$ is the likelihood of the specified model. $R_{LR}^2$ is in the interval $[0,1]$ and can be interpreted in the same way as the standard coefficient of determination from the linear regression analysis. LR was realized using the "glmfit" and "glmval" functions from the statistics toolbox of Matlab (The MathWorks Inc. 2006), whereas $R_{LR}^2$ was estimated additionally via the LOGISTIC procedure of SAS 9.2 (SAS Institute Inc. 2008). Results from both software packages were compared and yielded the same results.

#### 2.3.2.2. Random forest

The random forest (RF) algorithm is another approach to perform classifications, which was first proposed by Breiman (2001). In his paper, he defines RF as "a classifier consisting of a collection of tree-structured classifiers […] and each tree casts a unit vote for the most popular class at input $x$." (Breiman 2001). In other words: $n$ decision trees are created. Every tree consists of several binary decisions. After a cascade of decisions throughout a decision tree, observation $x$ is assigned to a class. This procedure is repeated for all $n$ decision trees, so $x$ is $n$ times assigned to a class. Usually, not every decision tree will assign $x$ to the same class. The idea is, that the majority of all trees (= the

whole "forest") assigns $x$ to the right (true) class. Finally, RF chooses the class for $x$ which was assigned by most trees.

RF is a supervised algorithm which needs to be trained. So the original data set has to be split up into a training and a prediction subset. Every decision branch of a decision tree is called "node", where every node leads either to another node or a final assignment to a class, which is called "leaf" (Ho 1995). The structure of the forest can be controlled via two free parameters: the number of trees grown and the dimension of the trees. The tree dimension depends on the number of explanatory variables the decisions are based on. The more feature variables are submitted to the algorithm, the more decisions can be done and the more complex are the trees. Commonly used values for the two parameters are $500$ and the integer part of the number of feature variables divided by $3$, respectively, which were also adopted in this work. In case the second parameter is $< 1$, then it is set to $1$. Sub splits of the training dataset are selected randomly as proposed by Dietterich (2000). Breiman (2001) showed that RF are not prone to the overfitting problem.

The RF algorithm was applied using Matlab (*classRF_train.m* and *classRF_predict.m* from https://github.com/PetterS/hep-2/tree/master/randomforest-matlab/RF_Class_C [accessed April 2 2014]). This Matlab implementation of RF is derived from the RandomForest implementation for R. The first file is used together with the training data set and creates the forest and the second file uses this forest structure to predict the classes for the remaining data. In this thesis the leave-one-out cross-validation (LOOCV) procedure was used: only one observation of the original dataset was left out from the training dataset (size of the training dataset is $n - 1$). Afterwards, the class of the single observation was estimated using the created forest. This was repeated $n$ times, so that every observation of the original dataset was left out once. The performance of the RF approach was then evaluated via calculation of the percentages of true and false class assignments.

#### 2.3.2.3. Support vector machines

Support vector machines (SVM) is a further method to solve multiple classification and regression problems, which was first proposed by Cortes and Vapnik (1995). In this thesis SVM is used to solve a binary classification problem. The starting point are $n$ pairs of observations $\boldsymbol{x} = (\boldsymbol{x}_1, \ldots, \boldsymbol{x}_n)$ and $\boldsymbol{y} =$

$(y_1, \dots, y_n)$ where $\boldsymbol{x}_i \in \mathbb{R}^d$ $(i = 1, \dots, n)$ consists of $d$ input variables and $y_i \in \{-1,1\}$ contains a binary class label. The pairs of $\boldsymbol{x}$ and $\boldsymbol{y}$ from the training dataset are used to create the SVM. Once trained, the SVM can be later used for classification of unknown data. The training dataset can be divided into two sub datasets: one for the SVM creation and one to validate the SVM's classification performance.

To separate $\boldsymbol{x}$ into two classes, the optimal hyperplane

$$\boldsymbol{w} \cdot \boldsymbol{z} + b = 0 \tag{2.7}$$

has to be found, where $\boldsymbol{w}$ is the parameterizing vector of the hyperplane, $\boldsymbol{z}$ consists of the vectors within the optimal hyperplane and $b$ is a constant. An example from $\mathbb{R}^2$ is presented in Figure 2.2. Additionally the constraint

$$y_i(\boldsymbol{w} \cdot \boldsymbol{x}_i + b) \geq 1 \quad \forall i \tag{2.8}$$

needs to be fulfilled by $\boldsymbol{w}$ and $b$. $\boldsymbol{w} \cdot \boldsymbol{x}_i + b = 1$ is the upper hyperplane and $\boldsymbol{w} \cdot \boldsymbol{x}_i + b = -1$ is the lower hyperplane which both together form the borders between which there are no observations (solid lines in Figure 2.2). Constraint (2.8) is necessary, because it ensures that no observations are between the upper and the lower hyperplane. The upper and lower hyperplane contain the observations which are nearest to the optimal hyperplane. These observations are also called "support vectors". Only the support vectors have influence on the optimal hyperplane, all the other observations are not used for calculations. Under the constraint (2.8), the distance between the upper and lower hyperplane $\rho(\boldsymbol{w}, b)$ should be maximized to become the best class separation possible (Burges 1998):

$$\max\big(\rho(\boldsymbol{w}, b)\big) = \max\left(\frac{2}{\|\boldsymbol{w}\|}\right) \Leftrightarrow \min(\|\boldsymbol{w}\|)\,. \tag{2.9}$$

In case that there is no linear separation possible without wrong classification of single observations, e.g. because of overlapping of the two true classes, Cortes & Vapnik (1995) proposed the slack variable $\boldsymbol{\xi} = (\xi_1, \dots, \xi_n)$ which has to fulfill the constraint:

$$y_i(\boldsymbol{w} \cdot \boldsymbol{x}_i + b) \geq 1 - \xi_i \quad \forall i \tag{2.10}$$

where $\xi_i \geq 0 \ \ \forall i$ and the value of $\xi_i$ is the deviation from the constraints. $\xi_i$ is zero in cases of correct classification. To find the optimal hyperplane in the case of not linear separable data, $\min(\sum_{i=1}^{n} \xi_i)$ has

to be found additionally. An integrated function which solves the two minimization problems simultaneously is (Cortes & Vapnik 1995)

$$\min\left(\frac{1}{2}\|\boldsymbol{w}\| + C\sum_{i=1}^{n}\xi_i\right), \tag{2.11}$$

which is subjected to the constraint (2.10) and $C$ is a constant. The higher $C$ the more important is a correct classification and the lower $C$, the more wrong classifications are accepted during support vector estimation (Boswell 2002).

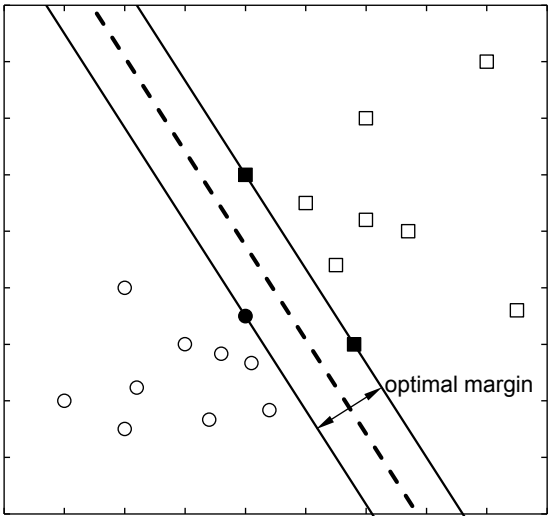


**Figure 2.2** Example of a classification problem in $\mathbb{R}^2$. Circles = class 1, squares = class 2, filled symbols = support vectors, dashed line = optimal hyperplane, solid lines = upper and lower border of widest separation margin. Modified from: Cortes & Vapnik (1995).

If the data set is not linear separable, having a significant number of wrong classifications, kernels can be used for nonlinear classification. The basic idea is to find a linear hyperplane in a higher dimensional space than $\mathbb{R}^d$ instead and to use this hyperplane in $\mathbb{R}^d$ as separation function. Then the hyperplane does not necessarily need to be linear in $\mathbb{R}^d$ anymore and it even does not need to be continuous. One can interpret this strategy also the other way around: $\boldsymbol{x}$ is transformed into the higher dimensional space via some basis function $\Phi(\boldsymbol{x})$ and becomes linear separable in its own dimensional space. Finding $\Phi(\boldsymbol{x})$ can require extensive computation resources (Boswell 2002). For simplification purposes and to avoid $\Phi(\boldsymbol{x})$, so called "kernel functions" in a dual form were introduced (Boswell 2002; Burges 1998; Cortes & Vapnik 1995):

$$K(\boldsymbol{x}_i, \boldsymbol{x}_j) = \Phi(\boldsymbol{x}_i) \cdot \Phi(\boldsymbol{x}_j) \tag{2.12}$$

Therefore the explosion of the number of parameters is impeded, implying manageable complexity and preventing from overfitting (Burges 1998). Two typically used kernels are the polynomial (Boswell 2002)

$$K(\boldsymbol{x}_i, \boldsymbol{x}_j) = (\boldsymbol{x}_i \cdot \boldsymbol{x}_j + 1)^p \tag{2.13}$$

and the Gaussian radial basis function kernel (Burges 1998)

$$K(\boldsymbol{x}_i, \boldsymbol{x}_j) = \exp\left(-\frac{\|\boldsymbol{x}_i \cdot \boldsymbol{x}_j\|^2}{2\sigma^2}\right) \tag{2.14}$$

where $p$ and $\sigma$ are adjustable parameters.

The SVM algorithm was realized in Matlab using the external provided routines *svmtrain.mexw32* and *svmpredict.mexw32*, which were built from the LIBSVM distribution (http://www.csie.ntu.edu.tw/~cjlin/libsvm/ [accessed April 9 2014]). The first file is used for the training data set and creates the SVM and the second file uses the SVM to predict the classes for the remaining data. The LOOCV validation procedure was used again, as described for RF (section 2.3.2.2). Eq. (2.14) was chosen as kernel function and the parameter values of $C$ and $\sigma$ were set to 10.0 and 0.18, respectively, based on a fourfold cross validation.

## 2.4. Measurement of leaf area index

In 2011, it became obvious that direct measurements of LAI in lettuce and kohlrabi are too laborious to achieve the necessary number of measurements during the field trials. For establishing a less labor and time intensive method of leaf area index measurement, an additional field trial was carried out. For details of the field trial layout see Sandmann et al. (2013).

They tested different non-destructive LAI estimation methods: digital photography from two different view zenith angles (0° and 57.5°) and the plant canopy analyzer LI-2200 with different cap views and measurement geometries (LICOR Bioscience USA 2011).

The reason for their choice of the view zenith angle at 57.5° is illustrated in Figure 2.3. The mean projection of unit foliage area ($G$) is shown for several view zenith angles ($\theta$) and mean leaf inclination angles ($\theta_l$) in Figure 2.3A. From Figure 2.3B it can be seen, that deviations from $G = 0.5$

are minimized for $\theta = 57.5°$. $G$-functions were calculated following the early proposal from Warren Wilson (1960):

$$G(\theta, \theta_l) = \frac{1}{360} \sum_{\phi=0}^{360} |\cos(\theta_l) \sin(\theta) - \sin(\theta_l) \cos(\theta) \cos(\phi)| , \quad (2.15)$$

where $\phi$ is azimuth angle.

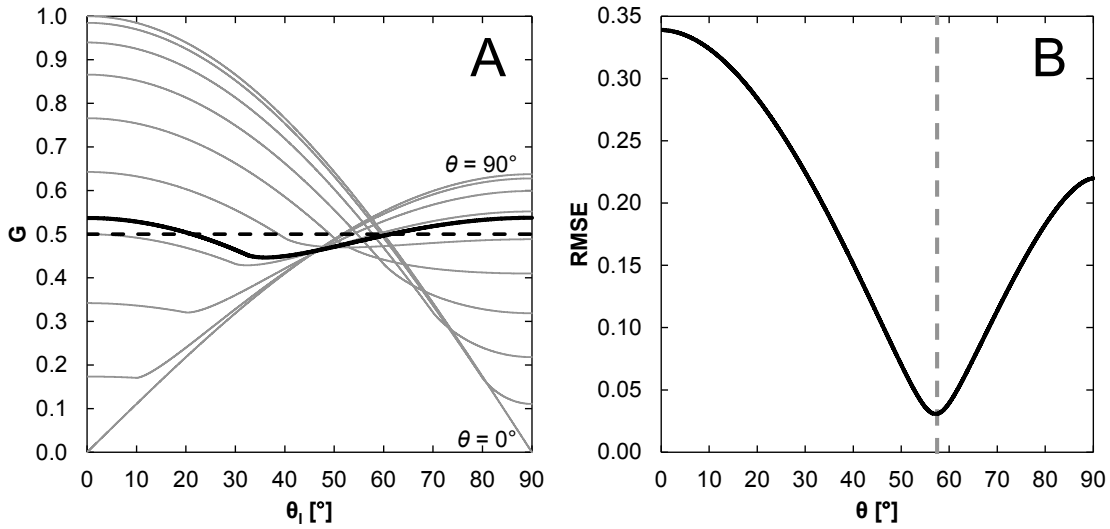


**Figure 2.3** (A) Mean projection of unit foliage area $G$ and view zenith angle $\theta$ against mean leaf inclination angle $\theta_l$. $\theta$ is varied from 0° to 90° in steps of 10° (grey lines). Solid black line: $\theta = 57.5°$, Dashed black line: $G(\theta_l) = 0.5$. (B) Root mean squared error from deviations of $G$ from 0.5 against view zenith angle. Dashed grey line is at $\theta = 57.5°$.

The simplification of setting $G = 0.5$ at $\theta = 57.5°$ therefore introduces only a negligible error in LAI computation. A comprehensive description of LAI computation using digital photography and LI-2200 is given by Sandmann et al. (2013). For validation of non-destructive estimations of LAI they performed additional destructive measurements as a reference.

## 2.5. Modeling microclimate and plant growth

For modeling microclimate and plant growth below plastic covers, whenever possible, already available and well-established approaches from the literature were used and in case of the non-availability of suited models, new models were developed. The group of established models and the corresponding parameter estimation procedure will be described in the following sections 2.5.1 to

2.5.4. Those models describe the volumetric soil water content following the approach from Durner (1994), soil water conductivity (Mualem 1976), soil thermal conductivity (Johansen 1975), stomata conductance (Ball et al. 1987), diffuse fraction of incident solar radiation (Erbs et al. 1982; Skartveit & Olseth 1987; Spitters et al. 1986), leaf angle distribution (Campbell 1990), clumping index (Pinty et al. 2006) and the extinction coefficient (Campbell 1986; Campbell 1990).

Own developed models will be described in the results and discussion chapter of this thesis in the sections 3.2.1 to 3.2.4. The wetness status and the surface morphology are described in section 3.3.2 and in Graefe & Sandmann (2014).

### 2.5.1. Soil water flow

The volumetric soil water content ($\theta_s$) and unsaturated soil water conductivity ($K$) are the most important characteristics to describe soil water flow, which is usually obtained from the solution of the Richards equation (Jury & Horton 2004). They are estimated for the two sites GR and GO and at three soil depths (0 to 15 $cm$, 15 to 30 $cm$ and 30 to 45 $cm$). Six undisturbed soil samples per site and depth were taken in a regular grid along the area of the field trials in 2012.

#### 2.5.1.1. Model functions

A classical approach to describe the relationship of $\theta_s$ and water tension ($h$) was proposed by van Genuchten (1980). But his assumption that there is only one maximum in the pore size distribution does not hold for all soil types. Durner (1994) therefore proposed a bimodal model, based on the van Genuchten model, which allows for two maxima in the pore size distribution. Multimodal extensions of this approach are possible (Durner 1994). Using the bimodal van Genuchten model, $\theta_s$ is then estimated from

$$\theta_s(h) = \left[\theta_{res} + (\theta_{sat} - \theta_{res})\left(\sum_{i=1}^{2} w_i \left(\frac{1}{1+(\alpha_i h)^{n_i}}\right)^{1-\frac{1}{n_i}}\right)\right] \tag{2.16}$$

where the parameters $\theta_{res}$ (residual water content), $\theta_{sat}$ (water content at saturation), $w_i$ (weights of the partial functions, where $\sum w_i = 1$), $\alpha_i$ (inverse value of the bubble point potential) and $n_i$ (pore size distribution) must be fitted and tension ($h$) is the input variable (UMS GmbH München 2012).

Typical values of $n_i$ are in the interval [1.17, 10.4] (Van Genuchten 1980). $n_i$ can be interpreted as a measure for the uniformity of pore sizes. An increased $n_i$ causes a steeper retention function which indicates a concentration of pore sizes around the maximum slope of $\theta_s(h)$. The estimation of $K$ is commonly done via the Mualem approach (Mualem 1976). All the previously mentioned parameters can be utilized for the estimation of $K$ as well, except $\theta_{res}$ and $\theta_{sat}$. Instead, the parameters $K_s$ (saturated conductivity) and $\tau$ (tortuosity) are implemented into the Mualem model:

$$K = K_s\left(\sum_{i=1}^{2} w_i[1+(\alpha_i h)^{n_i}]^{\frac{1}{n_i}-1}\right)^{\tau} \cdot \left(\frac{\sum_{i=1}^{2} w_i\alpha_i\left\{1-(\alpha_i h)^{n_i-1}[1+(\alpha_i h)^{n_i}]^{\frac{1}{n_i}-1}\right\}}{\sum_{i=1}^{2} w_i\alpha_i}\right)^{2}. \quad (2.17)$$

2.5.1.2. Parameterization with the ‘Hyprop’ system

The evaporation method (Peters & Durner 2008) was used to measure tension in dependency to $\theta_s$, which has the advantage of determining simultaneously the unsaturated water conductivity ($K$) over a relevant $\theta_s$ range. Undisturbed soil core samples (volume $V = 250\ cm^3$, height $z = 5\ cm$) taken at the center depth of each soil layer, were analyzed in the laboratory via the Hyprop system (**Hy**draulic **prop**erties) (UMS GmbH München 2012).

The first step of a Hyprop measurement is to saturate the soil sample with water. Then, the heads of two tensiometers are placed in the middle of the upper and the lower half of the soil sample (Figure 2.4). After these preparations, water can evaporate freely at the upper surface of the soil sample until the lower tensiometer reaches its operation limit. One additional measurement can be taken for the tension $8.5 \times 10^3\ hPa$, although this is far behind the operation limit of the tensiometers. Nevertheless, at this tension the “bubble-point” of the tensiometers is reached, where air is able to infiltrate the tensiometers. This certain tension is a known material constant of the Hyprop tensiometer heads (UMS GmbH München 2012). The observable characteristic of the “bubble-point” is the abrupt decrease of measured tension towards 0 $hPa$. During the evaporation process, tensions $h_1$ and $h_2$ in the heights $z_1 = 0.75z = 3.75\ cm$ and $z_2 = 0.25z = 1.25\ cm$ are measured in $10\ min$ intervals and the weight of the soil sample is measured twice a day. Between the measurements, the weight is linearly interpolated. At the end of the measurement, the sample is oven dried ($105°C$, $24\ h$) to obtain

the dry weight of the soil. Assuming that $\theta_s(\overline{h}) \approx \overline{\theta_s}(\overline{h})$, where $\overline{h}$ is the mean value of the measured tensions $h_1$ and $h_2$ and $\overline{\theta_s}$ is the mean volumetric water content of the soil sample, allows one to create data pairs of tension and volumetric water content. The assumption implies a linear increase of tension and a linear decrease of volumetric water content from bottom to top of the soil sample, which is not perfectly satisfied in reality. But the linearization error can be neglected as long as the measurement lasts at maximum a week (Peters & Durner 2008). Using the second assumption that half of the water flow $q$, which is evaporated, has its origin in the lower half of the soil sample, enables one to estimate $K(\overline{h})$ approximately via

$$K(\overline{h}) = \frac{0.5q}{\frac{\Delta h}{\Delta z} - 1} \tag{2.18}$$

where $\Delta h$ is the mean tension difference between two measurement intervals and $\Delta z$ is the difference between $z_1$ and $z_2$, which allows to create data pairs of tension and unsaturated soil water conductivity.

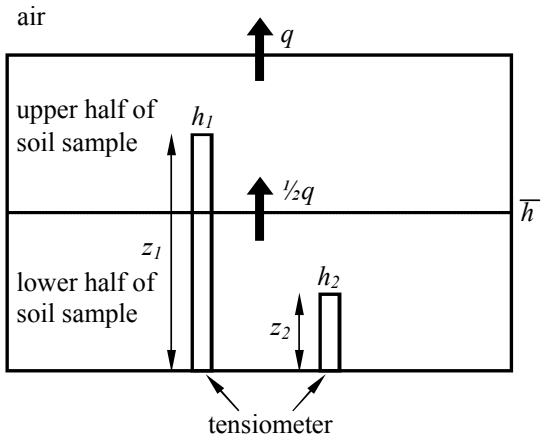


**Figure 2.4** Schematic of the Hyprop-system.

Parameter identification was performed using the Hyprop-Fit software (UMS GmbH München 2012). Comparisons of different models, which are commonly used, showed, that the described bimodal van Genuchten approach (van Genuchten (1980); Durner (1994)) ($\theta_s$) in combination with the Mualem approach (Mualem 1976) ($K$) fitted the data best.

### 2.5.2. Soil heat flow

To describe the soil heat flow via Fourier's law (Jury & Horton 2004), one necessary characteristic is the thermal conductivity of the soil ($\lambda$ [$W\,m^{-1}K^{-1}$]). Soil samples were taken from three soil depths (0-15 $cm$, 15-30 $cm$, 30-45 $cm$) and at the two sites GR and GO. There were two samples for every combination of site and soil depth, resulting in twelve samples.

#### 2.5.2.1. Model function

$\lambda$ was estimated by using the model from Johansen (1975) which was summarized by Lu (2007):

$$\lambda = (\lambda_s - \lambda_r) \cdot \left(\log_{10}\left(\frac{\theta_s}{\theta_{sat}}\right) + 1\right) + \lambda_r \tag{2.19}$$

where $\lambda_s$ is the thermal conductivity for a water saturated soil and $\lambda_r$ is thermal conductivity in a dry soil. $\lambda_s$ and $\lambda_r$ are to be parameterized and $\theta_s$ and $\theta_{sat}$ are input variables. Furthermore, the original proposal of Johansen (1975) includes a factor which distinguishes between fine- and coarse-textured soils and there are additional equations given for calculation of $\lambda_s$ and $\lambda_r$. These model expansions and also the more sophisticated proposal by Côté and Konrad and the proposal by Lu et al., which are described in Lu et al. (2007), did not lead to more precise predictions of $\lambda$ than the here adopted simplified Johansen-model.

#### 2.5.2.2. Parameterization with the Hukseflux TP01 sensor

Own data for parameterization of $\lambda_s$ and $\lambda_r$ in Eq. (2.19) were gained from measurements, with a heated thermopile (TP01 sensor, Hukseflux Thermal Sensors, Delft, NL), which was inserted in a cylindrical soil samples ring with a volume of 250 $cm^3$ and a height of 5 $cm$ (Figure 2.5). To enable insertion of TP01 from the side of the soil core, the cylinder wall was prepared at one side with a tiny slit which exceeded slightly the thermopile thickness. Each sample was water saturated at the beginning of the measurement procedure. Hourly measurements of thermal conductivity and cylinder weight were taken automatically over a broad water content range from about $\theta_{sat}$ to $\theta_{res}$, while the cylinder was allowed to evaporate freely at the upper side. One measurement of thermal conductivity lasted 180 $s$ where the internal heater is switched on. The subsequently applied heating power per

meter $Q = 0.8\,W/m$, results in an increase of soil temperature around the sensor of about $1\,K$ (Hukseflux Thermal Sensors 2003). The thermopile gives a voltage output before ($U_0$) and after ($U_{180}$) heating. Then $\lambda$ can be estimated from

$$\lambda = E_\lambda \frac{Q}{U_{180} - U_0} \tag{2.20}$$

where $E_\lambda$ is a sensor specific calibration factor.

After approaching an almost constant cylinder weight, the overall procedure was finished and the sample was dried at $105\,°C$ for 24 hours. From the difference between dry weight and saturated weight, the initial water content and the water content at sample times during the drying process were calculated.

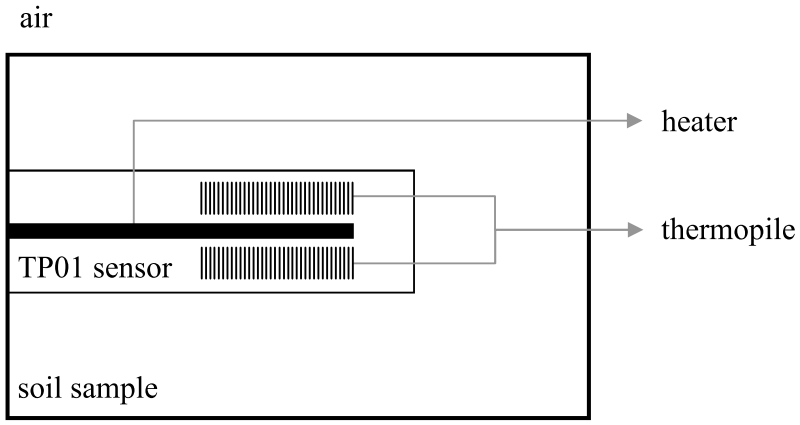


**Figure 2.5** Schematic of soil thermal conductivity measurements.

### 2.5.3. Ball-Berry-Leuning model of stomata conductance

For the estimation of stomata conductance ($g_{sc}$) data from the field trial carried out in GR in 2012 were used. A portable photosynthesis system (LI-6400 XT, LICOR Biosciences Inc., Nebraska, USA) was used to measure stomata conductance and several auxiliary variables in lettuce and kohlrabi grown under NWF or without cover. The semi-empirical model from Ball et al. (1987) with modifications proposed by Leuning (1995) was used for parameterization:

$$g_{sc} = g_0 + \frac{a_1 A}{(c_s - \Gamma) \cdot \left(1 + \frac{D_s}{D_0}\right)} \tag{2.21}$$

where $A$ is assimilation rate, $g_0$ is stomata conductance when there is no irradiation (which implies that $A$ is set to $\max(A, 0)$), $D_s$ is the air humidity deficit at the leaf surface, Γ is $CO_2$ compensation point, $c_s$ is $CO_2$ concentration at the leaf surface and $D_0$ and $a_1$ are empirical coefficients. $g_0$, $a_1$ and $D_0$ are fitting parameters and $A$, $c_s$ and $D_s$ are measured input variables. Γ was estimated from the measured leaf temperature via Farquhar et al. (1980):

$$\Gamma = \frac{\Gamma^* + K_c\left(1 + \frac{O}{K_o}\right)\frac{R_d}{V_{c_{max}}}}{1 - \frac{R_d}{V_{c_{max}}}} \tag{2.22}$$

where $K_c$ and $K_o$ are Michaelis-Menten constants for $CO_2$ and $O_2$, correspondingly, $O$ is the partial pressure of oxygen in the leaf air and is assumed to be $210\,mbar$, $R_d$ is the mitochondrial "dark respiration" which continues during leaf illumination, $V_{c_{max}}$ is maximum carboxylation rate and Γ* is $CO_2$ compensation point without dark respiration ($R_d$). The ratio $R_d/V_{c_{max}}$ was set to $0.01$. To account for the leaf temperature dependence of Γ*, $K_c$ and $K_o$ an estimation from Tenhunen et al. (1976) with the modifications from Bernacchi et al. (2001) was used:

$$\begin{aligned}
\Gamma^* &= \exp\left(c(\Gamma^*) - \frac{\Delta H_\alpha(\Gamma^*)}{R \cdot T_k}\right), \\
K_c &= \exp\left(c(K_c) - \frac{\Delta H_\alpha(K_c)}{R \cdot T_k}\right), \\
K_o &= \exp\left(c(K_o) - \frac{\Delta H_\alpha(K_o)}{R \cdot T_k}\right),
\end{aligned} \tag{2.23}$$

where $c$ and $\Delta H_\alpha$ are fitting parameters, $T_k$ is leaf temperature and $R$ is the molar gas constant ($= 0.0083145\ kJ\ K^{-1}\ mol^{-1}$). Preliminary tests with the function

$$f_w = \min\left(1.0, \frac{10(\theta_s - \theta_{min})}{3(\theta_{max} - \theta_{min})}\right) \tag{2.24}$$

as an additional factor into Eq. (2.21) to account for the sensitivity of stomata to soil water content ($\theta_s$, $\theta_{min}$ = water content at wilting point, $\theta_{max}$ = water content at field capacity) as proposed by Wang and Leuning (1998) did not lead to better results, indicating a rather optimal water supply during the field trial. Therefore, $f_w$ was not included into the model in this thesis. Parameters were fitted separately for each combination of species and cover material using the "lsqnonlin" function of the

MATLAB “optimization toolbox”, which solves nonlinear least squares problems via a subspace trust region method (The MathWorks Inc., USA).

### 2.5.4. Radiation transfer

The path of incident radiation through all flux participating surfaces as cover materials, canopy and soil surface and the nature of the interactions between all these surfaces and the incident radiation has to be known for modeling of the short wave radiation budget (see section 3.3.2). In this context the separation of diffuse and direct fractions of incident radiation, needs to be estimated, because those fractions can interact differently with the flux participating surfaces (Campbell & van Evert 1994). Different approaches are discussed in section 2.5.4.1. Afterwards, the methods of determination of optical properties of cover materials, leaves and soil surface are presented in section 2.5.4.2. The structure of the canopy has a strong influence on the fractions of transmitted, reflected and absorbed radiation, too. The main canopy structure features are the leaf angle distribution and the clumping factor. Furthermore, the extinction coefficient, which is an important measure for short wave transfer of canopies, is a function of leaf angle distribution. An explanation of these features and their mathematical definitions are given in section 2.5.4.3.

#### 2.5.4.1. Fractions of diffuse and direct short wave radiation

Due to the non-availability of separate data of incident direct ($I_0$) and diffuse ($I_0^d$) radiation above the covers (only the incident global radiation ($I_g$) was usually measured, which includes both diffuse and direct contributions), it is necessary to model these fractions from available variables. Those fractions are defined via

$$I_0^d = f^d \cdot I_g \text{ and}$$
$$I_0 = \left(1 - f^d\right) \cdot I_g \tag{2.25}$$

where $f^d$ is the relative diffuse fraction of $I_g$. In the literature, numerous models were proposed for this task, e.g. Dervishi and Mahdavi (2012) compared several approaches. Here, three of the most commonly utilized approaches (Spitters et al. (1986), Erbs et al. (1982) and Skartveit and Olseth (1987)) were tested, using measurements of $I_0^d$ from 20.03.2012 to 10.05.2012 at GR site for model

validation. The Spitters model is one of the most straightforward. It has only one input variable $k$, which is called the clearness index. $k$ is in the interval $[0, 1]$ and is the ratio of measured global radiation at the earth's surface and the instantaneous extraterrestrial radiation at the outer atmosphere. According to Spitters et al. (1986), $f^d$ is calculated via

$$f^d = \begin{cases} 1 & \text{if} \quad k < 0.07 \\ 1 - 2.3 \cdot (k - 0.07)^2 & \text{if} \quad 0.07 \leq k < 0.35 \\ 1.33 - 1.46k & \text{if} \quad 0.35 \leq k < 0.75 \\ 0.23 & \text{if} \quad 0.75 \leq k \end{cases}. \tag{2.26}$$

Erbs et al. (1982) departed the range of $k$ only into three intervals and proposed a fourth degree polynomial for the main interval of $k$ to determine $f^d$:

$$f^d = \begin{cases} 1 - 0.09k & \text{if} \quad k < 0.22 \\ 0.9511 - 0.1604k + 4.388k^2 - 16.638k^3 + 12.336k^4 & \text{if} \quad 0.22 \leq k < 0.80 \\ 0.165 & \text{if} \quad 0.80 \leq k \end{cases}. \tag{2.27}$$

The approach of Skartveit and Olseth (1987) is more sophisticated and was improved by the extensions of Dumortier for $\theta > 55°$ as reported in Hammer (2000). According to Skartveit and Olseth (1987), $f^d$ is estimated via

$$f^d = \begin{cases} 1 & \text{if} \quad k \leq 0.2 \\ 1 - (1 - d_{min})\left(a\sqrt{K} + (1 - a)K^2\right) \text{ where} & \\ \qquad K = 0.5\left(1 + \sin\left(\pi\left(\frac{k - 0.2}{k_1 - 0.2} - 0.5\right)\right)\right) & \text{if} \quad 0.2 < k \leq k_2 \\ 1 - k_2 \dfrac{1 - \left(1 - (1 - d_{min})\left(a\sqrt{K} + (1 - a)K^2\right)\right)}{k} \text{ where} & \\ \qquad K = 0.5\left(1 + \sin\left(\pi\left(\frac{k_2 - 0.2}{k_1 - 0.2} - 0.5\right)\right)\right) & \text{if} \quad k > k_2 \end{cases} \tag{2.28}$$

Some additional parameters need to be estimated for this model:

$$\begin{gathered} k_1 = \begin{cases} 0.82 - 0.51 \cdot \exp(-0.06 \cdot (90 - \theta)) & \text{if} \quad \theta > 55 \\ 0.87 - 0.56 \cdot \exp(-0.06 \cdot (90 - \theta)) & \text{if} \quad \theta \leq 55 \end{cases} \\ k_2 = 1.09 \cdot k_1 \\ d_{min} = \begin{cases} 0.12 + 0.46 \cdot \exp(-0.06 \cdot (90 - \theta)) & \text{if} \quad \theta > 55 \\ 0.15 + 0.43 \cdot \exp(-0.06 \cdot (90 - \theta)) & \text{if} \quad \theta \leq 55 \end{cases} \\ a = 0.27 \end{gathered} \tag{2.29}$$

where $k_1$ is the clearness index at $d_{min}$ which is the minimum diffuse fraction. $k_2$ and $a$ are additional parameters of the Skartveit approach. A comparison of all three models is shown in Figure 2.6.

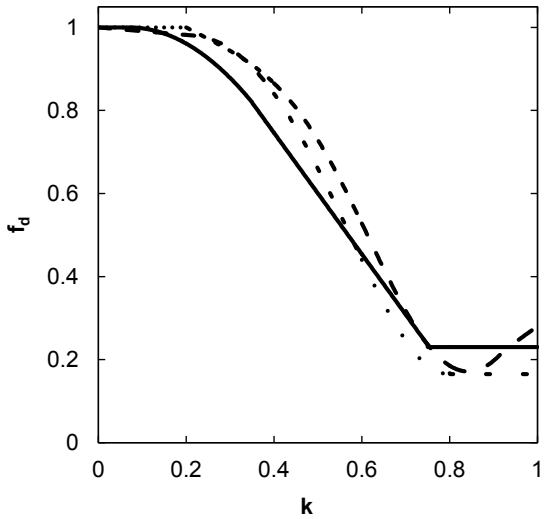


**Figure 2.6** Diffuse fraction ($f_d$) against clearness index ($k$) for three tested model approaches. Solid line = Spitters et al. (1986), dashed line = Erbs et al. (1982), dotted line = Skartveit and Olseth (1987).

### 2.5.4.2. Optical properties of flux participating surfaces

Measurements of the optical properties (transmittance $\tau$ and reflectance $\rho$) of cover materials, leaves and soil surface were done using a benchtop UV-VIS-NIR spectrometer (V-670, Jasco Corporation, Japan) with an Ulbricht-sphere ILN-725 accessory (internal diameter $15\ cm$). This device is able to measure directional-hemispherical reflectance and transmittance over the spectral range from $220\ nm$ to $2200\ nm$ with a resolution of $1\ nm$. Material samples have a size of about $2 \times 3\ cm$. Due to its small scale heterogeneity, 20 repetitions had to be made for every NWF sample. Only two repetitions were necessary for PF samples. For comparisons of dry and wet cover materials, only eight repetitions were made, where exactly the same spot of the material was taken for the measurement of reflectance and transmittance of NWF and FF. The double layer covers were wetted only on the NWF side because in the field the material is also wetted from this side whereas the surface of the PF is mostly dry due to free evaporation to the atmosphere.

Directional-directional light transmittance of cover materials ($\tau_{DIR}(\delta)$) was assessed at incidence angles ($\delta$) 0°, 30°, 45°, 60° and 75° using a variable angle transmittance accessory (VTA-752 film holder, Jasco, Japan) with the light polarisation angle set at 45°. Additional measurements of directional-hemispherical transmittance ($\tau(\delta)$) were taken using a smaller integrating sphere (internal diameter: $7.62\ cm$) with a red laser (peak wavelength $655\ nm$) at incidence angles 0°, 30°, 45°, 60°

and 70° and a UV-VIS-NIR diode array spectrometer (EPP 2000, StellarNet, USA). Possible substitution errors were estimated, and the corrections obtained were applied accordingly. The angular responses of $\tau_{DIR}(\delta)$ and $\tau(\delta)$ obtained were fitted with empirical functions for subsequent use. Both function fits were constrained to yield zero transmittance at $\delta = 90°$. Using an analogue setup, directional-hemispherical reflectance was measured with a laser incidence of 45°.

Leaf samples were repeated five times, where each repetition came from another plant of the same treatment. Reflectance and transmittance of leaves were measured at the adaxial side. Measurements on leaves were carried out weekly during the field trial in 2012 in GR.

Reflectance of the soil was measured via a non-stationary Ulbricht-sphere HISN-729 accessory for the V-670 system (spectral range from $250\ nm$ to $2000\ nm$). This was done for six soil samples from GR and GO sites in 2013. Soil samples were taken at $0-5\ cm$ soil depth in a cylinder with a volume of $250\ cm^3$. They were saturated with water and dried afterwards via free evaporation in the laboratory. Soil water content was estimated gravimetrically two to three times per day. After the end of spectral measurements the soil dry weight was estimated after oven drying at $105\ °C$ for $24\ h$. Spectral measurements were aborted after a visible color change of the soil surface was judged to be completed.

To obtain mean reflectance and transmittance values in the major wavelength ($\lambda$) bands of photosynthetic active radiation (PAR, $400-700\ nm$) and near-infrared radiation (NIR, $701-2200\ nm$), weighted means were calculated for all measurements using the Ulbricht-sphere. The spectral distribution of solar radiation (via Planck's distribution of blackbody spectral emissive power ($E$)) was used as weighting function:

$$E(\lambda, T) = \frac{C_1}{\lambda^5 \left(\exp\left(\frac{C_2}{\lambda \cdot T}\right) - 1\right)} \tag{2.30}$$

where $C_1$ and $C_2$ are the first and second radiation constants, respectively. $T$ is absolute temperature of the black body. In this case $T = 5800\ K$ is the absolute surface temperature of the sun (Figure 2.7). $C_1$ and $C_2$ can be determined with the following equations:

$$C_1 = 2 \cdot \pi \cdot h \cdot c_0^2 = 3.742 \cdot 10^8 \, W \, \mu m^4 m^{-2} \tag{2.31}$$

$$C_2 = \frac{h \cdot c_0}{k} = 1.439 \cdot 10^4 \, \mu m K \tag{2.32}$$

where $h = 6.6256 \cdot 10^{-34} \, Js$ is universal Planck constant, $c_0 = 2.998 \cdot 10^8 \, ms^{-1}$ is speed of light in vacuum and $k = 1.3805 \cdot 10^{-23} \, JK^{-1}$ is Boltzmann constant (Incropera & DeWitt 2002).

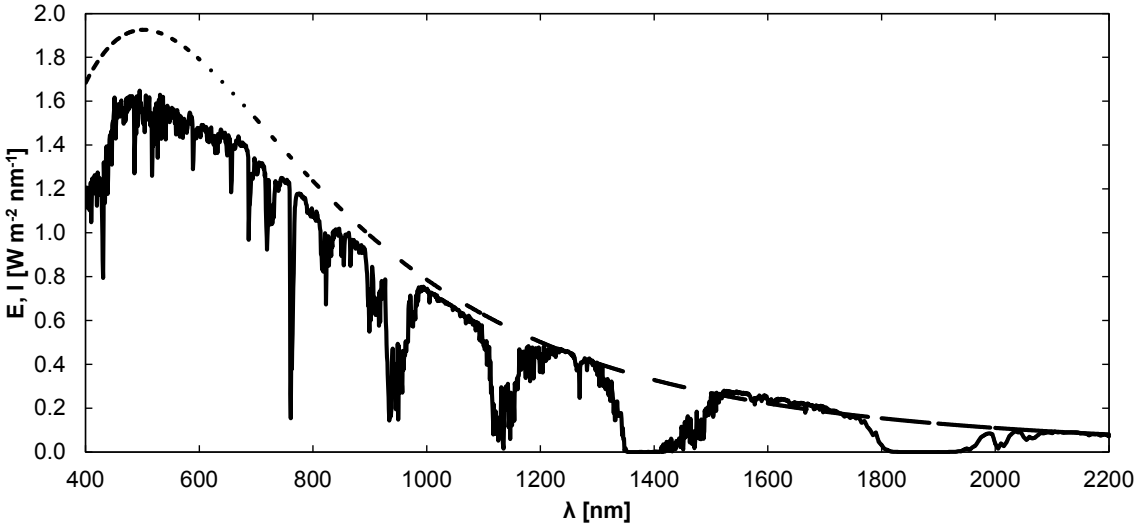


**Figure 2.7** Planck's distribution ($E$, dashed line) and the global radiation ($I$, solid line) against wavelength ($\lambda$). The Planck distribution is based on the surface temperature of the sun $T = 5800 \, K$ as the radiation source. The global radiation spectrum is provided by the American Society for Testing and Materials (ASTM) as a terrestrial reference spectrum for photovoltaic performance evaluation (http://rredc.nrel.gov/solar/spectra/am1.5/ ASTMG173.html [accessed March 20 2014]).

Weighted means based on the Planck distribution were also compared to weighted means based on a global radiation spectrum. The chosen spectrum is provided by the American Society for Testing and Materials (ASTM) as a terrestrial reference spectrum for photovoltaic performance evaluation and was modelled under the following conditions: 37° north (latitude on earth's surface) and $\theta = 48.19°$ (solar zenith angle) (http://rredc.nrel.gov/solar/spectra/am1.5/#1962 [accessed March 20 2014]). The comparison yielded no significant differences of the mean values, which might be explained by the influence of water, which absorbs mainly radiation at the same wavelengths in the atmosphere and in the tested flux participating surfaces, e.g. around $1400 \, nm$ and $1900 \, nm$. It is not important whether the weights have small values at these wavelengths or the measured reflectance or transmittance – the result is very similar. Due to the easier handling of the Planck distribution, Eq. (2.30) was preferred as weight function.

2.5.4.3. Leaf angle distribution function, clumping factor and extinction coefficient

The leaf angle distribution function is important for canopy radiation transfer calculations because the extinction coefficient ($K$) and mean projection of unit foliage area ($G$) are depending on the angle between incident radiation and leaf surface. The leaf angle distribution is often approximated by the distribution of the surface angles on a sphere (Campbell 1986) or on an ellipsoid. Campbell (1990) proposed a leaf angle density function $g$ which can describe all distributions from homogeneous horizontal to homogenous vertical leaves in the canopy, including spherical and ellipsoidal distributions. One advantage of this function is, that only one parameter ($x$) is necessary:

$$g(\alpha, x) = \frac{2x^3 \sin\alpha}{(x + 1.744(x + 1.182)^{-0.733})(\cos^2\alpha + x^2 \sin^2\alpha)^2} \tag{2.33}$$

where $\alpha$ is the leaf inclination angle. $x$ can be interpret as the ratio of vertical to horizontal projections of canopy elements (Campbell 1990) and its codomain reaches from $x = 0$ (vertical leaves only) over $x = 1$ (spherical distribution) to $x \to \infty$ (horizontal distribution). The parameter $x$ for kohlrabi was measured via the LAI-2200 plant canopy analyzer. For lettuce $x = 1$ was assumed.

Regarding radiation transfer calculations and indirect LAI measurements, an important characteristic of canopy structure is the clumping index $\Omega$. Possible values of $\Omega$ can be in the interval [0, 1], where 1 stands for no clumping and values $< 1$ mean that there is clumping. Clumping occurs if canopy elements are not randomly distributed in space, e.g. normally there are canopy structures like branches and in the space around them the leaves are concentrated (or *clumped*). It should be noted, that canopies with a quite regular or systematic leaf display are over-dispersed ($\Omega$ >1). Clumping falsifies the indirect measured LAI usually by underestimation, also indicated as effective LAI ($LAI_{eff}$). $\Omega$ is depending on $\theta$ (Kucharik et al. 1999). One useful approach to describe this relationship was proposed by Pinty et al. (2006)

$$\Omega(\theta) = q_1 + q_2 \cdot (1 - \cos(\theta)) \tag{2.34}$$

where $q_1$ and $q_2$ are two fitting parameters. From the indirect LAI measurements via digital photography at $\theta = 0°$ and $\theta = 57.5°$ and parallel performed direct LAI measurements (Sandmann et al. 2013), $\Omega_0$ and $\Omega_{57.5}$ are known. The parameters $q_1$ and $q_2$ can now be obtained by (Graefe & Sandmann 2014)

$$q_1 = \min(\Omega_0, \Omega_{57.5}) \tag{2.35}$$

and

$$q_2 = \frac{\Omega_{57.5} - q_1}{1 - \cos(57.5)}. \tag{2.36}$$

A third structural characteristic of canopies is the extinction coefficient $K$. Campbell (1986) defined $K$ as the average projection of leaves on to a horizontal surface. He proposed also a model for estimation of $K$ in dependence of $\theta$ and $x$. In this thesis a modified version given by Campbell (1990) was used:

$$K(\theta, x) = \frac{\sqrt{x^2 + \tan^2\theta}\cos(\theta)}{x + 1.774(x + 1.182)^{-0.733}}. \tag{2.37}$$

# 3. Results and Discussion

## 3.1. Leaf area index measurement methods

Sandmann et al. (2013) show that non-destructive estimation of LAI in lettuce and kohlrabi can be realized with sufficient precision. Their linear regressions between non-destructively and destructively measured LAI revealed high coefficients of determination ($R^2_{adj} > 0.95$). They recommend digital images of the canopy taken from a zenith angle of $57.5°$ because this is easy to realize in the field (fast, few equipment necessary, independent of sky conditions) and post processing on a computer can be widely automatized.

In Sandmann et al. (2013) the leaf area meter LI-3100 (LICOR Bioscience USA 1996) is used for the majority of destructive measurements of LAI. They do not mention the precision of this device, which produced their reference data. Therefore the precision of LI-3100 was tested in an additional trial, to legitimize this version of direct LAI measurements (Figure 3.1). Six different rectangles with known areas ($25$, $50$, $75$, $100$, $150$ and $200\,cm^2$) were measured thirty times each, using the LI-3100. Additionally, a $50\,cm^2$ calibration disk was used. The mean relative error over all $180$ measurements was $1.8\,\%$. This is higher than the value mentioned in the manual, which is $1\,\%$ (LICOR Bioscience USA 2011). But the observed value is still small enough to be sufficient. The increased difference between the test area size $75\,cm^2$ and LI-3100 measurement might result from the elongated shape of the test area ($5\,cm \times 15\,cm$).

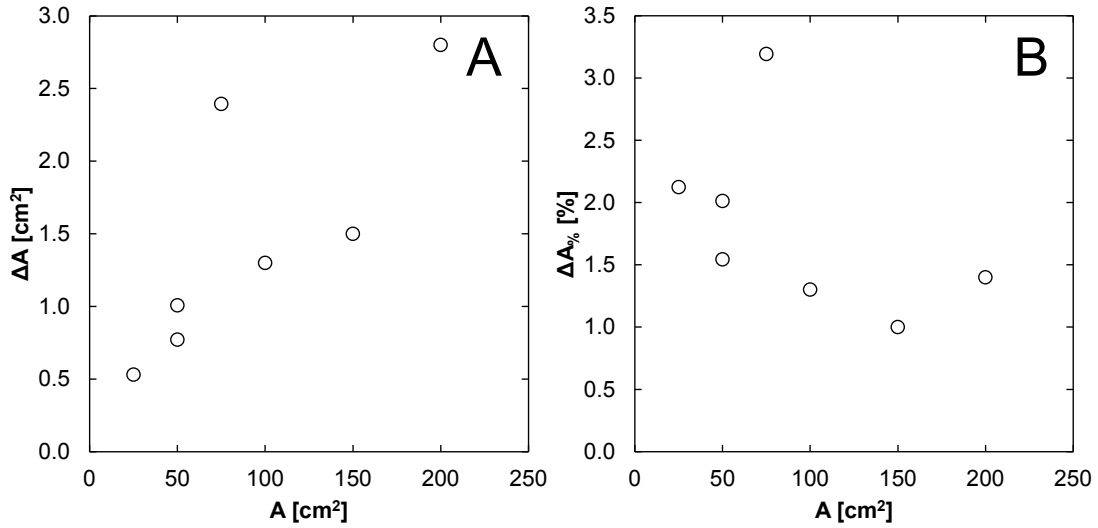


**Figure 3.1** Results from the test of the precision of the leaf area meter LI-3100 (LICOR Bioscience USA 1996). (A) Absolute difference of LI-3100 measurements and test area size ($\Delta A$) against test area size ($A$). (B) Relative difference of LI-3100 measurements and test area size ($\Delta A_{\%}$) against test area size ($A$).

## 3.2. Parameterization and test of established submodels

Soil water flow, soil thermal conductivity, stomata conductance and radiation transfer models, which are established in the literature and explained in section 2.5, will be parameterized for the special conditions of the present production system (section 1.1.1) in the following sections.

### 3.2.1. Parameters describing soil water flow

The results from measurements and model parameterizations of the main soil water flow describing characteristics are given in the following two sections. Those soil characteristics are soil water retention and unsaturated hydraulic conductivity and they are discussed for two sites and three soil depths.

#### 3.2.1.1. Soil water retention

Results of the parameter fitting for volumetric soil water content are given in Table 3.1. For three soil depths on both sites seven parameters had to be fitted to Eq. (2.16), respectively. The parameter $w_1$ (weight of the first partial function) is not given in Table 3.1. But it can be calculated easily via $w_1 = 1 - w_2$. All parameter-values are significantly different from zero, except the residual water content ($\theta_{res}$) in GR ($\alpha = 0.05$) which is still reasonable. The resulting retention curves are presented in

Figure 3.2. Especially the two soil layers from 0 to 15 $cm$ and from 15 to 30 $cm$ in GO show a pronounced dint in the area around $pF = 3$. $pF$ is defined as the decadic logarithm of the water tension ($h$): $pF = \log_{10}(h)$ (Blume et al. 2002). This is an indication for a bimodal pore size distribution of the soil. Residual water content ($\theta_{res}$) and saturated water content ($\theta_{sat}$) are smaller in the GR soil than in the GO soil and the water retention curves from GO are less steep than those from GR. This is in accordance with results from other studies which compared soils with different grain size distributions (Minasny et al. 1999; Peters & Durner 2008). Additionally the mean bulk density ($\rho_b$) of the soil was computed (Table 3.1). It increases with increasing soil depth at both sites, whereas $\rho_b$ is smaller in GO than in GR. The smaller $\rho_b$ at GO site is caused by the higher porosity of clay compared to sand (Blume et al. 2002). As described in section 2.1.2. there is a different particle size distribution in GO and GB resulting in different porosities.

**Table 3.1** Results from the volumetric soil water content parameterization ($n = 6$ soilsamples with $\approx 100$ measurements per soilsample). Additional the mean bulk density ($\rho_b$) is listed. GR = Großbeeren, GO = Golzow, [a] = not significant different from zero ($\alpha = 0.05$).

| Site | Depth [$cm$] | $\alpha_1$ | $n_1$ | $\theta_{res}$ | $\theta_{sat}$ | $\alpha_2$ | $n_2$ | $w_2$ | $\rho_b$ [$g/cm^3$] |
|---|---|---|---|---|---|---|---|---|---|
| GR | 0 to 15 | 0.0208 | 2.662 | 0.000[a] | 0.339 | 0.0553 | 1.137 | 0.501 | 1.497 |
| GR | 15 to 30 | 0.0240 | 12.800 | 0.022[a] | 0.346 | 0.0083 | 1.674 | 0.731 | 1.567 |
| GR | 30 to 45 | 0.0146 | 6.655 | 0.000[a] | 0.326 | 0.0772 | 1.254 | 0.722 | 1.690 |
| GO | 0 to 15 | 0.2445 | 1.424 | 0.228 | 0.509 | 0.0004 | 8.000 | 0.248 | 1.387 |
| GO | 15 to 30 | 0.1327 | 1.608 | 0.246 | 0.467 | 0.0004 | 8.000 | 0.368 | 1.398 |
| GO | 30 to 45 | 0.0371 | 2.115 | 0.208 | 0.413 | 0.0015 | 3.000 | 0.585 | 1.457 |

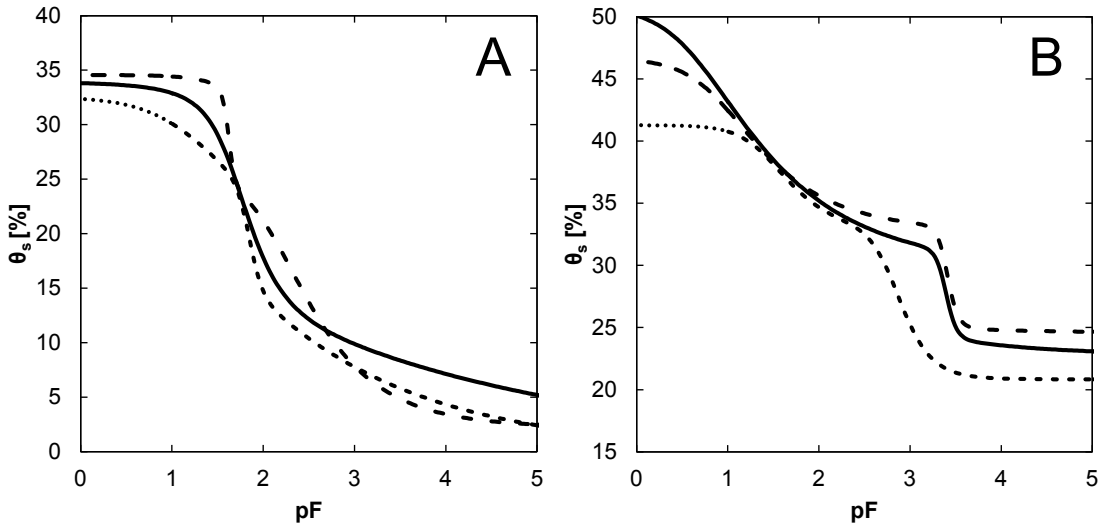


**Figure 3.2** Soil water content ($\theta_s$) against $pF = \log_{10}(h)$ for Großbeeren (A) and Golzow (B). Solid line = 0 to 15 $cm$ soil depth, dashed line = 15 to 30 $cm$ soil depth, dotted line = 30 to 45 $cm$ soil depth.

### 3.2.1.2. Unsaturated hydraulic conductivity

The two additional parameters, $\tau$ and $K_s$, for modeling the unsaturated hydraulic conductivity (Eq. (2.17)) are listed in Table 3.2. All parameters are significantly different from zero ($\alpha = 0.05$). $K_s$ is much higher in the upper two soil layer in GO than in GR. However, the opposite was observed for the lowest soil layer.

**Table 3.2** Results from the model parameterization of unsaturated hydraulic conductivity ($n = 6$ soilsamples with ≈ 100 measurements per soilsample). GR = Großbeeren, GO = Golzow.

| Site | Depth [$cm$] | $\tau[-]$ | $K_s$ [$cm\,d^{-1}$] |
|---|---|---|---|
| GR | 0 to 15 | -4.632 | 3.451 |
| GR | 15 to 30 | -1.671 | 1.679 |
| GR | 30 to 45 | -1.322 | 70.985 |
| GO | 0 to 15 | -2.797 | 75.255 |
| GO | 15 to 30 | -2.220 | 25.460 |
| GO | 30 to 45 | -2.155 | 0.323 |

Analogously to the volumetric soil water content, an indication for a bimodal pore size distribution of the soil can be observed in the two soil layers from 0 to 15 $cm$ and from 15 to 30 $cm$ in GO, as they show dints in the area around $pF = 3$ (Figure 3.3). Those two soil layers in GO also reach higher $\log_{10} K$ for $pF < 1$.

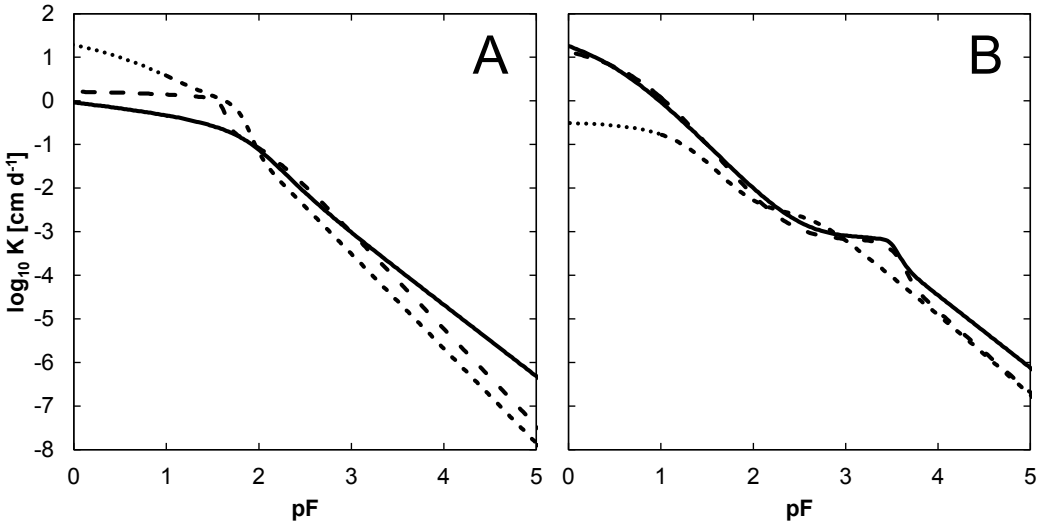


**Figure 3.3** Decadic logarithm of unsaturated hydraulic conductivity ($K$) against $pF$ for Großbeeren (A) and Golzow (B). Solid line = 0 to 15 $cm$ soil depth, dashed line = 15 to 30 $cm$ soil depth, dotted line = 30 to 45 $cm$ soil depth.

### 3.2.2. Soil thermal conductivity

Parameter estimates of thermal conductance function ($\lambda$, Eq. (2.19)) of the soil are summed up in Table 3.3. The resulting conductivity curves for a water content range from zero to $\theta_{sat}$ are given in Figure 3.4. These results are in good accordance with published works for sandy and loamy soils (Lu et al. 2007; Tarnawski et al. 2009). It can be seen, that $\lambda$ tends to increase with increasing soil depth. An explanation might be the increasing bulk density ($\rho_b$) with increasing soil depth (Table 3.1). In Figure 3.5, the comparison of measured and estimated thermal conductance for all soil depths and sites is shown ($R^2 = 0.959$, $n = 2245$). In general, there is a good performance although the relatively simple model of Johansen (1975) was applied.

**Table 3.3** Results from the soil thermal conductivity parameterization. GR = Großbeeren, GO = Golzow.

| Site | Depth $[cm]$ | $\lambda_s$ $[W\ m^{-1}\ K^{-1}]$ | $\lambda_r$ $[W\ m^{-1}\ K^{-1}]$ | $R^2$ |
|---|---|---|---|---|
| GR | 0 to 15 | 1.94721 | 0.92879 | 0.9526 |
| GR | 15 to 30 | 2.07214 | 0.94423 | 0.9556 |
| GR | 30 to 45 | 2.24738 | 1.15558 | 0.9249 |
| GO | 0 to 15 | 1.38588 | 0.29762 | 0.7768 |
| GO | 15 to 30 | 1.44028 | 0.65465 | 0.9161 |
| GO | 30 to 45 | 1.59841 | 0.36541 | 0.9954 |

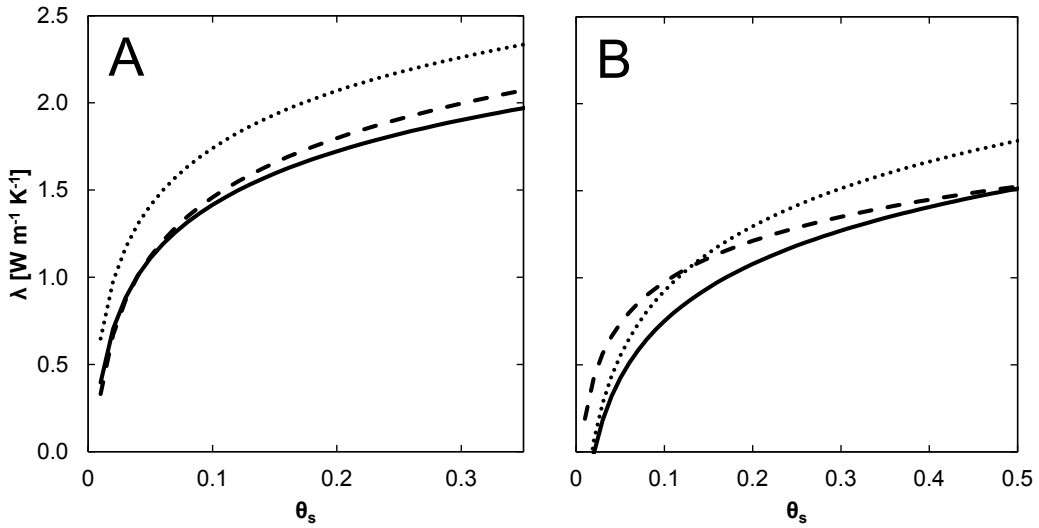


**Figure 3.4** Thermal conductivity of the soil ($\lambda$) against volumetric soil water content ($\theta_s$) for Großbeeren (A) and Golzow (B). Solid line = 0 to 15 $cm$ soil depth, dashed line = 15 to 30 $cm$ soil depth, dotted line = 30 to 45 $cm$ soil depth.

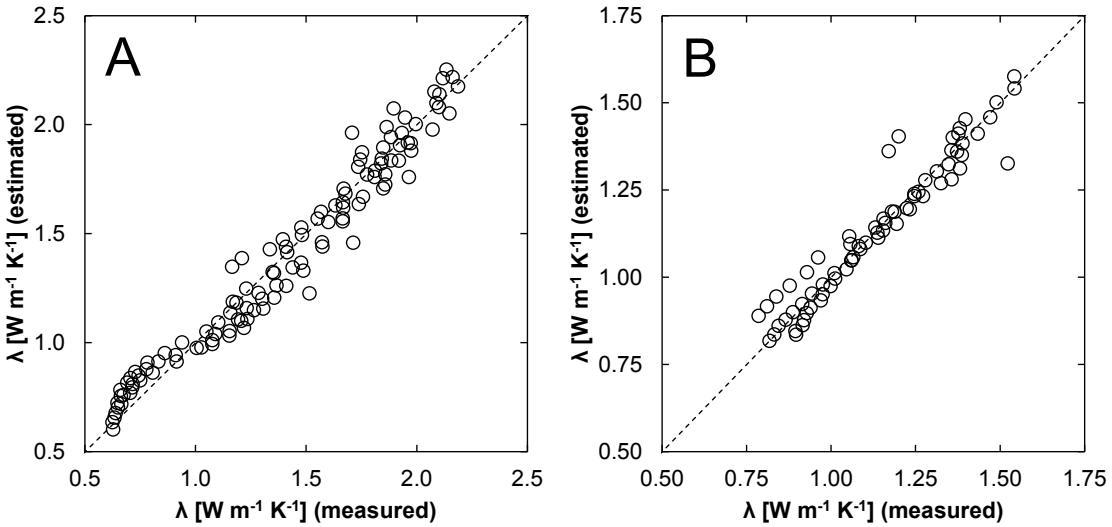


**Figure 3.5** Estimated against measured thermal conductivity of the soil ($\lambda$) for Großbeeren (A) and Golzow (B). For the purpose of clarity ($n = 2245$), only two values per day are plotted (noon and midnight). Dashed line = 1:1.

### 3.2.3. Ball-Berry-Leuning model of stomata conductance

The used parameters for describing temperature dependence of Γ are given by Bernacchi et al. (2001) and presented in Table 3.4.

**Table 3.4** Parameters ($c$ and $\Delta H_\alpha$) describing temperature dependence of the $CO_2$ compensation point. $\Gamma^*$ = $CO_2$ compensation point without dark respiration, $K_c$ = Michaelis-Menten constant for $CO_2$, $K_o$ = Michaelis-Menten constant for $O_2$ (Bernacchi et al. 2001).

| Parameter | $c$ | $\Delta H_\alpha$ |
|---|---|---|
| $\Gamma^*$ | 19.02 | 37.83 |
| $K_c$ | 38.05 | 79.43 |
| $K_o$ | 20.30 | 36.38 |

All results from the parameter identification are given in Table 3.5. $R^2$ values for the comparisons of estimated and measured conductance (Figure 3.7) range between 0.7 and 0.9 (Table 3.5). $g_0$ is negative or not significantly different from zero for all four treatments ($\alpha = 0.05$). This could be a special attribute of the observed species but it is in accordance with results from other species (Leuning 1995). $D_0$ and $a_1$ are significant different from zero in all investigated cases ($\alpha = 0.05$).

**Table 3.5** Results from the stomata conductance parameterization. NWF = non-woven fabric.

| Species | Cover material | Fitted parameter | Parameter value | Confidence lower limit | Confidence upper limit | P value | $R^2$ |
|---|---|---|---|---|---|---|---|
| lettuce | none | $g_0$ | -0.0005 | -0.0107 | 0.0097 | 0.9206 | 0.7059 |
| lettuce | none | $a_1$ | 4.1366 | 3.2543 | 5.0188 | <0.0001 | |
| lettuce | none | $D_0$ | 2228.9300 | 798.3611 | 3659.4989 | 0.0026 | |
| lettuce | NWF | $g_0$ | -0.1495 | -0.2091 | -0.0899 | <0.0001 | 0.8811 |
| lettuce | NWF | $a_1$ | 63.3413 | 28.6631 | 98.0195 | 0.0006 | |
| lettuce | NWF | $D_0$ | 211.2983 | 25.6683 | 396.9282 | 0.0265 | |
| kohlrabi | none | $g_0$ | -0.0168 | -0.0380 | 0.0044 | 0.1170 | 0.8784 |
| kohlrabi | none | $a_1$ | 6.5314 | 5.4595 | 7.6034 | <0.0001 | |
| kohlrabi | none | $D_0$ | 1253.1872 | 776.7729 | 1729.6014 | <0.0001 | |
| kohlrabi | NWF | $g_0$ | -0.0816 | -0.1413 | -0.0220 | 0.0084 | 0.7174 |
| kohlrabi | NWF | $a_1$ | 10.0532 | 7.3513 | 12.7552 | <0.0001 | |
| kohlrabi | NWF | $D_0$ | 1794.7538 | 567.4100 | 3022.0975 | 0.0051 | |

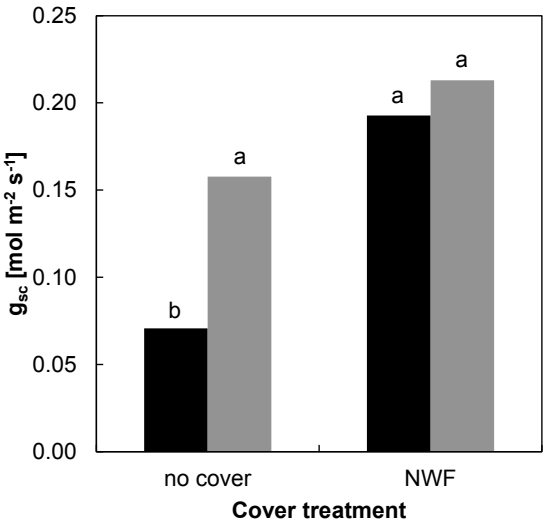


**Figure 3.6** Measured stomata conductance ($g_{sc}$) against cover treatments for lettuce (black) and kohlrabi (grey). NWF = non-woven fabric. Least squares means are presented.

An analysis of variance via the MIXED procedure of SAS 9.2 with two fixed factors (species and cover treatment) revealed a significant interaction of the two factors (F-test, $p = 0.0388$). Consequently, only comparisons between factor combinations are possible. Using the differences of least squares means and the Tukey-Kramer adjustment for multiple testing (Kramer 1956), two homogeneous groups can be identified (Figure 3.6). Only lettuce, grown without cover, has significantly smaller $g_{sc}$ than all other factor combinations. Although not significant, some tendencies can be observed: Kohlrabi has higher $g_{sc}$ than lettuce and plants, grown under NWF, have higher $g_{sc}$ than those grown without cover, whereas the difference of $g_{sc}$ between the cover treatments is higher for lettuce than for kohlrabi.

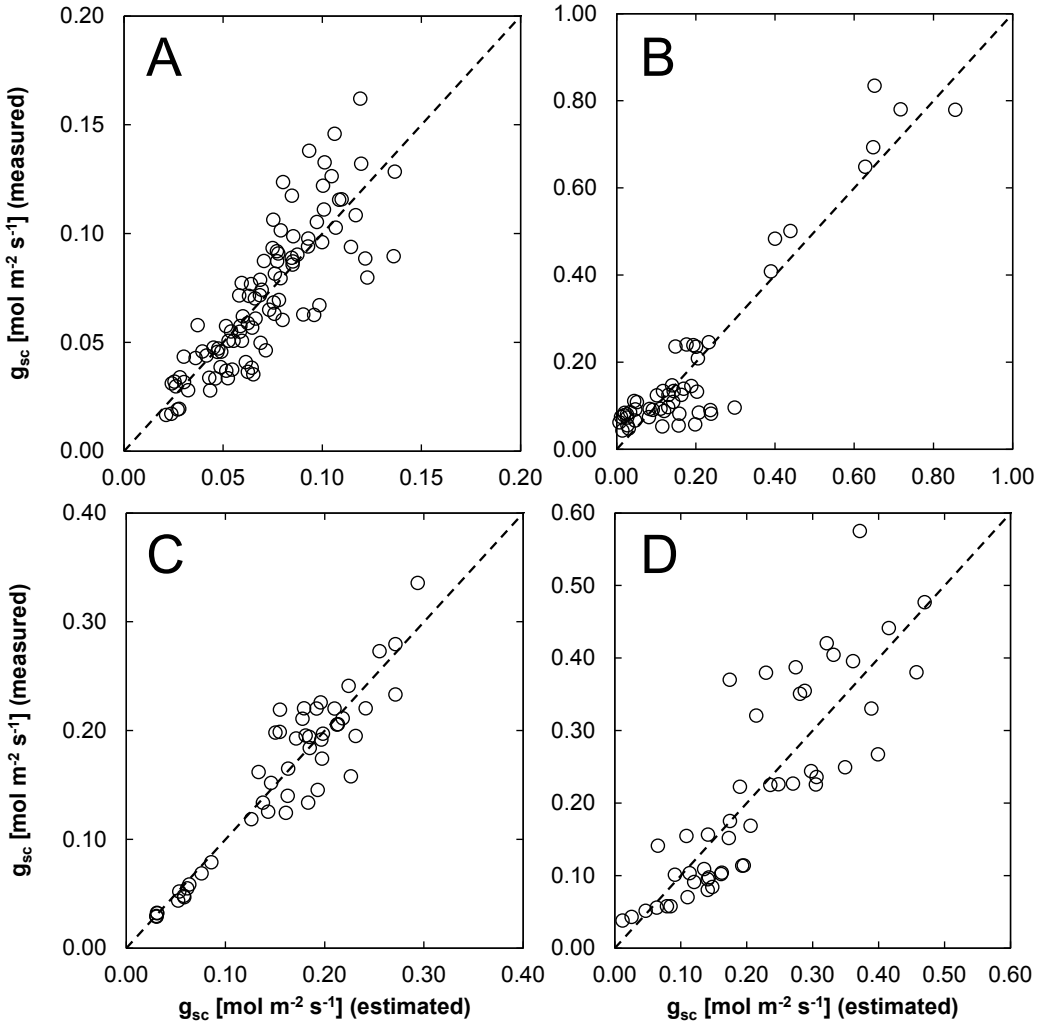


**Figure 3.7** Measured against estimated stomata conductance ($g_{sc}$). Dashed line = 1:1. A = lettuce without cover ($n = 96$), B = lettuce under non-woven fabric ($n = 52$), C = kohlrabi without cover ($n = 48$), D = kohlrabi under non-woven fabric ($n = 48$).

### 3.2.4. Radiation transfer

In the following sections (1) the comparison of the diffuse fraction models, which were described in section 2.5.4.1, using own data is performed and (2) based on the results, the decision, which one of the approaches will be used in the short wave radiation budget model, will be made. Afterwards, the optical properties of cover materials, leaves and soil surface will be discussed in detail for different conditions and wavelength ranges. Finally, the determined leaf angle distribution, clumping index and extinction coefficient are presented.

3.2.4.1. Test of the diffuse fraction models

A validation data set of $I_0^d$ was collected from 20.03.2012 to 10.05.2012 at Großbeeren site and it consists of 2436 measurements (see section 2.1.3.1). The modelled values of the three tested models (SP = Spitters et al. (1986) (Eq. (2.26)), ER = Erbs et al. (1982) (Eq. (2.27)), SK = Skartveit and Olseth (1987) (Eq. (2.28) and Eq. (2.29))) were compared to the measurements using linear regression analysis (Table 3.6).

**Table 3.6** Results of linear regression analysis between modelled (independent variable) and measured (dependent variable) values of diffuse PAR for three model approaches. Measurements were taken from 20.03.2012 to 10.05.2012 at Großbeeren site ($n = 2436$, $\alpha = 0.05$, CL = confidence limits, SE = standard error, SP = Spitters et al. (1986), ER = Erbs et al. (1982), SK = Skartveit and Olseth (1987)).

| Model | SP | ER | SK |
|---|---|---|---|
| $RMSE$ | 19.7911 | 21.8527 | 22.8771 |
| $R^2_{adj}$ | 0.8369 | 0.8131 | 0.8156 |
| Intercept | 5.7643 | 5.5315 | 3.8563 |
| CL intercept | [4.7520; 6.7767] | [4.4137; 6.6493] | [2.6861; 5.0265] |
| SE intercept | 0.5132 | 0.5700 | 0.5967 |
| Slope | 0.8932 | 0.9081 | 0.9585 |
| CL slope | [0.8775; 0.9088] | [0.8908; 0.9254] | [0.9404; 0.9766] |
| SE slope | 0.0080 | 0.0088 | 0.0092 |

$RMSE$ is lowest and $R^2_{adj}$ is highest for SP. However, ER and SK have higher $RMSE$ and lower $R^2_{adj}$ values than SP but those two approaches show almost a similar model performance according to the validation data set (Table 3.6). For all approaches, intercept and slope are significant different from 0 and 1, correspondingly, as indicated by the 95 % confidence limits in Table 3.6. Therefore, the SP model was further used with the calibration $I_o^d = 0.8932 I_{0SP}^d + 5.7643$, where $I_{0SP}^d$ is the originally modelled value from the SP approach.

Afterwards a correction of $f^d$ which is accounting for circumsolar fraction after Hay (1979) was included to the SP approach via

$$f^d(corrected) = f^d(uncorrected)\left(1 - \left(k\left(1 - f^d(uncorrected)\right)\right)\right), \qquad (3.1)$$

where $k$ is the clearness index and $f^d(corrected)$ will be used for further calculations and it will be denoted as $f^d$.

#### 3.2.4.2. Optical properties of flux participating surfaces

In the following three sections, the results of measurements of the optical properties reflectance $\rho$ and transmittance $\tau$ of each flux participating surface (covers, leaves and soil) are presented. Each surface is regarded separately. Generalization from leaf to canopy and consideration of multiple interactions between the flux participating surfaces are made in section 3.3.2, where selected aspects of a new short wave radiation budget model approach by Graefe & Sandmann (2014) are presented. The results discussed in the following three sections are the foundation of the new radiation model.

##### 3.2.4.2.1. *Covers*

In the beginning of this section the results from directional-hemispherical measurements of reflectance and transmittance are discussed, where the incidence angle was $\delta = 5°$ and covers were hold plane during measurements. Afterwards the incidence angle dependent direct transmittance $\tau_{DIR}(\delta)$ (directional-directional) of NWF and FF is presented, whereas the incidence angle dependent diffuse transmittance $\tau(\delta)$ (directional-hemispherical) will be discussed in conjunction with the short wave radiation budget model in section 3.3.2.

Directional-hemispherical reflectance and transmittance depend on several factors. One is the material, which reflects and transmits only certain amounts of radiation – even if unused; another influencing factor is the usage duration or cover material age. Mainly due to accumulating dirt and incrustation of algae during the plant growth period reflectance and transmittance characteristics are changing. A further reason for this effect might be changes in the chemical structure of the material in time due to the influence of solar radiation, particularly the radiation in the UV wavelength band. As Figure 3.8 shows, these changes can be found for different cover materials. Reflectance of NWF and PF increases with usage duration, whereas this effect is much stronger for NWF than for PF (Figure 3.8A). The increase of reflectance can be observed over the whole wavelength band range of the measurements. Reflectance of PF is monotonic decreasing with increasing wavelength and reflectance of NWF is increasing in the UV wavelength band and in the visible and NIR wavelength band it is nearly constant. Changes of reflectance with time occur mainly for wavelengths $> 400\,nm$. Absolute values of reflectance are higher for NWF than for PF. Transmittance shows almost the inverse behavior

(Figure 3.8B). It is decreasing with increasing wavelength for PF. But for NWF this behavior changes from decreasing to constant transmittance with increasing usage duration. As expected, transmittance is lower for used than for new cover materials. For the better part of the measured wavelength range, transmittance of PF is higher than of NWF. One exception is the interval of wavelength below $600\ nm$. The absolute values of transmittance of new PF (Figure 3.8B) are in good agreement with early results from Heissner (1965), who found $\tau = 90.8$ % for polyethylene film (thickness 60 $\mu m$) at nadir incidence.

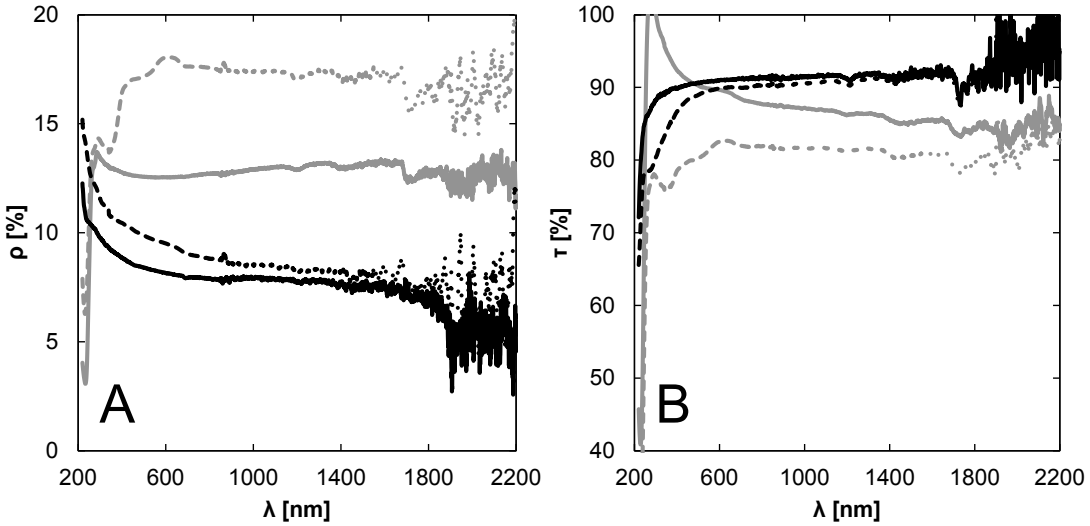


**Figure 3.8** Directional-hemispherical reflectance $\rho$ (A) and transmittance $\tau$ (B) for new and used cover materials against wavelength $\lambda$. Grey = non-woven fabric ($19\ g/m^2$), black = perforated film, solid lines = new cover material, dashed lines = used cover material (usage duration: $78\ d$), $\delta = 5°$.

Material thickness also influences its optical properties. In Figure 3.9 reflectance and transmittance spectra of NWF with three different thicknesses ($19\ g/m^2$, $23\ g/m^2$ and $30\ g/m^2$) are presented. One general conclusion can be derived from Figure 3.9: reflectance is increasing and transmittance is decreasing with increasing material thickness. The shape of the graphs is the same for all thicknesses, they are just vertical shifted. Separate mean values for the PAR and NIR wavelength band and all materials in new and used condition are given in Table 3.7.

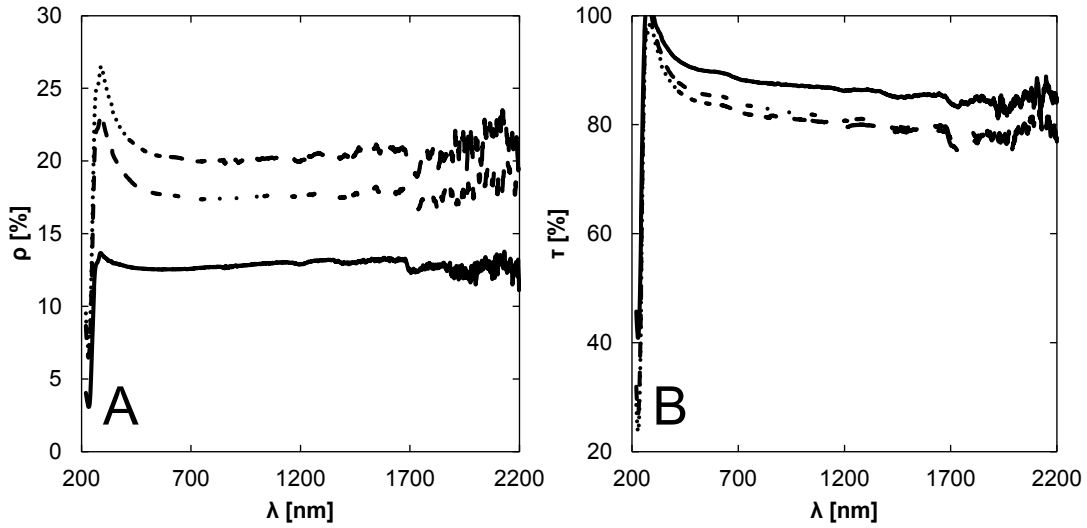


**Figure 3.9** Directional-hemispherical reflectance $\rho$ (A) and transmittance $\tau$ (B) of non-woven fabric with different thicknesses against wavelength $\lambda$. Solid lines = 19 $g/m^2$, dashed lines = 23 $g/m^2$, dotted lines = 30 $g/m^2$, $\delta = 5°$.

**Table 3.7** Measured directional-hemispherical reflectance and transmittance of covers for an incidence angle $\delta = 5°$ in the PAR ($400 - 700\,nm$) and NIR ($701 - 2200\,nm$) wavelength band. NWF = non-woven fabric (19 $g/m^2$), NWF2 = non-woven fabric (23 $g/m^2$), NWF3 = non-woven fabric (30 $g/m^2$), FF = double layer cover consisting of non-woven fabric and perforated film (usage duration: 78 $d$; NWF and FF data from Graefe & Sandmann (2014)).

| Material | State | Reflectance | | Transmittance | |
|---|---|---|---|---|---|
| | | PAR | NIR | PAR | NIR |
| NWF | New | 0.127 | 0.129 | 0.872 | 0.871 |
| NWF2 | | 0.181 | 0.176 | 0.866 | 0.820 |
| NWF3 | | 0.208 | 0.203 | 0.850 | 0.808 |
| FF | | 0.209 | 0.198 | 0.789 | 0.780 |
| NWF | Used | 0.150 | 0.161 | 0.777 | 0.814 |
| FF | | 0.263 | 0.241 | 0.681 | 0.749 |

The wetness condition of the cover material has to be taken into account, too, as Figure 3.10 shows. Very obvious differences between dry and wet covers occur around $1400\,nm$ and $1900\,nm$. These are the wavelength bands, where water is absorbing a substantial amount of radiation. Reflectance is smaller for wet FF than for dry. But it is almost constant for NWF for wavelengths $< 1300\,nm$, which was not expected, as wetted NWF appeared somewhat darker. In wet condition, transmittances of NWF and FF are almost identical. It is increasing for wavelengths $< 1400\,nm$, compared to the dry cover materials and for higher wavelengths it is mainly influenced by radiation absorption of the water. The visually sensed darkening of NWF while moistening might be explained by the increased

transmittance coefficient. This effect made the (relatively dark) background better visible, which resulted in the visual impression of a darkening of the cover material. Nevertheless, other reasons like a decreased relevance of isotropic reflectance are possible, too. Differences between mean values of reflectance and transmittance of dry and wet cover materials are summed up in Table 3.8.

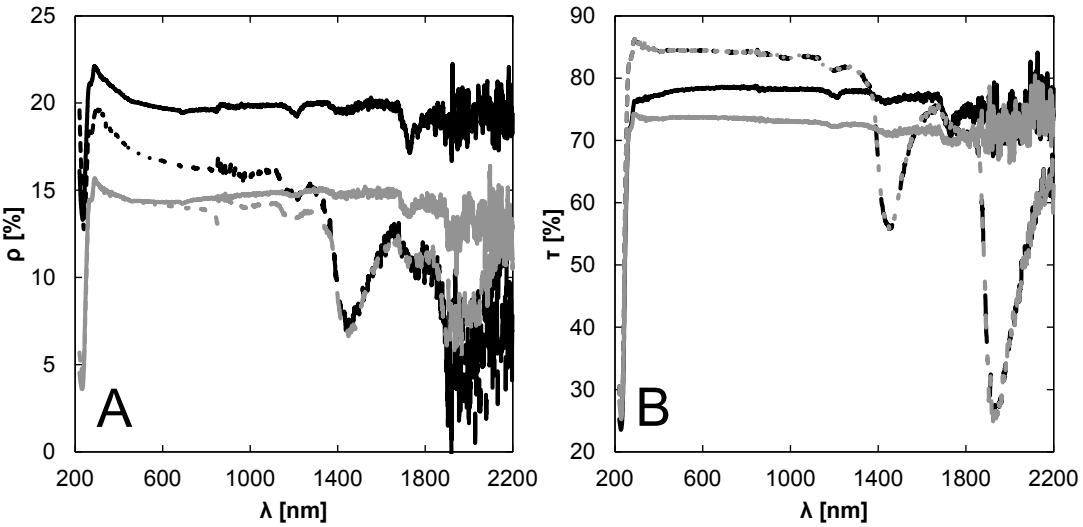


**Figure 3.10** Directional-hemispherical reflectance $\rho$ (A) and transmittance $\tau$ (B) of cover materials with different wetness states against wavelength $\lambda$. Grey = non-woven fabric (19 $g/m^2$), black = double layer consisting of non-woven fabric and perforated film, solid lines = dry covers, dashed lines = wet covers, $\delta = 5°$.

**Table 3.8** Differences in optical properties of cover materials under dry and wet conditions (differences are calculated as wet minus dry). NWF = non-woven fabric (19 $g/m^2$), PF = perforated film, $\delta = 5°$ (data from Graefe & Sandmann (2014)).

| Material | Reflectance difference | | Transmittance difference | |
|---|---|---|---|---|
| | PAR | NIR | PAR | NIR |
| NWF | -0.0015 | -0.0150 | 0.0027 | -0.0431 |
| FF | -0.0298 | -0.0505 | 0.0350 | -0.0179 |

Directional-directional transmittance in dependence of incidence angle is presented in Figure 3.11 for dry and wet NWF and FF, respectively. Measurements were done in 15° steps from 0° to 75° incidence angle. Transmittance at $\delta = 90°$ was assumed to be zero. Transmittances are decreasing with increasing incidence angle and they are constantly lower for FF than for NWF.

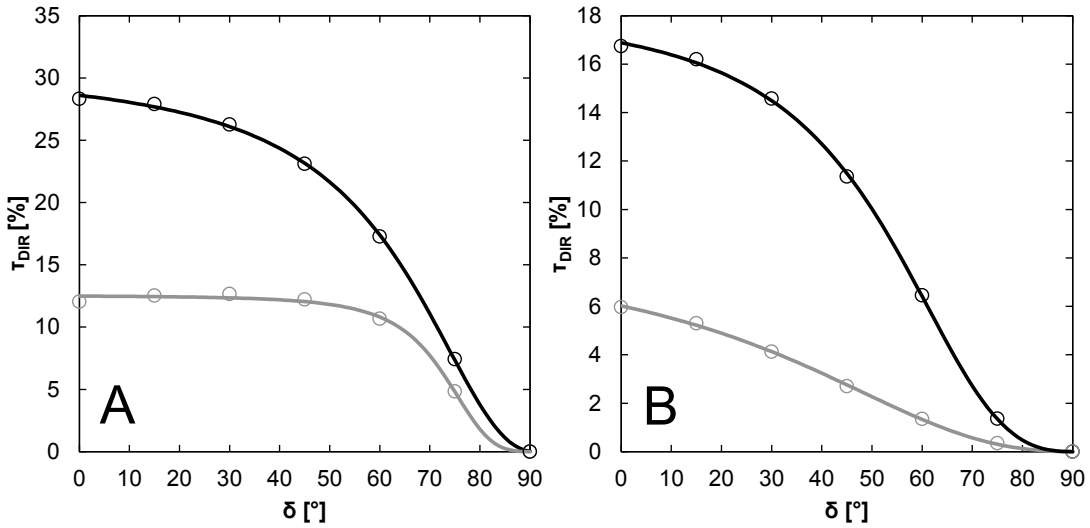


**Figure 3.11** Directional-directional transmittance ($\tau_{DIR}$) against incidence angle ($\delta$) for non-woven fabric (A) and a double layer consisting of non-woven fabric and perforated film (B). Black = dry covers, grey = wet covers, circles = measurements, lines = model.

To obtain values for arbitrary incidence angles $\delta$, the relation of directional-directional transmittance to incidence angle was fitted to the here proposed empirical model

$$\tau_{DIR}(\delta) = \frac{g_1 g_2 (91 - \delta)^{g_3}}{1 + g_2 (91 - \delta)^{g_3}}, \tag{3.2}$$

where $g_1$ to $g_3$ are fitting parameters (Table 3.9). The associated model graphs are shown in Figure 3.11. Model performance is very good for all cover materials and usage durations ($R^2_{adj} > 0.999$, $RMSE < 0.15$ % transmittance).

**Table 3.9** Parameters for the directional-directional transmittance model. NWF = non-woven fabric, FF = double layer consisting of non-woven fabric and perforated film.

| Cover | Condition | $g_1$ | $g_2$ | $g_3$ |
|---|---|---|---|---|
| NWF | dry | 30.7786 | 0.00080586 | 2.1507 |
| NWF | wet | 12.5335 | 0.00003909 | 3.4898 |
| FF | dry | 18.2610 | 0.00002594 | 2.8963 |
| FF | wet | 8.3422 | 0.00004564 | 2.4265 |

3.2.4.2.2. *Leaves*

Mean spectra of reflectance and transmittance of lettuce and kohlrabi leaves are plotted in Figure 3.12 ($n = 35$ for each species). The general appearance of the spectra is in accordance with the literature, for example referring to data from tobacco leaves (Knipling 1970). Around $550\ nm$ there is a distinct peak for reflectance and transmittance, respectively (Figure 3.12 A and B). In this wavelength region, there is the visible green light and its reflectance peaks contributes to the green color appearance of plants. As expected, blue ($\approx 400\ nm$) and red light ($\approx 700\ nm$) are absorbed more efficiently by leaves. Most of NIR is either reflected or transmitted. Due to this completely different optical behavior of leaves in the PAR and NIR band, it is appropriate to distinguish between these two wavelength bands for further radiation budget modeling. Around $1400\ nm$, a remarkable valley can be observed for both reflectance and transmittance. This is caused by a strong absorption band of the leaves' water.

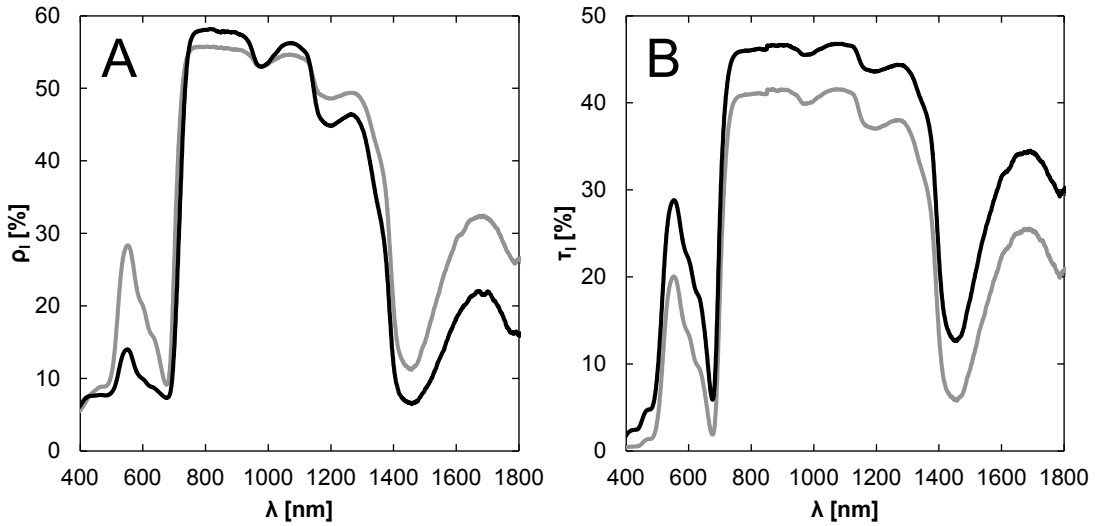


**Figure 3.12** Reflectance $\rho_l$ (A) and transmittance $\tau_l$ (B) of leaves against wavelength $\lambda$ ($n = 35$). A: grey = lettuce, black = kohlrabi, both grown without cover. B: grey = without cover, black = non-woven fabric and perforated film, both lettuce, $\delta = 5°$.

Additionally, from Figure 3.12 it becomes also clear, that a distinction between species (Figure 3.12A) and cover treatment (Figure 3.12B) is necessary.

Results from weekly measurements of reflectance and transmittance of lettuce leaves and kohlrabi leaves revealed that there is no systematic trend over time Figure 3.13. In most cases the slope of the linear regression function between DAP and reflectance or transmittance is not significant different

from zero ($\alpha = 0.05$), in the other cases the 95 % confidence limits of the slopes are only slightly different from zero. For this reason, reflectance and transmittance coefficients of leaves are regarded as constant throughout the growing period. But from Figure 3.13 it can be seen that there are differences between PAR and NIR (filled vs. blank symbols), between species (grey vs. black symbols) and between cover materials (circles vs. triangles).

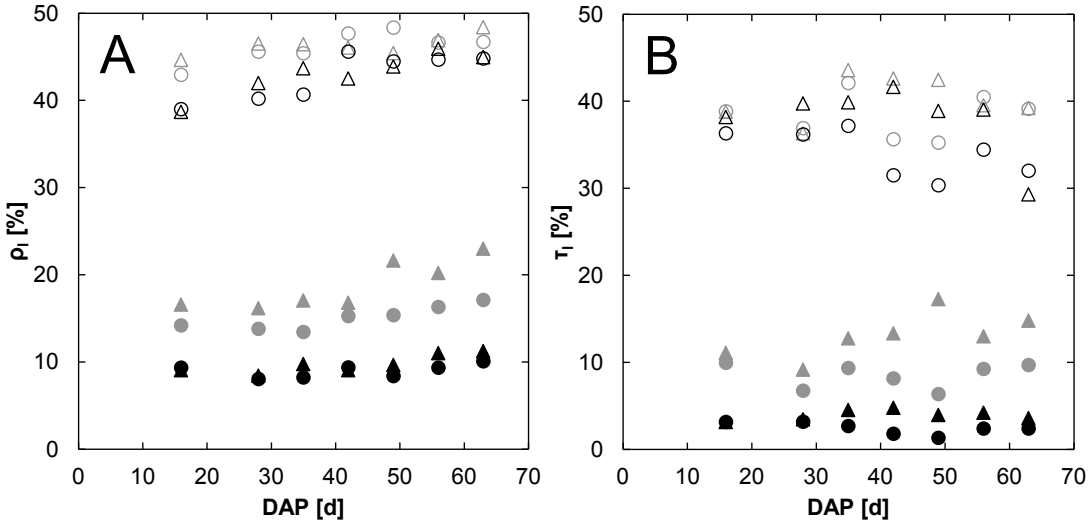


**Figure 3.13** Reflectance $\rho_l$ (A) and transmittance $\tau_l$ (B) of lettuce leaves (grey) and kohlrabi leaves (black) against days after planting (DAP). Filled symbols = photosynthetic active radiation, blank symbols = near-infrared radiation, circles = plants grown without cover, triangles = plants grown under non-woven fabric and perforated film.

These mentioned group means of reflectance and transmittance of leaves are listed in Table 3.10.

**Table 3.10** Optical properties of leaves ($\rho$ = reflectance coefficient, $\tau$ = transmittance coefficient, $\alpha$ = absorbtance coefficient). Measured direct-hemispherical reflectances and transmittances for a zenith angle $\delta = 5°$ in the photosynthetic active radiation (PAR) and near-infrared (NIR) wavelength band. NWF = non-woven fabric, FF = cover consisting of NWF and perforated film.

| Species | Cover treatment | $\rho$ | | $\tau$ | | $\alpha$ | |
|---|---|---|---|---|---|---|---|
| | | PAR | NIR | PAR | NIR | PAR | NIR |
| lettuce | without cover | 0.1506 | 0.4617 | 0.0848 | 0.3832 | 0.7646 | 0.1551 |
| lettuce | NWF | 0.1696 | 0.4574 | 0.1113 | 0.4032 | 0.7191 | 0.1394 |
| lettuce | FF | 0.1877 | 0.4633 | 0.1304 | 0.4034 | 0.6819 | 0.1333 |
| kohlrabi | without cover | 0.0899 | 0.4275 | 0.0240 | 0.3398 | 0.8861 | 0.2327 |
| kohlrabi | NWF | 0.0911 | 0.4291 | 0.0326 | 0.3628 | 0.8763 | 0.2081 |
| kohlrabi | FF | 0.0973 | 0.4308 | 0.0394 | 0.3809 | 0.8633 | 0.1883 |

Differences between species are smaller in the NIR band than in the PAR band, whereas both reflectance and transmittance coefficients in the NIR band are much higher than in the PAR band (Table 3.10, Figure 3.12 and Figure 3.13). Obviously, the absorbed fraction of radiation in the PAR band is higher than in the NIR band, which was expected. This is in accordance with Campbell and van Evert (1994). Another finding is that reflectance and transmittance coefficients are increasing from no cover to NWF to the double layer cover. During spectroscopic measurements there was already a distinct appearance: leaves from the covered treatments appeared paler than the leaves from the non-covered treatments. One possible explanation of these findings might be that the artificial protection against strong wind, transpiration and radiation leads to thinner leaves with a bigger area where the chlorophyll content per leaf area is smaller. Kohlrabi leaves also show a darker green than lettuce leaves in the field, which is confirmed by lower reflectance coefficients of kohlrabi leaves in the PAR band (Table 3.10, Figure 3.12 and Figure 3.13).

3.2.4.2.3. *Soils*

The development of soil reflectance $\rho_s$ during a dry down measurement is shown in Figure 3.14. From high to low volumetric water contents $\theta_s$, $\rho_s$ is increasing over the whole spectrum. Remarkable are the local minima of $\rho_s$ around $1400\,nm$ and $1900\,nm$, which are caused by water absorption. With decreasing volumetric soil water content $\theta_s$ there is also a decrease of amplitude of these local minima.

The dependence of $\rho_s$ from $\theta_s$ is illustrated in Figure 3.15. For a description of the transformation from spectra to mean values see section 2.5.4.2. $\rho_s$ in the PAR band (Figure 3.15A) is about half of $\rho_s$ in the NIR band (Figure 3.15B). In general it can be said, that the dryer the soil, the higher $\rho_s$, where the increase of $\rho_s$ is highest in the beginning of the measurements (near water saturation) and in the phase when the surface of the soil sample changes its color noticeably. In the intermediate phase (the normal soil condition during vegetable production), there is only a slight change of $\rho_s$ and after the second phase of high increase there is no further variation of $\rho_s$. The experiment was performed with soil samples from GR site and GO site. The higher clay content of the GO soil samples results in an

earlier visible color change at higher volumetric water contents and $\rho_s$ reaches finally smaller values than observed with the GR samples.

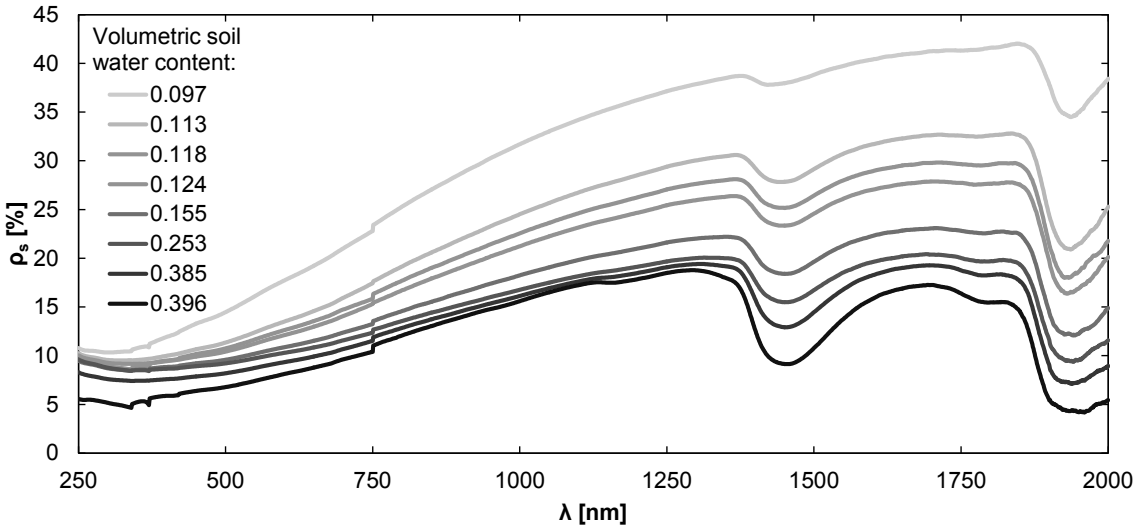


**Figure 3.14** Soil reflectance ($\rho_s$) against wavelength ($\lambda$) for various volumetric soil water contents ($\theta_s$) (decreasing $\theta_s$ from black to light grey, see also the legend). Soil sample was taken from Großbeeren site on 11.10.2013.

Graefe & Sandmann (2014) fitted the data from the GR site to a mixture of logistic functions and yielded $R^2_{adj} > 0.93$ for both PAR and NIR wavelength band:

$$\rho_s = \frac{s_1}{1 + \exp\big(s_2 \cdot (\theta_s - s_3)\big)} + \frac{s_4}{1 + \exp\big(s_5 \cdot (\theta_s - s_6)\big)}, \tag{3.3}$$

where $s_1$ to $s_6$ are six parameters which have to be fitted for each site and wavelength band. Here supplementary results from the GO site are presented in Table 3.6. All parameters from the GO site are significant different from zero (t-test, $\alpha = 0.05$), where $R^2_{adj}$ values (PAR: 0.778, NIR: 0.799) are smaller than from GR site.

**Table 3.11** Parameter estimates of the soil surface reflectance model at Golzow site. PAR = photosynthetic active radiation, NIR = near-infrared radiation.

| Parameter | PAR | NIR |
|---|---|---|
| $s_1$ | 0.0457 | 0.1250 |
| $s_2$ | 74.4283 | 47.5833 |
| $s_3$ | 0.1933 | 0.1991 |
| $s_4$ | 0.0950 | 0.1443 |
| $s_5$ | 26.5396 | 33.3358 |
| $s_6$ | 0.5000 | 0.5000 |

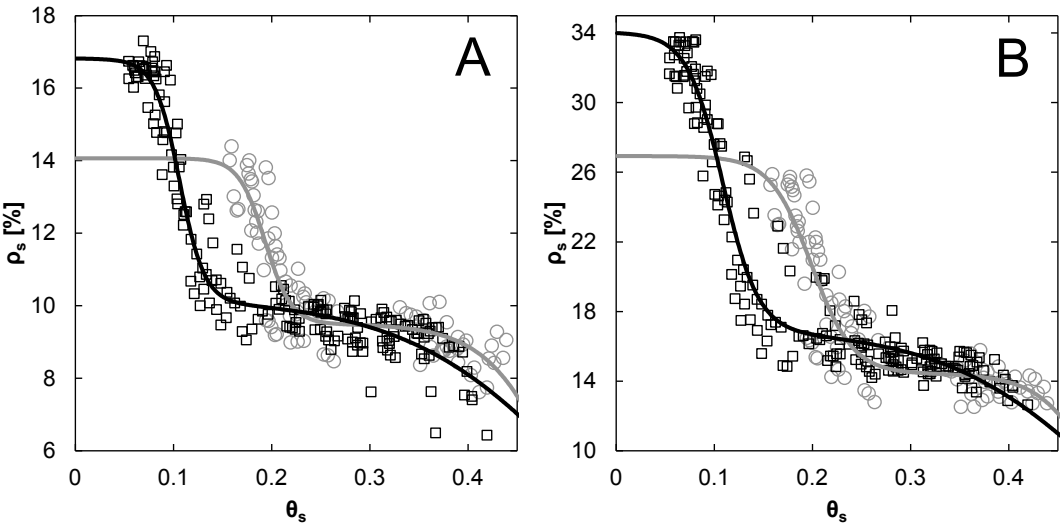


**Figure 3.15** Soil surface reflectance ($\rho_s$) against volumetric soil water content ($\theta_s$) in the (A) photosynthetic active radiation wavelength band ($PAR$, $400\,nm - 700\,nm$) and in the (B) near-infrared wavelength band ($NIR$, $701\,nm - 2000\,nm$). Black lines = model Großbeeren site, grey lines = model Golzow site, squares = measurements Großbeeren site, circles = measurements Golzow site (modified from Graefe & Sandmann (2014)).

### 3.2.4.3. Leaf angle distribution function, clumping index and extinction coefficient

From LAI-2200 measurements for kohlrabi, the parameter $x$ (Eq. (2.33)) from the leaf angle density function was used to estimate a mean value for the species. Graefe & Sandmann (2014) found that $x$ depends on $LAI$ and cover material. They fitted functions of the type $x = a \cdot LAI^b$ and give parameter values for $a$ and $b$ for kohlrabi stands without cover, NWF and FF. In Figure 3.16A the relationship between $LAI$ and $x$ is shown for kohlrabi grown without covers. Measurements with LAI-2200 are not feasible with lettuce. Therefore, for lettuce a spherical leaf angle distribution ($x = 1$), which is the most straightforward and common distribution, was assumed. In Figure 3.16B the leaf angle

distribution functions for $x = 1.0$ to $x = 2.5$ are presented. According to these distributions, the mean inclination angles (weighted mean of inclination angles; weights are the according values of $g(\alpha, x)$) are 57.3° to 32.6°, respectively. Hence, leaves of kohlrabi are less erected than the spherical leaf angle distribution. Furthermore, with increasing $LAI$ and $x$ the kohlrabi leaves are aligned more and more horizontally.

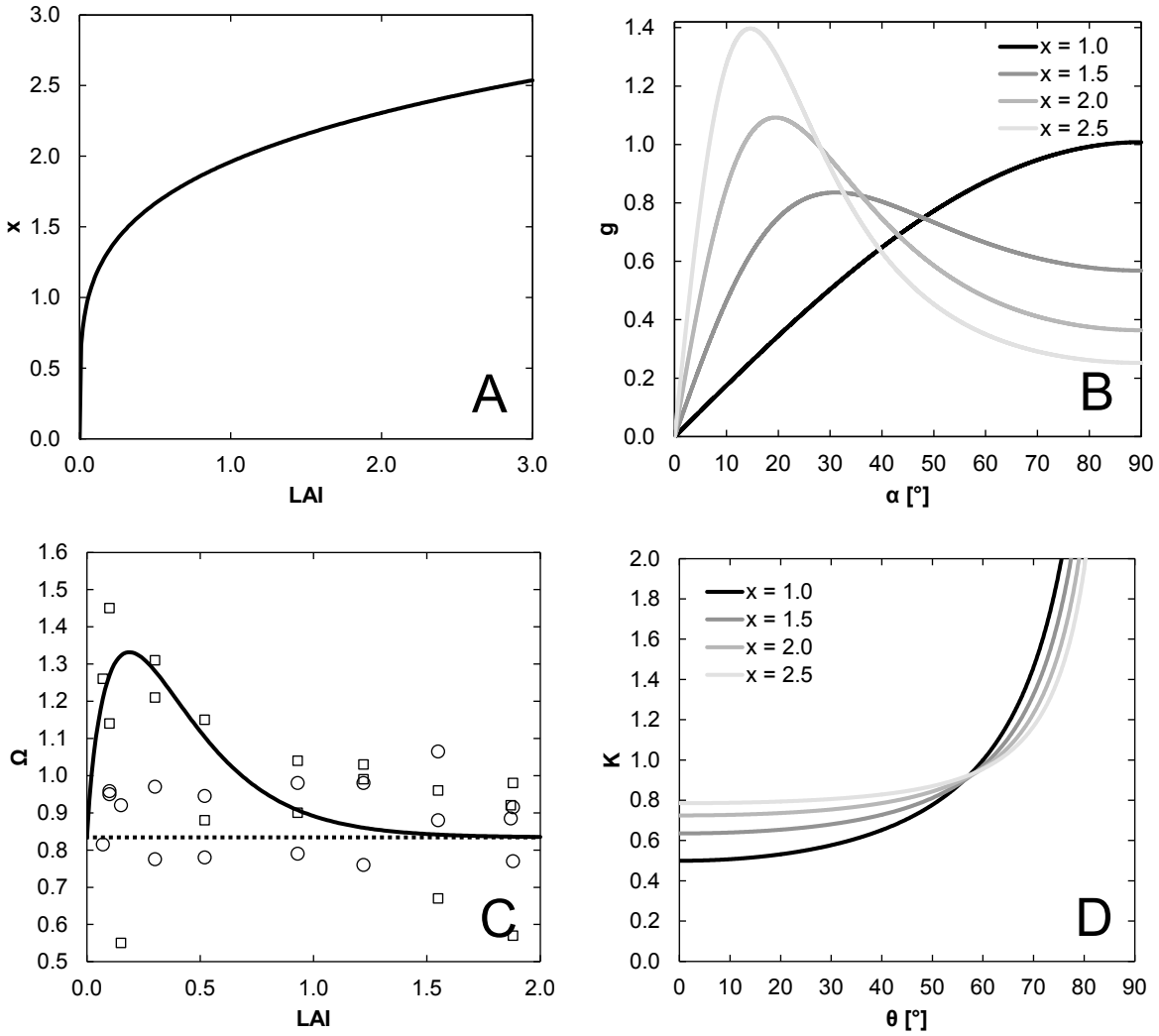


**Figure 3.16** (A) Parameter $x$ from leaf inclination angle density function ($g(\alpha, x)$) against leaf area index ($LAI$) for uncovered kohlrabi; $x = 1.96 \cdot LAI^{0.235}$. (B) Leaf inclination angle density function $g(\alpha, x)$ against leaf inclination angle ($\alpha$). (C) Fitted clumping factor $\Omega$ at 0° (squares) and 57.5° (circles) view zenith angles against $LAI$ in kohlrabi. $n = 17$; $\Omega_{57.5} = 0.834$ (dotted line); $\Omega_0(LAI) = 0.834 + 4.32 \cdot LAI^{0.807} \cdot \exp(-4.32 \cdot LAI)$ (solid line) (Graefe & Sandmann 2014). (D) Extinction coefficient $K$ against sun zenith angle $\theta$.

The modelled clumping index $\Omega(LAI)$ (Figure 3.16C from Graefe & Sandmann (2014)) is smaller for $\theta = 57.5°$ than for $\theta = 0°$. But the difference decreases with increasing $LAI$. From Figure 3.16C

(Graefe & Sandmann 2014) it becomes clear, that $\Omega_0$ is dependent on $LAI$ and $\Omega_{57.5}$ is not. In Figure 3.16D $K(\theta)$ for $x = 1.0$ (spherical leaf angle distribution) to $x = 2.5$ (ellipsoidal leaf angle distribution) in steps of $0.5$ is shown. There is a clear difference between the leaf angle distributions. Thus, it is important to account for the observed deviation from the spherical leaf angle distribution in kohlrabi for further calculations in the radiation model (see section 3.3.2).

## 3.3. Development and test of new submodels

Three new submodels are presented now, each concerning one special aspect of the regarded production system (section 1.1.1). At first the model derivation will be given and afterwards the parameterization and validation will be described. The three aspects covered are:

1. leaf area growth,
2. short wave radiation budget and
3. dry matter accumulation

and they are described in the following three sections.

### 3.3.1. A dynamic model for leaf area growth in lettuce and kohlrabi

For a general model approach of the microclimate below covers in early year vegetable production, the LAI has to be provided at least on a daily basis. This cannot be achieved by measurements (no matter whether direct or indirect methods are applied). Thus, a model is necessary which estimates the leaf area index in any temporal resolution desired using easily available input data. Such a model was developed and it is described in the following section. After the mathematical description, the calibration and validation of the model is outlined in section 3.3.1.2.

#### 3.3.1.1. Derivation of the model

Leaf area growth is modelled for both lettuce and kohlrabi. Hourly air temperatures at $10\ cm$ height within the crops are used as input (sensors are described in section 2.1.3.1). Temperature and leaf area index data from 2010-2012 (GR and GO) and from different cover materials (none, NWF, FF) and

treatments (e.g. removal-strategies) (Table 2.1) were used for parameterization. A logistic growth equation with a hourly iteration step was adopted which consists of the equation

$$LAI_t = LAI_{t-1} + \Delta LAI \tag{3.4}$$

with

$$\Delta LAI = a(T) \cdot LAI_{t-1} \cdot \left(1 - \frac{LAI_{t-1}}{LAI_{max}}\right) \tag{3.5}$$

and the initial value $LAI_0$ with $t = 1$ is estimated from

$$LAI_0 = p_5 \cdot e^{p_6 \cdot DAP} \tag{3.6}$$

where $LAI$ is leaf area index, $t$ is time step, $LAI_{max}$ is maximum leaf area index, $T$ $[K]$ is air temperature, $a(T)$ is temperature response function of leaf area growth, $DAP$ is days after planting and $p_5$ and $p_6$ are empirical parameters. $LAI_0$ is not $LAI$ at the moment of planting, which is almost constant, due to a quite comparable development stage of the plant in that moment. $LAI_0$ is the estimated initial $LAI$ for the time, when temperature recording started. Logistic approaches are often used to describe leaf area growth, e.g. in grapevine (Schultz 1992) and maize (Lizaso et al. 2003). Estimation of $LAI_0$ is necessary, because it was not always possible to record temperature up from planting on, e.g. in GR in 2010 temperature records started 10 $d$ after planting. For the period of time between planting and the first temperature measurements a species specific exponential growth of $LAI$ was assumed. As temperature response function of leaf area growth the approach of Leuning (2002) was modified, who used it as a temperature response function for the maximum electron transport rate of photosynthesis:

$$a(T) = p_1 \cdot \left( \exp\left(\frac{p_4 \cdot (T - T_{ref})}{R \cdot T \cdot T_{ref}}\right) \times \frac{1 + \exp\left(\frac{T_{ref} \cdot p_3 - p_2}{R \cdot T_{ref}}\right)}{1 + \exp\left(\frac{T \cdot p_3 - p_2}{R \cdot T}\right)} \right). \tag{3.7}$$

Originally, this formula was proposed by Johnson et al. (1942) who used it to describe the temperature dependence of the velocity of the enzyme catalysis in bacterial luminescence. $T_{ref}[K]$ is the reference temperature which was set to $T_{ref} = 25 + 273.15\ K$, $R$ is ideal gas constant and $p_1$ to $p_4$ are model parameters. $T_{ref}$ is an arbitrary choice, but in the context of photosynthesis modeling a reference temperature has to be chosen because of the temperature dependency of a variety of photosynthesis

related parameters, which need to be normalized e.g. for comparisons among species and environmental conditions. As shown by Leuning (2002) most studies in this field use $T_{ref} = 20\ °C$ or $T_{ref} = 25\ °C$, where he chose the latter one.

#### 3.3.1.2. Calibration and validation

The results of the parameter fitting for both species are presented in Table 3.12. For lettuce, all parameters except of $p_4$ are significantly different from 0 at the significance level $\alpha = 0.05$, where the p value of $p_4$ is only a little higher than the prescribed $\alpha$. The corresponding temperature response curve (Eq. (3.7)) is shown in Figure 3.17A. The curve has a plausible shape with a base temperature of approximately $5°C$ and a maximum leaf area growth rate of $0.025\ [m^2\ \text{leaf area}/h]$ at $25°C$. For kohlrabi the results of the model fit gave two parameters, that are not significantly different from zero: $p_4$ and $p_5$ ($\alpha = 0.05$). The temperature response curve has its maximum at about $22°C$ and a maximum growth rate of $0.012\ [m^2\ \text{leaf area}/h]$. The growth rates of kohlrabi reach only about half as high values as those of lettuce. The maximum growth rate of kohlrabi will be realized at $3\ K$ cooler temperatures compared to lettuce. Therefore, there is a tendency that kohlrabi might be adapted to lower temperatures than lettuce. This finding is in accordance with Vogel et al. (1996), who gives similar temperature intervals for optimal growth for lettuce ($15$ to $25\ °C$) and kohlrabi ($14$ to $20\ °C$). Figure 3.17B illustrates the estimated exponential growth (Eq. (3.6)) of leaf area index in the first three weeks after planting for lettuce and kohlrabi. $LAI_0$ is always higher for lettuce than for kohlrabi, which is plausible because own measurements of $LAI$ at planting date confirm this finding ($0.03$ for lettuce and $0.02$ for kohlrabi). But the growth of leaf area for kohlrabi accelerates faster towards the end of the first three weeks after planting than the growth of leaf area for lettuce.

**Table 3.12** Results from the leaf area index parameterization.

| Species | Fitted parameter | Parameter estimate | Confidence limit (lower) | Confidence limit (upper) | p value |
|---|---|---|---|---|---|
| lettuce | $p_1$ | 0.0244 | 0.0112 | 0.0376 | 0.0003 |
| lettuce | $p_2$ | 278.9421 | 85.4452 | 472.4390 | 0.0050 |
| lettuce | $p_3$ | 0.9378 | 0.3122 | 1.5634 | 0.0036 |
| lettuce | $p_4$ | 163.6397 | -5.0351 | 332.3145 | 0.0571 |
| lettuce | $LAI_{max}$ | 3.3109 | 2.9749 | 3.6468 | <0.0001 |
| lettuce | $p_5$ | 0.1208 | 0.0263 | 0.2152 | 0.0126 |
| lettuce | $p_6$ | 0.0812 | 0.0323 | 0.1301 | 0.0013 |
| kohlrabi | $p_1$ | 0.0100 | 0.0031 | 0.0169 | 0.0046 |
| kohlrabi | $p_2$ | 276.5340 | 66.5647 | 486.5033 | 0.0100 |
| kohlrabi | $p_3$ | 0.9409 | 0.2144 | 1.6674 | 0.0113 |
| kohlrabi | $p_4$ | 164.5986 | -100.2532 | 429.4504 | 0.2222 |
| kohlrabi | $LAI_{max}$ | 2.1572 | 1.9578 | 2.3566 | <0.0001 |
| kohlrabi | $p_5$ | 0.0154 | -0.0024 | 0.0333 | 0.0904 |
| kohlrabi | $p_6$ | 0.1739 | 0.1049 | 0.2430 | <0.0001 |

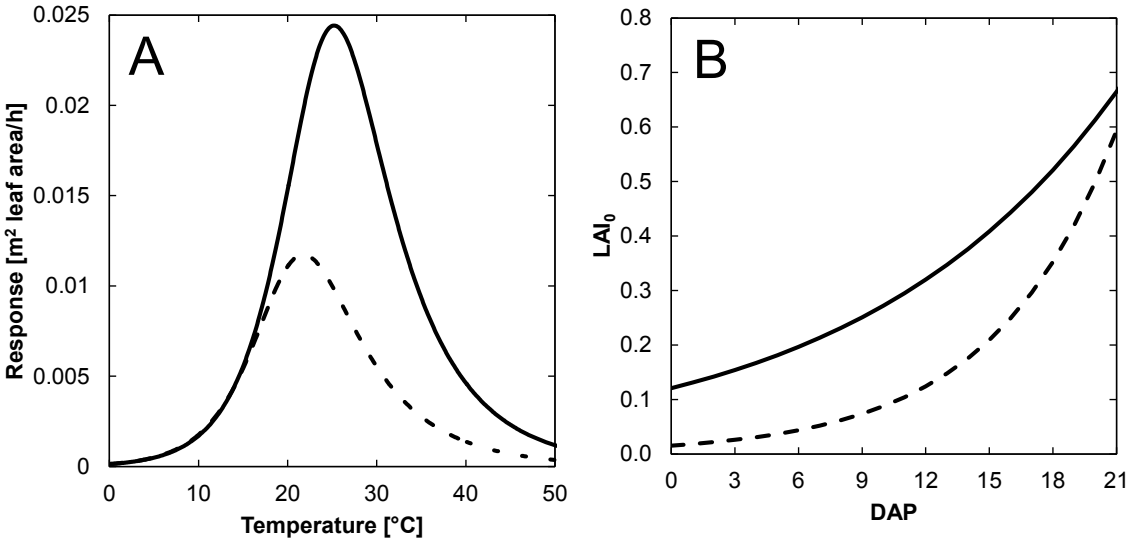


**Figure 3.17** Temperature response curve for hourly leaf area growth (A) and estimation of the initial leaf area index $LAI_0$ (B). DAP = days after planting, solid line = lettuce, dashed line = kohlrabi.

A comparison of measured and estimated leaf area indexes of lettuce and kohlrabi crops can be seen in Figure 3.18. For kohlrabi (Figure 3.18B) the obtained model fit reaches only an intermediate goodness

($R^2 = 0.6990$, $RMSE = 0.4365$, $n = 271$) whereas the prediction of LAI for lettuce (Figure 3.18A) is much better ($R^2 = 0.8548$, $RMSE = 0.5019$, $n = 154$).

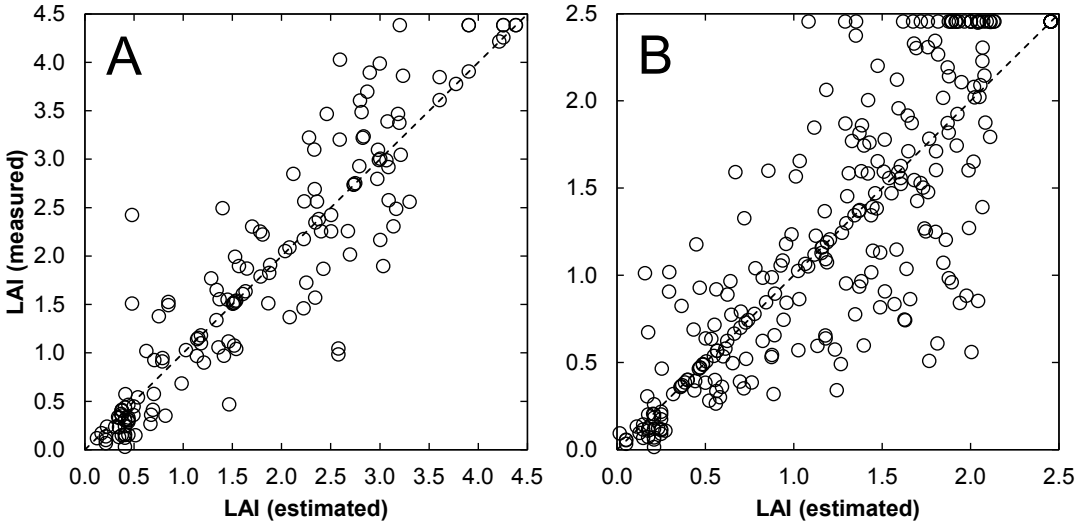


**Figure 3.18** Measured against estimated leaf area index for lettuce ($n = 154$, A) and kohlrabi ($n = 271$, B). Dashed line = 1:1.

For demonstration purposes, the modeled and measured *LAI* development for one plant per species is given in Figure 3.19. From these arbitrary examples it becomes obvious that the prediction can be of varying precision in individual cases.

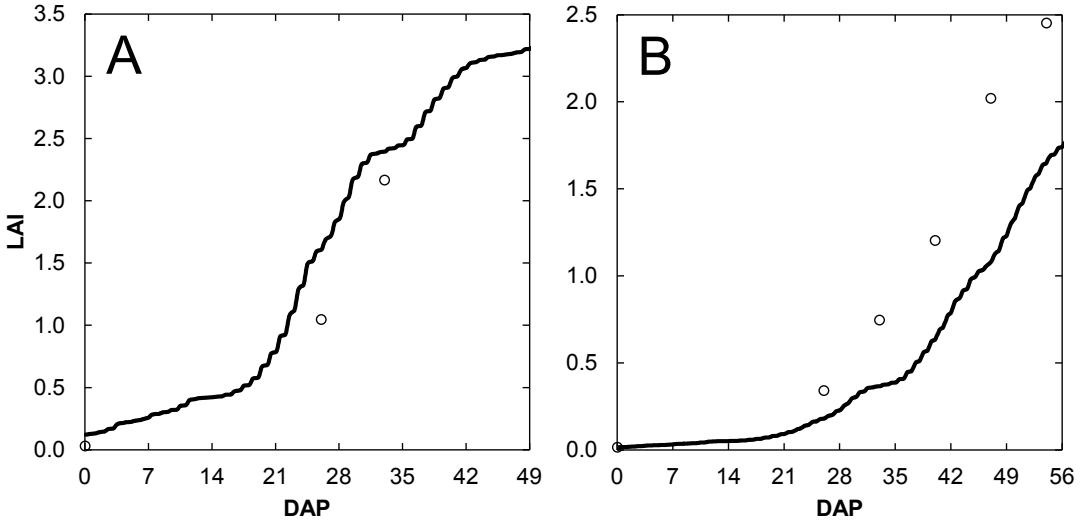


**Figure 3.19** Examples for the comparison of modelled (black lines) and measured (circles) leaf area index (*LAI*) for lettuce (A) and kohlrabi (B). DAP = days after planting. Data are from Großbeeren 2011 and without cover.

### 3.3.2. The short wave radiation budget of film covered canopies

Graefe & Sandmann (2014) propose a model for the short wave radiation budget of film covered canopies. For such a model, a lot of interactions have to be taken into account. An overview of the path of incident direct and diffuse radiation from above the cover to the soil surface, as accounted for in the model is given in Figure 3.20 and Figure 3.21, correspondingly. Altogether 23 portions of radiation are computed in the basic version of the model. For separation of incident shortwave radiation according to its angular distribution, Graefe & Sandmann (2014) used the procedure which is explained in section 2.5.4.1.

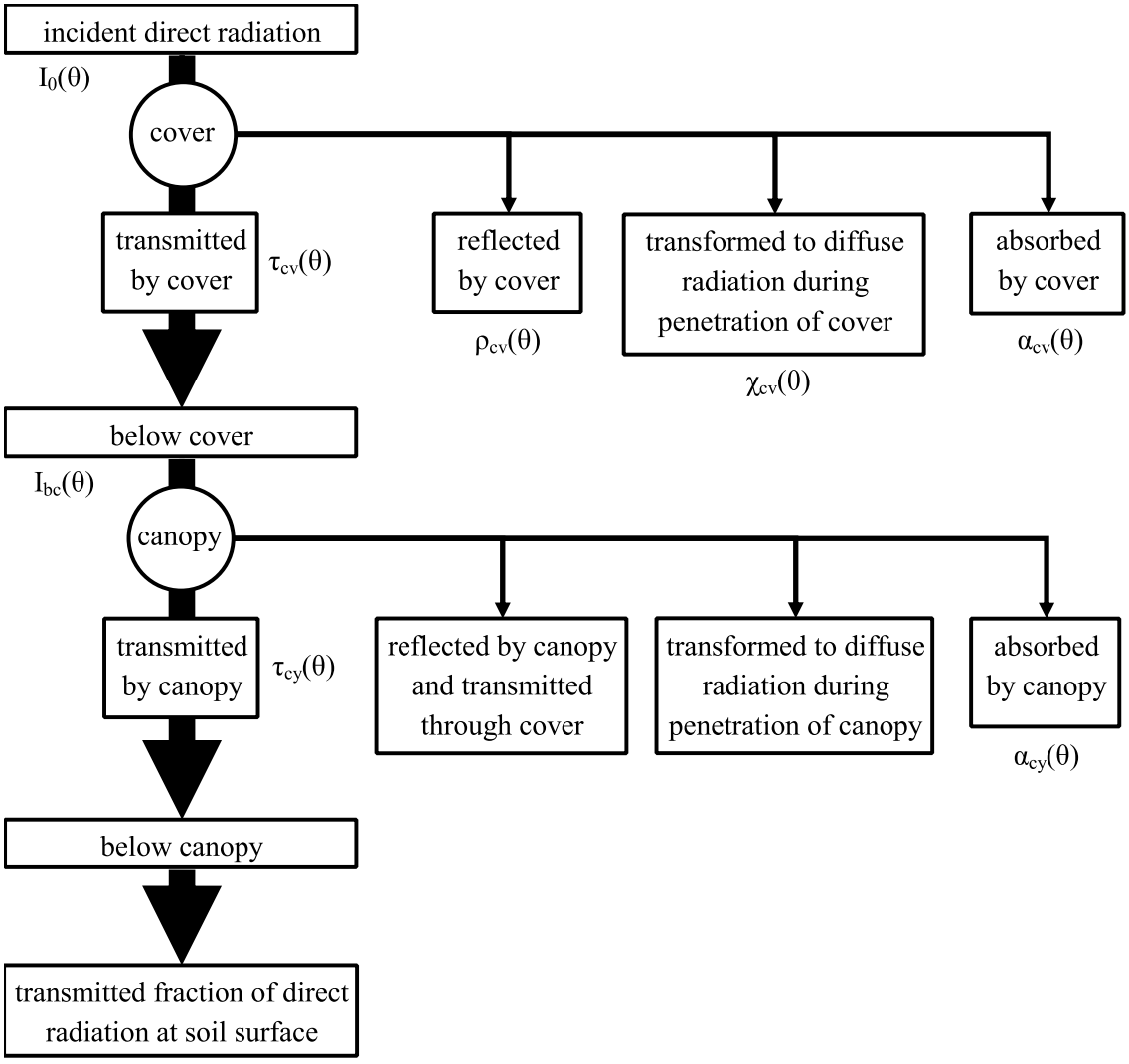


**Figure 3.20** Overview of the path of incident direct radiation from above the cover to the soil surface (thick arrows on the left side) and all fractions of lost direct radiation (thin arrows) as accounted for in the approach from Graefe & Sandmann (2014) and the according symbols as they are used there.

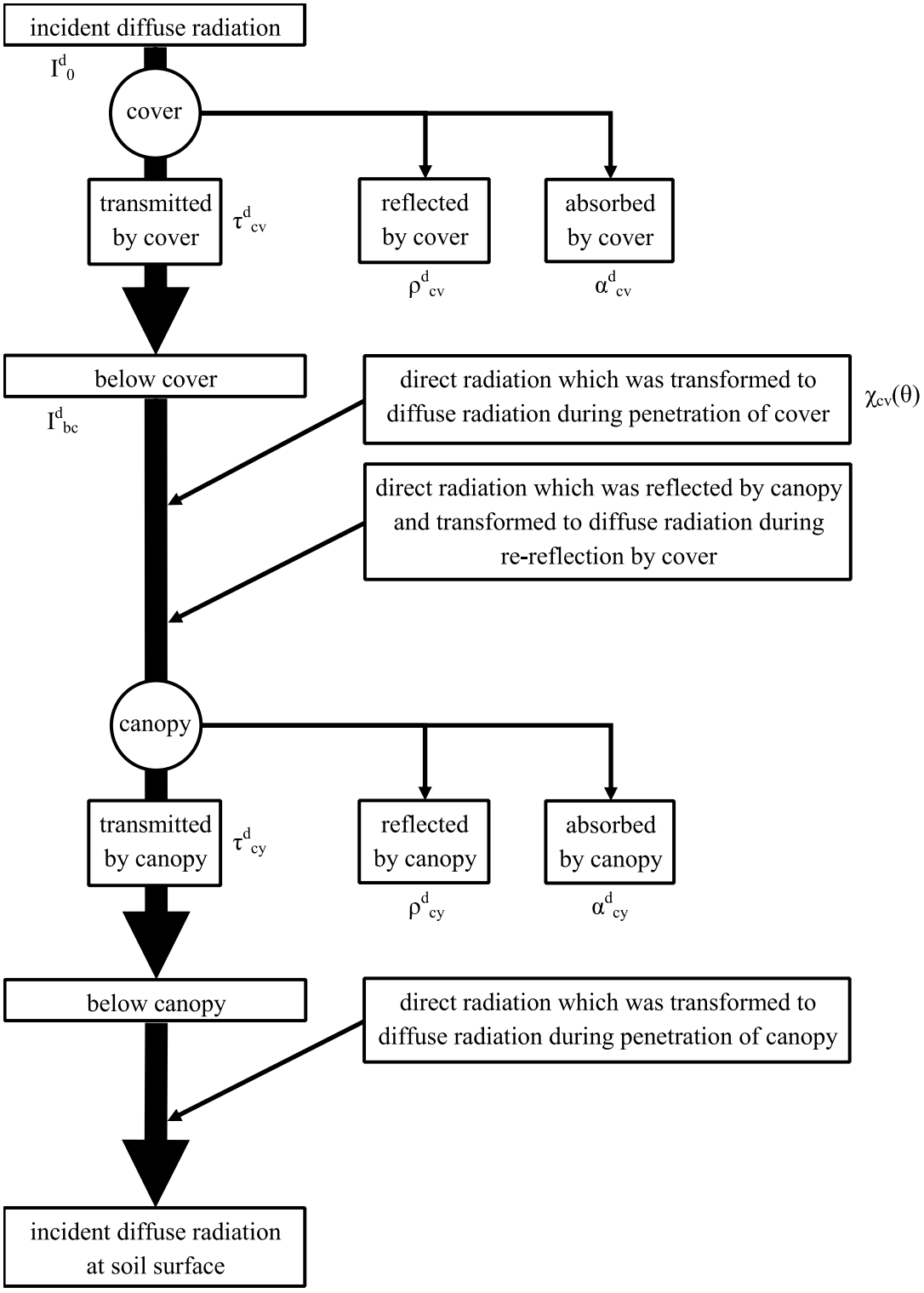


**Figure 3.21** Overview of the path of incident diffuse radiation from above the cover to the soil surface (thick arrows on the left side) and all fractions of lost and gained diffuse radiation (thin arrows) as accounted for in the approach from Graefe & Sandmann (2014) and the according symbols as they are used there.

They accounted also for changes of cover geometry during time. In their Figure 4, an overview of cover surface roughness depending on plant development is shown, where they describe the cover surface roughness using a Fréchet distribution, which has only one free parameter ($\alpha_b$). $\alpha_b$ is also

called “shape parameter” and is in the interval $(0,\infty)$ where small $\alpha_b$ indicates smooth cover surfaces and increasing $\alpha_b$ indicates increasing cover roughness. In the context of plastic cover roughness, values for $\alpha_b$ in the interval $(0,1]$ are plausible.

A geometric detail is the distinction between macroroughness and microroughness of the cover (Figure 3.22). The microroughness can be recorded as many small-surface facets randomly distributed in space and time. Those facets have all an individual slope (Figure 3.22). The distribution of the small-surface facet slopes $D(\beta)$ can be described by the Beckmann distribution (Walter et al., 2007).

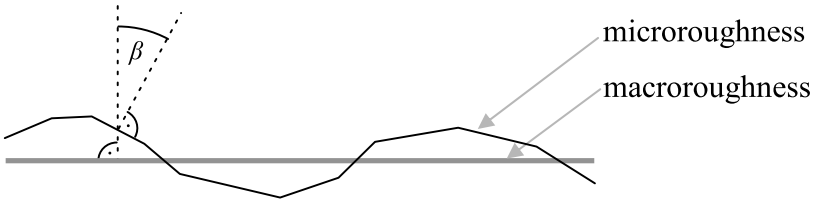


**Figure 3.22** Macroroughness and microroughness of the cover material. Additionally, one exemplary facet slope $\beta$ is represented, which is the angle between the macroroughness normal and the facet normal.

But Graefe & Sandmann (2014) extended this distribution to account for the projected area of the facets. This area is proportional to the cosine of the incidence angle ($\cos(\delta)$) as shown in Figure 3.23.

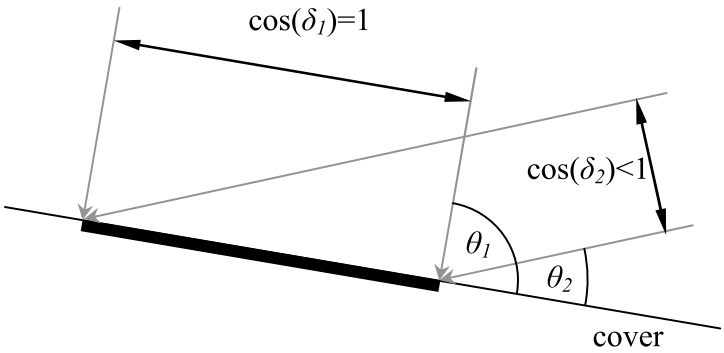


**Figure 3.23** Schematic of the proportionality of projected area (black arrows) of a cover facet (bold black line) for different zenith angles ($\theta_1$ and $\theta_2$) to the cosine of according incidence angles ($\delta_1$ and $\delta_2$).

Furthermore, they included a visibility function $V(\theta,\beta,\phi)$ as an additional factor into the Beckmann distribution. $V(\theta,\beta,\phi)$ is one for positive $\cos(\delta)$ and zero otherwise. Only a ray incidence from the facet upside will contribute to the computations (Figure 3.24).

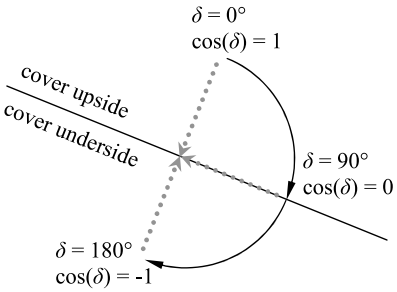


**Figure 3.24** Angle of incidence in the interval [0°, 180°] and the related cosines. Negative cosines occur only for angles of incidence > 90°, which means they arrive at the cover underside.

Graefe & Sandmann (2014) found that the fraction of direct radiation, which is transformed to diffuse radiation during penetration of the cover depends on light incidence angle (haze function). From the haze functions, plotted in their Figure 6, it can be seen, that most of incident direct radiation is transformed to diffuse radiation during penetration of the cover. As expected, FF covers transform a higher ratio of direct incident radiation into diffuse radiation during penetration of the cover. In contrary to NWF, for FF the increase of $\theta$ leads to a smooth increase of $\chi(\theta)$. As the sun approaches the horizon, $\chi(\theta)$ reaches almost 100 %.

The actual degree of cover roughness is broadly modified by plant growth. From Figure 9 in Graefe & Sandmann (2014) three growth stages A to C have been defined for kohlrabi (see Figure 4 in Graefe & Sandmann (2014)) and assigned to LAI thresholds. The surface roughness of the covers (NWF and FF) is at micro roughness during stage A until $LAI \approx 0.2$ for FF and $LAI \approx 0.6$ for NWF. Cover surface roughness reaches its maximum at $LAI \approx 0.8$ for FF and $LAI \approx 1.4$ for NWF and is decreasing fast with increasing $LAI$ from that point on.

### 3.3.3. Modeling the dry matter accumulation in kohlrabi

Dry matter accumulation is an important issue in plant growth modeling. Several model approaches were proposed in the past. Kage & Stützel (1999) simulated dry matter production in cauliflower as product of intercepted PAR by the canopy and its light use efficiency (LUE, mass of produced dry matter per received radiation portion) and connected this relationship with some other empirical submodels, which describe leaf number, vernalization and dry matter fractions per plant organ. LUE is also used by other authors for this purpose e.g. Amir & Sinclair (1991) for wheat and Tei et al. (1996)

for lettuce, onion and red beet. Using the results from the previously described submodels for leaf area growth and radiation transfer it is now possible to model the dry matter accumulation during vegetable production below covers in the field. One necessary input in this context is the absorbed radiation by the canopy $I_a$ , which is delivered by the model described in section 3.3.2 by additional calculations via the following equations:

$$I_a = I_{a,cy} + I^d_{a,cy}, \tag{3.8}$$

where absorbed direct radiation by the canopy $I_{a,cy}$ is estimated from

$$I_{a,cy} = I_{bc} \cdot \alpha_{cy}(\theta) \tag{3.9}$$

and absorbed diffuse radiation by the canopy $I^d_{a,cy}$ is estimated from

$$I^d_{a,cy} = \alpha^d_{cy} I^d_{bc}\left(1 + \rho^d_{cy}\rho^d_{cv}\right). \tag{3.10}$$

Absorptance coefficients of the canopy for direct and diffuse radiation ($\alpha_{cy}(\theta)$ and $\alpha^d_{cy}$) are outputs of the *JRC2S* canopy radiation transfer code (Pinty et al. 2006). Eq. (3.10) considers multiple interactions between canopy and soil and one to two reflection events from the cover.

Another important input variable is the air temperature below the cover $T_a$. For this thesis, $T_a$ was taken directly from measurements but it will be modelled in the future as well. Hourly values over the growing period were summed up and related to the measured plant dry matter $D$ of kohlrabi (including turnip) via linear regression analysis. The most straightforward model approach only takes the sum of $I_a$ into consideration:

$$D = b_1 \sum I_a + b_0, \tag{3.11}$$

where $b_0$ and $b_1$ are the estimates of regression constant and coefficient, correspondingly. Estimates for both parameters were $b_0 = 5.762$ and $b_1 = 0.173$, where $n = 21$, $R^2_{adj} = 0.583$ and $RMSE = 6.596\ g$ (Figure 3.25A). As this approach resulted in a non-satisfying prediction, several more complex relations were tested.

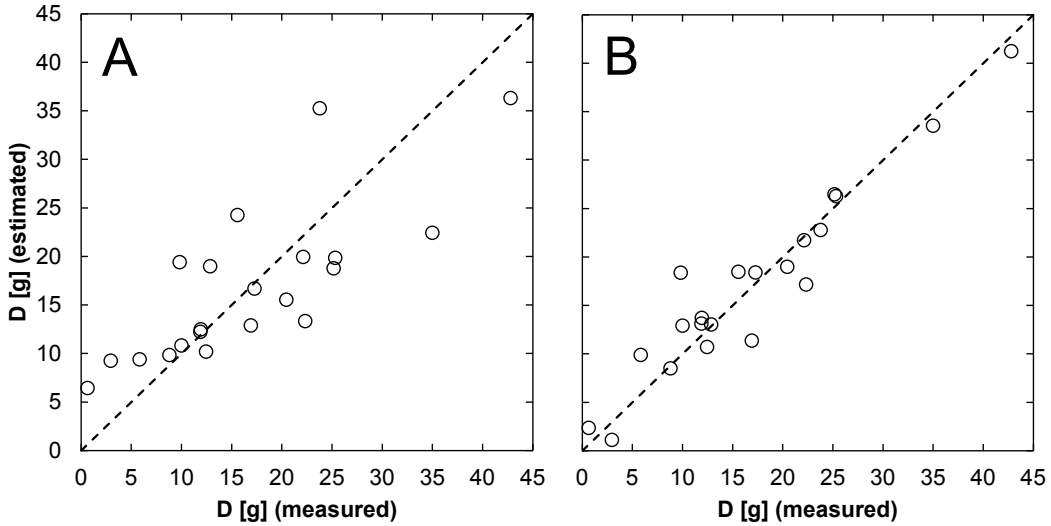


**Figure 3.25** Simulated against measured dry matter ($D$) of kohlrabi grown under non-woven fabric and a double layer consisting of non-woven fabric and perforated film. (A) Simplest model approach from Eq. (3.11), (B) Multiple linear regression approach from Eq. (3.12). Mean values per plot from intermediate and terminal harvests in Großbeeren (2010 to 2012), $n = 21$.

The most accurate results were obtained with the following model

$$D = b_1 \sum I_a + b_2 \sum I_a T_a + b_3 \sum I_a T_a^2 + b_4 \sum T_a \,. \tag{3.12}$$

From Figure 3.25B and Table 3.13 it can be seen, that this multiple linear regression approach without intercept estimates dry matter of kohlrabi using $I_a$ and $T_a$ as inputs quite precise ($RMSE = 3.3336\ g$, $R^2_{adj} = 0.9710$). All estimated parameters are significant different from zero as the p-values from t-tests and related confidence limits show (Table 3.13, $\alpha = 0.05$). The same approach, but with an additional intercept, resulted in a smaller $R^2_{adj}$ and the intercept parameter was not significant different from zero ($\alpha = 0.05$).

**Table 3.13** Results from the multiple linear regression model approach (Eq. (3.12)) for estimation of dry matter for kohlrabi. $b_1$ to $b_4$ are regression coefficients, $p$ is from t-test of regression coefficients, $n = 21$, $RMSE = 3.3336\ g$ and $R^2_{adj} = 0.9710$.

| Parameter | Estimate | Standard error | $p$ | Confidence limits ($\alpha = 0.05$) |
|---|---|---|---|---|
| $b_1$ | -1.8743 | 0.4116 | 0.0003 | [-2.7428; -1.0058] |
| $b_2$ | 0.2039 | 0.0388 | <0.0001 | [0.1250; 0.2888] |
| $b_3$ | -0.0048 | 0.0008 | <0.0001 | [-0.0065; -0.0030] |
| $b_4$ | 0.0006 | 0.0001 | 0.0002 | [0.0003; 0.0009] |

It was also tested whether the $CO_2$ content of the air below the cover influences dry matter accumulation. But no further improvement of performance was observed when $CO_2$ data were included to the model. These results show, that relative simple growth models can explain most of the variation in observed plant dry matter for kohlrabi, given that precise estimates of hourly absorbed radiation and temperature are available.

## 3.4. Modeling vegetable quality

Due to the fact that evaluation of plant quality is always influenced by subjectivity, it is no trivial task to precisely predict quality characteristics. Subjectivity introduces some kind of unsteadiness to the data. Therefore, it was necessary to simplify the problem to the fundamental question: Is the present plant marketable or not, if a distinct historically record of microclimate conditions has been received? To answer this question, many classification and regression methods are available, which are more or less complex. Three commonly used methods were chosen for the following analyses: LR, RF and SVM. They are described in more detail in chapters 2.3.2.1, 2.3.2.2 and 2.3.2.3, correspondingly. Intermediate quality scores (Table 2.4) were treated as non-marketable, because only for the score “1” it is certain that the scored plant is marketable. Whereas the objectification of quality scorings is a known prerequisite for the application of classification methods, not in all cases this precondition could be realized successfully. The processes leading to marketability or non-marketability are still unknown. Here it is attempted to reconnoiter the reason for the different ratios of marketable plants over the years at the tested sites (Figure 3.26).

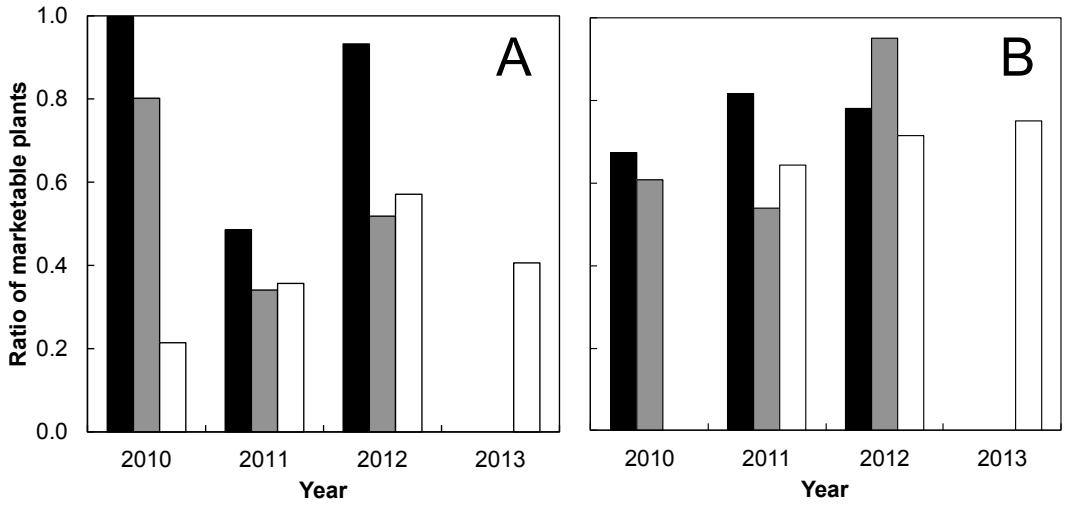


**Figure 3.26** Mean ratio of marketable plants grown without cover, under non-woven fabric and under a double layer cover consisting of non-woven fabric and perforated film where the perforated film was removed using different removal strategies for certain quality aspects. (A) Side shoots in lettuce. (B) Turnip form in kohlrabi. Black = Großbeeren, grey = Golzow, white = Schifferstadt.

### 3.4.1. Objectification of head consistency scorings

To get information about the precision of the scoring for head consistency, persons 2 and 3 repeated the scoring of 63 lettuce plants three times, each. In Figure 3.27 the mean range of the old scorings for each person is shown. The mean range was calculated as the mean of the differences between the highest and the lowest score given for each plant during the scoring repetitions. Mean scoring is the median of all scorings over both persons and all repetitions. Obviously the very soft and very hard lettuce heads were detected in every repetition. But true intermediate scorings had a much higher range. E.g. the eight lettuce plants which had the scoring five in median of all repetitions of both persons had a scoring range of about 2.5 units for both persons. Detection of extremes is easy, even for untrained persons, but it is very difficult to detect differences and to decide for a certain scoring unit, if there is a plant with a medium head consistency. Therefore, a reduction of the rating scheme as proposed in section 3.4, would generate a data set with distinct heteroscedasticity.

The comparison of the scorings of the experienced person 1 with the scorings of inexperienced persons 2 and 3 via a linear regression analysis yielded an $R^2_{adj} = 0.52$ and 0.68, respectively (Table 3.14). Considering the 95 % confidence limits, the regression coefficients where statistically significant different from 0 and the slopes of the obtained regression functions are not significantly different from 1 in both cases. So, there is a rather weak relationship between scorings of different

persons for the same plant. This fact is also supported by the relatively high $RMSE$ values (person 2: 1.7319, person 3: 1.4155), which arise mainly from the uncertainties in scoring at intermediate head consistencies (Figure 3.27 and Figure 3.28). The scoring-uncertainty for head consistency occurs not only within persons but also between them.

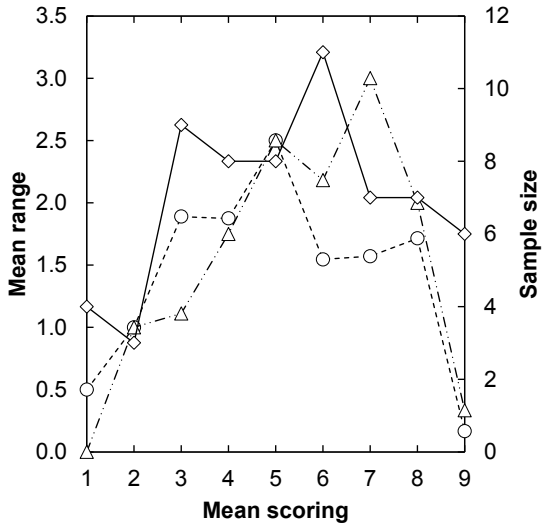


**Figure 3.27** Mean scoring range of repeated scorings for head consistency (circles = person 2, triangles = person 3) and the number of plants scored (diamonds) against mean scoring. Each plant was scored three times per person. Mean scoring is the median of all six scorings and was assumed to be the true head consistency. For scoring scheme see Table 2.4.

**Table 3.14** Results of linear regression analysis between scorings of the scoring experienced person 1 (independent variable) and scoring unexperienced persons 2 and 3 (dependent variables). $\alpha = 0.05$, CL = confidence limits, SE = standard error.

| Person | 2 | 3 |
|---|---|---|
| $n$ | 252 | 189 |
| $RMSE$ | 1.7319 | 1.4155 |
| $R^2_{adj}$ | 0.5240 | 0.6761 |
| Intercept | 0.1475 | -1.1161 |
| CL intercept | [-0.5020; 0.7969] | [-1.7300; -0.5022] |
| SE intercept | 0.3298 | 0.3112 |
| Slope | 0.9354 | 1.0515 |
| CL slope | [0.8248; 1.0461] | [0.9469; 1.1561] |
| SE slope | 0.0562 | 0.0530 |

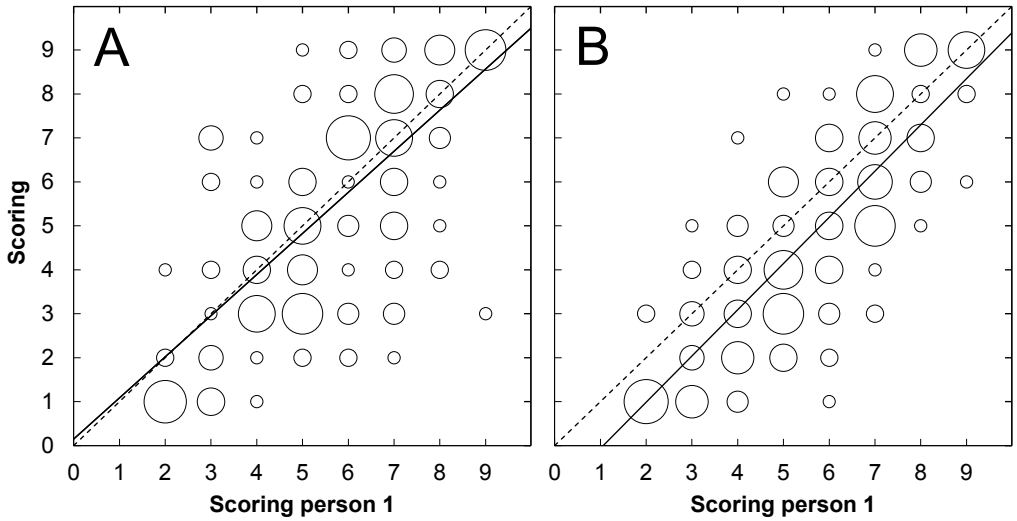


**Figure 3.28** Comparison of head consistency scorings, where person 1 is the reference. The bubble size indicates the number of identical data points (from 1 = small to 13 = large). A = person 2, B = person 3, solid line = linear regression function, dashed line = identity. For scoring scheme see Table 2.4.

The attempt of objectifying head consistency scoring through physically Instron measurements (see section 2.1.3.3) failed, as it can be seen clearly from Figure 3.29 and Table 3.15. In Figure 3.29 (D) a characteristic path force diagram, resulting from a lettuce head squeezing measurement, is presented. Due to the linear slope in the force region from 10 to 20 $N$, this data region was chosen to calculate a linear regression coefficient for each of the 63 lettuce heads. Other force regions were also tested but did not result in an increased estimation precision. The coefficients were then compared to the scorings of persons 1 to 3. The highest $R^2_{adj}$ (0.1778) was achieved by scoring unexperienced person 2, the lowest $R^2_{adj}$ (0.0679) was calculated for the scoring experienced person 1 (Table 3.15), whereas person 1 has the smallest RMSE (1.8902). This is still really high compared to the scoring scheme from 1 to 9. In Figure 3.29 (A), (B) and (C) the regression coefficients from linear regression analyses from Instron measurements are plotted against the scorings of persons 1, 2 and 3, separately. No relations are distinguishable. At least the positive regression coefficients, meaning that more force is necessary to squeeze a lettuce head with a higher scoring (hard) than for those with lower scorings (soft), are plausible.

**Table 3.15** Results of linear regression analysis between regression coefficients from Instron measurements (independent variable) and scorings of persons 1, 2 and 3 (dependent variables). $\alpha = 0.05$, CL = confidence limits, SE = standard error.

| Person | 1 | 2 | 3 |
|---|---|---|---|
| $n$ | 63 | 252 | 189 |
| $RMSE$ | 1.8902 | 2.2762 | 2.3766 |
| $R^2_{adj}$ | 0.0679 | 0.1778 | 0.0869 |
| Intercept | 2.8314 | 0.1661 | 1.0689 |
| CL intercept | [0.4765; 5.1863] | [-1.2304; 1.5626] | [-0.6175; 2.7554] |
| SE intercept | 1.1777 | 0.7091 | 0.8549 |
| Slope | 0.3889 | 0.7415 | 0.5228 |
| CL slope | [0.0577; 0.7201] | [0.5451; 0.9379] | [0.2856; 0.7599] |
| SE slope | 0.1656 | 0.0997 | 0.1202 |

This negative result was unexpected, but it shows, that manual determination of lettuce head consistency is relatively complex and may not be imitated sufficiently by a one dimensional squeeze of an Instron test facility. Furthermore, the results of the interpersonal comparisons have shown the variability of the given scoring. E.g. the nine plants that got the scoring six from reference person 1, were scored from two to nine by person 2 (where the scoring six was given only once in three scoring turns by person 2) and were scored from one to eight by person 3 (where the scoring six was given only five times in three scoring turns by person 3). Due to the stated uncertainties and the impossibility of objectifying head consistency scorings with the present data, further investigations with this quality indicator in lettuce were not performed.

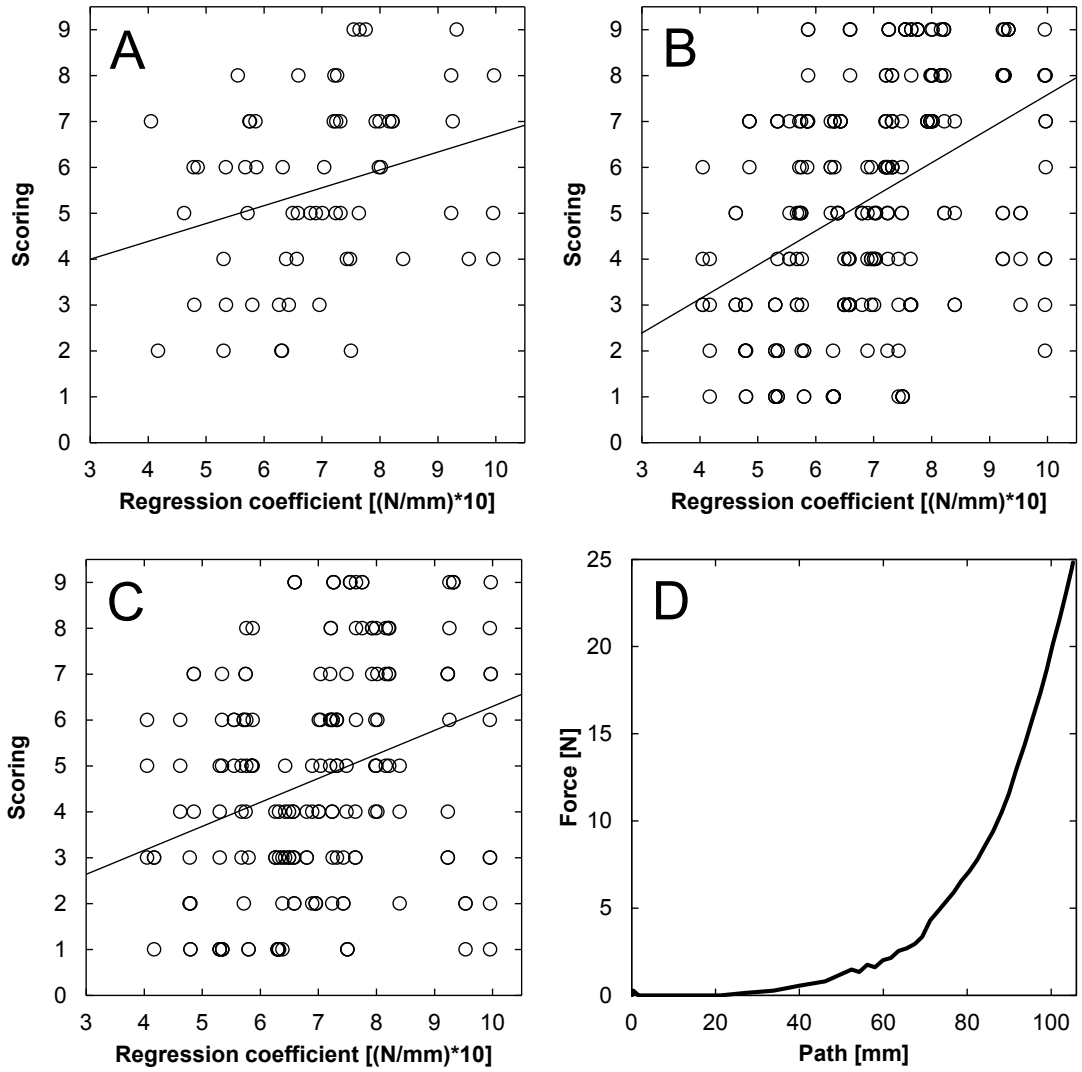


**Figure 3.29** Comparison of regression coefficients from Instron measurements and scorings of persons 1 (A), 2 (B) and 3 (C) for head consistency. D = Example for a squeeze path against squeeze force diagram from Instron measurements of lettuce. For scoring scheme see Table 2.4.

### 3.4.2. Modeling the presence of side shoots in lettuce

Side shoots in lettuce were modeled by the means of three different data mining methods (LR, RF and SVM), whose basic characteristics were described in sections 2.3.2.1, 2.3.2.2 and 2.3.2.3.

Depending on the incidence and development of side shoots, the lettuce plants were divided into marketable and non-marketable, where the new proposed scoring scheme (Table 2.4) was further simplified: intermediate plants were treated as non-marketable plants, so there were only two classes left. For the modeling process, the fraction of marketable plants per treatment and date was used as a reference, where an optimization procedure was carried out to find the threshold ratio $\tau$ for marketability. $\tau$ was found to be 0.9 for RF and SVM (criterion: lowest percentage of non-marketable

plants that were wrongly predicted as marketable ($p_f$)). As input variables the daily mean temperature of $n_d$ days before harvest and the sum of the daily mean temperatures prior that $n_d$ days lasting period are used for RF and SVM, where the summands of the temperature sum were restricted to be between $T_{min}$ and $T_{max}$. $T_{min}$ is the minimum temperature below which side shoot formation is constricted, because the lettuce plant grow is limited at all and $T_{max}$ is the maximum temperature above which the lettuce plant is limited, too. The summand is daily mean temperature minus $T_{min}$. In case the result is negative, then it is set to zero. The first four days after planting are neglected and the temperature sum has a maximum value, $\Sigma T_{max}$. $\Sigma T_{max}$ is interpreted as necessary for the lettuce plant to change from juvenile to adult growing stage, where there is assumed that side shoots cannot be formed in the juvenile phase. $\Sigma T_{max}$, $T_{min}$ and $T_{max}$ were parameterized simultaneously. Parameter optimization was carried out in two steps (Table 3.16). In the first step a relatively wide interval of parameter values along with coarse step sizes was chosen. However, RF and SVM were performed for all 540 possible parameter combinations and the best results (criterion: $p_f$) were used to refine parameter search intervals. In the second step smaller intervals and step sizes were used (Table 3.16) and again all 252 possible combinations were checked. The following parameter values were finally obtained: $\Sigma T_{max} = 300$, $T_{min} = 3$, $T_{max} = 12$ and $\tau = 0.9$. $n_d$ was fixed to 28.

**Table 3.16** Two step parameter search grid for maximum sum of daily mean temperature $\Sigma T_{max}$, minimum temperature $T_{min}$, maximum temperature $T_{max}$ and threshold $\tau$ which are involved in the marketability prediction of lettuce plants with regard to side shoot formation. Lower and upper limits of parameters search intervals and the step sizes are given.

| Parameter | First step of optimization | | | Second step of optimization | | |
|---|---|---|---|---|---|---|
| | Lower limit | Step size | Upper limit | Lower limit | Step size | Upper limit |
| $\Sigma T_{max}$ | 200 | 20 | 300 | 290 | 5 | 320 |
| $T_{min}$ | 2 | 1 | 6 | 2.5 | 0.5 | 3.5 |
| $T_{max}$ | 7 | 1 | 12 | 11.5 | 0.5 | 12.5 |
| $\tau$ | 0.7 | 0.1 | 0.9 | 0.8 | 0.05 | 0.95 |

For LR only the sum of mean temperature of the last $n_d$ days before harvest was used as input variable. Eq. (2.1) was used as linking function in the LR model.

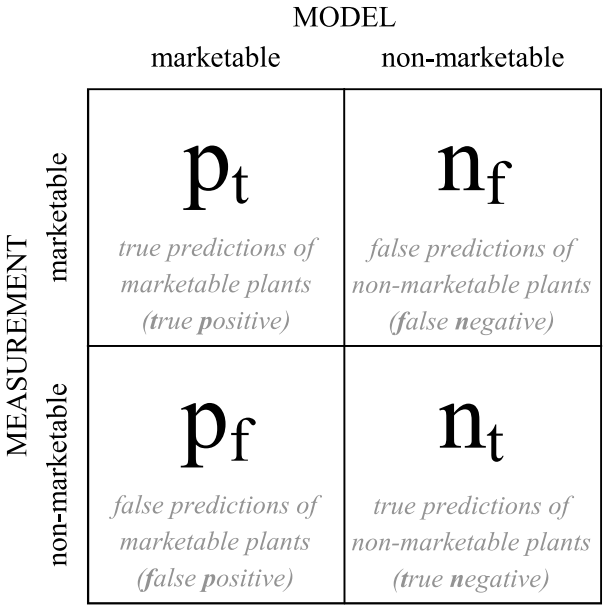


**Figure 3.30** Scheme of the four possible situations in classification problems.

Afterwards, $n_d$ was also varied from 1 to 28 for RF, SVM and LR. The results are summed up in Figure 3.31. As the most important measure $p_f$ (Figure 3.30) was taken, because in praxis the economic risk of declaring lettuce plants as marketable, which are actual non-marketable, is the most serious one. So $p_f$ should be minimized. In Figure 3.31 $p_f$ is represented by solid black lines. $p_f$ reaches for all methods values $< 0.1$. For RF it is smallest if data from $26\,d$ before harvest are included to the calculations, for SVM the minimum is reached for the first time with $n_d = 9\,d$ and for LR with $n_d = 11\,d$. At these values of $n_d$ the fraction of false predictions on non-marketable lettuce plants ($n_f$, Figure 3.30) also reaches values near its absolute minimum. Four different situations for the predictions are possible and they can be combined via

$$p_f + n_f + p_t + n_t = 1\,, \tag{3.13}$$

where $p_t$ and $n_t$ are the fractions of correctly predicted marketability and non-marketability of lettuce plants regarding side shoots (Figure 3.30), respectively. Logically, $p_f$ and $n_t$ show inverted graphs in Figure 3.31. The same fact is valid for $n_f$ and $p_t$.

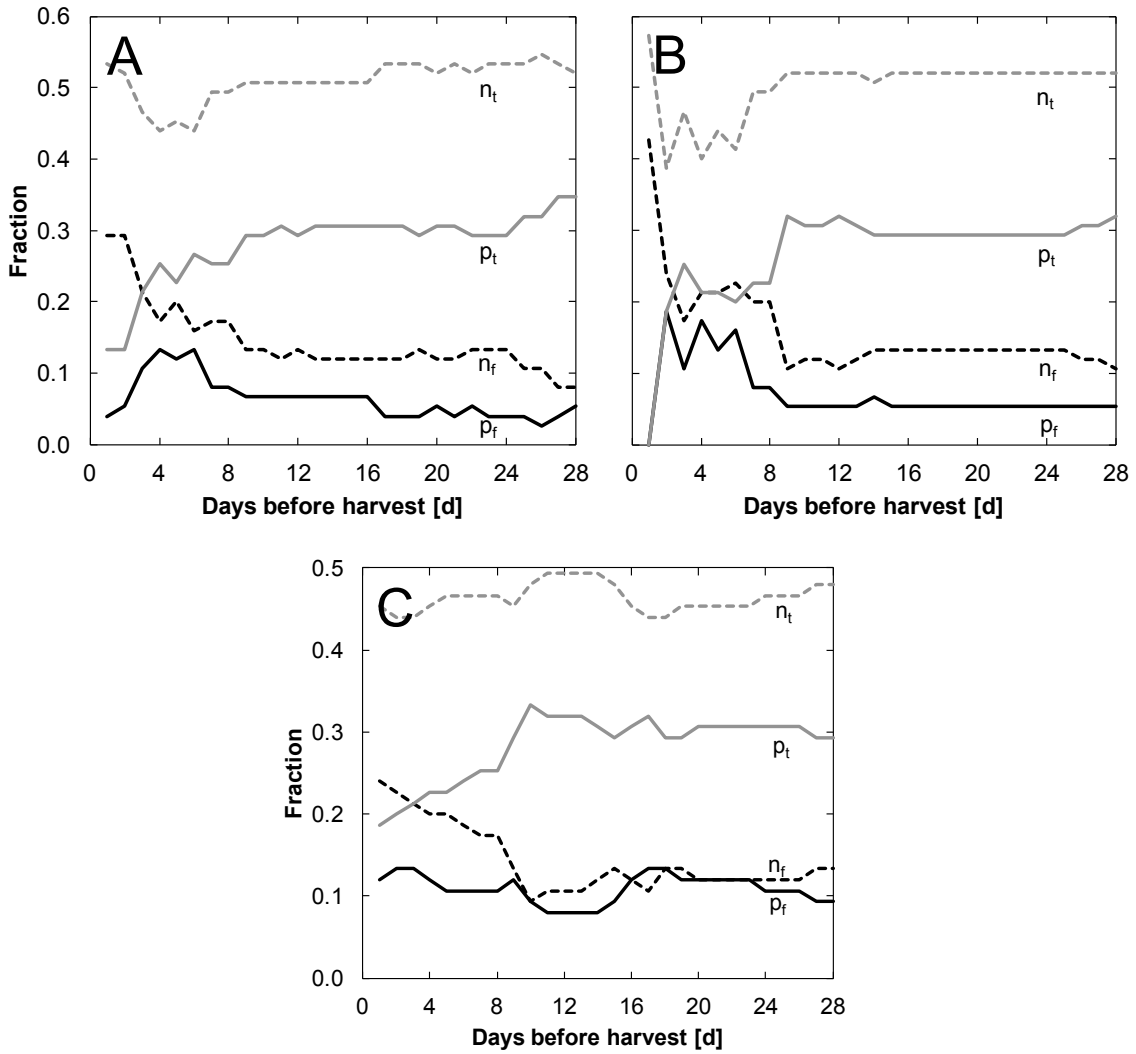


**Figure 3.31** Performance of marketability predictions of lettuce plants, regarding side shoots for three data mining methods: random forest (A), support vector machines (B) and logistic regression (C). The amount of input data was varied for this analysis (via the number of days before harvest). Black = fraction of false predictions, grey = fraction of true predictions, solid lines = marketable plants according to the model, dashed lines = non-marketable plants according to the model, $n = 75$ (one value per plot, data from all cover treatments and from Großbeeren, Golzow and Schifferstadt from 2010 to 2013), see Figure 3.30 for the meaning of the symbols.

Additionally $\tau$ for LR has to be found. In case of LR, $\tau$ is the probability of the LR model below which marketability is assumed and above which non-marketability is assumed, e.g. the output of LR is a fraction of non-marketable plants of 0.6. Here non-marketability is assumed for all plants grown under the conditions, which were the input of LR, if $\tau$ is lower than 0.6. It is commonly set to 0.5 (Backhaus et al. 2011). Both measured and modeled fractions of non-marketable plants were classified by the same $\tau$, which was varied from zero to one (Figure 3.32A). The lowest fractions of false predictions appeared for $\tau = 0.75$. In Figure 3.32B measured fractions of non-marketability of lettuce plants and the finally chosen LR model are presented. The parameters of the LR model are $\beta_0 =$

$-2.2671$ and $\beta_1 = 0.0187$, where the p-values from t-tests for both parameters are $< 0.001$. From Figure 3.32B the relatively small $R^2_{LR} = 0.1858$ is plausible. The residuals between modelled and measured values are relatively high but after the transformation into the two classes, the conformity is satisfactory. According to the logistic regression model the risk of non-marketable plants is increasing with increasing temperature sum (Figure 3.32B).

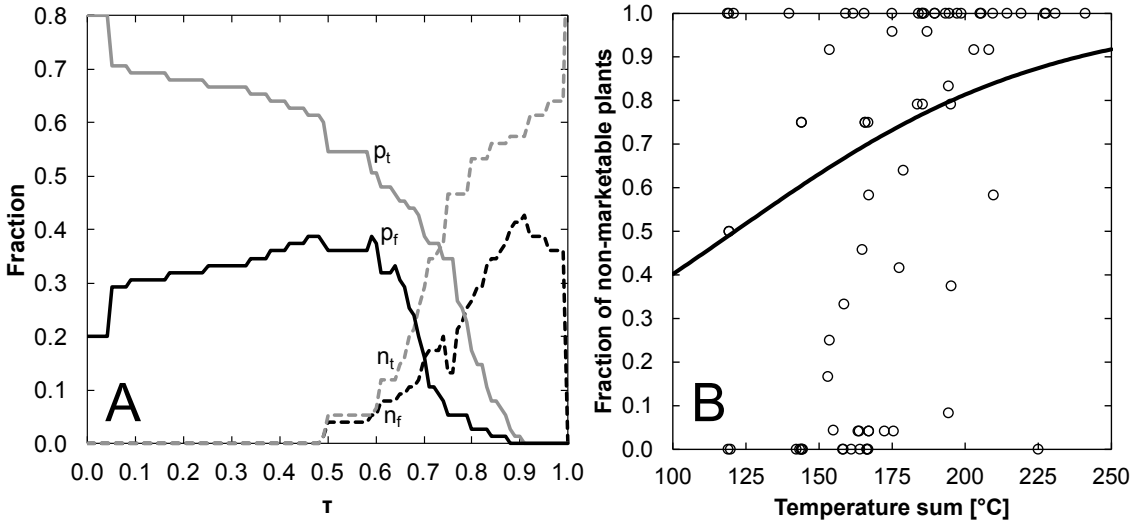


**Figure 3.32** (A) Performance of marketability predictions of lettuce plants as judged from side shoot formation using logistic regression for different decision thresholds ($\tau$). Black = fraction of false predictions, grey = fraction of true predictions, solid lines = marketable plants according to the model, dashed lines = non-marketable plants according to the model, $n_d = 11$, $n = 75$ (one value per plot, data from all cover treatments and from Großbeeren, Golzow and Schifferstadt from 2010 to 2013), see Figure 3.30 for the meaning of the symbols. (B) Fraction of non-marketable plants against sum of daily mean temperature of the last 11 days before harvest. Circles = measurements, black line = model from logistic regression, $\tau = 0.75$, $n_d = 11$, $n = 75$ (one value per plot, data from all cover treatments and from Großbeeren, Golzow and Schifferstadt from 2010 to 2013).

In Table 3.17 all fractions from Eq. (3.13) are presented for the three data mining methods. The best prediction is achieved by RF, where $p_f$ is the smallest for the three investigated methods (implying the highest $n_t$). $n_f$ of LR, RF and SVM are equal (implying an equal $p_t$). A disadvantage of RF is, that the method requires $n_d = 26\,d$ to reach the highest conformity between measured and modelled marketability-decisions, where LR and SVM reach their best results using $n_d = 11$ and 9, respectively. Comparing the performance of the three methods based on side shoot formation in lettuce, does not yield a distinct result. Which method should be preferred depends on whether the prediction is aimed to be as reliable as possible (than it would be RF) or it has to be a compromise

between reliability and less required input data. For the second case the decision would be rather tend to SVM because of a slightly lower value for $n_d$.

**Table 3.17** Fractions of true and false predictions of marketability (positive) and non-marketability (negative) of lettuce for three data mining methods (LR = logistic regression, RF = random forest, SVM = support vector machines, $p_t$ = true positive, $p_f$ = false positive, $n_t$ = true negative, $n_f$ = false negative, $n_d$ = number of days before harvest used for calculations, $n = 75$ (one value per plot, data from all cover treatments and from Großbeeren, Golzow and Schifferstadt from 2010 to 2013)).

| Method | $n_d$ | $p_t$ | $p_f$ | $n_t$ | $n_f$ |
|---|---|---|---|---|---|
| LR | 11 | 0.3200 | 0.0800 | 0.4933 | 0.1067 |
| RF | 26 | 0.3200 | 0.0267 | 0.5467 | 0.1067 |
| SVM | 9 | 0.3200 | 0.0533 | 0.5200 | 0.1067 |

### 3.4.3. Modeling the turnip form in kohlrabi

Modeling of turnip form in kohlrabi was done similar to the modeling of presence of side shoots in lettuce (section 3.4.2). Input data were the measured temperatures below the cover and the observed fractions of marketable plants from field trials in GB, GO and SC (2010-2012), resulting in a sample size of $n = 44$. The procedure of the stepwise parameterization of $\Sigma T_{max}$, $T_{min}$, $T_{max}$ and $\tau$ are given in Table 3.18. In the first step 180 parameter combinations and in a refined second step 560 parameter combinations were tested. Resulting parameter estimates are $\Sigma T_{max} = 280\ °C$, $T_{min} = 6\ °C$, $T_{max} = 15\ °C$ and $\tau = 0.6$.

**Table 3.18** Two step parameter search grid for maximum sum of daily mean temperature $\Sigma T_{max}$, minimum temperature $T_{min}$, maximum temperature $T_{max}$ and threshold $\tau$ which are involved in the marketability prediction of kohlrabi plants with regard to turnip form. Lower and upper limits of parameter search intervals and step sizes are given.

| Parameter | First step of optimization | | | Second step of optimization | | |
|---|---|---|---|---|---|---|
| | Lower limit | Step size | Upper limit | Lower limit | Step size | Upper limit |
| $\Sigma T_{max}$ | 100 | 100 | 300 | 280 | 10 | 320 |
| $T_{min}$ | 1 | 1 | 6 | 3 | 1 | 6 |
| $T_{max}$ | 7 | 5 | 17 | 12 | 1 | 18 |
| $\tau$ | 0.5 | 0.1 | 0.9 | 0.4 | 0.1 | 0.7 |

To find the minimum number of days necessary for sufficient predictions of marketability, the already found parameter estimates were used and the number of days integrated to the calculations was varied from 1 to 28. The results are presented in Figure 3.33. Surprisingly, RF needs data from just three days before harvest to predict the marketability with the same low error rate ($p_f = 0.0682$) as if 28 days were used. SVM reaches its minimum value of $p_f$ after 11 days and LR needs only eight days (Table 3.19).

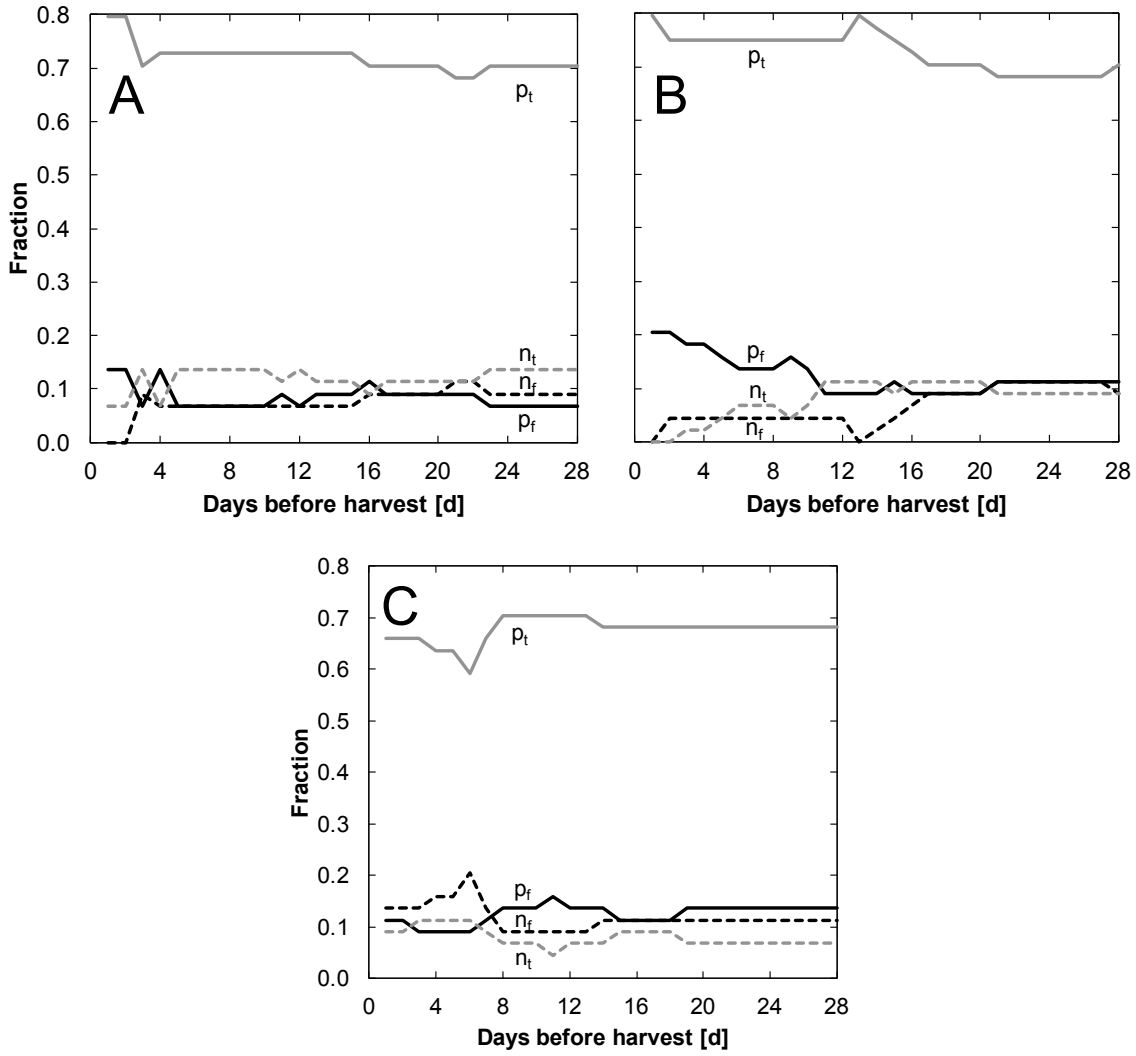


**Figure 3.33** Performance of marketability predictions of kohlrabi plants, regarding turnip form for three data mining methods: random forest (A), support vector machines (B) and logistic regression (C). The amount of input data was varied for this analysis (via the number of days before harvest). Black = fraction of false predictions, grey = fraction of true predictions, solid lines = marketable plants according to the model, dashed lines = non-marketable plants according to the model, $n = 44$ (one value per plot, data from all cover treatments and from Großbeeren, Golzow and Schifferstadt from 2010 to 2013), see Figure 3.30 for the meaning of the symbols.

Further investigations with LR revealed, that the overall $\tau = 0.6$ also is the optimum probability below which non-marketability is assumed using LR (Figure 3.34A). The parameters of the LR model are $\beta_0 = 5.5321$ and $\beta_1 = -0.0488$, where the p-values from t-tests for both parameters are $< 0.001$. Compared to side shoot formation in lettuce here again only a relatively small $R^2_{LR} = 0.2021$ is achieved. As Figure 3.34B shows, the model from LR is not well suited to predict the exact fraction of marketable plants or rather the exact risk of non-marketability. But from the general appearance of the curve it can be concluded, that increasing temperature sums lead to a decreasing fraction of marketable plants.

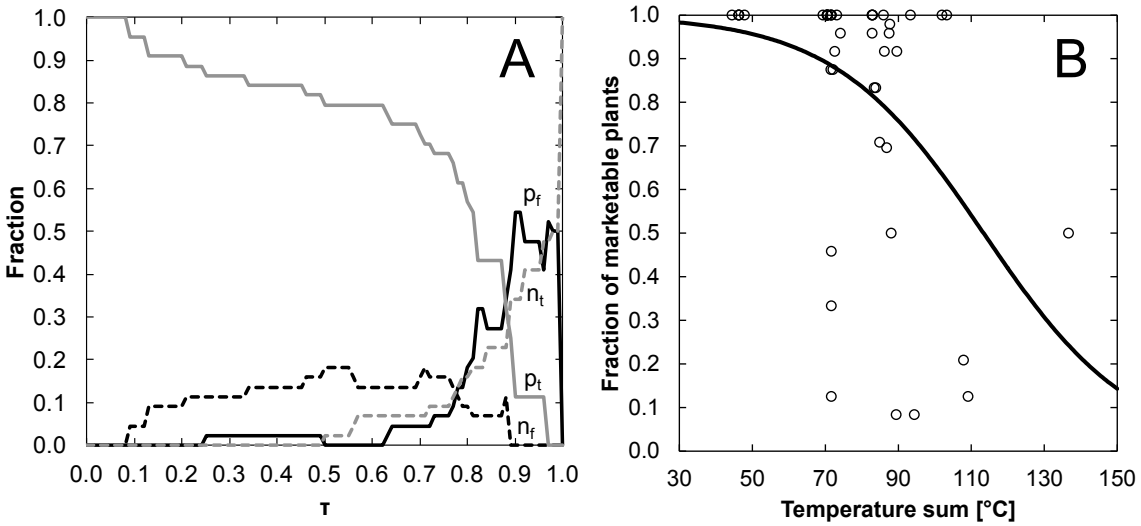


**Figure 3.34** (A) Performance of marketability predictions of kohlrabi plants, regarding turnip form for logistic regression, for different decision thresholds ($\tau$). Black = fraction of false predictions, grey = fraction of true predictions, solid lines = marketable plants according to the model, dashed lines = non-marketable plants according to the model, $n_d = 8$, $n = 44$ (one value per plot, data from all cover treatments and from Großbeeren, Golzow and Schifferstadt from 2010 to 2013), see Figure 3.30 for the meaning of the symbols. (B) Fraction of marketable plants against sum of daily mean temperature of the last 8 days before harvest. Circles = measurements, black line = model from logistic regression, $\tau = 0.6$, $n_d = 8$, $n = 44$ (one value per plot, data from all cover treatments and from Großbeeren, Golzow and Schifferstadt from 2010 to 2013).

But the more general absolute decision whether a kohlrabi plant is marketable or not can be done by the LR model with sufficient precision as the summarized data in Table 3.19 show. According to the fractions of false predictions of marketability, LR has the lowest precision ($p_f = 0.1136$) compared to the other methods. However, according to the fractions of false predictions of non-marketability, SVM reaches the lowest value, which is below 5 %. Integrated over all statistics in Table 3.19, one can say that RF provides the smallest amount of false predictions and uses only data from three days before

harvest for the prediction. LR has too many false predictions of non-marketability ($n_f = 0.1364$) and marketability ($p_f = 0.1136$), where SVM has too many false predictions of marketability, too, which is the main risk for vegetable growers.

**Table 3.19** Fractions of true and false predictions of marketability (positive) and non-marketability (negative) of kohlrabi for three data mining methods (LR = logistic regression, RF = random forest, SVM = support vector machines, $p_t$ = true positive, $p_f$ = false positive, $n_t$ = true negative, $n_f$ = false negative, $n_d$ = number of days before harvest used for calculations, $n = 44$ (one value per plot, data from all cover treatments and from Großbeeren, Golzow and Schifferstadt from 2010 to 2013)).

| Method | $n_d$ | $p_t$ | $p_f$ | $n_t$ | $n_f$ |
|---|---|---|---|---|---|
| LR | 3 | 0.6591 | 0.1136 | 0.0909 | 0.1364 |
| RF | 3 | 0.7045 | 0.0682 | 0.1364 | 0.0909 |
| SVM | 11 | 0.7500 | 0.0909 | 0.1136 | 0.0455 |

# 4. Conclusions

This thesis intends to establish the fundamentals for a more sophisticated model, which describes microclimate, plant growth and vegetable quality below plastic covers, than a currently rather simple model (section 1.2) which is in common use but fails in case of weather deviations from long to mid-term means. Several submodels for the aspired overall model were parameterized, which give the approach a scientifically more reliable foundation. Therefore it is reasonable to expect the overall model to be superior to the currently used model in terms of temperature predictions, plant growth and plant quality development.

During the first field trials, the need for a less time consuming method of LAI estimation became obvious. Therefore, potential useful methods were tested in an additional field trial. Sandmann et al. (2013) show that non-destructive methods of LAI estimation are suited for lettuce and kohlrabi although the tested methods were originally developed for LAI estimation in agricultural and forestall species with quite different morphology.

The simulation of leaf area growth (section 3.3.1) using a new developed model showed a species dependent difference. The prediction of leaf area seems to be easier for lettuce than for kohlrabi. Further work might be necessary for improvements of the performance, e.g. including a biochemical model which describes leaf gas exchange and photosynthetic activity as a crucial input variable for leaf area growth. One promising candidate for integration into the leaf area growth model might be the approach from Farquhar et al. (1980), which is still broadly utilized in photosynthesis modeling, although its origin dates back more than three decades.

A preliminary work towards the integration of a biochemical model is the parameterization of the stomata conductance model from Ball et al. (1987) in section 3.2.3. This model shows an intermediate performance with $R^2 > 0.7$, whereas parameterization has to be made separately for each combination of cover treatment and species. A possible reason might be the high sensitivity of the plants towards changing environmental conditions during leaf gas exchange measurements (e.g. incident radiation intensity and wind speed).

Graefe & Sandmann (2014) developed a model which describes the short wave radiation budget of film covered canopies sufficiently precise. The radiation model represents one of the two key-

components to describe the microclimate of the production system of vegetable production using plastics in the field in spring.

For the other key-component, a model for the air temperature below the cover materials, some preliminary work was conducted here by modeling the thermal conductivity of the soil (section 3.2.2), which is depending on the water status of the soil. This in turn can be modeled using the results from the parameterization of the soil water retention model and the soils unsaturated hydraulic conductivity model (sections 3.2.1.1 and 3.2.1.2). The radiation model might be considered as a second preliminary work for the air temperature model, because radiation absorptance by each compartment of the production system, which is one of the possible outputs of the model, influences the energy balance and therefore the air temperature, too.

Plant growth was not only modeled in the form of leaf area growth, but also as dry matter accumulation during the production process in the field (section 3.3.3). Dry matter could be estimated surprisingly precise for kohlrabi ($R^2 = 0.97$) by just using the air temperature below the cover and absorbed radiation by the plants. An expected significant influence of $CO_2$ content of the air below the cover could not be detected with the existent data.

Modeling of vegetable quality turned out to be more problematic than expected, due to strong subjectivity of quality scorings. As the process of objectification worked relatively well for side shoots in lettuce and turnip form in kohlrabi, which could be interpret as semi-quantitative characteristics, there is still not enough known about the true factors and processes leading to marketability or non-marketability. Therefore empirical model approaches were chosen for modeling of vegetable quality formation instead of mechanistic ones. Another constraint had to be made according to the data resolution: it had to be downscaled from the ordinal to the alternative scale (e.g. marketability: yes or no?). The proposed models in this thesis yielded low error probabilities for plants, which are identified as marketable by the model, but that are not marketable in fact: 0.03 to 0.05 based on side shoot criteria in lettuce and 0.07 to 0.09 based on turnip form in kohlrabi. Further research in this field should first concentrate on finding ways of measuring vegetable quality in an objective way and afterwards reveal and understand the inner processes leading to good or bad quality of the vegetables grown below plastic covers.

One fundamental aspect of an overall microclimatic model could not be realized within the bounds of this thesis: the energy balance of the production system, including the air temperature below the cover model. It will be left to future work to bring together the overall microclimatic model, the enhanced plant growth model and, if possible, the mechanistic vegetable quality model. The long-term objective should be the transfer of this work into praxis to enhance production safety e.g. via an online prediction service for points in time of cover removal and the development of vegetable quality.

# 5. Summary

Plastic film management is economically of importance for vegetable growing in the field in early spring, but the prediction of the best moment of removal of plastics from the crops is currently too imprecise to fulfill contemporary requirements in production safety (risk of quality losses). The broadly used approach for prediction is of empirical nature and is depending on current reference data from below covers, which are expensive to gather.

The aim of this thesis was to develop the scientific foundations for a more mechanistic model approach, based on the physical and biological understanding of the energy balance, plant growth and plant quality formation process below plastic covers in order to increase future production safety.

Field trials at three sites, with two species and several cover materials and removal strategies were carried out to gain data from plants and microclimate beneath and above covers for parameterization of new and established submodels. Additionally, laboratory experiments were performed to understand e.g. the optical properties of plastics, leaves and soil. Furthermore, a new method for determining leaf area index in lettuce and kohlrabi was adopted and established for a more efficient plant data collection (Sandmann et al. 2013).

As a result, several processes of vegetable production using plastic covers are now better understood and can be described mathematically and sufficiently precise, e.g. the short wave radiation budget (Graefe & Sandmann 2014), soil thermal and unsaturated hydraulic conductivity, soil water retention, leaf area growth, dry matter accumulation and stomata conductance.

Most, but not all aims of the thesis could be achieved. Further work will be necessary according to modeling of air temperature below the covers, leaf gas exchange and the development of a mechanistic approach for plant quality formation. Here, plant quality could only be modelled via an empirical approach, due to subjectively influenced data. Common plant quality data acquisition should be reconsidered to yield as much as possible objective values in the future.

On a medium term perspective, a completion and transfer of the new model into the praxis e.g. via an online based decision support system for the best moment of cover removal and a concurrently plant quality formation prediction, should be realized to strengthen commercial vegetable production.

Folienmanagement ist von wirtschaftlicher Bedeutung im Freiland-Gemüsebau im Frühjahr. Aber die Prognose des optimalen Zeitpunktes der Abnahme von Plastik-Abdeckungen vom Bestand ist mit den bereits verfügbaren Mitteln zu ungenau, um die heutigen Anforderungen an die Produktionssicherheit zu erfüllen (Risiko von Qualitätsverlusten). Der bislang allgemein verwendete empirische Ansatz hängt von jeweils aktuellen Referenzmessungen unter den Abdeckungen ab, welche kostspielig sind. Das Ziel dieser Arbeit war es, die wissenschaftlichen Grundlagen eines mehr mechanistischen Modellansatzes zu entwickeln, welcher auf dem physikalischen und biologischen Verständnis von Energiehaushalt, Pflanzenwachstum und den Prozessen der Qualitätsentwicklung unter den Abdeckungen beruht, um die zukünftige Produktionssicherheit zu verbessern. Feldversuche an drei Standorten mit zwei Spezies und mehreren Abdeck-Materialien und Abnahme-Strategien wurden durchgeführt, um Daten zum Pflanzenwachstum und Mikroklima unter und über der Abdeckung zu erhalten und neue sowie etablierte Untermodelle zu parametrisieren. Weiterhin wurden Laborversuche zum Verständnis z.B. der optischen Eigenschaften der Abdeckungen, Blätter und des Bodens ausgeführt. Außerdem wurde eine neue Methode zur Bestimmung des Blattflächenindex bei Kopfsalat und Kohlrabi geprüft und für die effiziente Erhebung der Pflanzendaten etabliert (Sandmann et al. 2013). Im Ergebnis können nun verschiedene Prozesse der Gemüseproduktion unter Abdeckungen besser verstanden und mit hinreichender Genauigkeit mathematisch beschrieben werden, z.B. Strahlungshaushalt (Graefe & Sandmann 2014), Wasserretention sowie Wärme- und Wasserleitfähigkeit des Bodens, Blattflächenwachstum, Trockenmassebildung und Stomata Leitfähigkeit. Zwar wurden die meisten, aber nicht alle Ziele der Arbeit erreicht. Weitere Arbeit ist notwendig für die Modellierung der Lufttemperatur unter der Abdeckung, den Gaswechsel der Blätter und die Entwicklung eines mechanistischen Ansatzes zur Beschreibung der Entwicklung der Pflanzenqualität. Hier konnte die Pflanzenqualität wegen der subjektiv beeinflussten Daten nur über einen empirischen Ansatz modelliert werden. Die übliche Erfassung der Pflanzenqualität sollte überdacht werden, um zukünftig möglichst objektive Werte zu erhalten. Mittelfristig sollte der neue Ansatz vervollständigt und z.B. über ein online gestütztes Entscheidungs-Unterstützungs-System für den besten Zeitpunkt der Abdeckungsabnahme bei gleichzeitiger Pflanzenqualitätsprognose in die Praxis überführt werden, um den kommerziellen Gemüsebau zu stärken.

# 6. Appendix

## 6.1. Experimental designs

### 6.1.1. Großbeeren 2010

| | | | | | | | | | | | |
|---|---|---|---|---|---|---|---|---|---|---|---|
| 41 | 61 | 71 | 11 | 21 | 31 | 51 | 72 | 62 | 12 | 52 *4 | 22 |
| 10 | 10 *3 | 10 | 10 *3 | 20 | 20 *3 | 20 | 20 *2,3 | 30 | 30 *3 | 30 | 30 *2,3 |
| 12 | 22 | 42 | 11 | 21 | 61 | 71 | 51 *4 | 41 *4 | 31 | 32 | 42 *4 |
| 52 | 32 | 72 | 62 | 11 | 21 | 31 | 41 *4 | 51 *4 | 61 | 72 | 32 |
| 22 | 62 | 12 | 52 | 71 | 42 *4 | 20 | 20 *4 | 20 | 20 *4 | 10 | 10 *4 |
| 51 | 21 | 61 | 11 | 52 *4 | 12 | 30 | 30 *4 | 30 | 30 *4 | 10 | 10 *4 |
| 62 | 42 | 32 | 22 | 71 | 41 | 31 | 72 | | | | |

Treatments

batch: dark = first batch, light = second batch (for planting dates see Table 2.2)

species: green = lettuce, yellow = kohlrabi

first numeral: cover treatment (1 = without cover, 2 = non-woven fabric, 3 = non-woven fabric + perforated film [FF], 4 = first fixed removal date of FF, 5 = second fixed removal date of FF, 6 = third fixed removal date of FF, 7 = fourth fixed removal date of FF [for exact dates see Table 2.2])

second numeral: number of replication (0 = main sensor measurement plots without intermediate harvests)

Sensors

next to the plots: wind speed (1x in 40 cm height)
air temperature (1x in 40 cm height)
relative air humidity (1x in 40 cm height)
$CO_2$ gas concentration (1x in 40 cm height)
PAR sensor (1x in 40 cm height)

*2: PAR line sensor at the soil (2x)

*3: soil temperature (2x in 5 cm depth and 2x 15 cm depth)
air temperature (2x in 10 cm height)
volumetric soil water content (2x in 0-30 cm depth)
relative air humidity (1x in 10 cm height)
$CO_2$ gas concentration (1x in 10 cm height)

*4: air temperature (2x in 10 cm height)

### 6.1.2. Großbeeren 2011

| | | | | | | | | | | | |
|---|---|---|---|---|---|---|---|---|---|---|---|
| 21 | 12 | 22 | 42 *4 | 62 | 31 | 32 | 52 *4 | 71 | 41 | 61 | 72 |
| 20 | 20 *2,3 | 10 | 10 *3 | 30 | 30 *2,3 | 20 | 20 *3 | 10 | 10 *3a | 30 | 30 *3b |
| 11 | 51 | 21 | 42 | 72 | 41 *4 | 51 | 31 | 22 | 32 | 12 | 52 *4 |
| 71 | 61 | 11 | 62 | 51 *4 | 61 | 32 | 52 | 12 | 41 *4 | 31 | 21 |
| 72 | 71 | 22 | 62 | 11 | 42 | 30 | 30 *4 | 20 | 20 *4 | 30 | 30 *4 |
| 51 *4 | 71 | 21 | 72 | 22 | 32 | 10 | 10 *4 | 10 | 10 *4 | 20 | 20 *4 |
| 62 | 41 *4 | 52 | 12 | 11 | 61 | 42 | 31 | | | | |

Treatments

batch: dark = first batch, light = second batch (for planting dates see Table 2.2)

species: green = lettuce, yellow = kohlrabi

first numeral: cover treatment (1 = without cover, 2 = non-woven fabric, 3 = non-woven fabric + perforated film [FF], 4 = first fixed removal date of FF, 5 = second fixed removal date of FF, 6 = third fixed removal date of FF, 7 = fourth fixed removal date of FF [for exact dates see Table 2.2])

second numeral: number of replication (0 = main sensor measurement plots without intermediate harvests)

Sensors

next to the plots: wind speed (1x in 40 cm height)
air temperature (1x in 40 cm height)
relative air humidity (1x in 40 cm height)
$CO_2$ gas concentration (1x in 40 cm height)
PAR line sensor (1x in 40 cm height)

*2: PAR line sensor at the soil (2x)

*3: soil temperature (2x in 5 cm depth and 2x 15 cm depth)
air temperature (2x in 10 cm height)
volumetric soil water content (2x in 0-30 cm depth)
relative air humidity (1x in 10 cm height)
$CO_2$ gas concentration (1x in 10 cm height)

*3a: same as *3 except: volumetric soil water content (3x in 0-30 cm depth)

*3b: same as *3 except: none volumetric soil water content

*4: air temperature (2x in 10 cm height)

### 6.1.3. Großbeeren 2012

| | | | | | | | | | | | |
|---|---|---|---|---|---|---|---|---|---|---|---|
| 52 | 41 *4 | 71 *4 | 51 *4 | 21 *4 | 22 | 11 *4 | 12 | 62 | 42 | 32 | 61 *4 |
| 10 *3 | 10 *3a | 10 *3,5 | 10 *3,5 | 80 *3b,5 | 80 *3b,5a | 20 *3 | 20 *2,3 | 20 *3,5 | 20 *3,5b | 80 *3 | 80 *2,3 |
| 62 | 31 *4 | 21 *4 | 61 *4 | 11 *4 | 51 *4 | 31 *4 | 72 | 80 *6 | 10 *6 | 20 *6 | |
| 42 | 72 | 12 | 71 *4 | 41 *4 | 22 | 52 | 32 | 80 *6 | 10 *6 | 20 *6 | |

Treatments

batch: only one batch (for planting date see Table 2.2)

species: green = lettuce, yellow = kohlrabi

first numeral: cover treatment (1 = without cover, 2 = non-woven fabric, 3 = non-woven fabric + perforated film [FF] with removal after occurrence of quality losses, 4 = removal of FF if $\Sigma T_{max} \geq 200°C$ (sum of the daily maximum temperatures in 2 m height since planting), 5 = removal of FF if $\Sigma T_{max} \geq 300°C$, 6 = removal of FF if $\Sigma T_{max} \geq 400°C$, 7 = removal of FF if $\Sigma T_{max} \geq 500°C$, 8 = without removal of FF [for exact dates see Table 2.2])

second numeral: number of replication (0 = main sensor measurement plots without intermediate harvests)

Sensors

next to the plots: wind speed (1x in 40 cm height)
air temperature (1x in 40 cm height)
relative air humidity (1x in 40 cm height)
$CO_2$ gas concentration (1x in 40 cm height)
PAR line sensor (1x in 40 cm height)
diffuse fraction of PAR (1x in 1m height)

*2: PAR line sensor at the soil (2x)

*3: soil temperature (1x in 5 cm depth and 1x 15 cm depth)
air temperature (2x in 10 cm height)
volumetric soil water content (1x in 0-30 cm depth)
relative air humidity (1x in 10 cm height)
$CO_2$ gas concentration (1x in 10 cm height)

*3a: same as *3 except: volumetric soil water content (2x in 0-30 cm depth)

*3b: same as *3 except: none volumetric soil water content

*4: air temperature (2x in 10 cm height)

*5: surface temperature of lettuce (3x)

*5a, *5b: same as *5 except: air flow (3x in 10 cm height, weekly alternation between *5a and *5b)

*6: gas exchange (2x portable systems, twice a week)

### 6.1.4. Golzow 2010

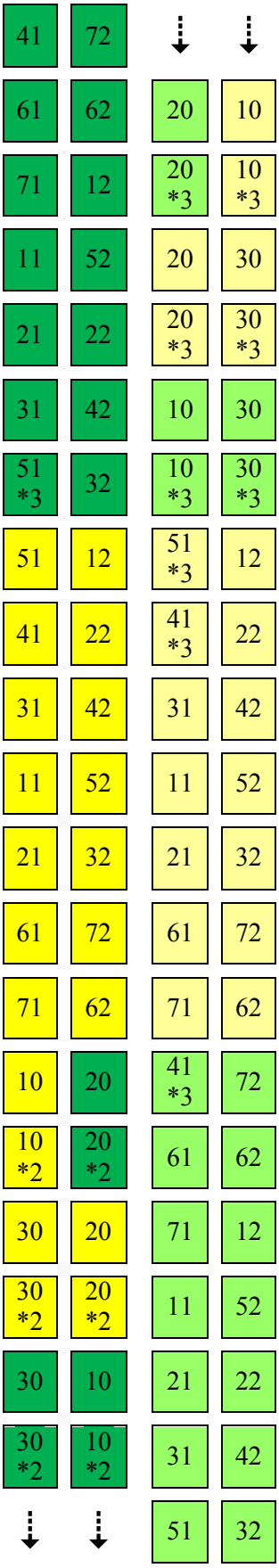


Treatments

batch: dark = first batch, light = second batch (for planting dates see Table 2.2)

species: green = lettuce, yellow = kohlrabi

first numeral: cover treatment (1 = without cover, 2 = non-woven fabric, 3 = non-woven fabric + perforated film [FF], 4 = first fixed removal date of FF, 5 = second fixed removal date of FF, 6 = third fixed removal date of FF, 7 = fourth fixed removal date of FF [for exact dates see Table 2.2])

second numeral: number of replication (0 = main sensor measurement plots without intermediate harvests)

Sensors

next to the plots: wind speed (1x in 40 cm height)
air temperature (1x in 40 cm height)
relative air humidity (1x in 40 cm height)
PAR sensor (1x in 40 cm height)

*2: soil temperature (2x in 5 cm depth and 2x 15 cm depth)
air temperature (2x in 10 cm height)
relative air humidity (1x in 10 cm height)

*3: air temperature (2x in 10 cm height)

### 6.1.5. Golzow 2011

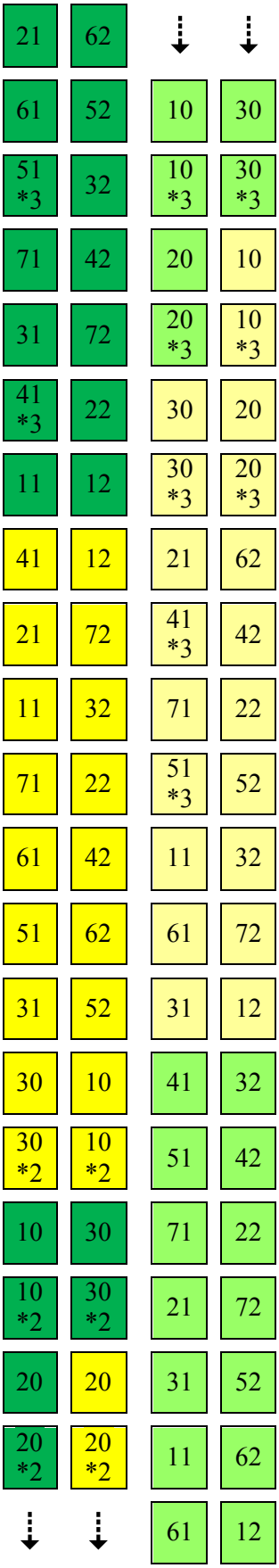


Treatments

batch: dark = first batch, light = second batch (for planting dates see Table 2.2)

species: green = lettuce, yellow = kohlrabi

first numeral: cover treatment (1 = without cover, 2 = non-woven fabric, 3 = non-woven fabric + perforated film [FF], 4 = first fixed removal date of FF, 5 = second fixed removal date of FF, 6 = third fixed removal date of FF, 7 = fourth fixed removal date of FF [for exact dates see Table 2.2])

second numeral: number of replication (0 = main sensor measurement plots without intermediate harvests)

Sensors

next to the plots: wind speed (1x in 40 cm height)
air temperature (1x in 40 cm height)
relative air humidity (1x in 40 cm height)
PAR sensor (1x in 40 cm height)

*2: soil temperature (2x in 5 cm depth and 2x 15 cm depth)
air temperature (2x in 10 cm height)
relative air humidity (1x in 10 cm height)

*3: air temperature (2x in 10 cm height)

### 6.1.6. Golzow 2012

| | |
|---|---|
| 21 *3 | 12 *3 |
| 41 *3 | 42 |
| 51 | 22 |
| 61 *3 | 62 |
| 31 | 32 *3 |
| 71 | 72 *3 |
| 11 | 52 *3 |
| 31 *3 | 42 *3 |
| 41 | 32 |
| 61 | 52 |
| 11 *3 | 12 |
| 21 | 22 *3 |
| 51 *3 | 72 |
| 71 *3 | 62 *3 |
| 80 *2 | 80 *2 |
| 80 *2a | 80 *2a |
| 20 *2 | 20 *2 |
| 20 *2a | 20 *2a |
| 10 *2 | 10 *2 |
| 10 *2a | 10 *2a |

Treatments

batch: only one batch (for planting dates see Table 2.2)

species: green = lettuce, yellow = kohlrabi

first numeral: cover treatment (1 = without cover, 2 = non-woven fabric, 3 = non-woven fabric + perforated film [FF] with removal after occurrence of quality losses, 4 = removal of FF if $\Sigma T_{max} \geq 200°C$ (sum of the daily maximum temperatures in 2 m height since planting), 5 = removal of FF if $\Sigma T_{max} \geq 300°C$, 6 = removal of FF if $\Sigma T_{max} \geq 400°C$, 7 = removal of FF if $\Sigma T_{max} \geq 500°C$, 8 = without removal of FF [for exact dates see Table 2.2])

second numeral: number of replication (0 = main sensor measurement plots without intermediate harvests)

Sensors

next to the plots: wind speed (1x in 40 cm height)
air temperature (1x in 40 cm height)
relative air humidity (1x in 40 cm height)
PAR sensor (1x in 40 cm height)

*2: soil temperature (1x in 5 cm depth and 1x 15 cm depth)
air temperature (1x in 10 cm height)

*2a: same as *2 except: relative air humidity (1x in 10 cm height)

*3: air temperature (2x in 10 cm height)

### 6.1.7. Schifferstadt 2010

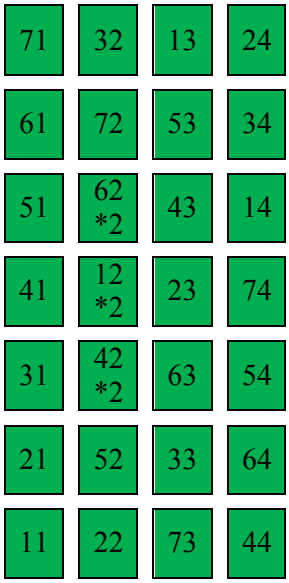


Treatments

batch: only one batch (for planting dates see Table 2.2)

species: green = lettuce (only one species)

first numeral: cover treatment (1 = non-woven fabric, 2 = non-woven fabric + perforated film [FF] with removal of FF if $\Sigma T_{max} \geq 200$°C (sum of the daily maximum temperatures in 2 m height since planting), 3 = removal of FF if $\Sigma T_{max} \geq 300$°C, 4 = removal of FF if $\Sigma T_{max} \geq 400$°C, 5 = removal of FF if $\Sigma T_{max} \geq 200$°C and at least 3 h with >30°C below FF, 6 = removal of FF if $\Sigma T_{max} \geq 500$°C, 7 = removal of FF if $\Sigma T_{max} \geq 200$°C and at least 3 h with >35°C below FF [for exact dates see Table 2.2])

second numeral: number of replication

Sensors

*2: soil temperature (2x in 5 cm depth)
air temperature (2x in 10 cm height)

### 6.1.8. Schifferstadt 2011

| | | | |
|---|---|---|---|
| 71 | 32 *2 | 13 *2 | 24 |
| 61 | 72 *2 | 53 | 34 |
| 51 | 62 | 43 | 14 |
| 41 | 12 *2 | 23 *2 | 74 |
| 31 | 42 | 63 | 54 |
| 21 | 52 | 33 *2 | 64 |
| 11 | 22 *2 | 73 *2 | 44 |
| 71 | 32 *2 | 13 *2 | 24 |
| 61 | 72 *2 | 53 | 34 |
| 51 | 62 | 43 | 14 |
| 41 | 12 *2 | 23 *2 | 74 |
| 31 | 42 | 63 | 54 |
| 21 | 52 | 33 *2 | 64 |
| 11 | 22 *2 | 73 *2 | 44 |

Treatments

batch: only one batch (for planting dates see Table 2.2)

species: green = lettuce, yellow = kohlrabi

first numeral: cover treatment (1 = without cover, 2 = non-woven fabric, 3 = perforated film, 4 = non-woven fabric + perforated film [FF] with removal of FF if $\Sigma T_{max} \geq$ 300°C (sum of the daily maximum temperatures in 2 m height since planting), 5 = removal of FF if $\Sigma T_{max} \geq$ 200°C and at least 3 h with >30°C below FF, 6 = removal of FF if $\Sigma T_{max} \geq$ 200°C and at least 3 h with >35°C below FF, 7 = removal of FF if $\Sigma T_{max} \geq$ 500°C [for exact dates see Table 2.2])

second numeral: number of replication

Sensors

*2: soil temperature (2x in 5 cm depth)
air temperature (2x in 10 cm height)

### 6.1.9. Schifferstadt 2012

| | | | |
|---|---|---|---|
| 71 | 32 *2 | 13 *2 | 24 |
| 61 | 72 *2 | 53 | 34 |
| 51 | 62 | 43 | 14 |
| 41 | 12 *2 | 23 *2 | 74 |
| 31 | 42 | 63 | 54 |
| 21 | 52 | 33 *2 | 64 |
| 11 | 22 *2 | 73 *2 | 44 |
| 71 | 32 *2 | 13 *2 | 24 |
| 61 | 72 *2 | 53 | 34 |
| 51 | 62 | 43 | 14 |
| 41 | 12 *2 | 23 *2 | 74 |
| 31 | 42 | 63 | 54 |
| 21 | 52 | 33 *2 | 64 |
| 11 | 22 *2 | 73 *2 | 44 |

Treatments

batch: only one batch (for planting dates see Table 2.2)

species: green = lettuce, yellow = kohlrabi

first numeral: cover treatment (1 = without cover, 2 = non-woven fabric, 3 = perforated film, 4 = non-woven fabric + perforated film [FF] with removal of FF if $\Sigma T_{max} \geq$ 300°C (sum of the daily maximum temperatures in 2 m height since planting), 5 = removal of FF if $\Sigma T_{max} \geq$ 200°C and at least 3 h with >30°C below FF, 6 = removal of FF if $\Sigma T_{max} \geq$ 200°C and at least 3 h with >35°C below FF, 7 = removal of FF if $\Sigma T_{max} \geq$ 500°C [for exact dates see Table 2.2])

second numeral: number of replication

Sensors

*2: soil temperature (2x in 5 cm depth)
air temperature (2x in 10 cm height)

### 6.1.10. Schifferstadt 2013

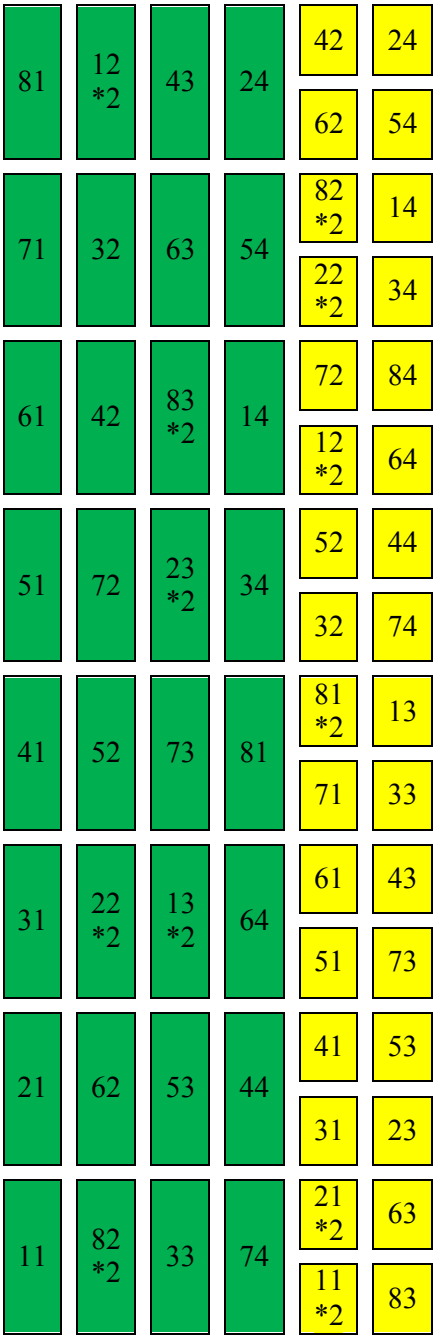


Treatments

batch: only one batch (for planting dates see Table 2.2)

species: green = lettuce, yellow = kohlrabi

first numeral: cover treatment
(1 = without cover,
2 = non-woven fabric,
3 = non-woven fabric + perforated film [FF] with removal of FF if $\Sigma T_{max} \geq 300°C$ (sum of the daily maximum temperatures in 2 m height since planting),
4 = removal of FF if $\Sigma T_{max} \geq 200°C$ and at least 3 h with >30°C below FF,
5 = removal of FF if $\Sigma T_{max} \geq 250°C$,
6 = removal of FF if $\Sigma T_{max} \geq 150°C$,
7 = removal of FF if $\Sigma T_{max} \geq 350°C$,
8 = removal of FF if $\Sigma T_{max} \geq 400°C$ [for exact dates see Table 2.2])

second numeral: number of replication

Sensors

*2: soil temperature (2x in 5 cm depth)
air temperature (2x in 10 cm height)

## 6.2. Plot designs

### 6.2.1. Großbeeren

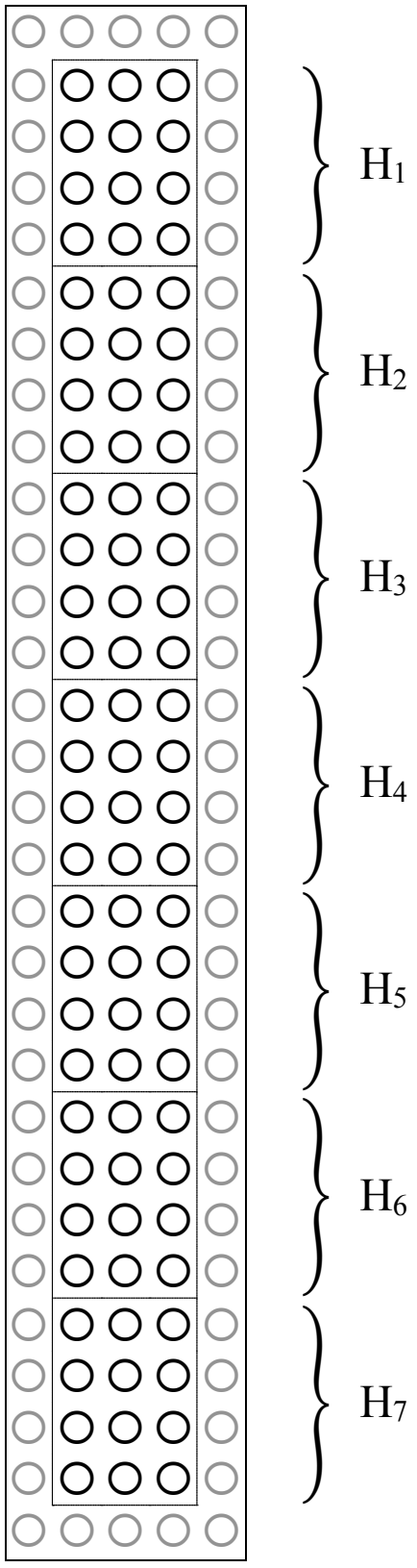


- five rows and thirty plants per row
- 150 plants per plot
- circles in the sketch represent plants
- border plants (grey circles) were not used for intermediate harvests
- $H_1$ to $H_7$ in the dashed frames are plants for up to seven intermediate harvests
- regular planting grid (30 $cm$ between rows and 30 $cm$ between plants within the rows)

### 6.2.2. Golzow

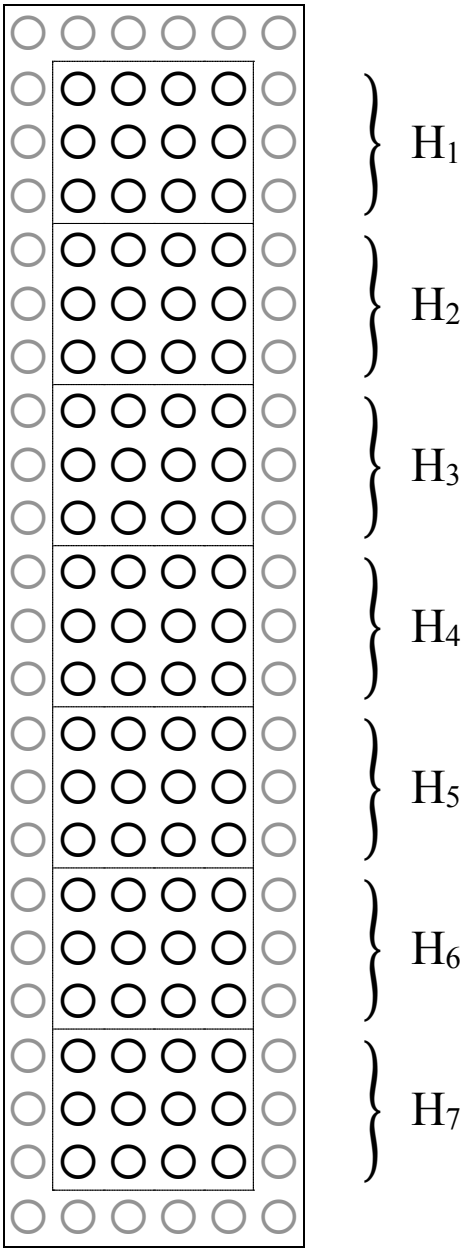


- six rows and 23 plants per row
- 138 plants per plot
- circles in the sketch represent plants
- border plants (grey circles) were not used for intermediate harvests
- $H_1$ to $H_7$ in the dashed frames are plants for up to seven intermediate harvests
- regular planting grid (30 $cm$ between rows and 30 $cm$ between plants within the rows)

### 6.2.3. Schifferstadt

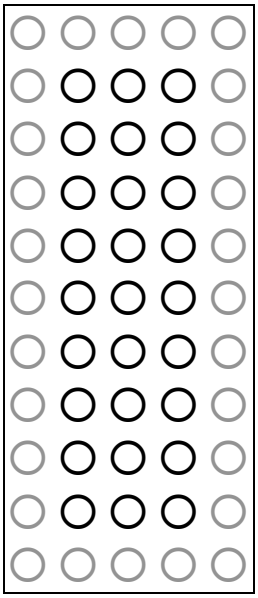

- five rows and eleven plants per row
- 55 plants per plot
- circles in the sketch represent plants
- border plants (grey circles) were not used for the terminal harvest
- regular planting grid (30 $cm$ between rows and 30 $cm$ between plants within the rows)
- in 2013 there were only nine plants per column

# 7. References


Alvensleben, R. (2000) Verbraucherpräferenzen für regionale Produkte: Konsumtheoretische Grundlagen. *agrarspectrum*, 30, 3-18.

Amir, J. & Sinclair, T.R. (1991) A Model of the Temperature and Solar-Radiation Effects on Spring Wheat Growth and Yield. *Field Crops Research*, 28, 47-58.

Backhaus, K., Erichson, B., Plinke, W. & Weiber, R. (2011) *Multivariate Analysemethoden - Eine anwendungorientierte Einführung*. Springer-Verlag: Berlin.

Ball, J., Woodrow, I. & Berry, J. (1987) A model predicting stomatal conductance and its contribution to the control of photosynthesis under different environmental conditions. *In:* J Biggins, *Progress in Photosynthesis Research*. Martinus Nijhoff: Leiden, The Netherlands, 221-224.

Beck, M. & Kleber, J. (2014) Grundlage Freiland-Bewässerung: so wird gesteuert. *Gemüse*, 50, 47-48.

Bernacchi, C.J., Singsaas, E.L., Pimentel, C., Portis, A.R. & Long, S.P. (2001) Improved temperature response functions for models of Rubisco-limited photosynthesis. *Plant Cell and Environment*, 24, 253-259.

Blume, H.P., Brümmer, G.W., Schwetmann, U., Horn, R., Kögel-Knabner, I., Stahr, K., Auerswald, K., Beyer, L., Hartmann, A., Litz, N., Scheinost, A., Stanjek, H., Welp, G. & Wilke, B.M. (2002) *Scheffer/Schachtschabel - Lehrbuch der Bodenkunde*. Springer: Heidelberg.

Boswell, D. (2002) Introduction to Support Vector Machines. 1-15.

Breiman, L. (2001) Random forests. *Machine Learning*, 45, 5-32.

Burges, C.J.C. (1998) A tutorial on Support Vector Machines for pattern recognition. *Data Mining and Knowledge Discovery*, 2, 121-167.

Campbell Scientific Inc.USA. (2011) *CS616 and CS625 Water Content Reflectometers - Instruction Manual*.

Campbell, G.S. (1986) Extinction Coefficients for Radiation in Plant Canopies Calculated Using An Ellipsoidal Inclination Angle Distribution. *Agricultural and Forest Meteorology*, 36, 317-321.

Campbell, G.S. (1990) Derivation of An Angle Density-Function for Canopies with Ellipsoidal Leaf Angle Distributions. *Agricultural and Forest Meteorology*, 49, 173-176.

Campbell, G.S. & van Evert, F.K. (1994) Light interception by plant canopies: efficiency and architecture. *In:* J.L.Monteith et al., *Resource Capture by Crops*. Nottingham University Press: Nottingham, 35-52.

Cortes, C. & Vapnik, V. (1995) Support-Vector Networks. *Machine Learning*, 20, 273-297.

Dervishi, S. & Mahdavi, A. (2012) Computing diffuse fraction of global horizontal solar radiation: A model comparison. *Solar Energy*, 86, 1796-1802.

Dietterich, T.G. (2000) An experimental comparison of three methods for constructing ensembles of decision trees: Bagging, boosting, and randomization. *Machine Learning*, 40, 139-157.

Durner, W. (1994) Hydraulic Conductivity Estimation for Soils with Heterogeneous Pore Structure. *Water Resources Research*, 30, 211-223.

Erbs, D.G., Klein, S.A. & Duffie, J.A. (1982) Estimation of the Diffuse-Radiation Fraction for Hourly, Daily and Monthly-Average Global Radiation. *Solar Energy*, 28, 293-302.

Farquhar, G.D., Caemmerer, S.V. & Berry, J.A. (1980) A Biochemical-Model of Photosynthetic Co2 Assimilation in Leaves of C-3 Species. *Planta*, 149, 78-90.

Fink, M. (2009) Prognose der Temperatur unter Bedeckungen. *Interner Forschungsbericht im Rahmen der Zusammenarbeit von Leibniz-Institut für Gemüse- und Zierpflanzenbau und Dienstleistungszentrum ländlicher Raum Rheinpfalz*.

Goudriaan, J. (1977) *Crop micrometeorology: a simulation study*. Centre for Agricultural Publishing and Documentation: Wageningen.

Graefe, J. & Sandmann, M. (2014) Shortwave radiation transfer through a plant canopy covered by single and double layers of plastic (*submitted 5/2014*). *Agricultural and Forest Meteorology*.

Graefe, J., Schmidt, S., Heissner, A., Rusin, W. & Wonneberger, C. (2005) Simulation of soil heating in ridges partly covered with plastic mulch, part II: Model calibration and validation. *Biosystems Engineering*, 92, 495-512.

Gutezeit, B., Herzog, F.N. & Wenkel, K.O. (1993) Das Beregnungsbedarfssystem für Freilandgemüse. *Gemuse*, 29, 106-108.

Hammer, A. (2000) Anwendungsspezifische Solarstrahlungsinformationen aus Meteosat-Daten. Carl von Ossietzky Universität Oldenburg: Oldenburg.

Hay, J.E. (1979) Calculation of Monthly Mean Solar-Radiation for Horizontal and Inclined Surfaces. *Solar Energy*, 23, 301-307.

Heissner, A. (1965) The measurement of the light-permeability of materials used for greenhouse construction - Die Messung der Lichtdurchlässigkeit von Materialien, die beim Gewächshausbau Verwendung finden. *Arch.Gartenb.*, 13, 399-413.

Henseleit, M., Kubitzki, S., Schütz, D. & Teuber, R. (2007) Verbraucherpräferenzen für regionale Lebensmittel - Eine repräsentative Untersuchung der Einflussfaktoren. *Agrarökonomische Diskussionsbeiträge*, 83, 1-32.

Ho, T.K. (1995) Random Decision Forest. *International Conference on Document Analysis and Recognition*, 278-282.

Hukseflux Thermal Sensors. (2003) TP01 Thermal Properties Sensor. *Manual*, 1-35.

Incropera, F. & DeWitt, D. (2002) *Fundamentals of Heat and Mass Transfer*. John Wiley & Sons, Inc.: Hoboken.

Johansen, O. (1975) Thermal conductivity of soils. Norwegian University of Science and Technology, Trondheim, 1-291.

Johnson, F.H., Eyring, H. & Williams, R.W. (1942) The nature of enzyme inhibitions in bacterial luminescence: sulfanilamide, urethane, temperature and pressure. *Journal of Cellular and Comparative Physiology*, 20, 247-268.

Jury, W.A. & Horton, R. (2004) *Soil physics*. John Wiley & Sons.

Kage, H. & Stützel, H. (1999) A simple empirical model for predicting development and dry matter partitioning in cauliflower (Brassica oleracea L. botrytis). *Scientia Horticulturae*, 80, 19-38.

Knipling, E.B. (1970) Physical and Physiological Basis for the Reflectance of Visible and Near Ir Radiation from Vegetation. *Remote Sensing of Environment*, 1, 155-159.

Kramer, C.Y. (1956) Extension of Multiple Range Tests to Group Means with Unequal Numbers of Replications. *Biometrics*, 12, 307-310.

Krishnapuram, B., Carin, L., Figueiredo, M.A.T. & Hartemink, A.J. (2005) Sparse multinomial logistic regression: Fast algorithms and generalization bounds. *Ieee Transactions on Pattern Analysis and Machine Intelligence*, 27, 957-968.

Kucharik, C.J., Norman, J.M. & Gower, S.T. (1999) Characterization of radiation regimes in nonrandom forest canopies: theory, measurements, and a simplified modeling approach. *Tree Physiology*, 19, 695-706.

Leuning, R. (1995) A Critical-Appraisal of A Combined Stomatal-Photosynthesis Model for C-3 Plants. *Plant Cell and Environment*, 18, 339-355.

Leuning, R. (2002) Temperature dependence of two parameters in a photosynthesis model. *Plant Cell and Environment*, 25, 1205-1210.

LICOR Bioscience USA. (1996) *LI-3100 Area Meter Instruction Manual*.

LICOR Bioscience USA. (2011) *LAI-2200 Plant Canopy Analyzer. Instruction Manual.*

Lizaso, J.I., Batchelor, W.D. & Westgate, M.E. (2003) A leaf area model to simulate cultivar-specific expansion and senescence of maize leaves. *Field Crops Research*, 80, 1-17.

Loureiro, M.L. & Umberger, W.J. (2005) Assessing consumer preferences for country-of-origin labeling. *Journal of Agricultural and Applied Economics*, 37, 49-63.

Lu, S., Ren, T., Gong, Y. & Horton, R. (2007) An improved model for predicting soil thermal conductivity from water content at room temperature. *Soil Science Society of America Journal*, 71, 8-14.

Maync, A., Naab, B. & Kuse, E. (1985) *Neustadter Hefte Versuchsberichte Gemüsebau*. Verein der Absolventen -Gartenbau- der Staatlichen Lehr- und Forschungsanstalt, Neustadt/Weinstraße und Schifferstadt: Neustadt an der Weinstraße.

Maync, V.A. (1989) *Folien und Vliese im Freilandgemüsebau*. Bernhard Thalacker.

Minasny, B., McBratney, A.B. & Bristow, K.L. (1999) Comparison of different approaches to the development of pedotransfer functions for water-retention curves. *Geoderma*, 93, 225-253.

Mualem, Y. (1976) New Model for Predicting Hydraulic Conductivity of Unsaturated Porous-Media. *Water Resources Research*, 12, 513-522.

Nagelkerke, N.J.D. (1991) A Note on A General Definition of the Coefficient of Determination. *Biometrika*, 78, 691-692.

Nett, L., Feller, C., George, E. & Fink, M. (2011) Effect of winter catch crops on nitrogen surplus in intensive vegetable crop rotations. *Nutrient Cycling in Agroecosystems*, 91, 327-337.

Peters, A. & Durner, W. (2008) Simplified evaporation method for determining soil hydraulic properties. *Journal of Hydrology*, 356, 147-162.

Pinty, B., Lavergne, T., Dickinson, R.E., Widlowski, J.L., Gobron, N. & Verstraete, M.M. (2006) Simplifying the interaction of land surfaces with radiation for relating remote sensing products to climate models. *Journal of Geophysical Research-Atmospheres*, 111.

Ruehlmann, J. & Ruppel, S. (2005) Effects of organic amendments on soil carbon content and microbial biomass - results of the long-term box plot experiment in Grossbeeren. *Archives of Agronomy and Soil Science*, 51, 163-170.

Sandmann, M., Graefe, J. & Feller, C. (2013) Optical methods for the non-destructive estimation of leaf area index in kohlrabi and lettuce. *Scientia Horticulturae*, 156, 113-120.

SAS Institute Inc. (2008) *SAS/STAT 9.2 User's Guide*. SAS Institute: Cary.

Schlaghecken, J., Engl, G., Maync, A. & Ziegler, J. (2002) *Neustadter Hefte Anbau- und Sortenhinweise für den Gemüsebau 2003/2004*. Verein der Absolventen -Gartenbau- der Staatlichen Lehr- und Forschungsanstalt, Neustadt/Weinstraße und Schifferstadt: Neustadt a. d. Weinstraße.

Schultz, H.R. (1992) An empirical model for the simulation of leaf appearance and leaf area development of primary shoots of several grapevine (Vitis vinifera L.) canopy-systems. *Scientia Horticulturae*, 52, 179-200.

Seitz, P. (1985) *Folien und Vliese für den Gartenbau*. Eugen Ulmer GmbH Co.: Stuttgart.

Skartveit, A. & Olseth, J.A. (1987) A Model for the Diffuse Fraction of Hourly Global Radiation. *Solar Energy*, 38, 271-274.

Spitters, C.J.T., Toussaint, H.A.J.M. & Goudriaan, J. (1986) Separating the Diffuse and Direct Component of Global Radiation and Its Implications for Modeling Canopy Photosynthesis .1. Components of Incoming Radiation. *Agricultural and Forest Meteorology*, 38, 217-229.

Statistisches Bundesamt. (2014) Gemüseerhebung - Anbau und Ernte von Gemüse und Erdbeeren. Statistisches Bundesamt: Wiesbaden.

Tarnawski, V.R., Momose, T. & Leong, W.H. (2009) Assessing the impact of quartz content on the prediction of soil thermal conductivity. *Geotechnique*, 59, 331-338.

Tei, F., Aikman, D.P. & Scaife, A. (1996) Growth of lettuce, onion and red beet .2. Growth modelling. *Annals of Botany*, 78, 645-652.

Tenhunen, J.D., Weber, J.A., Yocum, C.S. & Gates, D.M. (1976) Development of A Photosynthesis Model with An Emphasis on Ecological Applications .2. Analysis of A Data Set Describing Pm Surface. *Oecologia*, 26, 101-119.

The MathWorks Inc. (2006) *MATLAB Help*. The MathWorks Inc.: Natick USA.

UMS GmbH München. (2012) *Hyprop - User Manual*.

Van Genuchten, M.T. (1980) A Closed Form Equation for Predicting the Hydraulic Conductivity of Unsaturated Soils. *Soil Science Society of America Journal*, 44, 892-898.

Vogel, G., Hartmann, H.D. & Krahnstöver, K. (1996) *Handbuch des speziellen Gemüsebaues*. Ulmer Stuttgart,, Germany.

von Alvensleben, R. (2000) Verbraucherpräferenzen für regionale Produkte: Konsumtheoretische Grundlagen. *Schriftenreihe agrarspectrum*, 30, 3-18.

Wang, Y.P. & Leuning, R. (1998) A two-leaf model for canopy conductance, photosynthesis and partitioning of available energy I: Model description and comparison with a multi-layered model. *Agricultural and Forest Meteorology*, 91, 89-111.

Warren Wilson, J. (1960) Inclined point quadrats. *New Phytol*, 59, 1-8.

# 1. PUBLISHED ARTICLE

Sandmann, M., Graefe, J. & Feller, C. (2013): Optical methods for the non-destructive estimation of leaf area index in kohlrabi and lettuce. *Scientia Horticulturae*, 156, 113-120.

**Title:** Optical methods for the non-destructive estimation of leaf area index in kohlrabi and lettuce

**Authors:** Martin Sandmann [a, *], Jan Graefe [a], Carmen Feller [a]

[a] Leibniz-Institute of Vegetable and Ornamental Crops Großbeeren and Erfurt, Theodor-Echtermeyer-Weg 1, 14979, Großbeeren, Germany

[*] Author for correspondence, e-mail: sandmann@igzev.de, phone: +49 (0)33701 78362, fax: +49 (0)33701 55391

**Key words:** *Brassica oleracea var. gongylodes* L., *Lactuca sativa var. capitata* L., leaf area index, plant canopy analyser, gap fraction

**Abstract**

The dimensionless Leaf Area Index (LAI) is a fundamental crop characteristic. Since the direct measurement of LAI or leaf area is labour intensive and destructive, fast and reliable indirect methods have been devised to estimate LAI of different crops. The objective of this work was to test indirect methods for the non-destructive estimation of LAI in kohlrabi (*Brassica oleracea var. gongylodes* L.) and lettuce (*Lactuca sativa var. capitata* L.). Focusing on the gap fraction methodology, digital photographs and simultaneous radiation interception measurements were taken using a Li-Cor plant canopy analyser (LAI-2200) on 12 sampling dates from planting to harvest, with concurrent destructive estimations of the leaf area. Several geometric protocols of the LAI-2200 and inversion algorithms of the accompanying software were evaluated. Very good indirect-direct LAI relationships were obtained for kohlrabi ($R^2 > 0.97$, $n = 12$) and lettuce ($R^2 > 0.99$, $n = 9$) for the most suitable protocols and algorithms.

## 1 Introduction

The Leaf Area Index (LAI) of horticultural crops is an important plant characteristic, related directly to canopy photosynthesis and transpiration (Baret et al., 2010). Accordingly, the efficiency of many cultural treatments can be estimated using crop LAI (Campillo et al., 2010). LAI is defined as one-sided leaf area per stand area (Breda, 2003). The leaf area is usually considered to be the normal projected area of one leaf side. More generally, however, when considering needle-like leaves, for example, the leaf area is the hemi-surface area (Chen and Black, 1992). If non-leafy plant organs contribute substantially to the total surface (e.g. surface area of stems and fruits), the term plant area index (PAI), expressed as square metre of plant area per square metre of ground, is more appropriate.

Both indirect and direct methods can be applied to measure LAI. Direct estimation of LAI involves measuring the leaf area using imaging devices. Such estimations can be performed destructively using harvested leaves or non-destructively using in situ growing leaves. Since direct methods are very labour- and time-intensive, and consequently expensive, several indirect methods have been developed to circumvent these drawbacks (Campillo, 2010). Indirect methods are usually based on optical principles. An overview of the different indirect methods can be found in Jonckheere et al. (2004). Direct methods enable greater precision; indirect methods are more cost efficient and enable time-repeated measurements to be made of identical plots and spatial patches. The greater uncertainty of optical methods is frequently caused by a lack of discrimination between leaves, stems, branches and fruit. For this reason, PAI is usually obtained in place of LAI (Li-Cor, 2011). Although a certain non-leafy contribution by kohlrabi tubers is accounted for, the therm “LAI” is used throughout this study. A further problem is the mutual covering of leaves in a non-random or clustered fashion. This lack of randomness – known as clumping – depends on the plant distribution over the ground area and the leaf distribution within the plants’ envelope. Clumping frequently occurs in row

crops. Previous investigations revealed that indirect methods yield lower LAI than direct estimates (Breda, 2003; Gordon et al., 1994; Rover and Koch, 1995; Welles and Norman, 1991), thought to be caused primarily by clumping. The morphology of a single plant (e.g. location, distribution and size of leaves) and of the canopy (e.g. distribution of plants) can affect indirect measurements. To obtain reliable results, indirect methods have to be validated for each horticultural crop under investigation.

In this work, indirect measurements of LAI from gap fraction inversions are discussed and compared with direct reference LAI values for kohlrabi (*Brassica oleracea var. gongylodes* L.) and lettuce (*Lactuca sativa var. capitata* L.). Gap fractions are obtained from digital RGB (red, green and blue) images with a soil background (i.e. the camera points towards the soil) and multi-angular light interception measurements using an LAI-2200 plant canopy analyser (LAI-2200, Li-Cor).

## 2 Material and methods

At the field site of Leibniz-Institute for Vegetable and Ornamental Crops (Germany), kohlrabi (cv 'Lech' with a green tuber) and lettuce ('Torpedo') plants were set on 30 June 2011. The site is characterised by a sandy soil with 0.8% humus, 91% sand and 4.6% clay contents (Graefe et al., 2005). Both crops were grown in a double bed, with each bed comprising five rows. A regular planting grid of 0.3 x 0.3 m (distance between rows x within the row) was adopted, resulting in a planting density of about 111,000 plants/ha. From 1 July to 16 August 2011, 15 plants were sampled twice a week from the inner three rows of one bed, then analysed. On two sampling dates, the weather conditions were unsuitable for sampling and taking optical measurements.

### *2.1 Leaf area measurements*

All methods presented below where applied to the same 15 plants per date. Firstly, the non-destructive methods and afterwards the destructive one were performed. Measurements of LAI of the following date were accomplished by using 15 new plants. Digital photography provides the total area of green plantorgans (GAI). The plant canopy analyser measures PAI. As long as there are no senescent leaves, no significant differences occur between LAI, PAI and GAI in lettuce and (in case of green tubers) in kohlrabi.

#### *2.1.1 Digital photography*

Conventional digital RGB images were obtained using a Canon PowerShot G1 (10.5 Mpx); the optical axes were inclined at a nadir zenith angle $\theta$ = 0° (Campillo et al., 2008) and at 57.5° (Baret, 2010) (Fig. 1). Images were analysed using the software *CAN-EYE V6.1* (Weiss and Baret, 2010), which supports top-down viewing canopy images with soil background taken by conventional camera. Since the canopy is viewed from above, a crucial step is segmenting pixels representing soil and plants, which was achieved using the built-in classification algorithm in *CAN-EYE*. Potentially unsuitable image regions were masked out from further analysis. *CAN-EYE* uses focal length information from an EXIF header and a user-defined image sensor size to automatically vertical crop the image to ±5° of the target zenith angle (0°, 57.5°) in the vertical image domain. Following Baret et al. (2010), this was perpendicular to the row direction. The reason for choosing 57.5° is that the relationship between LAI and gap fraction ($P_0$) is independent of the leaf angle distribution for this particular zenith angle. The gap fraction is the fraction of soil pixels to the total number of pixels in the image (Baret et al., 2010), defined as follows:

$$P_0 = \exp(-G * LAI / \cos\theta),$$

where $G$ is the mean projection of unit foliage area. With the 57.5° zenith angle, the G-function is almost constantly 0.5 for all leaf angle distributions (Weiss et al., 2004). This fact

can be used to simplify LAI computation. From a gap fraction inversion of segmented and cropped 57.5° images, *CAN-EYE* computes LAI directly via

$$LAI = -2 * \ln(P_0) * \cos(57.5°) = -\ln(P_0) / 0.93,$$

where $P_0$ is the gap fraction at the zenith angle 57.5° (Weiss, 2006). In contrast, nadir images primarily produce the crop cover fraction (*CCF*). Monsi and Saeki (1953) found the relationship

$$I = I_0 * \exp(-K * LAI)$$

which connects CCF with LAI, where $I$ is the shaded light intensity beneath the canopy, $I_0$ is the incident light intensity above the canopy and $K$ is the extinction coefficient. CCF can be expressed as

$$CCF = 1 - I / I_0$$

and both equations can be combined and rearranged to

$$LAI = -\ln(1 - CCF),$$

implying an extinction coefficient of one.

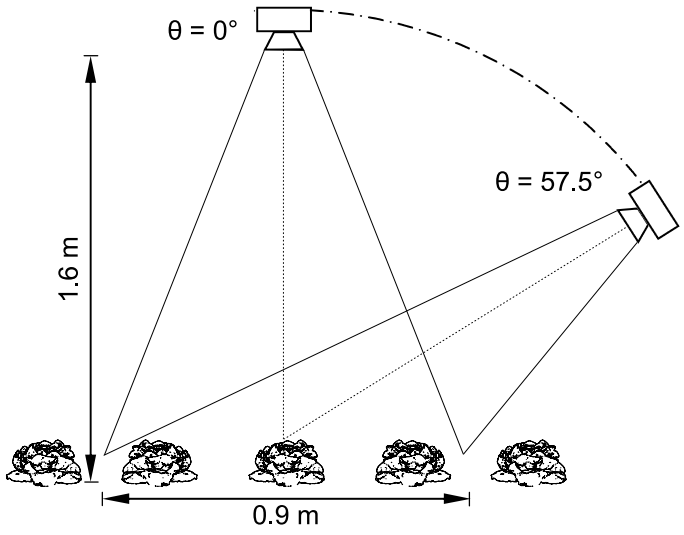


**Fig. 1.** Digital photography setup with zenith angles of θ=0° and θ=57.5° shown with lettuce.

### *2.1.2 Plant canopy analyser*

The LAI-2200 plant canopy analyser (LAI-2200) is a dedicated device for indirectly measuring LAI (LICOR Bioscience, USA, 2011). A fish eye-like optical lens estimates canopy gaps from radiation transmission measurements within five zenith angle ranges (centred angles: 7°–68°). Transmission is calculated as the ratio between below canopy (B readings) and above canopy (A readings) readings of radiation intensity within a wavelength ranging from 320 to 490 nm. To reduce multiple reflections, wavelengths exceeding 490 nm are rejected. A detailed description of the technically very similar LAI-2000 can be found in Welles and Norman (1991).

LAI-2200 measurements were conducted in kohlrabi plots only. Since lettuce crops have a low plant height and highly clustered leaves, they were considered inappropriate. Following the LAI-2200 manual (LICOR Bioscience, USA, 2011), three different protocols were tested throughout (Fig. 2). These protocols are similar to those employed by Boyd et al. (2002), Gordon et al. (1997), Grantz et al. (1993), and Hoffmann and Kluge-Severin (2010). Kohlrabi canopies have a row structure that is likely to clump. For this reason, only 90° and 45° view caps and diagonal transects were used, as recommended in the manual (Fig. 2).

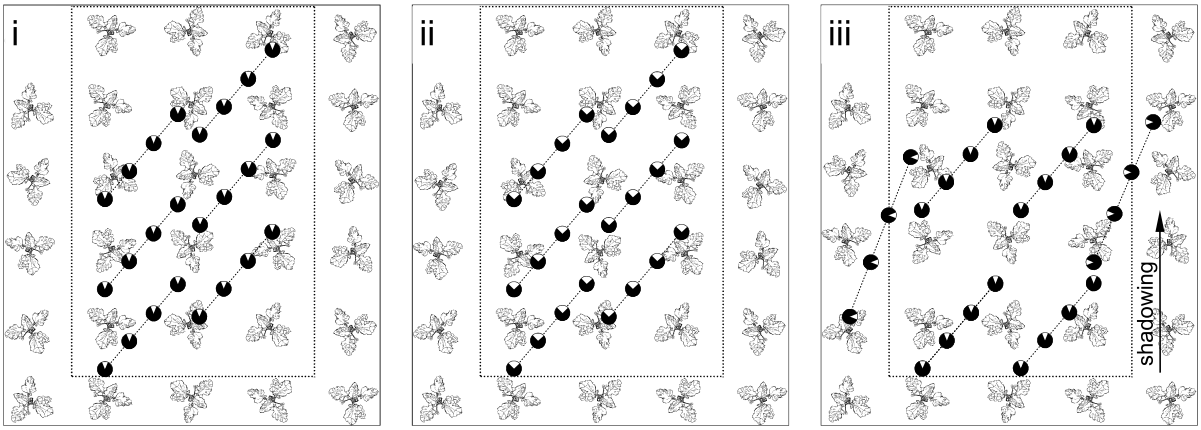


**Fig. 2.** Protocols used with precise locations of diagonal transects and indicated view cap opening. (i) Six transects (A readings) with four B readings per transect and 45° view cap. (ii) Same as (i) with 90° view cap. (iii) Same as (i) but with two transects where the view cap opens perpendicularly to the row direction. The dotted frame marks the digital photography and destructive plant sampling area.

Raw LAI-2200 readings were further processed offline using software *FV2200 1.2,* the LAI-2200 instrument software. This software offers diverse options for data processing and different inversion algorithms to calculate LAI. In this study, the following inversion algorithms were used:

- LAI: Default method, which accounts for the clumping factor (Li-Cor, 2011),
- CLS: Constrained least square method by Perry et al. (1988),
- Lang: Lang's method (Lang, 1987),
- Ellip: Least square method with ellipsoidal leaf angle distribution by Campbell (1986)

  and
- LAIeff: Default method without canopy clumping considerations (Li-Cor, 2011)

All inversion algorithms were fully combined and tested using further analysis options (A, C-F, see Table 1).

**Table 1** Protocols used and computation options for LAI calculation using software FV2200.

| Setup option | Code |
|---|---|
| *Protocol* | *A* |
| i | 1 |
| ii | 2 |
| iii | 3 |
| *Inversion algorithm* | *B* |
| LAI | 1 |
| CLS | 2 |
| Lang | 3 |
| Ellip | 4 |
| LAIeff | 5 |
| *Number of B readings per transect* | *C* |
| 2 | 1 |
| 4 | 2 |
| *Use of A readings* | *D* |
| preceding | 1 |
| closest in time | 2 |
| *Transmissions >1* | *E* |
| skip | 1 |
| set to 1.0 | 2 |
| *Angle logic used*[a] | *F* |
| 11111 | 1 |
| 01110 | 2 |
| 00010 | 3 |

[a] Each number represents one of the five zenith angles from 7° to 68°. 1 = zenith angle was used; 0 = zenith angle was not used for LAI computations.

The number of B readings per transect was varied by omitting the second and third B reading during computations. To compute single transmissions for each B reading, a corresponding A reading is selected from the measurement sequence. Two options were tested: use of the B reading preceding the A reading, or use of the closest in time A reading for transmission calculations of single B readings.

Singly calculated transmissions sometimes exceed one, because the sky radiation changes during a transect sequence and with large canopy gaps. *FV2200* offers two options to deal with this problem: either the B reading (and transmission) is omitted from the analysis or this transmission is set to one.

Furthermore, with so-called 'masking', a flexible number of zenith angles can be omitted from the analysis. In this work, three masks were tested: all angles, all angles except the smallest and the largest, and the second largest zenith angle only (53°). A full combination of all analysis options yielded 360 test cases for LAI calculation to be analysed (see Table 1).

### *2.1.3 Destructive measurements*

After completing the optical measurements as outlined above, 15 plants from the optically sensed area were harvested and analysed. Since it contributes to the overall sensed surface area, the diameter and height of the tuber of each kohlrabi plant were measured. Leaves from young plants were separated into lamina and petiole, and scanned using an Epson Perfection V700 PHOTO at 300 dpi resolution. From 9 August 2011, the leaves were horizontally aligned using a glass plate and photographed using a Canon EOS 400D with the optical axes normal to the glass plate. Scanned and photographed images were analysed using *Fiji* software (distribution of *ImageJA 1.45l)* to obtain the lamina area and width and petiole length and width at both ends.

The hemi-surface area $A_O$ ($m^2$) of $n$ kohlrabi plants is then given by

$A_0 = \Sigma^n_{i=1}(0.5T_i + 0.5P_i + L_i)$,

where $T_i$ is the tuber surface area, $P_i$ is the petiole surface area and $L_i$ is the one-sided projected laminar area of the $i$th plant. To calculate surface areas for tubers and petioles, ellipsoid and cone shapes were adopted, respectively. These organ surfaces are considered here in addition to leaves because they contribute to optical measurements and are involved in the mass and energy transfer of the crop.

The destructive LAI is finally obtained from

$$LAI_{destructive} = A_0 / (n * 0.09\ m^2), \quad (1)$$

where a mean soil surface area of 0.09 m² is attributed to each plant.

The lettuce plants were separated into head and 'hull' leaves, i.e. leaves which surround the head freely. The head diameter and height were measured; the one-sided projected area of hull leaves was obtained using an LI-3100 Area Meter (LICOR Bioscience, USA). The total semi-surface area of $n$ lettuce plants is given by

$A_0 = \Sigma^n_{i=1}(0.5H_i + L_i)$,

where $H_i$ is the surface area of the approximated head shape and $L_i$ is the one-sided projected area of hull leaves. The head shape was approximated by an ellipsoid. LAI is again computed from Eq. (1). The head was not separated further because the inner leaves do not contribute to either optical measurements or significantly to the mass and energy transfer of lettuce crops.

### *2.2 Statistical methods used*

Destructive and non-destructive measurements of LAI were compared in a linear regression approach using the REG procedure; tests for normality were performed using the UNIVARIATE procedure; Kruskal-Wallis tests to compare computation options in *FV2200* were conducted using the NPAR1WAY procedure (SAS 9.2, SAS Institute Inc., 2008). A risk of the first kind of $\alpha = 0.05$ was adopted for all tests.

## 3 Results

### *3.1 Destructive LAI measurements*

LAI of kohlrabi canopies increased continuously during the experiment from 0.02 on 1 July to 1.85 on 16 August 2011 (Fig. 3). At the same time, LAI of lettuce canopies rose from 0.01 to 5.2. However, there was a marked decline on the last sampling date; previous LAIs were about 6.2 (Fig. 3). This was caused in part by the fact that the cultivar used ('Torpedo') is adapted to spring temperatures and suffered under the high temperatures in July and August. From 5 August 2011, the oldest hull leaves started to senescence; this leaf decay extended rapidly to younger hull leaves and, finally, to the head.

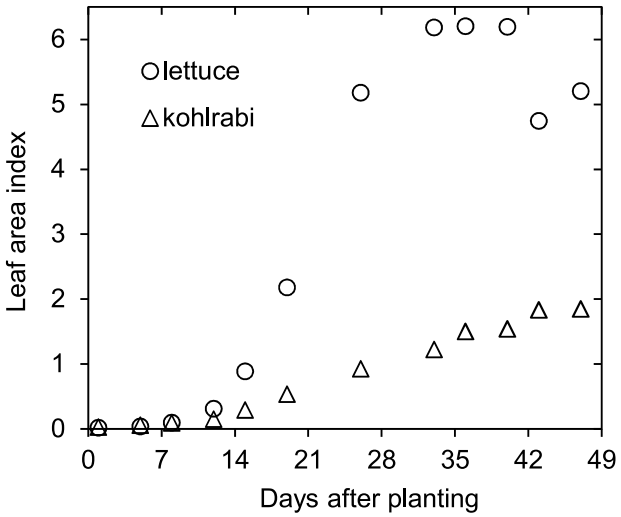


**Fig. 3.** Time course of destructively measured LAI of kohlrabi and lettuce crops.

### *3.2 LAI from digital images*

Table 2 shows the results of the linear regression between destructively measured LAI and LAI from images (x-axis). For images obtained at a nadir zenith angle ($\theta$ = 0°), LAI for both kohlrabi and lettuce are underestimated considerably, with slopes of 3.072 and 6.147, respectively. However, there is also a significant underestimation of LAI (i.e. slope > 1) for images

obtained at $\theta$ = 57.5° for both species, as the confidence range of the slope shows (see Table 2).

Real leaf area reductions are difficult to detect optically with lettuce at later sampling stages since decaying leaves are usually covered by younger leaves. The last two sampling dates were therefore treated as outliers, and additional comparisons are given for the reduced data set (Table 2). A higher $R^2$-adjusted value (0.978) is obtained for images with $\theta$ = 57.5° for the reduced data set, with similar results for kohlrabi. For nadir images, $R^2$-adjusted values are slightly higher for lettuce. With the reduced data set, the root mean squared error (RMSE) is also considerably reduced from 0.796 to 0.187 at $\theta$ = 0° and from 0.788 to 0.42 at $\theta$ = 57.5°. Since all estimated slopes differ significantly from one, it should be applied to remove the bias from indirect LAI assessments using digital images and *CAN-EYE*. For lettuce, the highest relation to destructively obtained LAIs is with zenith angle $\theta$ = 0° ($R^2$-adjusted value > 0.995); for kohlrabi, the highest precision of indirect LAI assessment can be found at $\theta$ = 57.5° ($R^2$-adjusted value > 0.978).

**Table 2** Linear regression slopes and intercepts of indirectly estimated LAI from digital photographs at $\theta$=0° and $\theta$=57.5° versus destructively measured LAI for kohlrabi and lettuce; RMSE = root mean squared error.

| Zenith angle | Species | n | Intercept | Slope | $R^2$-adjusted value | RMSE | Confidence interval of intercept ($\alpha$ = 0.05) | Confidence interval of slope ($\alpha$ = 0.05) |
|---|---|---|---|---|---|---|---|---|
| 0.0° | kohlrabi | 12 | 0.0385 | 3.0718[b] | 0.9629 | 0.1399 | [– 0.0993; 0.1764] | [2.6674; 3.4762] |
| 0.0° | lettuce | 11 | 0.0893 | 6.1471[b] | 0.9176 | 0.7958 | [– 0.7214; 0.8999] | [4.8355; 7.4587] |
| 0.0° | lettuce | 9[a] | – 0.0748 | 7.2931[b] | 0.9958 | 0.1875 | [– 0.2769; 0.1272] | [6.8957; 7.6906] |
| 57.5° | kohlrabi | 12 | – 0.0278 | 1.1663[b] | 0.9749 | 0.1151 | [– 0.0861; 0.1417] | [1.0407; 1.2919] |
| 57.5° | lettuce | 12 | – 0.1459 | 1.8655[b] | 0.9163 | 0.7877 | [– 0.6373; 0.9291] | [1.4883; 2.2426] |
| 57.5° | lettuce | 10[a] | 0.0072 | 2.1400[b] | 0.9783 | 0.4202 | [– 0.4295; 0.4440] | [1.8950; 2.3850] |

[a] Reduced data set without the last two sampling dates.
[b] Significantly different from 0 (intercept) and 1 (slope).

Fig. 4 shows regressions for both zenith angles and species (reduced data set for lettuce).

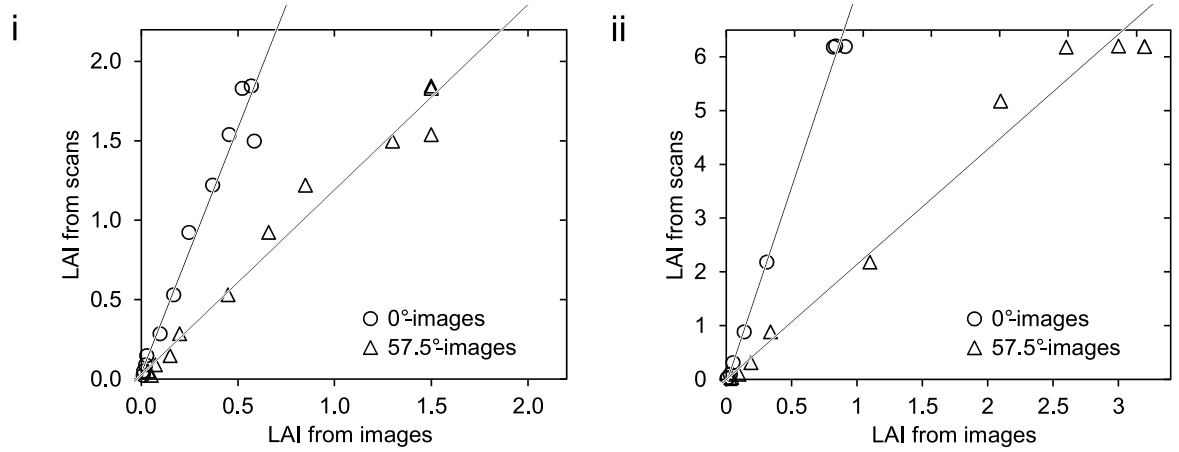


**Fig. 4.** Non-destructively estimated LAI from digital images versus destructively scanned LAI for kohlrabi (i) and lettuce (ii) at two incidence angles $\theta$=0° and $\theta$=57.5°. Line = regression function; $n_{lettuce} = 9$ (0°), $n_{lettuce} = 10$ (57.5°), $n_{kohlrabi} = 12$.

### *3.3 LAI-2200 measurements*

From a total of 360 linear regressions made between destructive and indirect measurements of LAI of kohlrabi crops, the ten best performing setups in terms of $R^2$-adjusted values are listed in Table 3. Only three LAI-2200 setups revealed $R^2 > 0.95$. For the second and third setups in that order, however, the estimated slope and intercepts do not differ significantly from 1 and 0, respectively ($\alpha = 0.05$). The lowest $R^2$-adjusted value, which occurred in setup 311212, was 0.4974 (for code see Table 1); most of the computed $R^2$-adjusted values (35%) were between 0.8750 and 0.9250 (data not shown). According to the results of the linear regressions the LAI of kohlrabi crops is therefore most precisely estimated indirectly using LAI-2200 with the following setup:

- Protocol ii (Fig. 2)
- Inversion algorithm Ellip
- Include all four B readings per transect
- Use closest A reading in time
- Skip transmissions >1
- Mask highest and smallest zenith angle (mask: 01110)

The setup with the second highest R²-adjusted is recommended here as it is bias-free and retrieved LAIs can be used without further correction. In contrast, LAI-2200-based LAI estimates with the setup with the highest R²-adjusted should be corrected by $LAI_{true} = -0.2465 + 1.1819 * LAI_{LAI\text{-}2200}$, as both the slope and intercept differ from 1 and 0, respectively (see Table 3).

**Table 3** Linear regression slopes and intercepts of indirectly estimated LAI from plant canopy analyser versus destructively measured LAI for kohlrabi for the ten best LAI-2200 setups. Coding (A-F) is from Table 1; $n = 12$.

| A | B | C | D | E | F | Intercept | Slope | R²-adjusted value | RMSE[a] | Confidence interval of intercept ($\alpha = 0.05$) | Confidence interval of slope ($\alpha = 0.05$) |
|---|---|---|---|---|---|---|---|---|---|---|---|
| 1 | 5 | 1 | 1 | 1 | 1 | – 0.2465[b] | 1.1819[b] | 0.9542 | 0.1555 | [– 0.4339; – 0.0591] | [1.0082; 1.3555] |
| 2 | 4 | 2 | 2 | 1 | 2 | – 0.0391 | 0.8720 | 0.9522 | 0.1589 | [– 0.2052; 0.1269] | [0.7409; 1.0030] |
| 2 | 4 | 2 | 1 | 2 | 3 | 0.0412 | 0.8962 | 0.9514 | 0.1601 | [– 0.1168; 0.1992] | [0.7604; 1.0320] |
| 3 | 5 | 2 | 2 | 2 | 3 | – 0.0371 | 1.3051[b] | 0.9484 | 0.1649 | [– 0.2094; 0.1353] | [1.1012; 1.5091] |
| 1 | 3 | 1 | 1 | 2 | 1 | – 0.0119 | 0.8568[b] | 0.9467 | 0.1677 | [– 0.1841; 0.1603] | [0.7205; 0.9931] |
| 1 | 4 | 1 | 1 | 1 | 1 | – 0.2036[b] | 0.9268 | 0.9461 | 0.1686 | [– 0.4016; – 0.0056] | [0.7786; 1.0750] |
| 1 | 5 | 1 | 1 | 1 | 3 | – 0.1745 | 1.1714 | 0.9455 | 0.1696 | [– 0.3698; 0.0207] | [0.9829; 1.3598] |
| 1 | 5 | 2 | 2 | 2 | 2 | – 0.0022 | 1.1750 | 0.9452 | 0.1700 | [– 0.1756; 0.1712] | [0.9854; 1.3645] |
| 2 | 4 | 2 | 2 | 1 | 3 | 0.0164 | 0.7925[b] | 0.9450 | 0.1702 | [– 0.1549; 0.1878] | [0.6645; 0.9206] |
| 2 | 3 | 2 | 2 | 1 | 2 | 0.0816 | 0.7949[b] | 0.9440 | 0.1719 | [– 0.0835; 0.2466] | [0.6651; 0.9247] |

[a] Root mean squared error
[b] Significantly different from 0 (intercept) and 1 (slope).

Fig. 5 shows the LAI-2200 setups with the four highest R²-adjusted. It can be seen that the setup with the third highest R²-adjusted is very reliable for small LAI values up to 1, where data points are closely matched by the regression line. This setup (code 242123, see Table 1) is recommended for young kohlrabi crops in particular.

Additionally, several statistical tests were performed to establish whether any patterns exist among the protocols used and the computation options according to $R^2$-adjusted values. Owing to the non-normality of the computed $R^2$-adjusted values (Kolmogorov-Smirnov test p-value <0.01), the Kruskal-Wallis test was chosen. Each setup option was tested on average of all others. The results are presented in Table 4, together with comparisons of the recommended setups, the setup with the lowest R²-adjusted and the options with the highest R²s-adjusted

values. According to these results, the inversion algorithm chosen (Code B) and the decision on which A reading to use (Code D) have no significant impact on $R^2$-adjusted values. There is a good consistency between the recommended setups and the options with the highest $R^2$-adjusted values. As expected, there is no consistency between the setup with the lowest $R^2$-adjusted and the options with the highest $R^2$-adjusted values (with the exception of the two options that have no impact on $R^2$-adjusted values).

**Table 4** *p*-Values from Kruskal-Wallis tests and comparisons of the recommended setups, the worst setup and the options with the best $R^2$s-adjusted values. Codes are from Table 1.

| Code | P-values | | | | Options with the best $R^2$-adjusted values | Recommended setups | | Worst setup |
|---|---|---|---|---|---|---|---|---|
| | global | 1 - 2 | 1 - 3 | 2 - 3 | | 2nd best | 3rd best | |
| A | <0.0001[b] | 0.1261 | <0.0001[b] | <0.0001[b] | 1, 2 | 2[a] | 2[a] | 3 |
| B | 0.3337 | | | | all equal | 4[a] | 4[a] | 1[a] |
| C | | <0.0001[b] | | | 2 | 2[a] | 2[a] | 1 |
| D | | 0.5156 | | | both equal | 2[a] | 1[a] | 2[a] |
| E | | <0.0001[b] | | | 2 | 1 | 2[a] | 1 |
| F | 0.0018[b] | 0.0008[b] | 0.5824 | 0.0119[b] | 1, 3 | 2 | 3[a] | 2 |

[a] In accordance with the results of Kruscal-Wallis tests.
[b] Significant differences ($\alpha = 0.05$).

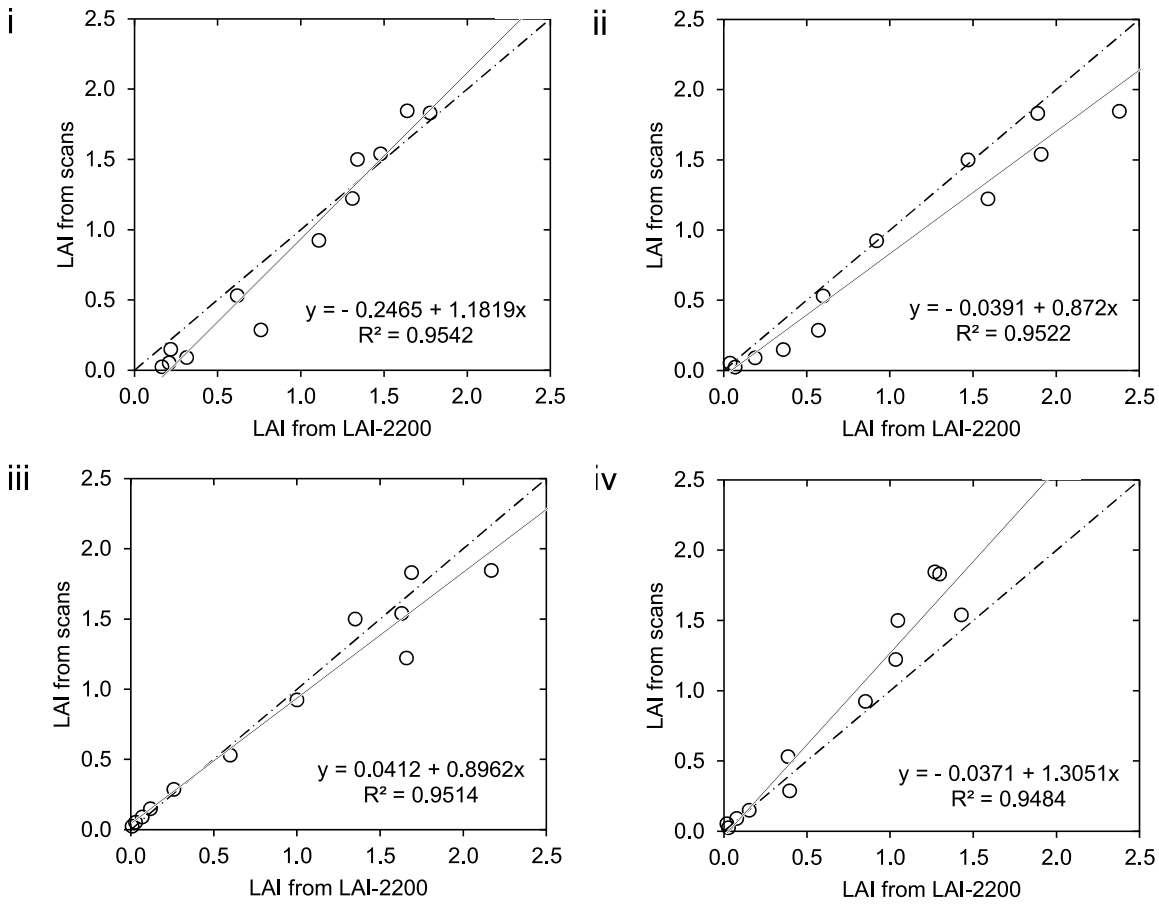


**Fig. 5.** Linear regression of non-destructively measured LAI with LAI-2200 using destructively measured LAI for the best performing setups: 151111 (i), 242212 (ii), 242123 (iii) and 352223 (iv). Line = regression function; Slash-dotted line = 1:1 ratio; coding is from Table 1.

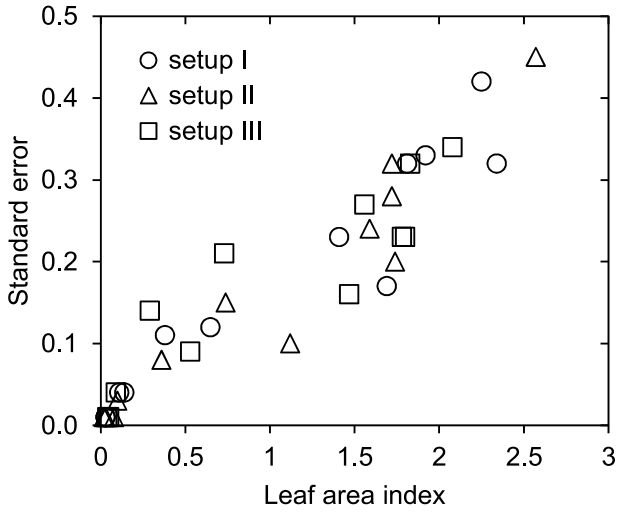


**Fig. 6.** Standard error of LAI computed using setups 11221 (I), 21221 (II) and 31221 (III); coding is from Table 1.

To get an idea of the precision of LAI values of kohlrabi crops collected using LAI-2200, the standard errors of LAI for three exemplary setups are shown in Fig. 6. Each symbol in this graph represents one LAI measurement, which is the mean of a sample with $n = 24$ (one value per B reading). Obviously, the standard error increases with increasing LAI. The mean coefficient of variation for all LAI measurements in Fig. 6 is 0.2222. The smallest and largest coefficients of variance are 0.0893 and 0.5000, respectively. These figures are only slightly different for other setups. According to the measures of variation, the relatively high number of 24 B readings is actually required to gain data in kohlrabi with certain reliability. However, this reliability still is not high, e.g. the wide confidence limit of LAI 2.57 (largest LAI in Fig. 6) with standard error 0.45 is (1.688; 3.452).

For small height crops such as kohlrabi, LAI-2200 measurements can be conducted with short distances between the sensor head and the leaves. The minimum required distance $D_{min}$ can be calculated from (LICOR Bioscience, USA, 2011)

$D_{min} = (d * w)/B$.

Here, $d$ is a tabulated distance parameter (LICOR Bioscience, USA, 2011) which depends on zenith angle $\theta$ and the view cap used, $w$ is leaf width in cm and $B$ is the number of total B readings of the protocol used. The smaller $\theta$ and azimuthal view cap opening, the larger the distance parameter.

$D_{min}$ was calculated from measured lamina widths recorded throughout the experiment (Table 5).

**Table 5** Required distance (m) between the sensor head of the LAI2200 and leaves. The values shown are means over all sampling dates.

| View cap | Number of B readings | Mean zenith angle 7° | 23° | 38° | 53° | 68° | *Mean* |
|---|---|---|---|---|---|---|---|
| 45° | 4 | 1.87 | 0.56 | 0.37 | 0.28 | 0.26 | *0.67* |
| 45° | 2 | 3.75 | 1.12 | 0.75 | 0.56 | 0.52 | *1.34* |
| 90° | 4 | 0.94 | 0.37 | 0.19 | 0.15 | 0.13 | *0.36* |
| 90° | 2 | 1.87 | 0.75 | 0.37 | 0.30 | 0.26 | *0.71* |
| *Mean* | | *2.11* | *0.70* | *0.42* | *0.32* | *0.30* | |

It can be seen from Table 5 that $D_{min}$ cannot always be met. For the centred ring with the mean zenith angle $\bar{\theta}$ = 7° and the 45° view cap, the minimum distance calculated (3.75 m) is much larger than the typical plant heights of kohlrabi. The lowest $D_{min}$ values are obtained for the 90° view cap. This could be one of the reasons why it is a feature of the LAI-2200 setup with the second highest R²-adjusted (Table 3).

The time required by an operator to complete the suggested protocols for one plot (see Fig. 2) was estimated. The mean values over all sampling dates were 5:05', 4:22' and 5:15' for protocols i, ii and iii, respectively. Fig. 7 shows that the completion time decreases initially during the learning stage and subsequently levels off.

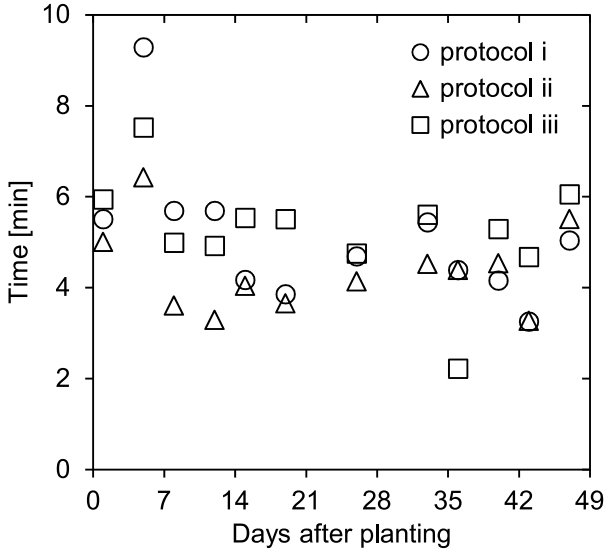


**Fig. 7.** Operation time to complete one LAI-2200 measurement per plot for different protocols as the difference between the first A reading and the last B reading time during the experiment; for protocols, see Fig. 2.

### *3.4 Gap fractions from digital images and LAI-2200 measurements*

*CAN-EYE* and *FV2200* provide also data for gap fractions ($P_0$). To compare the data of kohlrabi crops from both methods it was necessary for the LAI-2200 data to interpolate between the measured values of the centred angles 53° and 68°. A linear interpolation between these two angles was used to calculate $P_0$ for the zenith angle 57.5°. For every combination of the setup options "Protocol", "Use of A readings" and "Transmissions >1" (Table 1) $P_0$ was calculated. Linear regressions were performed between the *CAN-EYE* $P_0$ and twelve different

*FV2200* $P_0$ values. The smallest RMSE (0.066) and the highest $R^2$-adjusted values (0.964) were found for the setup options

- Protocol ii (Fig. 2)
- Use closest A reading in time
- Skip transmissions >1.

This is in accordance with the recommended setup in chapter 3.3. The equation of the linear regression is $y = -0.136 + 1.086x$ where $y$ is $P_0$ from LAI-2200 measurements and $x$ is $P_0$ from digital photography while the intercept is statistical significant and the slope is not ($\alpha = 0.05$). So $P_0$ values of kohlrabi crops from digital images are slightly smaller than those from LAI-2200 measurements.

## 4 Discussion

Both digital photography and LAI-2200-based methods for indirect LAI estimation performed well for kohlrabi, with $R^2 > 0.97$ and $R^2 > 0.95$, respectively (Tables 2 and 3). Compared to digital photography, LAI-2200-based LAI estimates do not require any correction for bias if the setups recommended here are followed; methods using digital photography significantly underestimated the true LAI.

For LAI-2200 measurements in kohlrabi, the proposed setup is comparable to Grantz et al. (1993), who undertook similar investigations with cotton. The RMSE of listed setups varies between 0.15 und 0.18 (Table 3), which is of a similar magnitude to an LAI-2200 test on potatoes conducted by Gordon et al. (1994).

As mentioned earlier, the LAI-2200 method was considered unsuitable for lettuce. However, the digital photography method yields very good estimates with $R^2 > 0.99$, and is therefore a good alternative to destructive sampling (Table 2), as long as leaves show no senescence. As shown in Table 2, precision and accuracy increase significantly if sampling dates where obvious signs of leaf decay were visible are rejected.

With regard to labour and time requirements, both indirect methods are superior to destructive sampling. Digital photographs can be taken quickly at the field site, because the region of interest or the patch is imaged in one operation. LAI-2200 measurements usually require more time; in this case (6 A readings and 24 B readings) for which the operator has to level the sensor head each time, 30 single readings were involved. An average of about 5 minutes is required for one LAI-2200 measurement (Fig. 7).

Regarding the time required to post-process the data, the relations between these indirect methods are reversed. Post-processing is simple and fast using software *FV2200,* which accompanies LAI-2200. The further processing of digital images is far more elaborate in terms of operation time.

In particular, the necessary segmentation between soil and vegetation pixels in images is still a manual classification process, which is a time-demanding process, despite being quite user-friendly when implemented in *CAN-EYE* software. A possible option for improvement seems to be the acquisition of near-infrared images, where the fractions of sunlight soil and vegetation, and the shaded fraction are more distinctly separate (Fitzgerald, 2004). Furthermore, the usage of high dynamic range images (HDR) should be considered in future studies. A high dynamic range can be achieved using sequential shots with different exposures times or using imaging sensors with a higher dynamic range (13-14 f-stops), rarely found even in professional digital cameras. Under field conditions, sequential shots are not feasible due to plant movements.

For both methods, an even, overcast sky is ideal. Highlights from direct sunlight – which can be reduced in part by circular polarising filters in imaging – induce strong multiple reflections, which are not accounted for by the inversion algorithms used by the LAI-2200, complicating the task of image segmentation, as with strong shadows (Baret, 2010; LICOR Bioscience, USA, 2011). Under strong light, segmentation is more difficult because sunlit soil and leaves are very bright and shaded soil and leaf patches are almost evenly dark. Even for

images obtained under strong sunlight, however, segmentation was accomplished using *CAN-EYE* and the corresponding estimated LAI values matched estimates under more favourable sky conditions. Li-Cor proposes special procedures for measurements conducted using the LAI-2200 in direct sunlight, e.g. using view caps, shading the sensor and shading the part of the canopy visible to the sensor (LICOR Bioscience, USA, 2011). However, it is difficult to shade the canopy if only one person is involved in measuring LAI. In addition to shading the canopy, the proposed procedure was followed in this study. Welles and Norman (1991) showed that LAI is underestimated by LAI-2200 measurements due to direct sunlight. The more gaps there are in the canopy, the more serious this problem becomes (LICOR Bioscience, USA, 2011). Regarding sky conditions, therefore, digital photography is less error prone than LAI-2200 measurements in low leaf area canopies of kohlrabi crops, which have many gaps.

The comparison of gap fractions estimated from digital photography and LAI-2200 measurements in kohlrabi (both for $\theta = 57.5°$) are in good accordance (chapter 3.4). This is interesting because it implicates that the viewing direction (from below or above the canopy) has no influence on the observed gap fraction, and later on on the estimated LAI.

Table 6 gives a summary of criteria, allowing the direct comparison of all discussed methods for LAI measurement. It becomes apparent that indirect methods are far less labour intensive than direct methods for LAI estimation; digital photography can even be conducted using simple point and shoot cameras. The direct method is exact and does not depend on light conditions.

**Table 6** General comparison of different LAI estimation methods.

| Criteria | Digital photography | Plant canopy analyser | Destructive measurements |
|---|---|---|---|
| Assessment type | indirect | indirect | direct |
| Instruments | digital camera tripod | LAI2200 | logistic leaf area meter scanner or digital camera + tripod |
| Software | *CAN-EYE* | *FV2200* | *Fiji* |
| Field work load | very low | low - medium | high |
| Lab work load | - | - | high |
| PC work load | low - high | low | high |
| Sky condition | overcast - clear | overcast | - |
| Precision | high | high | very high |

## 5 Conclusions

It was shown that indirect methods to measure LAI are a very good alternative to the destructive and labour-intensive estimation of leaf area for the horticultural species kohlrabi and lettuce. Indirectly estimated LAI values correlated well with direct estimates. Here, several measurement setups are suggested for both crops allowing, in the case of digital photography, the rapid and cost-effective assessment of LAI in the field. Moreover, the suggested approaches enable reliable leaf area measurements to be taken for kohlrabi and lettuce in field experiments with a large number of treatments, where the non-destructive approach enables repeated measurements to be taken of the same plot area over time. Especially for the setups proposed here, which have systematic errors, new planting patterns and cultivars should be recalibrated and modified before applying the setups.

Future research into soil viewing images should focus on the additional use of the near-infrared channel and test cameras with a high dynamic range to achieve a faster, or maybe even automatic, segmentation between vegetation and soil.

**Acknowledgements**

The authors like to thank Christel Richter for her helpful comments and Stefan Koeller, Alexander Koschker and Marcel Witt for their practical assistance. This work was supported by funding from the German Federal Ministry of Education and Research and from the Federal State Ministries: Lower Saxony Ministry of Science and Culture, Brandenburg Ministry of Infrastructure and Agriculture and Bavarian Ministry of State of Science, Research and Art.

**References**

Baret, F., de Solan, B., Lopez-Lozano, R., Ma, K., and Weiss, M., 2010. GAI estimates of row crops from downward looking digital photos taken perpendicular to rows at 57.5 degrees zenith angle: Theoretical considerations based on 3D architecture models and application to wheat crops. Agricultural and Forest Meteorology 150, 1393-1401.

Boyd, N.S., Gordon, R., and Martin, R.C., 2002. Relationship between leaf area index and ground cover in potato under different management conditions. Potato Research 45, 117-129.

Breda, N.J.J., 2003. Ground-based measurements of leaf area index: a review of methods, instruments and current controversies. Journal of Experimental Botany 54, 2403-2417.

Campbell, G.S., 1986. Extinction Coefficients for Radiation in Plant Canopies Calculated using an Ellipsoidal Inclination Angle Distribution. Agricultural and Forest Meteorology 36, 317-321.

Campillo, C., Prieto, M.H., Daza, C., Monino, M.J., and Garcia, M.I., 2008. Using digital images to characterize canopy coverage and light interception in a processing tomato crop. Hortscience 43, 1780-1786.

Campillo, C., Garcia, M.I., Daza, C., and Prieto, M., 2010. Study of a Non-destructive Method for Estimating the Leaf Area Index in Vegetable Crops using Digital Images. Hortscience 45, 1459-1463.

Chen, J.M. and Black, T.A., 1992. Defining Leaf-Area Index for Non-Flat Leaves. Plant Cell and Environment 15, 421-429.

Fitzgerald, G.J., 2004. Portable hyperspectral tunable imaging system (PHyTIS) for precision agriculture. Agronomy Journal 96, 311-315.

Gordon, R., Brown, D.M., and Dixon, M.A., 1994. Nondestructive Estimation of Potato Leaf-Area Index using a Fish-Eye Radiometer. Potato Research 37, 393-402.

Gordon, R., Brown, D.M., and Dixon, M.A., 1997. Estimating potato leaf area index for specific cultivars. Potato Research 40, 251-266.

Graefe, J., Schmidt, S., Heissner, A., Rusin, W., and Wonneberger, C., 2005. Simulation of soil heating in ridges partly covered with plastic mulch, part II: Model calibration and validation. Biosystems Engineering 92, 495-512.

Grantz, D.A., Zhang, X.J., Metheney, P.D., and Grimes, D.W., 1993. Indirect Measurement of Leaf-Area Index in Pima Cotton (Gossypium-Barbadense L) using a Commercial Gap Inversion Method. Agricultural and Forest Meteorology 67, 1-12.

Hoffmann, C.M. and Kluge-Severin, S., 2010. Light absorption and radiation use efficiency of autumn and spring sown sugar beets. Field Crops Research 119, 238-244.

Jonckheere, I., Fleck, S., Nackaerts, K., Muys, B., Coppin, P., Weiss, M., and Baret, F., 2004. Review of methods for in situ leaf area index determination - Part I. Theories, sensors and hemispherical photography. Agricultural and Forest Meteorology 121, 19-35.

Lang, A.R.G., 1987. Simplified Estimate of Leaf-Area Index from Transmittance of the Sun's Beam. Agricultural and Forest Meteorology 41, 179-186.

LICOR Bioscience, USA, 2011. LAI-2200 Plant Canopy Analyzer. Instruction Manual.

Monsi, M. and Saeki, T., 1953. Über den Lichtfaktor in den Pflanzengesellschaften und seine Bedeutung für die Stoffproduktion. Japanese Journal of Botany 14, 22-52.

Perry, S.G., Fraser, A.B., Thomson, D.W., and Norman, J.M., 1988. Indirect Sensing of Plant Canopy Structure with Simple Radiation Measurements. Agricultural and Forest Meteorology 42, 255-278.

Rover, A. and Koch, H.J., 1995. Indirect Determination of Leaf-Area Index of Sugar-Beet Canopies in Comparison to Direct Measurement. Journal of Agronomy and Crop Science-Zeitschrift fur Acker und Pflanzenbau 174, 189-195.

SAS Institute Inc., 2008. SAS/STAT 9.2 User's Guide. SAS Institute, Cary.

Weiss, M., 2006. CAN-EYE Output Variables. Definitions and theoretical background. INRA.

Weiss, M. and Baret, F., 2010. CAN-EYE V 6.1 USER MANUAL. INRA.

Weiss, M., Baret, F., Smith, G.J., Jonckheere, I., and Coppin, P., 2004. Review of methods for in situ leaf area index (LAI) determination Part II. Estimation of LAI, errors and sampling. Agricultural and Forest Meteorology 121, 37-53.

Welles, J.M. and Norman, J.M., 1991. Instrument for Indirect Measurement of Canopy Architecture. Agronomy Journal 83, 818-825.

# 2. PUBLISHED ARTICLE

Graefe, J. & Sandmann, M. (2015): Shortwave radiation transfer through a plant canopy covered by single and double layers of plastic. *Agricultural and Forest Meteorology*, 201, 196-208.

**Title:** Shortwave radiation transfer through a plant canopy covered by single and double layers of plastic

**Authors:** Jan Graefe [a, *], Martin Sandmann [a]

[a] Leibniz-Institute of Vegetable and Ornamental Crops Großbeeren and Erfurt, Theodor-Echtermeyer-Weg 1, 14979, Großbeeren, Germany

[*] Author for correspondence, e-mail: graefe@igzev.de, phone: +49 (0)33701 78363, fax: +49 (0)33701 55391

**Key words:**

Plastic covers, leaf area index, radiation transfer, clumping index, transmittance, reflectance, soil albedo

**Abstract**

A model that predicts radiation transfer through single and double layers of plastic covering over kohlrabi canopies is developed, parameterised and tested. This model will be the foundation of an energy balance and growth module for covered kohlrabi crops that can be used in cover management. Radiation transfer through covers is based on their laboratory-measured angular-resolved transmittances, which are upscaled to non-plane covers in the field. The upscaling procedure accounts for distributed facet slopes according to the Beckmann distribution and visibility, as well as interception preference according to the cosine of the facet-ray incidence angle. Additional measured and upscaled quantities include absorptance and the degree of haze at several angles. The effects of plastic aging and wetting are measured and implemented into the model using simple empirical approaches. Radiation transfer through the canopy is described by a thoroughly tested 1D canopy model, which accounts effectively for multiple reflections between leaves and the soil. A reanalysis of combined gap fraction and leaf area data from a previous study revealed a tendency of

kohlrabi canopies to overdisperse at early growth stages, when only minor leaf area overlapping occurs. Using hourly measurements of photosynthetic active radiation flux densities at the soil level over two growth seasons at one site, the overall model performed reasonably well for a non-woven fabric-based cover (n=1067, $R^2$ = 0.96, RMSE = 6.62 $Wm^{-2}$) and a combination of a low-density polyethylene perforated plastic on top of a non-woven fabric (n = 1112, $R^2$ = 0.97, RMSE = 5.11 W $m^{-2}$). Simulations showed rather low degree of model sensitivity to the specification of cover roughness, but a high level of sensitivity to a proper parameterisation of angular optical properties of covers and of canopy radiation transfer in the NIR spectral range.

## 1. Introduction

In spring, plastic covers enable field-grown vegetables to be harvested earlier by protecting them from late frosts and increasing the temperature under the cover markedly compared to uncovered crops. In Germany, one of the most important crops for this production system is kohlrabi (*Brassica oleracea var. gongylodes)*. Non-woven fabric (NWF) and perforated film (PF) on top of NWF (NWF+PF) are mainly used. However, there is a serious risk of crop quality losses if the air temperature under the cover is excessively high. One reaction of kohlrabi plants is to form upright tubers (instead of the more popular flat oval tubers). To avoid these risks, growers must decide when it is the right time to remove the cover, weighing up the risk of quality losses against the opportunity of yielding earlier harvests. There is a currently established temperature sum criterion based on a cumulated daily maximum temperature sum above the cover after planting. However, this empirical model is not precise enough for contemporary requirements in production safety.

Our long-term objective is therefore to develop a physically and physiologically based model of crop microclimates under plastic covers that interacts with plant growth and quality. In this study, we develop a radiation transfer model for PAR (photosynthetic active radiation, $400$ to $700\ nm$) and NIR (near-infrared radiation, $701$ to $3000\ nm$), which will be an essential part of the envisioned overall system model.

Previous studies on plastic covered plant–soil systems either assumed there was no interaction between the vegetation and shortwave radiation fluxes (Albright et al., 1989) or they not consider the plant compartment (De Luca and Ruocco, 2000, Graefe, 2005, Ham and Kluitenberg, 1994, Wu et al., 1996). Other studies placed greater emphasis on the light transmission of greenhouse structures (Critten, 1983, Pieters and Deltour, 1999, Wang and Boulard, 2000).

Modelling radiation transfer in horizontal homogeneous plant canopies is well established, and is generally solved by using the one-dimensional radiation transport equation (Ross, 1981). However, for routine applications that provide net radiation fluxes in soil–vegetation–atmosphere models, for example, approximations to the full theory of multiple scattering of radiation are often applied (Goudriaan, 1977, Pinty et al., 2006, Verhoef, 1984). The objective of this study is to develop a combined model that describes the radiation transfer of plastic covered plant canopies. The model will be parameterised from comprehensive measurements of optical and structural properties of various covers used, soils and kohlrabi canopies.

## 2. Material and methods

### 2.1. Site and experiment

Field trials were carried out at the site of Leibniz-Institute for Vegetable and Ornamental Crops in Großbeeren, Germany (52°21' N, 13°19' E) from 2011 to 2012. The site is characterised by silty sand with 5.5 % clay (Rühlmann and Ruppel, 2005). In spring (March to June), kohlrabi (cv 'Lech') was grown in beds, with each bed comprising five rows with thirty plants each. A regular planting grid of 0.3 m × 0.3 m (distance between rows × within the row) was adopted, resulting in a planting density of about 111,000 plants/ha. There were two cover treatments: NWF and NWF+PF. NWF, consisting of polypropylene fibres, weighs 19 $g/m^2$; PF is 40 μ$m$ thick polyethylene plastic with 500 $holes/m^2$ (hole diameter is 1 $cm$). Covers were placed directly over the plants without any supporting structure. The plants were fertilised and irrigated in line with current practice; they did not constitute limiting factors for plant growth.

### 2.2. Field measurements

All measurements were taken at hourly or ten-minute intervals, and were aggregated to hourly means. Incident PAR at the soil surface, $I_s$, was recorded using one (2012) or two (2011) LI-191 line quantum sensors (LI-COR Biosciences Inc., Lincoln, NE, USA) per treatment placed diagonally towards the rows of kohlrabi in NWF and NWF+PF plots. All quantum flux outputs were converted to $W\ m^{-2}$ using a factor of 0.235 (Campbell and Norman, 1998). Incident PAR at the top of the canopy was also measured with a LI-191 line quantum sensor in order to improve angular and spectral consistency.

Global radiation data was obtained from a weather station located 200 $m$ from the experimental site (CM11, Kipp & Zonen B.V., Delft, NL). The field soil moisture was measured using vertically inserted TDR sensors (CS625, Campbell Scientific Inc., Logan, UT, USA) at a 0 to 30 $cm$ soil depth. The leaf area index (LAI) was determined directly in 2011 using an LI-3100 area meter (LI-COR Biosciences Inc., Lincoln, NE, USA) and

indirectly in 2012 using an image-based gap fraction method (Sandmann et al., 2013). Additional LAI data was obtained using a plant canopy analyser (PCA) in 2011 (LI-2200, LI-COR Biosciences Inc., Lincoln, NE, USA). Weekly measured LAI were spline interpolated to hourly values using a continuously calculated thermal time since planting from the air temperature under the cover.

Furthermore, independent concurrent measurements of gap fraction (PCA, digital photography at nadir and 57° view angle) and LAI in uncovered kohlrabi crops (details given by Sandmann et al., 2013) were reanalysed. The leaf angle distribution parameter $X$ from the ellipsoidal distribution (Campbell, 1986) was estimated using the software program FV2200 (version 2.0, LI-COR Biosciences Inc., Lincoln, NE, USA). PCA-based gap fraction measurements from three different protocols (72 B readings altogether) were then linear averaged and analysed together with gap fraction estimates from segmented digital photographs for clumping index at different viewing zenith angles (0°, 7°, 22°, 38°, 53°, 57°).

### 2.3. Laboratory measurements

Measurements of the optical properties of cover materials and plant leaves were performed using a dual beam UV/VIS/NIR photometer (V-670, Jasco, J) equipped with a large integrating sphere (ILN-725, internal diameter: $15\ cm$). The properties measured were the directional (5°)-hemispherical reflectance and transmittance from $220$ to $2200\ nm$ at a resolution of $1\ nm$. Preliminary analysis revealed that a scan of 20 and 2 different patches was required for NWF and PF, respectively, to account for spatial inhomogeneity. Only eight repetitions were performed in order to compare dry and wet cover materials; exactly the same spot was chosen to measure the reflectance and transmittance of NWF and NWF+PF. NWF+PF covers were wetted (sprayed) from the NWF side only. The sprayed water was

completely absorbed by NWF with no obvious droplets present. The optical properties of the plastics used were assessed in 2012 after 78 days of field application.

Leaf sampling was repeated five times, whereby each repetition originated from another plant from the same treatment. Reflectance and transmittance spectra of leaves obtained from the adaxial leaf side were carried out weekly during the field trial in Großbeeren in 2012.

Directional-directional light transmittance of covers ($\tau_{DIR}(\delta)$) was assessed at incidence angles ($\delta$) 0°, 30°, 45°, 60° and 75° using a variable angle transmission accessory (VTA-752 film holder, Jasco, J) with the light polarisation angle set at 45°. Additional measurements of directional-hemispherical transmittance ($\tau(\delta)$) were taken using a smaller integrating sphere (internal diameter: $7.62\ cm$) with a red laser (peak wave length $655\ nm$) at incidence angles 0°, 30°, 45°, 60° and 70° and a UV/VIS/NIR diode array spectrometer (EPP 2000, StellarNet, USA). Possible substitution errors were estimated, and the corrections obtained were applied accordingly. The angular responses of $\tau_{DIR}(\delta)$ and $\tau(\delta)$ obtained were fitted with empirical functions for subsequent use; both were constrained to yield zero transmittance at $\delta = 90°$. Using an analogue setup, directional-hemispherical reflectance was measured with a laser incidence of 45°.

Soil reflectance was measured using a fibre-connected integrating sphere (HISN-729, 250 to $2000\ nm$, Jasco, J) for six soil samples. Top soil (0 to $5\ cm$) cores with a volume of $250\ cm^3$ were sampled non-destructively and saturated for $24\ h$ in a water bath. Subsequent changes in water content and reflectivity induced by passive evaporation were monitored gravimetrically and spectroscopically.

Mean values for all spectral-resolved reflectance and transmission data over the wavelength ($\lambda$) bands of PAR and NIR were calculated using Planck's function of blackbody (assuming $5800\ K$ to be the surface temperature of the sun) spectral emissive power.

### 2.4. Statistical and mathematical tools

Several response functions ($\tau_{DIR}(\delta), \tau(\delta)$) were fitted and verified using the MODEL procedure in SAS (Version 9.2, SAS Institute Inc., Cary, NC, USA). Robust nonlinear regression was performed using the MATLAB (Version 14, The Mathworks Inc., Natick, MA, USA) nlinfit function. The whole radiation transfer model was coded as MATLAB function. The original source code of the canopy radiation transfer routine *JRC2S* (Pinty et al., 2006) was interfaced as mex function to the overall MATLAB model. Parameter estimation of the overall model was performed using the genetic algorithm (ga) function from the Global Optimization Toolbox using default options, with the exception of the number of generations (30). This ensured fast and global solutions when used in conjunction with the Parallel Computing toolbox. Possible outliers within PAR measurements were removed by the criteria residual > 4 MAD, where MAD denotes the median absolute deviation of residuals between model simulations and measurements. Around 10 % of the measurements were marked as outliers and disregarded in the further analysis.

## 3. Model derivation and parameterisation

### 3.1. Overview

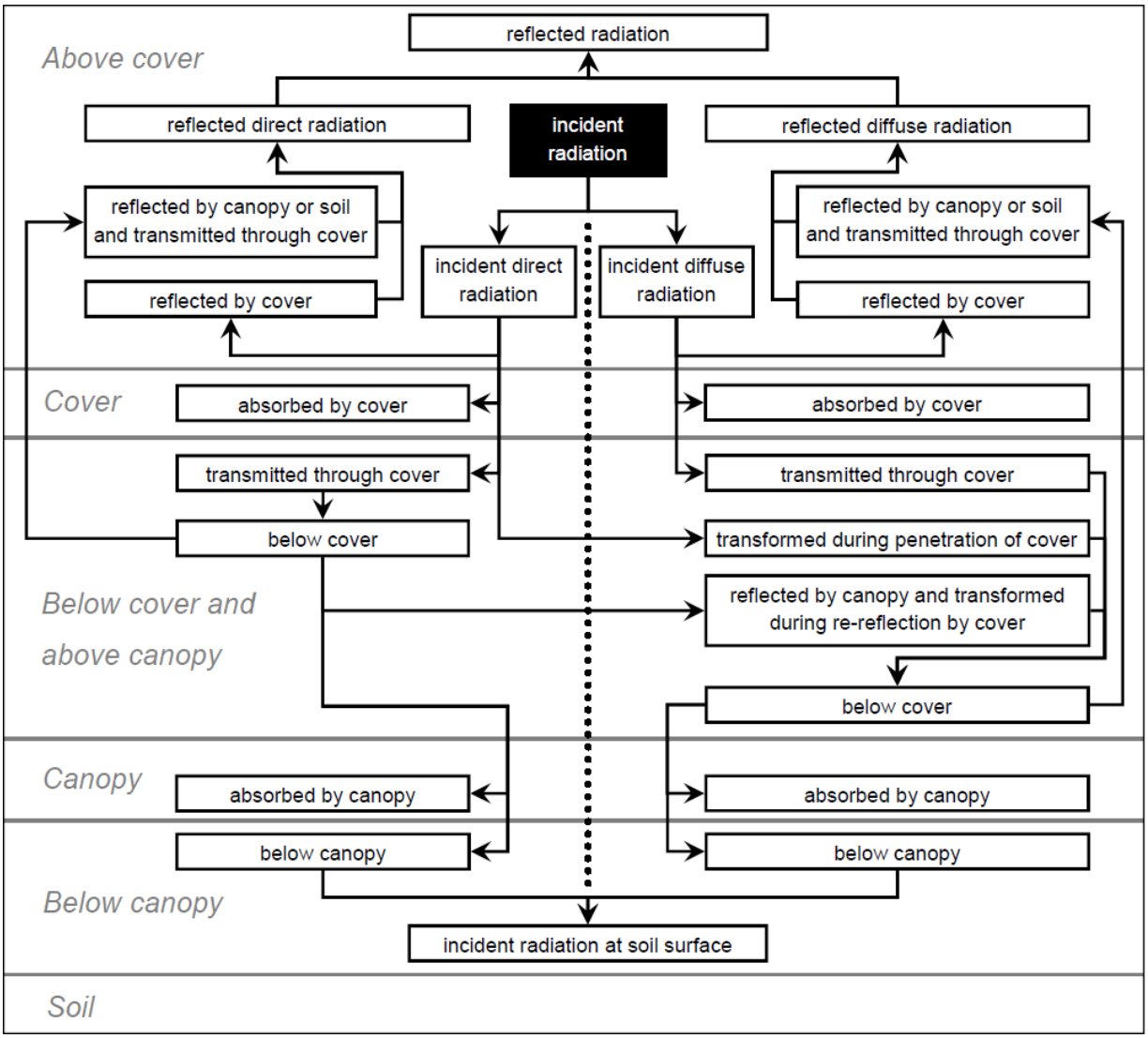


**Figure 1** Radiation–cover–canopy–soil interactions taken into account by the model. Direct radiation is illustrated on the left-hand side of the figure, diffuse radiation on the right.

Figure 1 gives an overview of all radiation–cover–canopy–soil interactions accounted for by the model. Incident shortwave radiation is composed of different fluxes that interact differently with cover materials, leaves and soil. Due to this non-homogeneity, incident shortwave radiation is usually segmented into portions that are treated separately (Goudriaan, 1977):

(1) Wavelength bands: PAR (400 to 700 $nm$) versus NIR (701 to 3000 $nm$)

(2) Angular distribution: single-angular (direct) radiation versus multi-angular (diffuse) radiation

The following equations only take into account the distinction between direct and diffuse radiation fluxes, as all equations used should be valid for both PAR and NIR wavelength ranges, likewise. Our model is based on established equations that describe diffuse and direct radiation transfer in scattering plant canopies over a reflecting soil. This well-proven theory can still be used under covers if direct and diffuse radiation fluxes are separated and account is taken of multiple reflections between the cover and the plant canopy.

### 3.2. Derivation of main fluxes

Incident radiation at soil surface $I_s$, which has accordingly transmitted the cover material and the canopy, can be calculated using

$$I_s = I_{bc}(\theta)\,\tau_{cy}(\theta) + I_{bc}^{d}\,\tau_{cy}^{d}, \tag{1}$$

where $I_{bc}(\theta)$ and $I_{bc}^{d}$ are incident direct and diffuse radiant flux densities at the canopy top below the cover and $\theta$ is the sun zenith angle. The subscripts used are: $cy$ = canopy, $l$ = leaf, $s$ = soil, $bc$ = below cover, 0 = above cover and $cv$ = cover. Superscript $d$ indicates a diffuse light property. The canopy transmittance of direct radiation $\tau_{cy}(\theta)$ accounts for multiple scattering between leaves and soil, respectively. $\tau_{cy}^{d}$ is the canopy transmittance for diffuse radiation, which accounts for multiple reflections within the canopy, between the canopy and soil, and between the canopy and the lower side of the plastic cover. $I_{bc}(\theta)$ is determined from

$$I_{bc}(\theta) = I_0(\theta)\,\tau_{cv}(\theta)\,\big(1 - \chi_{cv}(\theta)\big), \tag{2}$$

where $I_0(\theta)$ is the direct part of incident global radiation above the cover and $\chi_{cv}(\theta)$ the fraction of direct radiation transformed to diffuse radiation during cover transmission, denoted

further as the haze function. $I_{bc}^{d}$ is described as the sum of three different downward diffuse radiation fluxes

$$I_{bc}^{d} = I_{bc}^{d\prime} + I_{bc}^{d\prime\prime} + I_{bc}^{d\prime\prime\prime}, \tag{3}$$

which are defined by

$$I_{bc}^{d\prime} = I_0^{d}\,\tau_{cv}^{d}, \quad I_{bc}^{d\prime\prime} = I_0(\theta)\,\tau_{cv}(\theta)\chi_{cv}(\theta), \quad I_{bc}^{d\prime\prime\prime} = I_{bc}(\theta)\,\rho_{cy}(\theta)\,\rho_{cv}^{d}, \tag{4}$$

where $I_{bc}^{d\prime}$ is the transmitted diffuse sky radiation, $I_{bc}^{d\prime\prime}$ is the diffuse contribution from converting direct to diffuse radiation while transmitting the cover, and $I_{bc}^{d\prime\prime\prime}$ is generated by the interaction of the direct radiation flux $I_{bc}$ with the canopy–soil–cover system. $I_0^{d}$ is the diffuse part of incident global radiation, while partitioning into diffuse $I_0^{d}$ and direct $I_0(\theta)$ components is calculated using a procedure suggested by Spitters et al. (1986) with an added circumsolar part according to Hay (1979). $\tau_{cv}^{d}$ and $\rho_{cv}^{d}$ are the diffuse transmittance and reflectance values of the cover, respectively.

Due to multiple scattering between the canopy and the lower cover side, however, the diffuse radiation transmission coefficient $\tau_{cy}^{d}$ is somewhat higher. Considering $n$ interactions between upstream canopy fluxes and the lower side of the cover, this enhancement can be determined by inspecting the limit $n \to \infty$

$$\tau_{cy}^{d} = \tau_{cy}^{d\prime} + \lim_{n\to\infty} \tau_{cy}^{d\prime} \textstyle\sum_{i=1}^{n} \left(\rho_{cy}^{d\prime}\rho_{cv}^{d}\right)^{i}, \tag{5}$$

which yields

$$\tau_{cy}^{d} = \tau_{cy}^{d\prime} + \frac{\tau_{cy}^{d\prime}\rho_{cy}^{d\prime}\rho_{cv}^{d}}{1-\rho_{cy}^{d\prime}\rho_{cv}^{d}}. \tag{6}$$

In line with diffuse transmission, the effect of multiple scattering between the canopy and the cover is captured by a geometrical series

$$\rho_{cy}^{d} = \rho_{cy}^{d\prime} + \lim_{n\to\infty} \rho_{cy}^{d\prime} \sum_{i=1}^{n} \left(\rho_{cy}^{d\prime}\, \rho_{cv}^{d}\right)^{i}. \quad (7)$$

Solving Eq. (7) yields

$$\rho_{cy}^{d} = \rho_{cy}^{d\prime} + \frac{\rho_{cv}^{d} \left(\rho_{cy}^{d\prime}\right)^{2}}{1-\rho_{cv}^{d}\, \rho_{cy}^{d\prime}}. \quad (8)$$

The canopy transmission and reflection coefficients for direct and diffuse radiation ($\tau_{cy}(\theta), \tau_{cy}^{d\prime}, \rho_{cy}(\theta), \rho_{cy}^{d\prime}$) are calculated using the *JRC2S* 1D canopy radiation transfer code (Pinty et al., 2006), which was extensively validated during a recent radiation model intercomparison study (Widlowski et al., 2011). The *JRC2S* model requires the specification of leaf transmittance and reflectance values ($\tau_l, \rho_l$), the soil albedo $\rho_s$ and a leaf area clumping index for direct ($\Omega(\theta)$) and diffuse radiation ($\Omega(60°)$).

The observed variability in measured leaf reflectance and transmittance values (see **Table 1**) was only related to the cover treatment. No further trends (e.g. over time) were observed.

**Table 1** Measured directional-hemispherical reflectance and transmittance of kohlrabi leaves in the PAR and NIR spectral range (data obtained in 2012).

| Cover treatment | Leaf reflectance | | Leaf transmittance | |
|---|---|---|---|---|
| | PAR | NIR | PAR | NIR |
| Without cover | 0.090 | 0.430 | 0.024 | 0.340 |
| NWF | 0.091 | 0.430 | 0.033 | 0.363 |
| NWF+PF | 0.097 | 0.431 | 0.039 | 0.381 |

Soil reflectance $\rho_s$ versus soil water content $\theta_s$ measurements were fitted to the following mixture of logistic functions

$$\rho_s(\theta_s) = \frac{s_1}{1+\exp(s_2\,(\theta_s - s_3))} + \frac{s_4}{1+\exp(s_5\,(\theta_s - s_6))}, \quad (9)$$

where $s_1$ to $s_6$ are soil-specific parameters, listed in **Table 2**.

**Table 2** Soil surface reflection model parameters.

| Parameter | Spectral range | |
|---|---|---|
| | PAR | NIR |
| $s_1$ | 0.06638 | 0.17065 |
| $s_2$ | 79.36623 | 55.31782 |
| $s_3$ | 0.10630 | 0.10871 |
| $s_4$ | 0.10211 | 0.17015 |
| $s_5$ | 11.14054 | 12.04091 |
| $s_6$ | 0.52066 | 0.50000 |

The fitted dependence of $\rho_s$ on $\theta_s$ is illustrated in **Figure 2**. All parameters are significantly different from zero (t-test, $\alpha = 0.05$) with an $R^2_{adj}$ of 0.9458 (PAR) and 0.9383 (NIR).

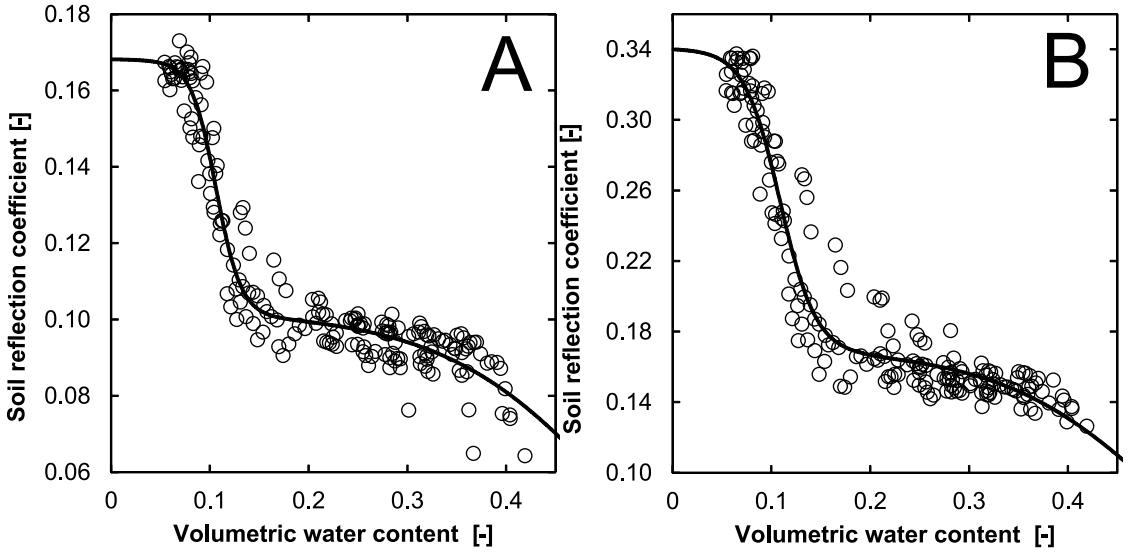


**Figure 2** Soil reflection coefficient in the PAR wave band (A) and the NIR wave band (B) versus soil volumetric water content (lines = model, circles = measurements).

Internally, *JRC2S* parameterises leaf area clumping as

$$\Omega(\theta) = a + b(1 - cos(\theta)), \tag{10}$$

where parameters $a$ and $b$ are empirical parameters. The *JRC2S* model call was adapted to enable the use of a variable G-function value ($G(\theta, X)$), which was calculated from the ellipsoidal leaf angle distribution (Campbell, 1986) with distribution parameter $X$:

$$G(\theta, X) = \frac{(X^2+\tan(\theta)^2)^{0.5}\cos(\theta)}{X+1.774(X+1.182)^{-0.733}}\,. \quad (11)$$

Furthermore, *JRC2S* approximates the transmission of diffuse light for spherical leaf angle distribution ($i.e.\ G(\theta,1) = 0.5$) and a constant clumping index ($\Omega\ (60°)$) according to:

$$\tau^d_{Black} \approx 2\int_0^{\frac{\pi}{2}} \exp\left(-\frac{0.5}{\cos(\theta)}\Omega(60°)LAI\right)\sin(\theta)\cos(\theta)\,d\theta. \quad (12)$$

This approximation is valid for random leaves with an angular clumping index given in Eq. (10). To allow for the more general ellipsoidal leaf angle distribution, the following equality must hold:

$$\int_0^{\frac{\pi}{2}} \exp\left(-\frac{0.5}{\cos(\theta)}\Omega_{eff}LAI\right)\sin(\theta)\cos(\theta)\,d\theta =$$

$$\int_0^{\frac{\pi}{2}} \exp\left(-\frac{G(\theta,X)}{\cos(\theta)}\,\Omega(\theta)\mathrm{LAI}\right)\sin(\theta)\cos(\theta)\;d\theta, \quad (13)$$

which is solved for $\Omega_{eff}$ and fed into *JRC2S* to calculate diffuse radiation transfer for non-spherical leaf angle distributions, i.e. $X \neq 1$. Note that the right-hand side of Eq. (13) is a commonly used equation for calculating diffuse radiation transfer (Campbell and Norman, 1998). Since the diffuse radiance distribution under a plastic cover is largely unknown, a uniform radiance distribution is adopted in this case.

Previously estimated gap fraction and leaf areas for uncovered kohlrabi crops (Sandmann et al., 2013) were reanalysed. The reanalysis involved using measured leaf areas and gap fractions obtained from digital photographs and PCA measurements at different viewing zenith angles $0° \ldots 57°$. The following parameterisation of canopy structure was finally obtained:

$$\begin{aligned} X &= 1.96\,LAI^{0.235} \\ \Omega_{57} &= 0.834 \\ \Omega_0 &= \Omega_{57} + 4.32LAI^{0.807}\exp(-4.32\,LAI) \end{aligned}\,. \quad (14)$$

The fitted functions for the clustering factor are shown in **Fig. (3)**. The leaf area clumping index at nadir viewing zenith angle depends nonlinearly on LAI and displays a degree of overdispersion at low LAI; no systematic change in leaf area was detected at 57°. Parameters $a$ and $b$ in Eq. 10 were then obtained by $a = \min(\Omega_0, \Omega_{57})$ and $b = (\Omega_{57} - a)/(1 - \cos(57°))$. Note that gap fraction data from all viewing zenith angles lower than 57° was included in the parameter estimation using a robust regression approach (iterated least squares with Huber weights). Several alternative functions to Eq. (10) were tested, but failed to improve the fit to the derived clumping index.

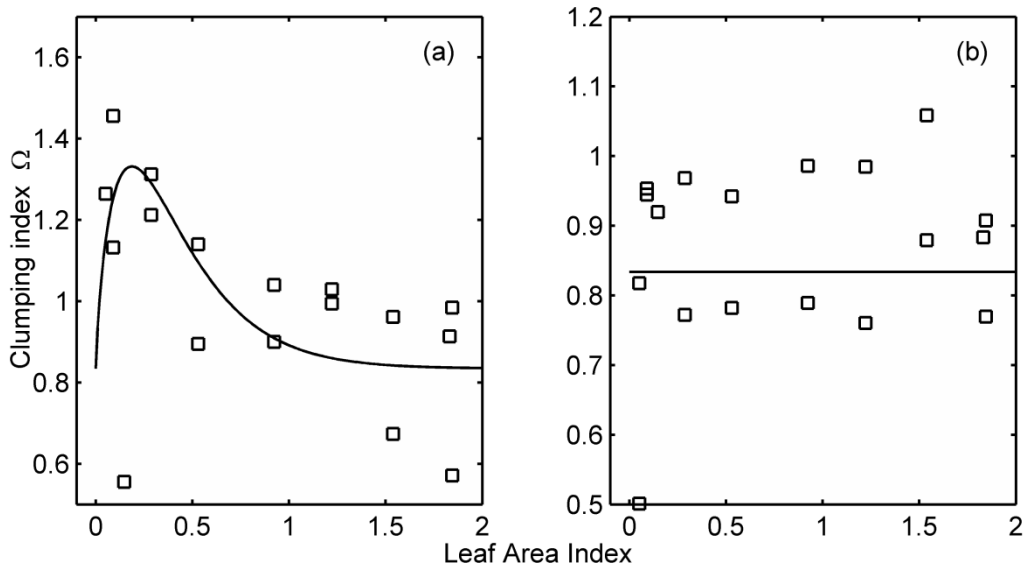


**Figure 3** Fitted (line) and estimated (symbols) clumping index at nadir (a) and 57° (b) view zenith angles versus *LAI*. The clumping indexes shown are estimated from model inversion using a prescribed G-function from PCA measurements, measured leaf area and linear averaged gap fractions.

During kohlrabi growth there is a plant size-induced shaping of the cover surface, which leads to a varying surface roughness during growth (**Figure 4**).

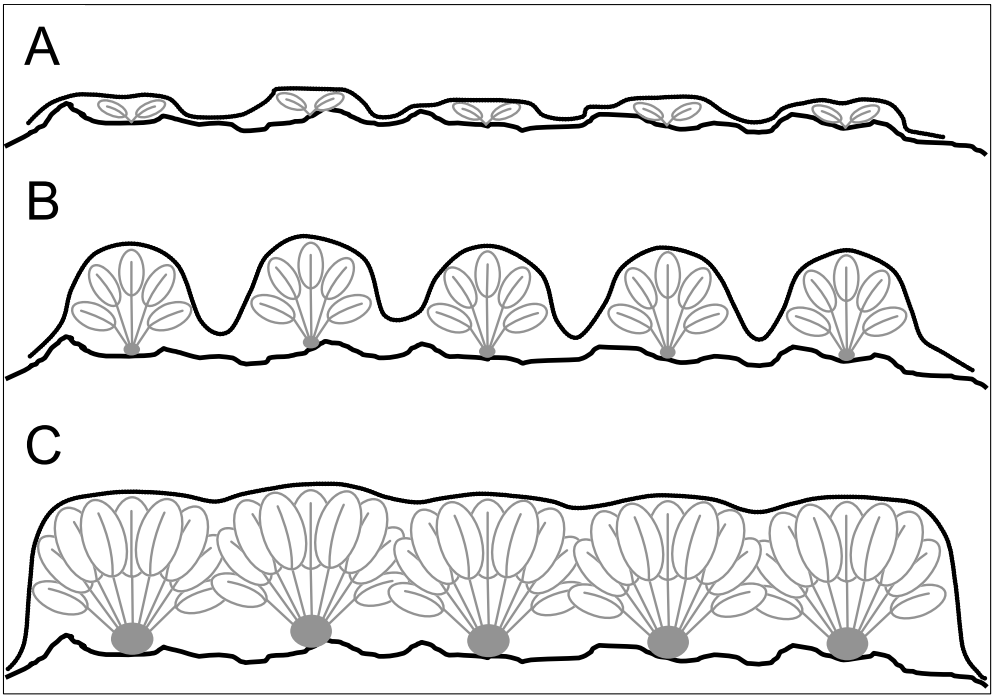


**Figure 4** Shape of the cover surface during kohlrabi growth at stages A to C.

This variation is empirically described by a scaled Fréchet distribution

$$\alpha_b(LAI) = \frac{c_1}{c_2}\left(\frac{LAI}{c_2}\right)^{-1-c_1} \exp\left(-\left(\frac{LAI}{c_2}\right)^{-c_1}\right) D_{max}^{-1}\left(\alpha_{b,max} - \alpha_{b,min}\right) + \alpha_{b,min,} \quad (15)$$

where $\alpha_b$ is a roughness parameter to be described below, $c_1$, $c_2$, $\alpha_{b,max}$ and $\alpha_{b,min}$ are free parameters and $D_{max}$ is the maximum density.

### 3.3. Optical properties of covers

Providing a comprehensive description of optical properties of plastic covers under field conditions is a challenging task, from both a theoretical and an experimental perspective. Cover transmittance and reflectance change according to the current state of surface wetness and light incidence, and therefore also with cover roughness.

Estimated directional-hemispherical transmittance and reflectance values for new and used dry plastic covers are summarised in **Table 3**. The differences between dry and wet covers are shown in **Table 4**.

**Table 3** Measured directional-hemispherical reflectance and transmittance of covers for an incidence angle $\theta = 5°$ in the PAR and NIR waveband before and after field use. NWF = non-woven fabric, PF = perforated film, usage duration = 78 $d$

| Material | State | Reflectance | | Transmittance | |
|---|---|---|---|---|---|
| | | PAR | NIR | PAR | NIR |
| NWF | New | 0.127 | 0.129 | 0.872 | 0.871 |
| NWF+PF | | 0.209 | 0.198 | 0.789 | 0.780 |
| NWF | Used | 0.150 | 0.161 | 0.777 | 0.814 |
| NWF+PF | | 0.263 | 0.241 | 0.681 | 0.749 |

**Table 4** Differences in optical properties of cover materials under dry and wet conditions (differences are calculated as wet minus dry).

| Material | Reflectance difference | | Transmittance difference | |
|---|---|---|---|---|
| | PAR | NIR | PAR | NIR |
| NWF | -0.0015 | -0.0150 | 0.0027 | -0.0431 |
| NWF+PF | -0.0298 | -0.0505 | 0.0350 | -0.0179 |

In general, reflection increases and transmission decreases during the ageing process of the cover materials. Since cover samples were only analysed at the beginning and end of the experiment (2012, duration = 78d), the adopted linear ageing process was parameterised with a variable effective duration $d_e$

$$\omega(t) = \omega_O + \frac{\omega_N - \omega_O}{\min(78, d_e)} \min(t, d_e), \tag{16}$$

where $\omega(t)$, $\omega_N$ and $\omega_O$ denote the current, new and old state of an optical property.

However, laboratory measurements of optical properties need to be properly scaled to field conditions to account for effects such as a distributed sun incidence angle over a non-flat cover surface. The overall approach followed here is based on measured angular transmittances and absorptances of plane plastics at selected incidence angles in the

laboratory. Angular reflection is then subsequently obtained from the radiation balance. These angular resolved properties are then averaged over the local incidence angle distribution of a rough cover surface, which comprises small surface patches or facets.

The density function $D(\beta)$ of small-surface facet slopes ($\beta$) is described by the Beckmann distribution (Walter et al., 2007) with roughness parameter $\alpha_b$. This distribution is further extended to account for the visibility of facets $V$ and the projected area of the facet, which is proportional to the cosine of the incidence angle ($\cos(\delta)$) of light

$$D(\theta,\beta,\phi) = \frac{\exp\left(-\frac{\tan(\beta)^2}{\alpha_b^2}\right)}{\cos(\beta)^4} V(\theta,\beta,\phi)\cos(\delta). \tag{17}$$

The cosine angle of incidence ($\delta$) between a light ray and a facet with slope $\beta$ and azimuth offset $\phi$ is calculated from (Goudriaan, 1988)

$$\cos(\delta) = cos(\theta)\, cos(\beta) + sin(\theta)\, sin(\beta)\, cos(\phi). \tag{18}$$

The visibility function $V(\theta,\beta,\phi)$ is one for positive cos($\delta$) and zero otherwise, indicating a ray incidence from the facet underside. If the measured directional-hemispherical absorptance function of covers ($\alpha(\delta)$) is now used, the mean cover absorptance for direct radiation at sun incidence angle $\theta$ with facets distributed according to the Beckmann distribution is

$$\alpha_{cv}(\theta) = N_c^{-1} \int_0^{\pi/2} \int_0^{\pi} D(\theta,\beta,\phi)\alpha(\delta) d\beta d\phi \ . \tag{19}$$

The normalisation constant $N_c$ is derived from the integration of Eq. (17)

$$N_c = \int_0^{\pi/2} \int_0^{\pi} D(\theta,\beta,\phi)\, d\beta d\phi \ . \tag{20}$$

Assuming a standard overcast sky radiation distribution (Moon and Spencer, 1942), the diffuse cover absorptance is given by (Papadakis et al., 2000):

$$\alpha_{cv}^{d} = 6/7 \int_0^{\pi/2} \alpha_{cv}(\theta) \sin(\theta)\cos(\theta)(1 + 2\cos(\theta))\, d\theta. \quad (21)$$

A similar approach could be taken for transmission, but additional losses could occur. As already mentioned, light is partly diffused during cover passage. For sloped cover facets, a fraction of this diffusely transmitted light is directed towards the upper hemisphere and lost, with the exception of some backward reflected contributions. Assuming a lambertian distribution of diffused light, the effective directional-hemispherical transmittance is approximated as:

$$\tau_e(\theta) = \tau(\theta)(1 - \chi(\theta)\ 0.5 \sin(\beta)^2\, \alpha_{cv}^{d} \tau_{cv}^{d}) \quad (22)$$

with haze function $\chi(\theta)$. The calculations required to obtain $\tau_{cv}(\theta)$ and $\tau_{cv}^{d}$ are then identical to the absorptance case (Eqs. 19 - 21), but use effective directional-hemispherical transmittance $\tau_e(\theta)$. Note that Eq. (22) approximates local absorption and transmission with bulk cover quantities and must be solved by iteration of Eqs. (19) - (22).

The directional and diffuse reflectance of the bulk cover is simply obtained from the radiation balance

$$\begin{array}{rcl} \rho_{cv}(\theta) & = & 1 - \alpha_{cv}(\theta) - \tau_{cv}(\theta) \\ \rho_{cv}^{d} & = & 1 - \alpha_{cv}^{d} - \tau_{cv}^{d} \end{array} . \quad (23)$$

Finally, the haze function $\chi(\theta)$ was estimated from the fitted angular responses of directional-hemispherical transmittance $\tau(\delta)$ and directional-directional transmittance $\tau_{DIR}(\delta)$: $\chi(\theta) = 1 - \tau_{DIR}(\delta)/\tau(\delta)$. However, in analogy to transmission, some diffusely transmitted light is lost to the upper hemisphere for sloped facets, leading to a reduction in the diffuse light fraction. The effective haze function can be stated as

$$\chi_e(\theta) = \chi(\theta)\ (1 - 0.5 \sin(\beta)^2\, \alpha_{cv}^{d} \tau_{cv}^{d}) \quad (24)$$

which is subsequently scaled to a cover property ($\chi_{cv}(\theta)$) with roughness parameter $\alpha_b$ according to Eq. (19). All numerical solutions to Eqs. (19) - (24) were obtained by the MATLAB quad function and tabulated for discrete $\alpha_b$ values (0.1,0.2…1.). During simulation, upscaled optical cover properties at intermediate $\alpha_b$ values are obtained by the linear interpolation of tabulated values.

The state of wetness of the lower surfaces of plastics is likely to change during the day. However, the state of wetness was not monitored or physically modelled. It was therefore assumed that plastics are wet until a distinct sum of incident global radiation since sun rise has been received, after which they are considered dry. This necessary radiation sum is regarded as a free parameter (one for each cover) that needs to be fitted.

## 4. Results

### 4.1. Angular-resolved optical properties of plane covers

Measured angular transmittance and absorptance functions ($\tau(\delta)$ and $\alpha(\delta)$) are presented in **Fig. 5** and **Table 5**.

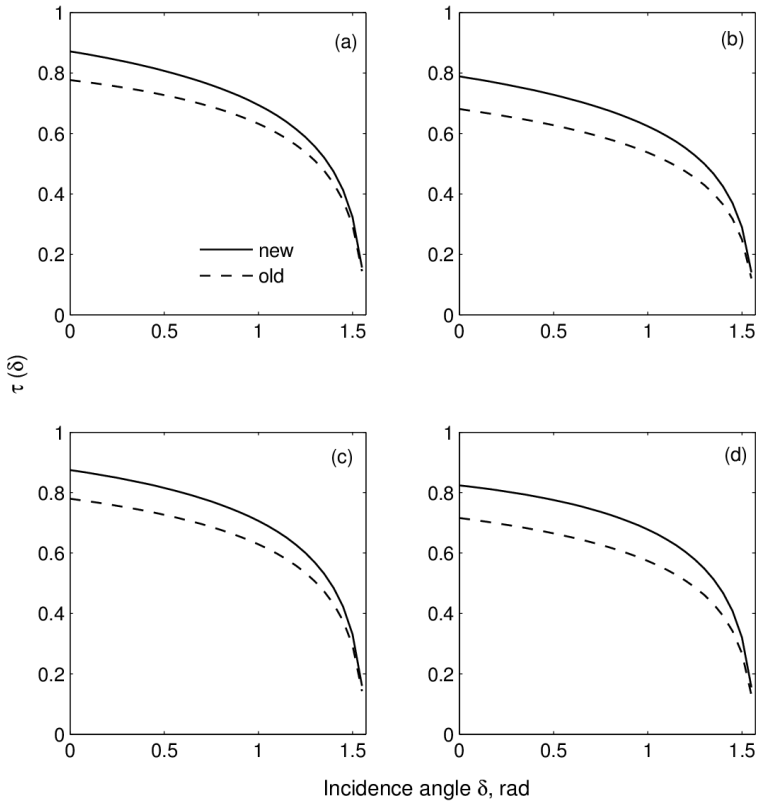


**Figure 5** Measured PAR transmittance versus light incidence angle of plane plastics: (a) NWF dry, (b) NWF+PF dry, (c) NWF wet, (d) NWF+PF wet.

Since transmission measurements with the larger integrating sphere are more reliable and cover the whole PAR range, red transmission values are scaled accordingly with effective PAR values (**Table 3**). The angular response of transmission is quite similar for the different plastics in different states (dry versus wet, old versus new). Absorptances at 0° and 45° are given in **Table 5**. As expected, absorptances increase with age and incidence angle. An angular response function is obtained from a spline interpolation with a zero absorption constraint at 90°, which results in a nearly symmetric response at around 45°. A reanalysis of angular absorptance data for polyethylene (Nijskens et al., 1985) confirmed this approach.

**Table 5** Measured PAR absorptance values at 0° (PAR) and 45° (red) light incidence, respectively, for plane plastics.

| Material | State | Absorptance dry | | Absorptance wet | |
|---|---|---|---|---|---|
| | | 0° | 45° | 0° | 45° |
| NWF | New | 0.001 | 0.046 | 0.005 | 0.053 |
| NWF+PF | | 0.002 | 0.052 | 0.010 | 0.060 |
| NWF | Used | 0.073 | 0.085 | 0.072 | 0.070 |
| NWF+PF | | 0.056 | 0.112 | 0.061 | 0.093 |

Incident direct light is shown to diffuse to a lesser extent in dry plastics and for near normal incidence angles (**Figure 6**). Almost all direct light is diffused as more oblique incidence angles are approached. As expected, the single layer cover (NWF) shows a slightly lower tendency to diffuse.

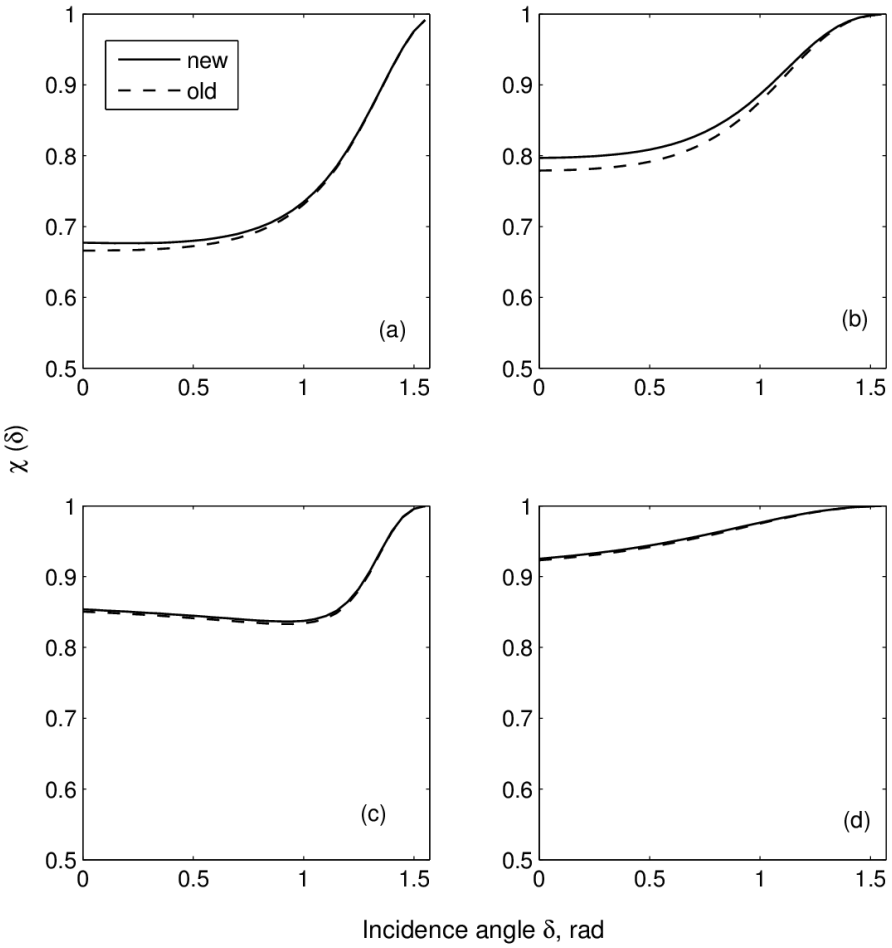


**Figure 6** Measured haze function $\chi(\delta)$ for plane plastics: (a) NWF dry, (b) NWF+PF dry, (c) NWF wet, (d) NWF+PF wet.

### 4.2. Transmittance of rough covers

Practical experience and preliminary model fits revealed that covers are usually in a wet state. Figure 7 shows transmission functions calculated for rough plastics for anticipated typical values of the Beckmann distribution ($\alpha_b$). Transmittance of direct light for rough plastics exhibits a shallower response to the sun incidence angle than plane plastics **(Fig. 5)**; surfaces with a different roughness behave very similarly at about 66°. With a further increase in the sun incidence angle, light transmission is enhanced for rougher surfaces.

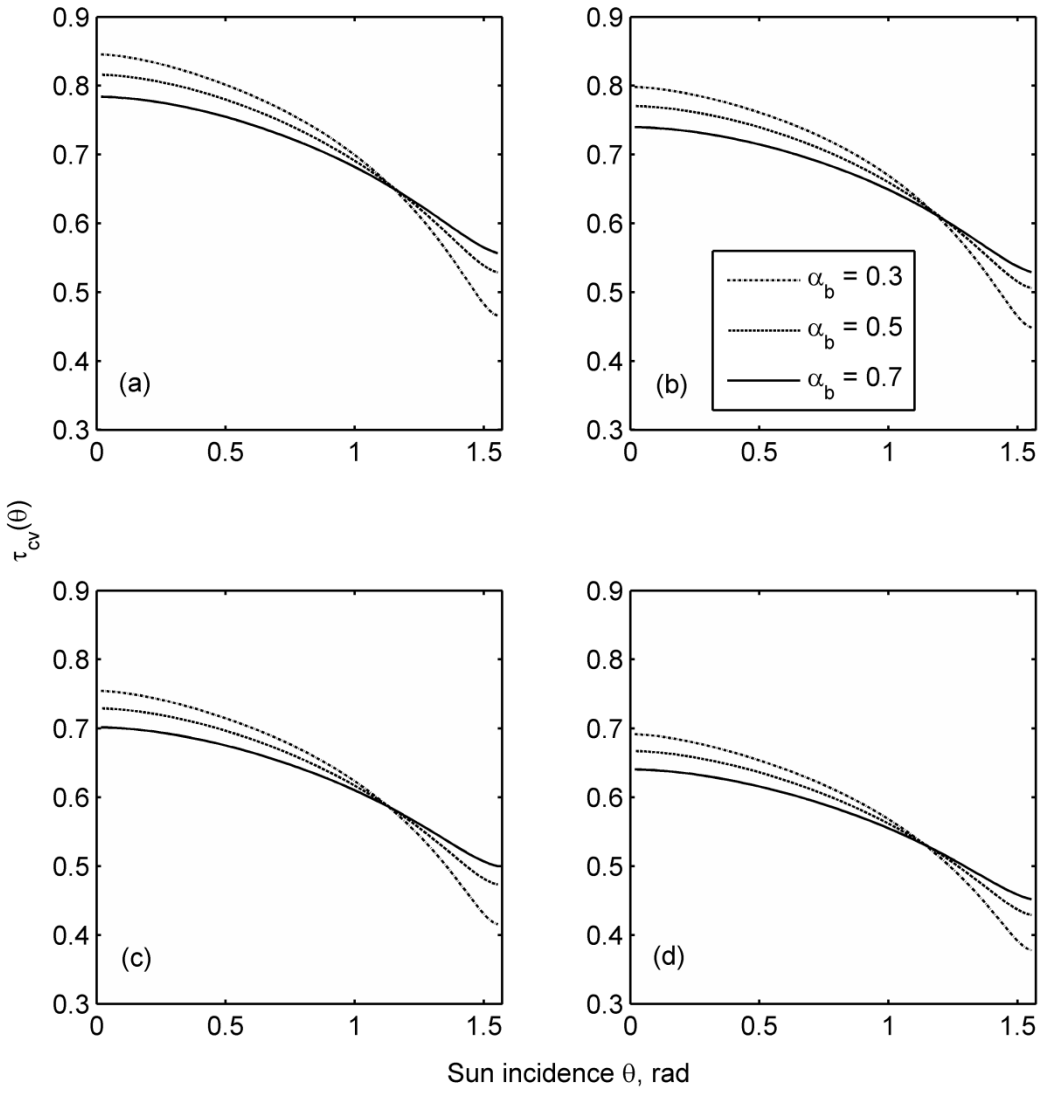


**Figure 7** Calculated PAR transmittance versus sun incidence angle of wet plastics calculated for different values of surface roughness $\alpha_b$: (a) NWF new, (b) NWF+PF new, (c) NWF old, (d) NWF+PF old.

Calculated diffuse transmittance decreases linearly with cover roughness (**Figure 8**), but the effect is smaller compared to changes caused by aging if medium roughness values ($\alpha_b \sim 0.5$) are considered.

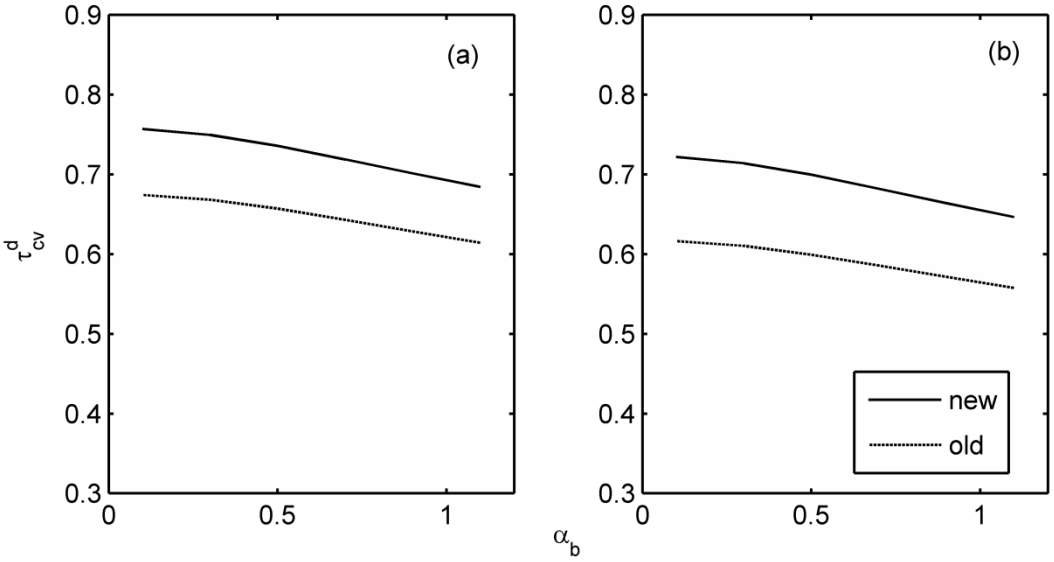


**Figure 8** Calculated diffuse PAR transmittance versus cover roughness parameter $\alpha_b$: (a) wet NWF , (b) wet NWF+PF.

### 4.3. Parameter estimation and model performance

Parameters related to the temporal change of cover roughness ($\alpha_{b,min}$, $\alpha_{b,max}$, $c_1$, $c_2$, Eq. (15)), the effective duration of the linear aging process ($d_e$, Eq. (16)), the required sum of incident global radiation for drying ($s_r$) and the parameters of the X function ($X = c_3 LAI^{c4}$, Eq. (14)) were optimised for each cover treatment (**Table 6**).

**Table 6** Estimated parameter values for each cover treatment.

| Cover | $\alpha_{b,max}$ | $\alpha_{b,min}$ | $c_1$ | $c_2$ | $c_3$ | $c_4$ | $d_e$ (d) | $s_r$ (kWh) |
|---|---|---|---|---|---|---|---|---|
| NWF | 0.99 | 0.104 | 2.12 | 1.70 | 1.62 | 0.0872 | 45.2 | 1.61 |
| NWF+PF | 0.99 | 0.105 | 1.38 | 1.21 | 2.89 | 0.0682 | 42.3 | 1.79 |

The estimates obtained for $\alpha_{b,min}$ and $\alpha_{b,max}$ approached the provided bound constraints to the ga search algorithm ($\alpha_{b,min}$: 0.1…0.3, $\alpha_{b,max}$: 0.31…1). The fitted relative change in cover roughness with leaf area ($c_1$, $c_2$, **Figure 9**) development increased strongly with leaf area and diminished again after peaking at medium LAI.

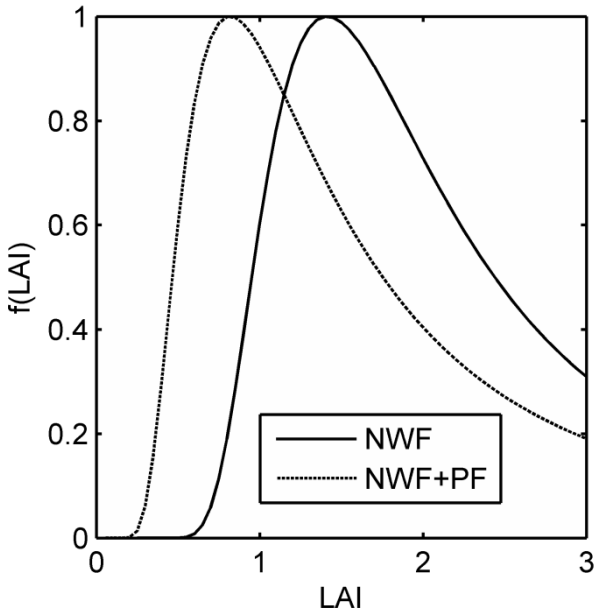


**Figure 9** Fitted normalised Fréchet distribution to describe the change in relative cover roughness for NWF and NWF+PF covers as a function of the leaf area index.

The estimated *X*-*LAI* relations ($c_3$, $c_4$, **Figure 10**) have a similar shape as the independently derived function for uncovered crops, although crops covered with a double layer tend to have more horizontally inclined leaf angle distributions.

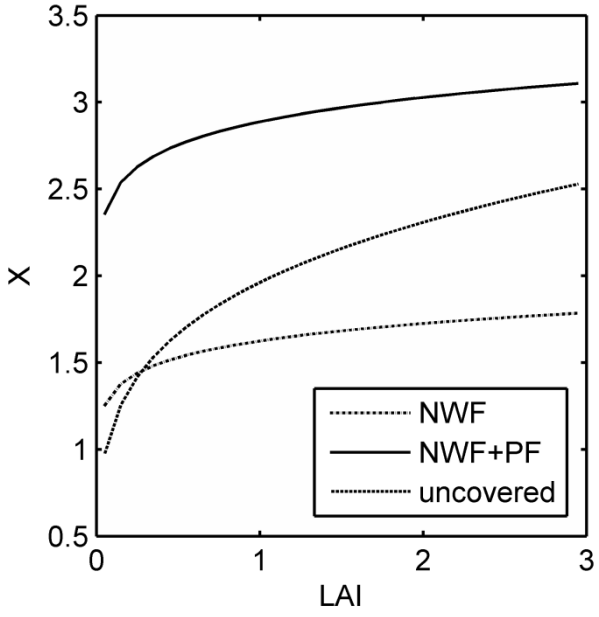


**Figure 10** Fitted *X* versus *LAI* relations for NWF and NWF+PF covers and the deduced function for uncovered crops from independent gap fraction measurements.

The estimated effective duration of cover aging ($d_e$) is significantly lower than the time span of actual observation (78 *d*), which indicates that more frequent measurements would be necessary to characterise this process fully. On average, NWF covers had become dry somewhat earlier in the day than NWF+PF covers, as indicated by the fitted $s_r$ parameter. The corresponding mean and standard deviations of decimal daytime hours (UTC+1) for this event are 11.7 ± 1.57 and 12.1 ± 1.72 for NWF and NWF+PF, respectively.

There is a good overall correspondence between simulated and measured radiant flux densities at the soil surface (**Figure 11**), as indicated by small root mean squared errors (RMSE) of 6.62 and 5.11 W m$^2$ for NWF and NWF+PF covers, respectively.

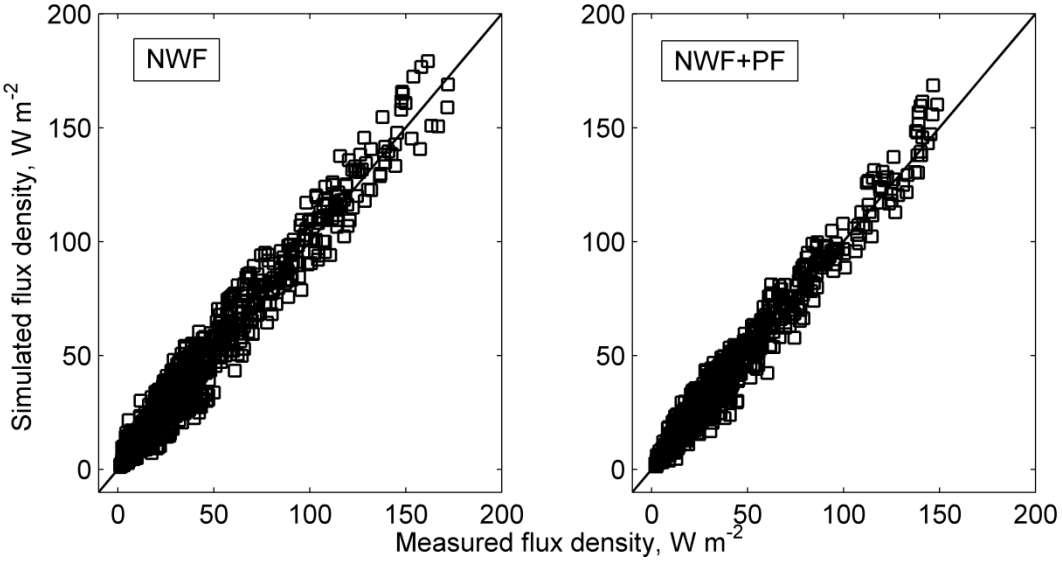


**Figure 11** Simulated versus measured radiant flux densities at the soil surface for NWF and NWF+PF covered kohlrabi crops. The line is a 1:1 response. NWF: $n = 1067$, $R^2 = 0.96$, $RMSE = 6.62$; NWF+PF: $n = 1112$, $R^2 = 0.97$, $RMSE = 5.11$.

The performance of the full model was compared to simplified model versions: 1) Model_A: Constant cover roughness ($\alpha_b = 0.1$); 2) Model_B: Setting all optical properties to laboratory values obtained at near normal ray incidence; 3) Model_C: Using a simple non-scattering canopy with spherical leaf angle distribution and single angle approximation for diffuse radiation ($\theta = 45°$). The performance of the model was poorest when angular and therefore also diffuse optical properties of the plastics were neglected (**Table 7**). Simplified

assumptions regarding canopy light transfer (Model_C) and cover roughness effects (Model_B) exhibit far less model performance degradation.

**Table 7** Comparison of the root mean squared error (RMSE) and the mean difference (BIAS) between simulated and measured PAR flux densities at the soil surface for models with reduced complexity.

| Cover | Full model | | Model_A | | Model_B | | Model_C | |
|---|---|---|---|---|---|---|---|---|
| | RMSE | BIAS | RMSE | BIAS | RMSE | BIAS | RMSE | BIAS |
| NWF | 6.62 | 4.28 | 6.77 | 2.76 | 10.97 | 8.77 | 6.87 | 2.84 |
| NWF+PF | 5.10 | 1.96 | 5.53 | 2.81 | 10.13 | 8.59 | 6.65 | 4.79 |

Since no measurements of flux densities at the soil level were available in the NIR spectral range, simplified model versions were compared to full model simulations (**Table 8**) with adopted optical properties to the NIR range. In order to make a fair comparison, the black leaf canopy Model_C was adapted to include a common multiple scattering approximation to the extinction coefficient: $K = 0.5 / \cos(\theta)(1 - \tau_l - \rho_l)^{0.5}$ (Goudriaan, 1977). Neglecting angular optical responses also had a strong degrading performance effect in the NIR spectral range. In addition, however, canopy fluxes need to be modelled with greater care than in the PAR spectral range (**Table 8**). Similarly, the neglecting effects of cover roughness only has a minor impact on the performance of the model.

**Table 8** Comparison of the root mean squared error (RMSE) and the mean difference (BIAS) between simulated NIR flux densities at the soil surface using simplified models and the full model.

| Cover | Model_A | | Model_B | | Model_C | |
|---|---|---|---|---|---|---|
| | RMSE | BIAS | RMSE | BIAS | RMSE | BIAS |
| NWF | 1.66 | 0.71 | 9.92 | 7.76 | 6.06 | 3.85 |
| NWF+PF | 2.06 | 1.08 | 10.37 | 8.46 | 7.60 | 5.28 |

## 5. Discussion

### 5.1. Measured optical properties

The soil reflectance characteristics we measured (**Figure 2**) are generally comparable to the results of Lobell and Asner (2002), although they used only $1\,mm$ thick soil samples as opposed to the $5\,cm$ thick samples used here. Lobell and Asner (2002) and Muller and Décamps (2001) used exponential functions for their soil reflectance models. Due to the

observation of the initial increase in $\rho_s$ and the constant $\rho_s$ after the colour of the soil surface changed (which was not observed by Lobell and Asner (2002) and Muller and Décamps (2001) because of their different experimental setup), we applied a mixture of logistic functions, as explained by Meyer (1994), for a variety of scenarios.

Al-Mahdouri et al. (2013) observed a zero complex index of refraction for a low-density polyethylene plastic over the short wave length range, meaning that new plastics only permit weak radiation absorption (**Table 5**). However, at an incidence angle of 45° we measured a finite absorptance of approximately 4 to 5 %, even for new plastics. In scattering plastic materials, absorbance is enhanced by an increased effective path length and classical Fresnel theory needs to be modified (Rosenfeld et al., 2001). Moreover, near normal and 45° incidence absorptance measurements derived from corresponding transmittance and reflectance measurements are noisy because they are derived from two measurements. A centre-mounted sample setup within an integrating sphere (ASTM, 1992) would yield the angular absorptance of plastics or covers more precisely. Clearly, the adopted spline interpolation of three prescribed absorptances (θ: 0°, 45°, 90°) is a rough assumption, but data from Nijskens et al. (1985) support this approximation. However, it is preferable to derive angular-resolved directional-hemispherical reflectance from the radiation energy balance (Eq. (23)) because it is very difficult to measure this quantity.

Visually, cover ageing is related to the presence of dirt and algal growth, leading to increased absorptance and reflectance, and lower transmittances (**Table 3**). Even under laboratory conditions, however, artificial weathering of different plastic materials over 480 hours increased the scattering coefficient significantly (Wallner and Lang, 2005). Using parameter optimisation, we estimated that ageing mainly occurred in the first 40 to 50 days of field cover use in our experiment (parameter $d_e$, **Table 6**). However, ageing effects are significant and should be taken into account more frequently in similar future experiments.

To our knowledge, no angular-resolved measurements of haze (Yu and Hsaio, 2009) for different plastics have been published yet. Here we proposed the relation: $\chi(\delta) = 1 - \tau_{DIR}(\delta)/\tau(\delta)$ to obtain an angular haze function from separate directional-directional and directional-hemispherical transmittance measurements. The observed trends of increasing haze with ray incidence angle and wetness are consistent with results obtained by Cabrera et al. (2009), Pieters et al. (2003) and Pollet et al. (2005).

Wetting covers usually degrades the transmittance of plastics if dropwise condensation is present (Pollet and Pieters, 2002). In this case, however, transmittances actually increased for the NWF+PF cover (**Table 4**). It was observed, however, that wetted underside NWF was virtually glued to the PF, meaning that interface water acted like an anti-reflective agent and prevents the occurrence of drops.

It proved effective to use the sum incident global radiation as a driver for different durations of cover underside wetness. Since crops usually dry in the morning, the estimate obtained in this case of around noon is reasonable, as turbulent exchange of canopy is largely restricted by covering. In a future model extension, radiation transfer will be solved simultaneously with the energy balance of the cover–canopy–soil system to obtain the wetness state of the cover dynamically, which should slightly improve the predictions.

### 5.2. Upscaling optical properties from plane to rough covers

There is a long tradition in computer graphics to derive more realistic bidirectional reflectance and transmittance distributions of materials from a prescription of the micro facet distribution of the material surface and the per facet application of the Fresnel equations (Cook and Torrance, 1982). Here we focus on a larger spatial scale of cover slope variation and use measured directional-hemispherical transmittances and absorptances of bulk samples in rather than Fresnel computations.

In fact, there are no independent measurements or previous studies available to verify the proposed upscaling procedure from plane to rough plastic surfaces (Eqs. (17) - (24)). Although the estimated relative change in cover roughness with leaf area (**Figure 9**) supports the initial hypotheses of plant size-induced seasonal roughness change, no sensible estimates of minimum and maximum roughness values were obtained (**Table 6**). After all, as we rather expected $\alpha_{b,min}$ and $\alpha_{b,max}$ estimates to differ greatly from the prescribed box constraints (0.1; 1) following the analysis of ad hoc generated surfaces with a similar appearance to covered canopies. Overall, the simulations were not very sensitive to the inclusion of cover roughness in the PAR (**Table 7**) or the NIR (**Table 8**) spectral range.

In order to describe the light microclimate under plastic covers appropriately, however, it is important to measure directional-hemispherical transmittance at various angles and to calculate diffuse transmittance weighted by a reasonable chosen diffuse sky radiance distribution (Eq. (21), **Table 7**, **Table 8**).

### 5.3. Parameterisation of kohlrabi canopy architecture

The measured and estimated relations of the $X$ parameter from the ellipsoidal leaf angle distribution with leaf area (**Figure 10**) growth are plausible because young kohlrabi plants tend to have more vertically inclined leaves and because the double cover exerts a significant mechanical load on the top leaf layer, promoting more horizontal leaf inclinations. Although clumping index estimates at viewing angles of 57° are more reliable, as the G-function is almost invariant to leaf angle distributions (Myneni et al., 1989), we believe that the trend obtained at nadir direction is also reasonable (**Figure 3**). We argue that crops grown on a regular planting pattern ($0.3 \times 0.3\ m$) with a minor degree of leaf overlapping are likely to tend to regular leaf dispersion at the nadir viewing direction at early stages of development. Baret et al. (1993) observed a maximum clumping factor of about 1.3 for sugar beet at 15°

viewing zenith angle, which declined with increasing zenith angle, as observed here. Furthermore, Andrieu and Sinoquet (1993) analysed regularly spaced artificial canopies and found a clumping factor of 1.26 at nadir viewing direction, which diminished towards unity at zenith angles > 30°. Since most canopy structure-related studies adopt the terminology of a clumping index (Demarez et al., 2008, Gonsamo and Pellikka, 2009), they always implicitly presume a leaf area dispersion coefficient (Nilson, 1971) smaller than unity, which usually results from local varying leaf area densities between samples as detected using the logarithm method first introduced by Lang and Yueqin (1986). The intrinsic processes apart from leaf area density clustering leading to overdispersion of leaf area towards nadir viewing zenith angles require further research. This refinement could improve the precision of plant growth and water use simulation models, especially at low latitudes and in early growth stages prior to significant leaf overlapping.

## 6. Conclusions

Provided that the leaf area, the optical properties of plastics, leaves and soil, and incident shortwave radiation flux density are known, the radiation transfer model developed here is suitable for predicting the radiation micro climate for kohlrabi canopies below a plastic cover in the field in both the PAR and NIR spectral range.

Model simulations are most sensitive to a sound specification of the angular optical properties of the covers applied. In addition, sound modelling of the multiple scattering between the soil, leaves and plastic is of similar importance in the NIR spectral range. Comprehensive upscaling from plane to rough plastics can be derived using the microfacet theory, but only small improvements in prediction accuracy can be achieved if the surface roughness of covers in the field is considered in greater detail.

During early growth stages with non-significant leaf overlapping, we further detected an overdispersion of leaf area, attributable to the regular planting grid used. The presented model will be the basis for a more complex energy balance model of the whole production system characterised by kohlrabi crops under single NWF and double NWF+PF plastics.

## 7. Acknowledgements

The authors would like to thank Ingo Hauschild, Ines Marten and Simone Starke for their practical assistance. This study was funded by the German Federal Ministry of Education and Research and the federal state ministries: Lower Saxony Ministry of Science and Culture, Brandenburg Ministry of Infrastructure and Agriculture, and Bavarian Ministry of State of Science, Research and Art.

## 8. Notation

| | |
|---|---|
| $I_0$ | direct part of incident shortwave radiation above the cover (W m$^{-2}$) |
| $I_{bc}(\theta)$ | direct radiation intensity at the canopy top below the cover (W m$^{-2}$) |
| $I^d_0$ | diffuse part of incident shortwave radiation above the cover (W m$^{-2}$) |
| $I^{d\prime}_{bc}$ | diffuse sky radiation transmitted by the cover (W m$^{-2}$) |
| $I^{d\prime\prime}_{bc}$ | downward diffuse contribution from converting direct radiation while transmitting the cover (W m$^{-2}$) |
| $I^{d\prime\prime\prime}_{bc}$ | downward diffuse radiation generated by one interaction of the direct radiation flux with canopy, soil and cover (W m$^{-2}$) |
| $I_s$ | incident radiation at the soil surface (W m$^{-2}$) |
| NIR | near-infrared radiation |
| NWF | non-woven fabric |
| PAR | photosynthetic active radiation |
| PF | perforated film |
| RMSE | root mean squared error |
| $r_s$ | global radiation threshold sum for the drying cover (kWh) |
| $X$ | parameter of the ellipsoidal leaf angle distribution |
| | **Greek symbols** |
| $\alpha_{cv}(\theta)$ | cover absorptance for direct radiation |
| $\alpha^d_{cv}$ | cover absorptance for diffuse radiation |
| $\beta$ | surface slope (radiant) |
| $\delta$ | collimated light source zenith angle (radiant) |
| $\chi(\theta)$ | cover haze function at incidence angle $\theta$ |
| $\phi$ | relative azimut between surface normal and light ray (radiant) |
| $\rho(\theta)$ | directional-hemispherical reflectance at incidence angle $\theta$ |
| $\rho^d$ | hemispherical-hemispherical reflectance |
| $\rho_s(\theta_s)$ | soil albedo at soil water content $\theta_s$ |

| | |
|---|---|
| $\tau(\theta)$ | directional-hemispherical transmittance at incidence angle $\theta$ |
| $\tau^d$ | hemispherical-hemispherical transmittance |
| $\tau_{DIR}(\delta)$ | directional-directional transmittance at incidence angle $\delta$ |
| $\theta$ | sun or view zenith angle (radiant) |
| $\theta_s$ | volumetric soil water content ($m^3\ m^{-3}$) |
| $\Omega(\theta)$ | leaf clumping index at zenith angle $\theta$ |
| $\Omega_{57}$ | leaf clumping index at 57° |
| $\Omega_0$ | leaf clumping index at nadir direction |

**Subscripts**

| | |
|---|---|
| *bc* | below cover |
| *cv* | cover |
| *cy* | canopy |
| $\lambda$ | leaf |
| *0* | above cover |
| s | soil |

**Superscripts**

| | |
|---|---|
| *d* | diffuse |
| ‘ | previously defined quantity |

## 9. References


Albright, L.D., Wolfe, D., Novak, S., 1989. Modeling row cover effects on microclimate and yield. 2. Thermal-model and simulations. J. Am. Soc. Hortic. Sci. 114, 569–578.

Al-Mahdouri, A., Baneshi, M., Gonome, H., Okajima, J., Maruyama, S., 2013. Evaluation of optical properties and thermal performances of different greenhouse covering materials. Sol. Energy 96, 21–32. doi:10.1016/j.solener.2013.06.029

Andrieu, B., Sinoquet, H., 1993. Evaluation of structure description requirements for predicting gap fraction of vegetation canopies. Agric. For. Meteorol. 65, 207–227.

ASTM, 1992. ASTM E 903-82. Standard test method for solar absorptance, reflectance, and transmittance of materials using integrating spheres.

Baret, F., Andrieub, B., Stevenc, M.D., 1993. Gap frequency and canopy architecture of sugar beet and wheat crops. Agric. For. Meteorol. 65, 261–279.

Cabrera, F.J., Baille, a., López, J.C., González-Real, M.M., Pérez-Parra, J., 2009. Effects of cover diffusive properties on the components of greenhouse solar radiation. Biosyst. Eng. 103, 344–356. doi:10.1016/j.biosystemseng.2009.03.008

Campbell, G.S., 1986. Extinction coefficients for radiation in plant canopies calculated using an ellipsoidal inclination angle distribution. Agric. For. Meteorol. 36, 317–321. doi:10.1016/0168-1923(86)90010-9

Campbell, G.S., Norman, J.M., 1998. An introduction to environmental biophysics. Springer New York, New York, NY. doi:10.1007/978-1-4612-1626-1

Cook, R.L., Torrance, K.E., 1982. A reflectance model for computer graphics. ACM Trans. Graph. 1 1, 7–24.

Critten, D.L., 1983. A computer model to calculate the daily light integral and transmissivity of a greenhouse. J. Agric. Eng. Res. 28, 61–76. doi:10.1016/0021-8634(83)90100-2

De Luca, V., Ruocco, G., 2000. A transient-spectral thermal model of soil under radiative-interfering cover. J. Agric. Eng. Res. 77, 93–102. doi:10.1006/jaer.2000.0565

Demarez, V., Duthoit, S., Baret, F., Weiss, M., Dedieu, G., 2008. Estimation of leaf area and clumping indexes of crops with hemispherical photographs. Agric. For. Meteorol. 148, 644–655. doi:10.1016/j.agrformet.2007.11.015

Gonsamo, A., Pellikka, P., 2009. The computation of foliage clumping index using hemispherical photography. Agric. For. Meteorol. 149, 1781–1787. doi:10.1016/j.agrformet.2009.06.001

Goudriaan, J., 1977. Crop micrometeorology : a simulation study. Agricultural University, Wageningen, NL.

Goudriaan, J., 1988. The bare bones of leaf-angle distribution in radiation models for canopy photosynthesis and energy exchange. Agric. For. Meteorol. 43, 155–169. doi:10.1016/0168-1923(88)90089-5

Graefe, J., 2005. Simulation of soil heating in ridges partly covered with plastic mulch, Part I: Energy balance model. Biosyst. Eng. 92, 391–407. doi:10.1016/j.biosystemseng.2005.07.010

Ham, J.M., Kluitenberg, G.J., 1994. Modeling the effect of mulch optical properties and mulch-soil contact resistance on soil heating under plastic mulch culture. Agric. For. Meteorol. 71, 403–424. doi:10.1016/0168-1923(94)90022-1

Hay, J.E., 1979. Calculation of monthly mean solar radiation for horizontal and inclined surfaces. Sol. Energy 23, 301–307. doi:10.1016/0038-092X(79)90123-3

Lang, A., Yueqin, X., 1986. Estimation of leaf area index from transmission of direct sunlight in discontinuous canopies. Agric. For. Meteorol. 37, 229–243. doi:10.1016/0168-1923(86)90033-X

Lobell, D.B., Asner, G.P., 2002. Moisture effects on soil reflectance. Soil Sci. Soc. Am. J. 66, 722–727. doi:10.2136/sssaj2002.7220

Meyer, P., 1994. Bi-logistic growth. Technol. Forecast. Soc. Change 47, 89–102. doi:10.1016/0040-1625(94)90042-6

Moon, P., Spencer, D.E., 1942. Illumination from a non-uniform sky. Illum. Eng. 37, 707–726.

Muller, E., Décamps, H., 2001. Modeling soil moisture–reflectance. Remote Sens. Environ. 76, 173–180. doi:10.1016/S0034-4257(00)00198-X

Myneni, R.B., Ross, J., Asrar, G., 1989. A review on the history of photon transport in leaf canopies. Agric. For. Meteorol. 45, 1–153.

Nijskens, J., Deltour, J., Coutisse, S., Nisen, A., 1985. Radiation transfer through covering materials, solar and thermal screens of greenhouses 35, 229–242.

Nilson, T., 1971. A theiretical analysis of the frequency of gaps in plant stands. Agric. Meteorol. 8, 25–38.

Papadakis, G., Briassoulis, D., Scarascia Mugnozza, G., Vox, G., Feuilloley, P., Stoffers, J. a., 2000. Radiometric and thermal properties of, and testing methods for, greenhouse covering materials. J. Agric. Eng. Res. 77, 7–38. doi:10.1006/jaer.2000.0525

Pieters, J.., Pollet, I.., Deltour, J., Verschoore, R., 2003. Angular dependence of forward scattering induced by condensate on greenhouse cladding materials. Agric. For. Meteorol. 119, 23–36. doi:10.1016/S0168-1923(03)00121-7

Pieters, J.G., Deltour, J.M., 1999. Modelling solar energy input in greenhouses. Sol. Energy 67, 119–130. doi:10.1016/S0038-092X(00)00054-2

Pinty, B., Lavergne, T., Dickinson, R.E., Widlowski, J.-L., Gobron, N., Verstraete, M.M., 2006. Simplifying the interaction of land surfaces with radiation for relating remote sensing products to climate models. J. Geophys. Res. 111, D02116. doi:10.1029/2005JD005952

Pollet, I.V., Pieters, J.G., 2002. PAR transmittances of dry and condensate covered glass and plastic greenhouse cladding. Agric. For. Meteorol. 110, 285–298. doi:10.1016/S0168-1923(01)00295-7

Pollet, I. V., Pieters, J.G., Deltour, J., Verschoore, R., 2005. Diffusion of radiation transmitted through dry and condensate covered transmitting materials. Sol. Energy Mater. Sol. Cells 86, 177–196. doi:10.1016/j.solmat.2004.07.003

Rosenfeld, J.L.., Platzer, W.., van Dijk, H., Maccari, A., 2001. Modelling the optical and thermal properties of complex glazing: overview of recent developments. Sol. Energy 69, 1–13. doi:10.1016/S0038-092X(01)00028-7

Ross, J., 1981. The radiation regime and architecture of plant stands. Kluwer Academic Publisher, Dordrecht.

Rühlmann, J., Ruppel, S., 2005. Effects of organic amendments on soil carbon content and microbial biomass – results of the long-term box plot experiment in Grossbeeren. Arch. Agron. Soil Sci. 51, 163–170. doi:10.1080/03650340400026651

Sandmann, M., Graefe, J., Feller, C., 2013. Optical methods for the non-destructive estimation of leaf area index in kohlrabi and lettuce. Sci. Hortic. (Amsterdam). 156, 113–120. doi:10.1016/j.scienta.2013.04.003

Spitters, C.J.T., Toussaint, H.A.J.M., Goudriaan, J., 1986. Separating the diffuse and direct component of global radiation and its implications for modeling canopy photosynthesis Part I. Components of incoming radiation. Agric. For. Meteorol. 38, 217–229. doi:10.1016/0168-1923(86)90060-2

Verhoef, W., 1984. Light scattering by leaf layers with application to canopy reflectance modeling: The SAIL model. Remote Sens. Environ. 16, 125–141. doi:10.1016/0034-4257(84)90057-9

Walter, B., Marschner, S.R., Li, H., Torrance, K.E., 2007. Microfacet models for refraction through rough surfaces. Eurographics Symp. Render. 195–206. doi:10.2312/EGWR/EGSR07/195-206

Wang, S.W., Boulard, T.B., 2000. Measurement and prediction of solar radiation distribution in full-scale greenhouse tunnels. Agronomie 20, 41–50.

Widlowski, J.-L., Pinty, B., Clerici, M., Dai, Y., De Kauwe, M., de Ridder, K., Kallel, a., Kobayashi, H., Lavergne, T., Ni-Meister, W., Olchev, a., Quaife, T., Wang, S., Yang, W., Yang, Y., Yuan, H., 2011. RAMI4PILPS: An intercomparison of formulations for the partitioning of solar radiation in land surface models. J. Geophys. Res. 116, G02019. doi:10.1029/2010JG001511

Wu, Y., Perry, K.B., Ristaino, J.B., 1996. Estimating temperature of mulched and bare soil from meteorological data. Agric. For. Meteorol. 81, 299–323.

Yu, H.-L., Hsaio, C.-C., 2009. Comparison of different measurement methods for transmittance haze. Metrologia 46, 233–237. doi:10.1088/0026-1394/46/4/S19